Signal Processing Techniques for Mobile Multimedia Systems

A thesis submitted in fulfillment of the requirements for
the degree of Doctor of Philosophy

Tasso Athanasiadis
B.Eng. (Honours), M.Eng.

School of Electrical and Computer Engineering
Science, Engineering and Technology Portfolio
RMIT University
May 2007

Declaration

I certify that except where due acknowledgement has been made, the work is that of the author alone; the work has not been submitted previously, in whole or in part, to qualify for any other academic award; the content of the thesis is the result of work which has been carried out since the official commencement date of the approved research program; and, any editorial work, paid or unpaid, carried out by a third party is acknowledged; ethics procedures and guidelines have been followed.

Signed: ..... Date: .....

Tasso Athanasiadis

This thesis is dedicated to my wife Vilma,
my parents Kyriakos and Anthi Athanasiadis,
and brothers Bill & Alex.

Acknowledgements

There are many people who I would like to acknowledge and thank for their support and encouragement during the course of this research. In particular, those people who have contributed their thoughts, ideas, and criticism to this study.

First, I wish to express my eternal gratitude to my supervisor Assoc. Prof. Zahir Hussain for giving me the opportunity to undertake this research study and for his continued support and understanding. I am truly grateful for his friendship, and in particular, for the many occasions spent sharing and discussing our personal life experiences; both philosophically and spiritually. This proved to be an invaluable source of inspiration. Without it this study would not have eventuated or reached its conclusion.

The generous financial support received from the School of Electrical and Computer Engineering at RMIT University, which made this research possible, is also gratefully acknowledged.

My research colleagues and friends, Dr. Kevin Lin, Dr. Yuu-Seng (aka Jimmy) Lau, and Dr. Jusak Jusak, are especially acknowledged for contributing their expertise to this research; through cooperative works in the publication of peer-reviewed conference and journal papers. In particular, I would like to express my deepest appreciation for Dr. Kevin Lin's efforts and contribution, in willingly giving his time and assisting in the development of a simulation framework to explore new ideas and challenges for mobile multimedia systems. This was valuable in forming the foundations of this study.

I would also like to thank my friends, past and present staff members of the School of Electrical and Computer Engineering at RMIT University, who have taken a keen interest in my personal, professional, and academic development, for their continued kind words of support and encouragement. A special thanks must also go to my past mentor and good friend, Dr. Rodney Staples, for offering to review my thesis and inspiring me to achieve my personal goals through our insightful discussions on life and work, and by making sure that my 'feet are firmly grounded'. Our casual luncheons have also been an immense source of motivation, particularly, resulting from our fruitful commentaries on issues concerning the telecommunica-

tions/broadcasting industry and current state of the tertiary education system in Australia.

Finally, but by no means least, I wish to sincerely thank my beloved wife Vilma for her unwavering love, patience, and support, especially, during our most difficult times; without which this work would not have been possible. I am also truly grateful to my family and extended family for their continued support and encouragement in all my endeavours.

Table of Contents

List of Figures

List of Tables

List of Abbreviations

1G	first-generation
1xRTT	1 times radio transmission technology
2G	second-generation
3G	third-generation
3GPP	third-generation partnership project
4G	fourth-generation
AAA	adaptive antenna array
ABPA	adaptive bit and power allocation
ATD	adaptive transmit diversity
AoA	angle-of-arrival
AS	angular spread
AWG	array weighting gain
AWGN	additive white Gaussian noise
BER	bit error rate
BPSK	binary phase shift keying
BS	base station
BTS	base transceiver station
CCI	co-channel interference
CDMA	code-division multiple access
CIR	channel impulse response
CMA	constant modulus algorithms
CNR	channel-to-noise ratio
CP	cyclic prefix
CSK	chaos shift keying
CWT	continuous wavelet transform
DCT	discrete cosine transform

DFBM	direct feedback method
DFT	discrete Fourier transform
DOA	direction of arrival
DS-CDMA	direct-sequence code division multiple access
DSP	digital signal processing
DWT	Discrete wavelet transform
EDGE	enhanced data rates for GSM evolution
EV-DO	evolution-data optimised
EVD	eigen-value decomposition
ESPRIT	estimation of signal parameters via rotational invariance technique
FB	feedback
FDD	frequency-division duplexing
FDMA	frequency-division multiple access
FEC	forward error coding
FFT	fast Fourier transform
FH-CDMA	frequency hopping - code division multiple access
FIR	finite impulse response
GBHDS	geometrical-based hyperbolic distributed scatterers
GPRS	general packet radio service
GSDF	geometrical scatterer density function
GSM	global system for mobile communications
IDFT	inverse discrete Fourier transformation
IFFT	inverse fast Fourier transformation
i.i.d.	independent and identically distributed
ISI	inter-symbol-interference
JPEG	joint photographic experts group
LAN	local area network
LCG	logistic chaotic generator
LM-ABPA	lookup matrix - adaptive bit and power allocation
LMS	least mean squared
LOS	line-of-sight
MAN	metropolitan area network
MEA	multi-element array

MIMO	multiple-input multiple-output
MISO	multiple-input single-output
MLD	maximum likelihood detector
MMSE	minimum mean-square error
MPEG	moving picture experts group
MRC	maximum ratio combiner
MS	mobile station
MSC	mobile switching centre
MSE	mean-square error
MUSIC	multiple emitter location and signal parameter estimation
MVDR	minimum variance distortionless-response
NG	next-generation
OFDM	orthogonal frequency division multiplexing
OSTBC	orthogonal space-time block coding
pdf	probability density function
PDP	power delay profiles
PEP	pairwise error probability
PL	path loss
PSK	phase-shift keying
PSNR	peak-signal-to-noise ratio
PSTN	public-switched telephone network
QAM	quadrature amplitude modulation
QPSK	quadrature phase shift keying
RF	radio frequency
RHS	right hand side
S-DSE-CMA	sinusoidally-distributed dithered signed-error constant modulus algorithm
SER	symbol error rate
SIMO	single-input-multiple-output
SINR	signal-to-interference-and-noise ration
SISO	single input single output
SNR	signal-to-noise ratio
STBC	space-time block coding
STC	space-time coding

STF	space-time-frequency
STTC	space-time trellis coding
SVD	singular-value decomposition
TCM	trellis coded modulation
TDD	time-division duplexing
TDMA	time-division multiple access
ToA	time-of-arrival
UCA	uniform circular array
ULA	uniform linear array
VRD	variable rate demodulator
WCDMA	wideband CDMA

List of Mathematical Notations

$\lvert \cdot \rvert$	Absolute value of a scalar; cardinality of a set
ϕ	Angle-of-arrival
ψ	Angle-of-departure
σ_ϕ	Angular spread
T_b	Bit period
f_c	Carrier frequency
λ_c	Carrier wavelength
T_c	Chip period
$\mathcal{CN}(m, v)$	Circularly symmetric complex Gaussian random process with mean m and variance v
$\mathcal{Q}(\cdot)$	Classical Gaussian Q-function
B_c	Coherence bandwidth
$(\cdot)^*$	Complex conjugation
σ_τ	Delay spread
$\det(\cdot)$	Determinant of a matrix
τ_0	Direct path delay
D	Distance between the base station and the mobile station
f_m	Doppler spread
ε_b	Energy per bit
ε_s	Energy per symbol
$\lVert \cdot \rVert_F$	Frobenius norm for matrices; Euclidean norm for vectors
$(\cdot)^H$	Hermitian transposition of a vector or a matrix
I_N	Identity matrix of a size $N \times N$
$\mathbf{A}$	Matrix $\mathbf{A}$
f_d	Maximum Doppler shift
$\tau_{e_{\max}}$	Maximum excess delay

$\tau_{\max}$	Maximum path delay
N_t	Number of transmit antennas
N_r	Number of receive antennas
N_c	Number of OFDM subcarriers
L	Number of dominant & resolvable multipaths
n	Path loss exponent
$S_r(f)$	Power spectral density
R	Radius of the scatterers' circle
d_o	Reference distance from the mobile station
a	Scalar a
c	Speed of light
v	Speed of the mobile
$\sqrt{\cdot}$	Square root of a scalar; Hermitian square root of a matrix
$\mathcal{E}\{\cdot\}$	Statistical expectation value
T_s	Symbol period
τ	Time-of-arrival
P_{T}	Total Transmitted power
Trace$(\cdot)$	Trace of a matrix
$(\cdot)^T$	Transposition of a vector or a matrix
$\underline{a}$ or $\mathbf{a}$	Vector $\underline{\mathrm{a}}$ or $\mathbf{a}$

Abstract

Recent trends in wireless communication systems show a significant demand for the delivery of multimedia services and applications over mobile networks - mobile multimedia. Today, it is not uncommon to find users accessing a variety of multimedia data through mobile devices such as video-capable cell phones. This can be attributed mainly to the rapid growth and popularity of a long list of applications for mobile communication systems that were considered impossible or impracticable only a few years ago like video telephony, multimedia messaging, mobile gaming, interactive and streaming video, etc. However, despite the ongoing development of key communication technologies that support these applications, the communication resources and bandwidth available to wireless/mobile radio systems are often severely limited. It is well known, that these bottlenecks are inherently due to the processing capabilities of mobile transmission systems, and the time-varying nature of wireless channel conditions and propagation environments. Therefore, new ways of processing and transmitting multimedia data over mobile radio channels have become essential which is the principal focus of this thesis.

In this thesis, we investigate the performance and suitability of various signal processing techniques and transmission strategies in the application of multimedia data over wireless/mobile radio links. The proposed transmission systems for multimedia communication use different data encoding schemes, which include source coding in the wavelet domain, transmit diversity coding (space-time coding), and adaptive antenna beamforming (eigenbeamforming). By integrating these techniques into a robust transmission system, we maximise the received quality (SNR, etc) of multimedia signals on mobile devices while mitigating the fast fading and multi-path effects of mobile channels. To support the transmission of high data-rate multimedia applications, we also make use of a well known multi-carrier transmission technology known as Orthogonal Frequency Division Multiplexing (OFDM). Apart from being bandwidth-efficient, OFDM systems offer many benefits that further enhance the error-rate performance of radio links, which includes the ability to transmit data with virtually zero intersymbol interference. Moreover, OFDM systems are effective in providing additional diversity branches in the frequency domain. As shown in

this study, this results in significant performance gains when combined with other techniques, such as space-time coding (STC).

To optimise signal transmission, we have proposed a novel unequal adaptive modulation scheme for the transmission of mutlimedia data over MIMO-OFDM systems. In this system, we use discrete wavelet transform/subband coding to compress data into their respective low-frequency and high-frequency components. Unlike traditional methods, however, data representing the low-frequency components are processed and modulated separately as they are more sensitive to the distortion effects of mobile radio channels. To make use of a desirable subchannel state, such that the quality (SNR) of the multimedia data recovered at the receiver is optimized, we employ a lookup matrix-adaptive bit and power allocation (LM-ABPA) algorithm. Apart from improving the spectral efficiency of OFDM, the modified LM-ABPA scheme, sorts and allocates subcarriers with the highest SNR to low-frequency data and the remaining to the least important data. To maintain a target system SNR, the LM-ABPA loading scheme assigns appropriate signal constellation sizes and transmit power levels (modulation type) across all subcarriers and is adapted to the varying channel conditions such that the average system error-rate (SER/BER) is minimised. To ensure that the maximum data-rate is achieved, knowledge of the subchannel gain is used to maximise the instantaneous channel-to-noise ratio (CNR) of OFDM subcarriers such that an optimum number of antenna output beams are selected with a corresponding power splitting ratio. The diversity gain of the system is also maximised by selecting a STC encoding matrix with a spatial dimension equal to the number of output beams determined by this process. When configured under a constant data-rate constraint, simulation results show significant performance gains over non-adaptive systems.

In addition to the above studies, we apply the multimedia framework presented in this thesis to investigate the performance of other signal processing techniques for multimedia communication such as blind channel equalization, and study the effectiveness of a secure communication system based on a logistic chaotic generator (LCG) for Chaos Shift Keying (CSK).

Chapter 1

Introduction

Over the past decade, there has been a phenomenal increase in the generation, transmission, and use of multimedia information over wireless communication systems, particularly, in mobile radio networks. The growing demand for high-speed multimedia services in mobile systems has enabled a multitude of applications for multimedia communication - mobile multimedia - such as mobile video telephony, multimedia messaging, wireless Internet (wireless access to data networks), digital video broadcasting [1–3], all of which are now inherent in current implementations of third generation (3G) WCDMA (Wideband Code Division Multiple Access) mobile communication systems [4, 5]. In addition, users of these applications are becoming more mobile and have a stronger requirement for wireless networks which provide the ability to communicate multimedia information with improved scalability, error resiliency, and energy efficiency. The need to access vast amounts of audio-visual information on multiple devices in different contexts at different locations and environments through ubiquitous terminals and networks is also now being realised. In fact, as more and more multimedia content becomes available in digital form, there is an increasing demand to make use of it in a wireless/mobile setting. As a result, mobile multimedia has attracted considerable interest by both the research community and industry to address the need for new key technologies that will enable data services to support wide-band high speed multimedia applications [6, 7].

Recent studies into next-generation (NG) mobile networks such as fourth generation (4G) systems, have reported a significant trend towards personalized mobile communications [8–10] and an impending requirement for modern communication products/devices that are able to transmit and process high rate multimedia data such as high-quality images and video; suggesting a significant paradigm shift in traditional mobile services, which have predominantly supported the transmission of voice data. This can be mainly attributed to the popularity and capabilities of data-oriented services increasingly made available in mobile radio networks. In fact, since the deployment of the first generation (1G) analogue mobile phone system in 1985, there has been a

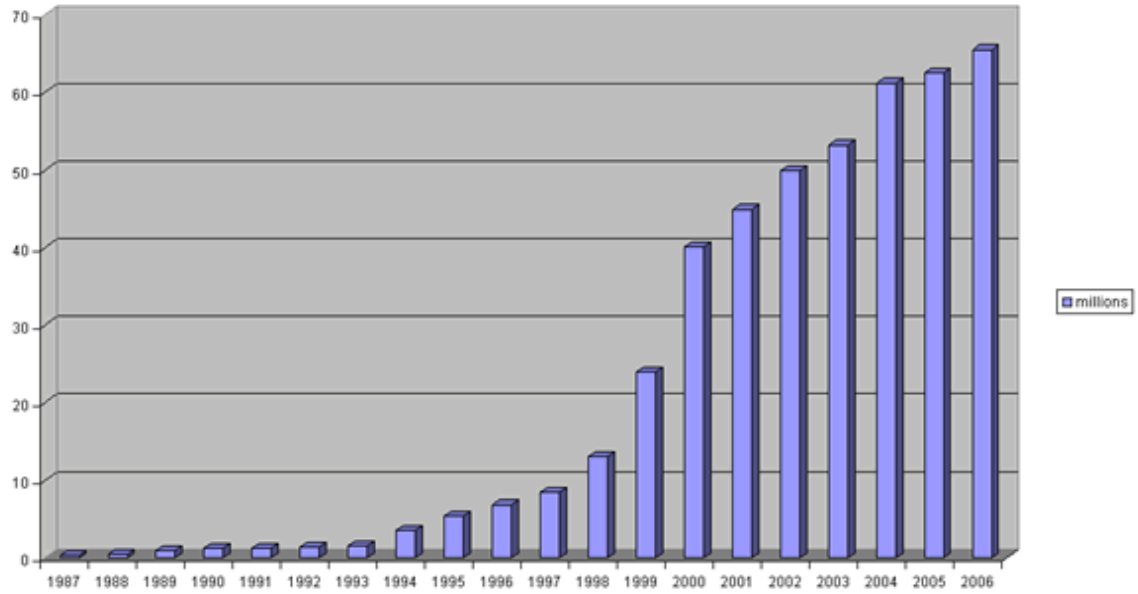

Figure 1.1: Number of mobile phone subscribers in the UK.

rapid growth in the number of mobile phone subscribers as mobile communication systems have evolved to support high data rate digital services. Figure 1.1, shows a typical growth pattern (experienced globally) over the past two decades in the number of users subscribing to a mobile service in the UK (United Kingdom) - adopted from [11]. According to Wireless Intelligence (www.wirelessintelligence.com), as of the end of the first quarter 2007 there are already close to 3 billion mobile phone subscribers worldwide with 115 million of those being 3GSM/W-CDMA subscribers [12].

Generally, this trend in mobile phone subscription can also be reflected in the many advancements made during this period with the provisioning and improved capabilities of data services available for mobile radio networks: from 9.6 Kbits/s in second generation (2G) GSM (Global System for Mobile Communications) systems [13] in 1992, up to 114 Kbit/s for 2.5G GPRS (General Packet Radio Service) [14] & CDMA2000 1xRTT (1 times Radio Transmission Technology) enabled systems [15] and 384 Kbit/s in 2.75G EDGE (Enhanced Data Rates for GSM Evolution) capable networks [14], to the more recent rates of 3 Mbit/s for CDMA2000 EV-DO (Evolution-Data Optimized) [15] and 1.8 Mbit/s, 3.6 Mbit/s, 7.2 Mbit/s & 14.4 Mbit/s currently specified in the HSDPA (High Speed Downlink Packet Access) standard for 3G W-CDMA systems [16]. Figure 1.2, illustrates the evolution of the GSM-based and CDMA (Code Division Mulitple Access) data access/transport technologies - adopted from [17]. It is also predicted that NG/4G mobile communication systems will offer a fully IP-based integrated system capable of providing 100 Mbit/s and 1 Gbit/s, respectively [18]; speeds of which are commonplace

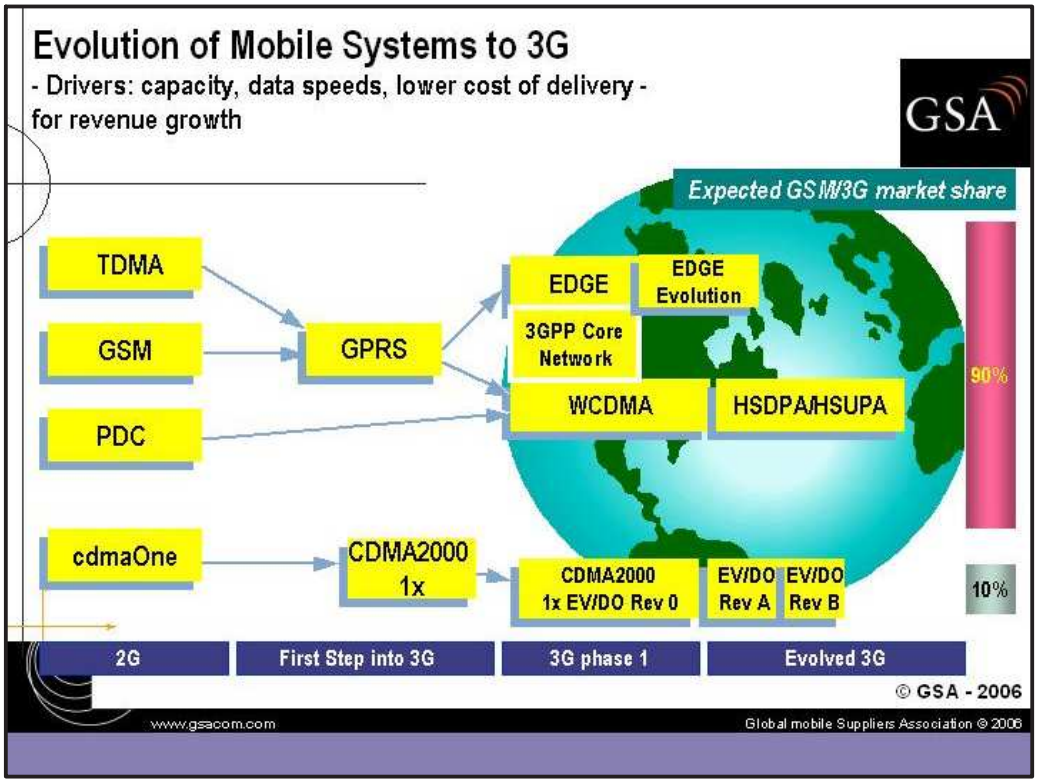

Figure 1.2: Evolution of mobile communication systems to 3G.

in current wireless LAN/MAN systems such as Wi-Fi & WiMax, which are based on the IEEE 802.11/16 standards [19, 20]. One of the key technologies that will enable this vision of ultra-broadband mobile data communications are adaptive array systems [9, 10]. However, despite the ongoing development of communication technologies to deal with multimedia communication, the transmission of multimedia data over wireless/mobiles channels invariably introduce significant bottlenecks.

There are several factors that contribute to the constraints introduced by mobile multimedia communication. In general, it is widely accepted that the communication bandwidth available to wireless systems and the processing capabilities of mobile systems/devices are often severely limited. Secondly, mobile radio channels must transmit user information in a highly compressed form, while making efficient use of available frequency spectrum and communication power. Thirdly, representing multimedia data such as high-quality digital images and video requires a large amount of the available information/channel resources, leading to high bandwidth, computational, and communication energy requirements. Finally, and more importantly, the time-varying nature of channel conditions and propagation characteristics in a wireless environment such as noise, interference, and particularly mulitpath fading [21] will cause severe degradation in communication performance, system latency, and the acceptable or subjective quality of data

received on mobile terminals/devices.

To deal with the problems commonly associated with the transmission of multimedia data over wireless communication channels several different signal-processing techniques have been developed. The most viable approach to alleviate the bandwidth demands of multimedia technology is data compression [22, 23], also referred to as *source coding* in digital communications literature [24]. In the context of multimedia communication, compression is concerned with transmitting image/video data with the highest quality and lowest bandwidth possible, and within a processing time acceptable by the user. Transform coding, such as the wavelet-based technique, has emerged as the most powerful method used in the compression of digital images and video [25–29], and are the basis of current JPEG [30, 31] and MPEG [32–34] standards introduced by the International Standards Organisation (ISO). In order to overcome the effects of noisy wireless/radio environments various 'adaptive' processing techniques such as adaptive modulation - to dynamically control communication parameters to suit variations in channel conditions, computational requirements, and available processing resources - have emerged [35]. For example, in [36], source coding parameters of the JPEG image compression algorithm are adapted to varying communication requirements; energy consumption, bandwidth, and latency. A methodology to select the optimal image compression parameters to minimize communication energy consumption given current channel conditions and constraints is also proposed. In [37], an adaptive joint source/channel coding scheme is used, which is based on a turbo-coded OFDM transmission system incorporating a wavelet coder, to transmit compressed images over band-limited frequency selective fading channels. Other techniques employed to mitigate the propogation effects of wireless channels include channel coding and transmit diversity schemes.

Traditionally, temporal domain processing or *channel coding* techniques such as turbo coding, convolutional coding, Reed-Solomon coding, and interleaving are employed to improve the reliability of mobile radio links by the detection and correction of errors [38]. Channel coding techniques can reduce the required signal-to-noise ratio (SNR) to achieve a desired probability of error P_E, but at the expense of transmission bandwidth or decoder complexity [39]. More recently, however, transmit diversity has attracted considerable interest by the research community as a powerful tool in mitigating the multipath propagation effects in wireless environments for multi-antenna transmission systems. One of the most important and extremely effective transmit diversity techniques developed is the well-known space-time block coding (STBC) scheme in [40], which has been further extended in [41–43] as orthogonal-STBC (OSTBC). Space-time coding significantly improves the bit error rate (BER) performance of mobile systems by introducing joint correlation in both the spatial and time domain of wireless channels; achieved by cleverly

encoding information data across a multi-antenna configuration [44]. Used on its own, however, STBC cannot mitigate the effects of coherent channel deep fading (which is the resultant effect when transmitted signals from all antennas are experiencing deep fade at the same time) due to the spatial correlation structure of the channel [45–47].

Another popular transmit diversity technique is antenna beamforming [48] such as the eigen-beamforming scheme adopted in the 3GPP (3rd Generation Partnership Project) standards [49]. In antenna beamforming, the gain of the pensile-like beams from the antenna array are resolved in a direction of the dominant propagating path such that the signal power at the receiver is maximised. When combined with STBC and a carrier modulation technique such as Orthogonal Frequency Division Multiplexing (OFDM), also referred to as discrete multitone modulation (DMT), significant gains in error-rate performance and spectral efficiency can be achieved with transmission systems incorporating adaptive transmit diversity (ATD) techniques; as shown in [50]. Importantly, however, there has been very little work done in demonstrating the use of these signal-processing techniques and exploring new ways of improving the performance of mobile transmission systems for multimedia applications - mobile multimedia. This is the principal focus of this thesis.

1.1 Objectives of this Dissertation

The growing demand for high speed/quality multimedia information in mobile networks has created an impending need for investigating different signal-processing approaches that will address the performance issues with mobile transmission systems to support the high bandwidth, computational energy, and communication energy requirements for multimedia communication. This dissertation is primarily concerned with the application (through simulation analysis and modeling) of various digital communication techniques such as data compression and adaptive transmit diversity (ATD), to improve the transmission performance of mobile multimedia systems. Although one of the requirements in multimedia communication is the integration of different types of media (data, audio, video, etc), the thesis focuses on the application of digital still images for the verification and presentation of the techniques applied. Nevertheless, the transmission systems proposed can be readily extendable to other types of multimedia data such as digital video. In the context of mobile multimedia, however, the study of service related issues in supporting different media such as the investigation of the 'quality of service' requirement is considered beyond the scope of the research conducted. The key objectives of this thesis, therefore, include the following:

1. To develop a simulation framework for multimedia applications that integrates different signal-processing techniques and advanced communication concepts such as data compression, transmit diversity coding (e.g. STBC), and adaptive antenna beamforming (AB), with an OFDM transmission system.
2. To evaluate the performance of the proposed transmission system in the application of 'real' multimedia data such as digital still images, and to use both objective and subjective performance measurement techniques in the analysis of simulated results.
3. To study the performance of the framework developed when combining source coding (based on wavelet decomposition) with adaptive transmit diversity schemes and simulating the transmission of compressed digital images.
4. To extend the simulation framework to include and study the effectiveness of the transmission system employing a space-time-frequency (STF) encoder, and to compare performance results with those obtained for STBC.
5. To develop a new approach in the optimisation of multimedia data transmission using an unequal modulation scheme based on a high spectrally efficient bit and power allocation algorithm known as LM-ABPA (Look-up Matrix-Adaptive Bit and Power Allocation), which is adaptive to the channel fading conditions and aims to maximise the received signal quality of multimedia data.
6. To apply the simulation framework resulting from this study to evaluate the performance of a blind channel equalization algorithm for multimedia communication and a secure communication system based on Chaos Shift Keying (CSK).

1.2 Contributions of this Dissertation

The overall contribution of this thesis is the design of a novel and efficient integrated compression (in the wavelet domain) and unequal adaptive modulation scheme for multimedia communication in mobile radio systems. In this dissertation, various signal-processing schemes are proposed for improving the quality of multimedia data in terms of the error rate performance, channel capacity, and spectral efficiency of mobile transmission systems. The main contributions of this thesis are summarised as follows:

1. A transmission system (multimedia simulation framework) for mobile multimedia applications based on data compression, transmit diversity, and OFDM has been introduced. By integrating space-time block coding (STBC) and an adaptive beamforming (AB) strategy with OFDM using a multi-antenna array configuration at the transmitter,

it is shown (by simulating the transmission of compressed digital images) that the degradation in system performance caused by the channel impairments of wireless channels such as multipath fading, is significantly reduced. This work was presented at the *IEEE International Conference on Information Technology and Applications - ICITA 2005*, in Sydney/Australia [51].

2. A transmission system using a combined compression and diversity scheme for multimedia communication has been proposed. To improve the bandwidth utilisation of the system when transmitting multimedia information, the data is compressed using a wavelet-based encoding before it is further processed by the STBC, AB, and OFDM blocks. This is shown to provide better control over a range of communication requirements such as the communication bandwidth, transmission power, etc. The results of this study have been published in [52].
3. A source-diversity coded OFDM system using a space-time-frequency (STF) coding algorithm has been proposed. When compared to a source-diversity coded OFDM system using STBC the additional diversity branches exploited by STF coding (space, time, and frequency domains) results in significant performance improvements, but at the expense of computational complexity. The findings of this work have been presented in [53].
4. A mobile transmission system for multimedia communication using a source combined unequal adaptive modulator is presented. To ensure that the quality of the multimedia data recovered at the receiver is optimized, data representing the low-frequency components from the wavelet-based compressor are processed and modulated separately using a a lookup matrix-adaptive bit and power allocation (LM-ABPA) algorithm, as they are more sensitive to the distortion effects of radio channels. In this system, the LM-ABPA loading scheme maintains a target system SNR by assigning appropriate signal constellation sizes and transmit power levels (modulation type) across all subcarriers and is adapted to the varying channel conditions such that the average system error-rate (SER/BER) is minimised. Simulation results show significant performance gains over other methods. This work was presented at the *IEEE Region 10 Conference - TENCON 2006*, in Melbourne/Australia [54].
5. The multimedia simulation framework developed to investigate the effectiveness of a combined source-diversity coded OFDM system is applied to study the performance of a blind channel equalisation technique, the sinusoidally distributed dithered signed-error constant modulus algorithm (S-DSE-CMA). Simulations using the transmission of compressed digital images show that the proposed method converges faster when compared

to other existing schemes. The results of this work led to the publication in [55].

6. A secure communication system using a modified logistic chaotic generator (LCG) for Chaos Shift Keying (CSK) is presented. It is shown that the newly proposed LCG algorithm provides an additional bifurcation parameter that can be used to enhance the security of the CSK system without sacrificing the communication performance (BER, stc). The multimedia simulation framework, developed for the investigation of source-diversity coded OFDM systems, has been modified to incorporate the CSK technique and to show the effectiveness of the bifurcation parameter in providing an extra level of security in spread spectrum communication systems. This work has been accepted for publication in the *Multimedia Cyberscape Journal* [56].

1.2.1 Publications & Awards

The contributions of this thesis have appeared in several refereed international conference proceedings [51–55], and includes the publication of a peer-reviewed international journal paper [56]. Also, in conjunction with the research work conducted at RMIT University, School of Electrical & Computer Engineering, the author has received 2 IEEE-Victoria awards. Details of the publications and awards are provided below.

Conference Publications

1. Tasso Athanasiadis, Kevin H. Lin, and Zahir M. Hussain, "An Unequal Modulation Scheme for the Transmission of Compressed Multimedia Data over Adaptive MIMO-OFDM Systems," *IEEE Region 10 Conference*, *TENCON 2006*, November 2006.

2. Tasso Athanasiadis, Kevin H. Lin, and Zahir M. Hussain, "Multimedia Transmission over Wireless Space-Time-Frequency coded OFDM Systems with Adaptive Beamforming," *Asia-Pacific Conference on Communications*, *APCC '06*, August 2006.

3. Tasso Athanasiadis, Kevin H. Lin, and Zahir M. Hussain, "Transmission of Compressed Multimedia Data over Wireless Channels using Space-time OFDM with Adaptive Beamforming," *IEEE Region 10 Conference*, *TENCON 2005*, November 2005.

4. Jusak Jusak, **Tasso Athanasiadis**, Zahir M. Hussain, "A Blind Equalization Algorithm for Wireless Multimedia Communication," *Asia-Pacific Conference on Communications*, *APCC 2005*, October 2005.

5. Tasso Athanasiadis, Kevin H. Lin, and Zahir M. Hussain, "Space-time OFDM with Adaptive Beamforming for Wireless Multimedia Applications," *Proc. IEEE International Conference on Information Technology and Applications*, *ICITA 2005*, vol. 2, pp. 381-386, July 2005.

Journal Publications

1. Yuu-Seng Lau, **Tasso Athanasiadis**, and Zahir M. Hussain, "A Secure Digital Communication System for Multimedia Applications Using a Chaotic Generator," *Multimedia Cyberscape Journal*, vol.5, no. 1, pp. 30-42, 2007.

Awards

1. IEEE-Victoria Chapter First Prize Award for Best Oral Presentation,"An Unequal Modulation Scheme for the Transmission of Compressed Multimedia Data over Adaptive MIMO-OFDM Systems," *RMIT University, School of Electrical & Computer Engineering, Annual Postgraduate Conference*, September 2006.

2. IEEE-Victoria Chapter First Prize Award for Best Oral Presentation, "Space-time OFDM with Adaptive Beamforming for Wireless Multimedia Applications," *RMIT University, School of Electrical & Computer Engineering, Annual Postgraduate Conference*, September 2005.

1.3 Thesis Outline

This dissertation consists of 8 chapters, which can be divided into two parts. With Chapter 1 & 2 being the introductory and review chapters, the first part of the thesis consists of Chapters 3, 4, and 5. These chapters present a communication framework based on wireless OFDM systems to investigate the use and performance of various signal processing techniques and transmission strategies for the efficient transport of multimedia applications over mobile radio links/channels. These techniques include, source coding in the wavelet domain, adaptive transmit diversity coding, adaptive antenna beamforming (eigen-beamforming), and a novel unequal adaptive modulation scheme. The second part consists of Chapters 6 and 7. These chapters contain applications of the multimedia system framework presented in the earlier parts of this thesis to study the performance of other signal processing techniques for multimedia communication such as, blind channel equalization, and a secure communication system based on Chaos Shift Keying (CSK).

Chapter 8, provides the thesis conclusions and suggestions for future research directions. An overall summary of the organisation of this dissertation is provided below.

Chapter 2: Overview of Multimedia & Mobile Communication Systems. In this chapter, an overview of some of the key aspects concerning multimedia signals and systems (acquisition, processing, compression, etc), and mobile communication systems is presented. In particular, it provides a brief review of current techniques used for image compression with the main focus on transform/sub-band coding of digital images using wavelets; as simulation results presented in this thesis are based on the transmission of compressed wavelet-coded images. This is followed by a review of the basic principles of mobile communication systems in general and the key signal processing functions of wireless transmission systems for digital communications. Finally, a description of the signal processing techniques and channel modelling used throughout the thesis such as, transmit diversity coding, antenna beamforming (eigenbeamforming), and a geometrical space-time channel model known as GBHDS (geometrical-based with hyperbolically distributed scatterers), are also detailed and presented in this chapter.

Chapter 3:Multimedia Communication over Space-Time Beamformed OFDM. Research studies have shown that transmit diversity and antenna beamforming techniques are highly effective in improving the performance and capacity of wireless systems utilizing OFDM. This chapter introduces a multimedia communication system employing a transmit diversity coding technique known as, space-time block coding (STBC), and an adaptive beamforming (AB) strategy. These techniques are integrated with an OFDM transmission system such that the diversity gain offered by STBC is maintained and the received SNR is maximised, while AB (eigenbeamforming) - adaptive antenna weighting scheme - provides a mechanism for mitigating the fast fading and multi-path effects of mobile channels. Simulation results, based on the transmission of compressed digital images over a geometrical space-time channel model called GBHDS (geometrical-based with hyperbolically distributed scatterers), showed that the performance improvement introduced by STBC-OFDM with adaptive beamforming are significant and can be readily observed even without extensive numerical analysis as traditionally expected.

Chapter 4: Integrated Source and Diversity Coding for Multimedia Communication. In this chapter, we extend the work presented in Chapter 3 by combining the STBC-OFDM-AB transmission system for multimedia communication with a perceptually-based compression coder, which consists of a 2-D discrete wavelet transform (DWT) based on biorthogonal wavelets,

an adaptive quantizer (with thresholding) and variable-length entropy encoding. This system is later adapted to include a space-time-frequency coder (STF-OFDM-AB) such that we exploit the additional diversity branches in the frequency domain of OFDM systems. As expected, simulation results based on the transmission of compressed images over a GBHDS space-time channel model, showed that the performance improvement introduced by both STBC-OFDM-AB & STF-OFDM-AB can be readily observed from inspecting the perceived quality of the reconstructed images and by using an objective measure or fidelity criteria known as the peak signal-to-noise ratio (PSNR). When compared to other transmission methods, STBC-OFDM-AB & STF-OFDM-AB, prove to be well suited to mobile multimedia communication.

Chapter 5: An Optimised Transmission Technique for Mobile Multimedia. This chapter proposes an optimum transceiver structure for a combined source-modulation coded MIMO-OFDM system with STBC and adaptive eigenbeamforming for mobile multimedia systems. Using an unequal adaptive modulator based on a lookup matrix-adaptive bit and power allocation (LM-ABPA) scheme, the channel-to-noise ratio (CNR), and more importantly, the data transfer rate is maximised by sorting and allocating subcarriers with the highest SNR to the low-frequency components of compressed data, which are more sensitive to the time-varying nature of wireless channels and propagation environments. With knowledge of the channel fading conditions, a loading algorithm is used to adaptively assign OFDM subcarriers with the appropriate baseband signal constellation size and required power such that a target error-rate constraint is achieved for the whole system. The same channel information is used to determine the optimal number of orthogonal output beams for each subcarrier and a STBC encoding matrix with the same spatial dimension such that maximum diversity is satisfied. In comparison to other transmission systems, simulation results based on the application of compressed images showed that the proposed unequal adaptive modulation scheme achieves significant performance gains under a constant data rate load.

Chapter 6: Application of a Blind Equalization Technique for Wireless Multimedia. In this chapter, we apply the multimedia simulation framework developed in the previous chapters to consider the implementation of a blind channel equalisation technique known as, sinusoidally-distributed dithered signed-error constant modulus algorithm (S-DSE-CMA), to deal with the effects of intersymbol interference (ISI) in mobile/wireless channels. In this work, the proposed S-DSE-CMA scheme is evaluated in the application of digital still images. Simulation results showed that the low computational complexity and the fast convergence rate of

the algorithm are the major advantages for employing this technique to support the transmission of multimedia data. Perceptual-based analysis as well as objective measurements obtained by evaluating the peak signal-to-noise ratio (PSNR) of the recovered images, showed that the proposed blind adaptive equalisation algorithm outperforms other DSE-CMA schemes.

Chapter 7: Chaos for Secure Multimedia Communication. In this chapter, the multimedia framework developed in the previous chapters is applied to study the performance of a secure communication system using Chaos Shift Keying (CSK). A comparison of two common chaotic logistic maps and a modified chaotic logistic map is provided. The newly modified logistic map provides similar bit error-rate (BER) performance to the best logistic map, but, it also provides an additional security parameter for the control of its bifurcation property. Simulation results, based on the transmission of digital still images, showed that the performance improvement in security introduced by the bifurcation behavior of a chaotic generator can be readily observed from analysis of the perceived quality of the reconstructed images and the PSNR objective measure.

Chapter 8: Conclusions and Future Directions. This chapter summarises the main findings of this dissertation and discusses some of the challenges for future research work.

Chapter 2

Overview of Multimedia & Mobile Communication Systems

2.1 Introduction

Multimedia is one of the most exciting developments in the field of mobile communications, and over the past decade, has greatly impacted on the way people make use of and share information. Today, it is not unusual to find users of these technologies communicating and accessing a diverse range of information or media such as, text, audio, image, and video - hence, the term *multimedia*. To adequately support the applications that are based on this type of information in mobile communication systems (e.g. audio and video streaming), a process for reducing the amount of data needed for its representation with an acceptable subjective quality is crucial in maintaining the bandwidth requirements for transmission over mobile radio links . This is generally achieved by reducing the statistical or temporal redundancy present in multimedia data using modern compression techniques such as wavelet-based coding. Data compression has, thus, become an important consideration for the realisation of broadband mobile multimedia applications.

Mobile networks, on the other hand, introduce complexities not found in wireline or fixed wireless communication systems. Apart from developing techniques to mitigate the effects of noise and interference from other signal sources, one the main areas of concern is the impact the mobile environment has on signal propagation, especially, the interaction of radio signals with physical objects (mountains, buildings, trees, etc) along the propagating path. There are several causes of degradation in the quality of the signal transmitted over wireless/mobile channels, but can be generally characterised by the complex fading effects resulting from changes in the transmission medium or introduced by the movement of a mobile antenna. It has been well established in wireless communications literature that, the channel conditions in a mobile environment are time-varying, dynamic, and unpredictable [21,57,58]. We also recall from Chapter 1,

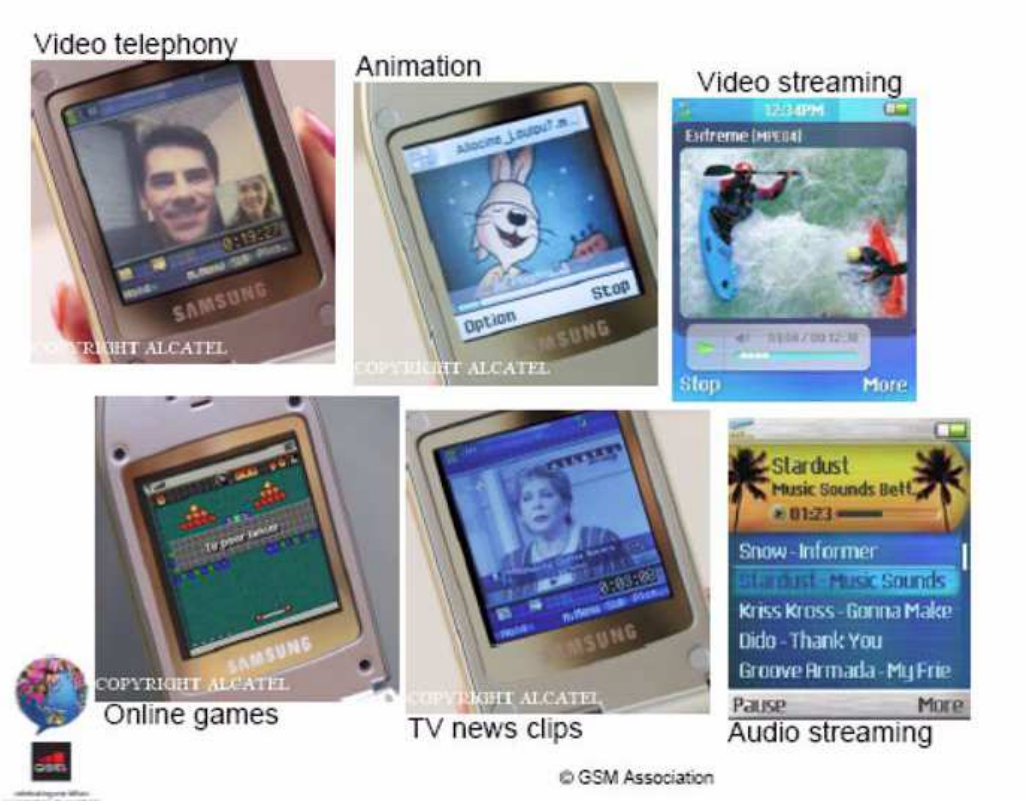

Figure 2.1: Examples of multimedia applications in 3G mobile communication systems.

that various digital communication or signal-processing techniques have been developed to overcome the effects of multipath fading (e.g. adaptive modulation, channel coding, etc). The most important breakthroughs, however, have come from the recent advent of antenna-array systems and transmit diversity techniques such as, antenna beamforming and space-time coding.

In this chapter, we review the basic concepts of data compression in terms of image coding, as the application of digital still images is used to form the basis of the simulation work presented in this thesis. Key implementation issues for mobile communication systems are also presented in this chapter, which includes a description of the propagation effects of mobile radio channels and an introduction into some of the current transmit diversity techniques employed in multi-antenna mobile transmission systems.

The organisation of this chapter is, therefore, as follows: a brief review of the image model and sampling technique used in the acquisition of multimedia data is given in section 2.2. In section 2.2.2, some of the basic concepts in image compression techniques is presented. The theory surrounding wavelet-based coding for image compression is also detailed in 2.2.3. Sections 2.2.4 and 2.2.5, look at the performance metrics and some of the standard test images used in evaluating the quality or fidelity of compressed images. A review of the important elements in mobile communication systems including the key signal-processing functions is then presented in

section 2.3. In particular, Section 2.3.2 provides a description of the various multipath propagation effects experienced in a mobile environment. Finally, details of the GHBDS channel model and a review of the transmit diversity techniques used in this thesis are presented in Sections 2.3.3 and 2.3.4, respectively. The chapter is then concluded with a summary in Section 2.4.

2.2 Multimedia Signals: Processing & Compression

In the context of mobile multimedia, there are different multimedia applications used to convey a multitude of information to the end user, that is, on mobile devices such as video-capable cell phones, wireless-enabled portable computers & PDA's (Portable Digital Assistants), etc. Figure 2.1, shows a typical range of multimedia data that a mobile phone subscriber could realistically access from today's 3G networks. The technologies which enable the development of these applications, rely on the generation, acquisition, compression, and storage of the different types of media readily available on current personal computing platforms; the most popular being audio, images, and video. Generally, multimedia systems support the use of both continuous (time-dependant) data such as, digital audio and video, or discrete (time-independent) media such as, text and digital images. Examples of multimedia systems in mobile communications, include the transmission of text documents, email, and streaming audio and video data. In order to understand the processes involved in the digitization of multimedia data the following sections will briefly examine the sampling and coding theory for image compression.

2.2.1 Multimedia Data Acquisition

To make use of multimedia data we need to be able to generate and process multimedia signals, which are generally *analogue* in nature. A variety of sources such as, microphones and cameras, are required to produce continuous-time analogue signals that can be sampled and digitized. Figure 2.2, shows the process of converting an image to a discrete form that can be further processed and stored by a digital camera (adopted from the Computer Desktop Encyclopedia, ©1998 The computer Language Co. Inc.). The main elements required for the digitisation of images are: an analog-to-digital converter (ADC) to convert the varying voltage levels from the CCD sensor into samples of discrete binary form, and a digital signal processor (DSP) to provide advanced filtering functions (anti-aliasing, etc) while formatting the sample sequences into a structured bitstream that can be further processed (compressed, stored, etc). In image processing, the number of bits (e.g. 8 or 24, 32 bits) that each sample or pixel (from a CCD

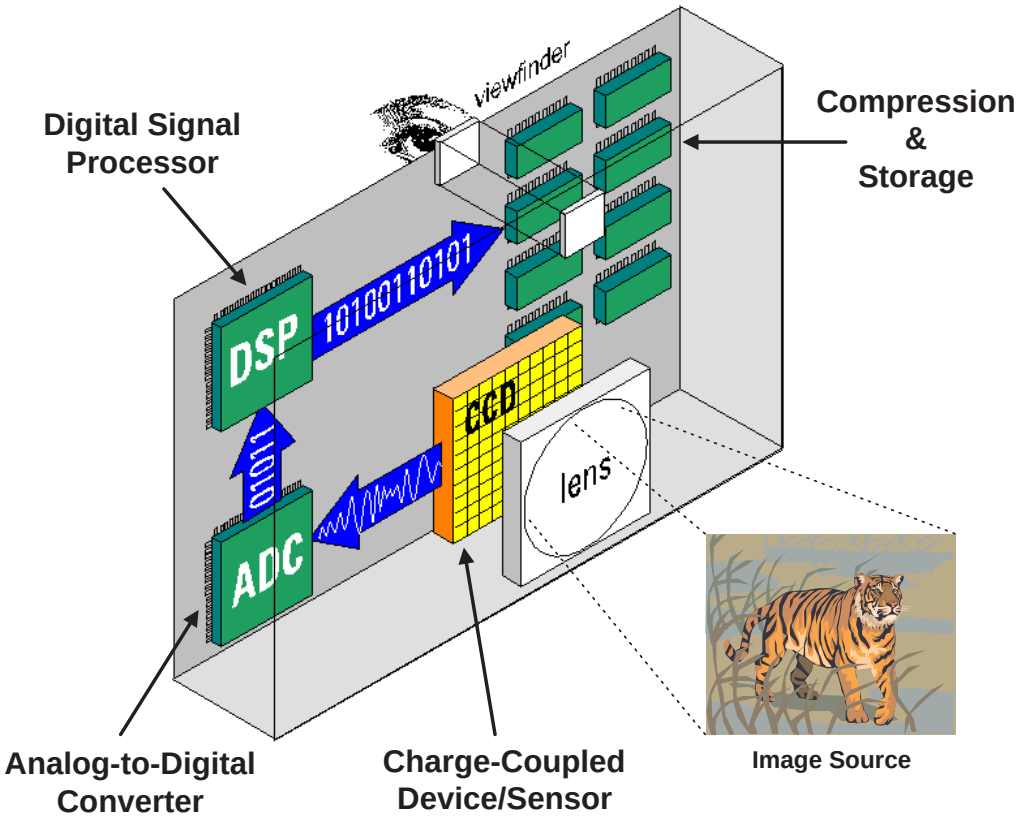

Figure 2.2: The digitization and processing of still images.

sensor) can be represented with finite precision is generally used to denote the resolution or quality of a digital image (bits/pixel). Similar inferences can also be made for digital audio and video.

The properties of the human visual system (HVS) can also be used to control the quality of digital images [59, 60]. For example, a gray level image can digitized with excellent quality with 8-bit resolution, which corresponds to 2^8 or 256 levels of gray. This is more than what the human eye can differentiate. Colour images are commonly digitized using a separate component to represent different levels of Red, Green, and Blue - {R,G,B} colour system. In modern cameras, individual sensors (channels) are employed to convert colour pixels with the desired resolution. An 8-bit/channel/pixel sensor can deliver a total of $2^8 \times 3$ bits for each colour pixel. This corresponds to 2^{24} or 16 million colours, which again, is more than what the human eye can differentiate. Therefore, most modern electronic devices are designed to produce digital image data with a lower resolution (e.g., 8-bit or 16-bit displays). The following sections will now present the mathematical models used in image processing.

A Simple Image Model

An image can be simply defined as a two-dimensional light intensity function $i(x, y, t)$ [28, 61], where the intensity (brightness) of the image is given by the amplitude of the function at a spatial coordinate (x, y) for a particular point in time t. It can also be represented as a function of two components: i) the amount of source light incident on the scene and ii) the amount of light reflected by the objects in the scene. These are referred to as the *illumination* component, $l(x, y, t)$ and *reflectance* component, $r(x, y, t)$, respectively. Thus, the image model can be described as follows:

$$i(x, y, t) = l(x, y, t)r(x, y, t) \tag{2.1}$$

where $0 < l(x, y, t) < \infty$ and $0 < r(x, y, t) < 1$. The image model represented by the function in Eq. (2.1) is also known as the coefficient model [61], where the image intensity function is directly proportional to the illumination component. We note that, images can be processed as either monochrome or color. A monochrome image is generally represented in terms of the instantaneous luminance of the light field defined by $i(x, y, t)$, while a color image is represented in terms of a set of tristimulus values that are linearly proportional to the amounts of red $(R(x, y, t))$, green $(G(x, y, t))$, and blue $(B(x, y, t))$ light. For digital images and video, x and y take on discrete values, which represent the pixel information acquired from the digitization process described in the previous section. In the case of digital images the model represents an image at a specific value of t, while for video it consists of a sequence of images ordered in time.

Sampling of Two-Dimensional images

Let an image captured by a device such as, the CCD sensor in a digital camera, be expressed using the continuous-time function $i(x, y, t)$ defined in Eq. (2.1). As the image is digitized for a specific value of t, this model can be reduced to $i(x, y)$, where x and y are the two spatial dimensions. Thus, the 2-D Fourier transform of the image can be expressed as

$$I(\omega_h, \omega_v) = \int_{-\infty}^{\infty} \int_{-\infty}^{\infty} i(x, y) e^{-j(\omega_h x + \omega_v y)} \, \mathrm{d}x \, \mathrm{d}y \tag{2.2}$$

where ω_h and ω_v are the horizontal and vertical spatial frequencies (expressed in *radian/degree*), respectively. The horizontal and vertical frequencies, f_h and f_v, in the 'frequency' domain are subsequently defined by $f_h = 1/2\pi\omega_h$ and $f_v = 1/2\pi\omega_v$. Let the image be considered bandlimited, and the maximum horizontal and vertical frequencies be denoted by f_H and f_V.

Now, assume that the digitization process samples and converts the image function $i(x, y)$

into a matrix with M rows and N columns by assigning (quantizing) each continuous sample with a discrete integer value. Also, consider the image function $i(x, y)$ to be a continuous range of samples split into K intervals. The finer the sampling (i.e., the larger M and N) and quantization (the larger K) the better the approximation obtained. If we let the continuous image function $i(x, y)$ be sampled using a discrete grid of sampling points, $x = m\Delta x$ and $y = n\Delta y$, the discrete image can be described as

$$\begin{aligned} i_s(x,y) &= i(x,y)s(x,y) \\ &= \sum_{m=1}^{M}\sum_{n=1}^{N} i(x,y)\delta(x - m\Delta x,\, y - n\Delta y) \\ &= i(m\Delta x, n\Delta y)\sum_{m=1}^{M}\sum_{n=1}^{N}\delta(x - m\Delta x,\, y - n\Delta y) \end{aligned} \tag{2.3}$$

where $s(x, y)$ is the 2-D sampling function defined by

$$s(x,y) = \sum_{m=1}^{M}\sum_{n=1}^{N}\delta(x - m\Delta x,\, y - n\Delta y) \tag{2.4}$$

and, Δx and Δy, are the spatial-sampling intervals with the sampling frequencies in the horizontal and vertical directions given by $1/\Delta x$ and $1/\Delta y$ (in *samples/degree*), respectively. Applying the Nyquist−Shannon sampling theorem [62, 63] to two-dimensions, it can be shown that the image $i(x, y)$ can be reproduced precisely if the following conditions are satisfied:

$$\frac{1}{\Delta x} \geq 2f_H \qquad \text{and} \qquad \frac{1}{\Delta y} \geq 2f_V \tag{2.5}$$

Note, that the periodic repetition of the Fourier transform in Eq. (2.2) may under certain conditions cause distortion of the image which is commonly referred to as *aliasing*. This occurs when individual digitized components of $I(\omega_h, \omega_v)$ overlap. If the image function $i(x, y)$ has a bandlimited spectrum then the Fourier transform $I(\omega_h, \omega_v) = 0$ outside a certain interval of frequencies, that is for $|f_h| > f_H$ and $|f_v| > f_V$. According to general sampling theory [62, 63], that the overlapping of the periodically repeated results of $I(\omega_h, \omega_v)$ can be prevented if the sampling interval is chosen according to Eq. (2.5). Thus, the sampling interval should be chosen in size such that it is less than or equal to half of the smallest detail required in the image. In practise, however, the sampling function is not the Dirac distribution in real digitizers; synthesised narrow impulses with limited amplitude are used instead. In real image digitizers a sampling interval about ten times smaller than that indicated by the Shannon sampling theorem

is used, as the algorithms used for image reconstruction are based on a step function.

2.2.2 Fundamentals of Image Compression

The amount of data (bits) required to represent a digital image resulting from the sampling process can be quite significant and generally require large storage systems. However, most of the information is highly redundant and can therefore be compressed (reduced) to a more manageable form. In terms of image compression, this is achieved by removing various redundancies present in the 2-D structure of images so that it can be reproduced with an acceptable degree of goodness, whether being subjective or perceived. Superior compression is therefore obtainable by exploiting the statistical, spatial, structural redundancies [26, 28]. A description of each type is provided in the following.

Statistical redundancy: Refers to the non-uniform probabilities of the occurrences of the different pixel values. The pixel values that occur more frequently should be given a smaller number of bits than the less probable values.

Spatial redundancy: Refers to the correlation between neighboring pixels in an image. This intra-image or intra-frame redundancy is typically removed by employing compression techniques such as predictive coding, and transform coding.

Structural redundancy: We note that an image is originally a projection of 3-D objects onto a 2-D plane. Therefore, if the image is encoded using structural image models that take into account the 3-D properties of the scene, a high compression ratio can be achieved. For example, a segmentation coding approach that considers an image as an assembly of many regions and encodes the contour and texture of each region separately, can efficiently exploit the structural redundancy in an image.

In addition to the above, psychovisual redundancies or the properties of the human visual system (HVS) [64] can also be exploited to achieve high compression ratios and improve the overall subjective quality of a sampled digital image [65, 66]. The typical HVS properties that are useful in image compression include:

1. Greater sensitivity to distortion in dark areas in images.
2. Greater sensitivity to distortion in smooth areas compared to areas with sharp changes (i.e., areas with higher spatial frequencies).
3. Greater sensitivity to signal changes in the luminance component compared to the chrominance component in color images.

The compression techniques that are based on removing these types of redundancies in im-

age compression are generally classed into two categories, i.e., *lossless* techniques and *lossy* techniques. With lossless compression, the reconstructed image is identical to the original image, and hence no distortion is introduced (the image is perfectly recovered). Applications that might typically require this type of compression technique include, medical and satellite imaging. Lossless compression techniques, however, encode images with a very low compression rate and thus have a greater storage requirement. These techniques are generally based on entropy and run-length coding. Lossy compression, on the other hand, such as predictive coding, transform coding, and vector quantization, generally encode images with a high compression ratio, but, at the expense of subjective quality (distortion or noise). Therefore, there is a trade-off between a reduction in the amount of overall data obtained from the compression process and the sacrifice to fidelity. The areas where lossy compression techniques are considered acceptable are the Web-based applications found on the Internet, and the multimedia applications developed for wireless/mobile communication systems. The following section will now explore some of the popular lossless and lossy compression techniques that exist for image processing.

Image Coding Techniques

Over the past few years, there have been a number of lossless and lossy compression techniques that have been developed. In general, there are four main directions established in image compression: entropy coding, predictive coding, vector quantization, and transform coding. These coding methods are briefly described below - for further details the reader is referred to [22,26,29].

Entropy Coding

Entropy coding relies on an uneven distribution of values to be encoded to achieve compression, that is, the non-uniform probability density function (*pdf*) is exploited to remove the statistical redundancy of a given source. For example, it is well known that the pixel values for an image to do not have a uniform *pdf*. The entropy of the image can, therefore, be calculated and a suitable encoder can then be designed with a coding rate or bit−rate (bits/pixel) to match the entropy of the original image source. The compression ratio using this method is in most cases negligible (1:1). Entropy coding is, however, generally used to encode the transform coefficients of an image and is not directly applied to the sampled pixels. Two popular encoding schemes, are *Huffman* coding and *arithmetic* coding [26, 29].

Predictive Coding

Predictive coding works on the basis that adjacent pixels in an image are very similar, and thus the redundancy between successive pixels can be removed and only the the residual between the

actual and predicted pixel values are encoded. For example, an image having a constant gray level can be fully predicted from the gray level value of its first pixel. In images with multiple gray levels, the gray level of an image pixel can be predicted with high accuracy from the values of its neighboring pixels. The prediction error is then encoded instead of the original pixels, and thus, a high compression ratio is achieved. Differential pulse code modulation (DPCM) is the basic compression scheme used in predictive coding techniques.

Vector Quantization

Unlike entropy coding, vector quantization (VQ) achieves compression by reducing the spatial redundancy of a given source. A set of reproduction vectors (code−words) called a VQ codebook or VQ table containing code−words is used to achieve compression. The principal idea behind VQ, is that both the encoder and decoder have an identical copy of the codebook with each codeword made up of the same number of sampled pixel. Representative pixel blocks are chosen from the source to be compressed such that each data vector is matched with or approximated by a codeword in the codebook, and is labelled with an address or index of that codeword. It is these indices that are transmitted through a communication channel instead of the data vector itself. At the receiving end or decoder, the index is mapped back to the codeword (by matching it to an entry in the codebook) corresponding to the sampled pixel block used to represent the original data vector. One of the advantages of this technique is that only table lookups are required at the decoder. A major drawback of vector quantization, however, is that it is highly image-dependent and its computational complexity grows exponentially with the vector dimension. In addition, it is difficult to design a good codebook that is representative of all the possible occurrences of pixel combinations in a block.

Transform Coding

Transform coding achieves compression by converting the source data into a small number of coefficients. Although a wide variety of transforms have been proposed the most popular for representing signals are unitary transforms due to their orthogonality, energy conservation and compaction property. Unitary transforms are used to convert data from the spatial domain to an alternate domain, which can then be encoding further by use of a scalar or vector quantization technique. Higher compression ratios can then be achieved by passing the quantized data through an entropy coder.

The unitary transform is a reversible linear transform whose kernel describes a set of complete orthonormal basis functions. The objective of transform coding is to decorrelate the original signal and to repack the energy into fewer coefficients. In the case of a two dimensional image a 2−D unitary transform is required. Assuming an image sampled with a matrix dimension $N \times N$

is denoted by $I = [i(m,n)]$ the forward and inverse transforms are defined as

$$\theta(k,l) = \sum_{m=0}^{N-1}\sum_{n=0}^{N-1} \omega(k,l;m,n)i(m,n) \qquad 0 \leq k,l \leq N-1 \tag{2.6}$$

$$i(m,n) = \sum_{k=0}^{N-1}\sum_{l=0}^{N-1} v(m,n;k,l)\theta(k,l) \qquad 0 \leq m,n \leq N-1 \tag{2.7}$$

where $\omega(.)$ and $v(.)$ are the forward and inverse transform kernels. Orthonormal transforms such as the $2-$D unitary transform exhibit important properties which are very well suited to image coding applications. These include the following:

- **Energy Conservation:** $2-$D unitary transforms satisfy Parseval's relation i.e.the total energy in the frequency domain is equal to that of the spatial domain defined by

$$\sum_{m=0}^{N-1}\sum_{n=0}^{N-1} \Big|i(m,n)\Big|^2 = \sum_{k=0}^{N-1}\sum_{l=0}^{N-1} \Big|\theta(k,l)\Big|^2 \qquad \text{, i.e., } \Big\|I\Big\|^2 = \Big\|\Theta\Big\|^2 \tag{2.8}$$

  The unitary transform, thus, preserves the signal energy or alternatively the length of the vector I in the N^2 dimensional vector space.

- **Sum of Squared Error:** Assume that the transform coefficients for an image change from $\theta(k,l)$ to $\hat{\theta}(k,l)$ due to an error introduced during data compression or errors caused by the transmission of data through a communication channel. The reconstructed image $\hat{i}(m,n)$ will be different from the original image $i(m,n)$. It can be shown that the total squared error between the original and the reconstructed image is equal to the total squared error between the original coefficients and the coefficients in error, and can be expressed mathematically as follows

$$\sum_{m=0}^{N-1}\sum_{n=0}^{N-1} \Big|i(m,n) - \hat{i}(m,n)\Big|^2 = \sum_{k=0}^{N-1}\sum_{l=0}^{N-1} \Big|\theta(k,l) - \hat{\theta}(k,l)\Big|^2 \tag{2.9}$$

  The same holds true for the mean square error, whereby, the mean square reconstruction error in the spatial domain is equal to the mean square quantization error in in the frequency domain.

- **Separable Basis:** The $2-$D kernels are separable and symmetric and can be expressed as the product of the two $1-$D orthogonal basis functions. If we denote the $1-$D transform

operator by Φ, then the forward and reverse transformations can be expressed as

$$\Theta = \Phi^* I \Phi^T \tag{2.10}$$

$$I = \Phi^T \Theta \Phi^* \tag{2.11}$$

Hence, the transformation can be done in two stages: i) by taking the unitary transform (1−D) of each row of the image array and then ii) taking the transform of each column of the intermediate result [26].

In the case of image compression, the transformation of generally results in a set of coefficients that are nonstationary, and is statistically optimal if it satisfies the following two criteria: (i) Correlation among the coefficients should not exist i.e., the autocorrelation matrix should be diagonal, and (ii) it should pack the energy in as few coefficients as possible. The unitary transform that satisfies both criteria is the Karhunen-Loeve transform (KLT) [28]. However, KLT is image dependent and has a higher computational complexity. Therefore, image independent sub-optimal transforms such as *discrete cosine transform* (DCT) and *wavelet transform* are used in practice, as their rate-distortion performance is closest to KLT [28]. Hence, DCT and wavelet-based coding have been adopted as the compression technique in image and video coding standards such as, JPEG, JPEG2000 [67], MPEG, H.261, and H.263 [29, 68].

2.2.3 Image Compression Using Wavelets

The wavelet transform (also known as subband coding) has emerged as one of the most popular tools in the field of image processing [69–77]. In particular, the discrete wavelet transform (DWT) has been adopted as a standard tool in image compression applications due to their superior data reduction capability. The basic principle behind the wavelet transform, is the representation of any arbitrary function as a superposition of a set of 'wavelets' or basis functions (defined recursively from a set of scaling coefficients and scaling functions), which are obtained by scaling and shifting from the mother wavelet. Compared to other coding techniques, wavelet-based image compression is more robust to transmission and decoding errors and can facilitate the progressive transmission of images. They are inherently multiresolution in nature and importantly are suitable to applications where scalability and tolerable degradation are an important system requirement.

Specifically, the DWT offers a number of performance enhancements over traditional Fourier-based techniques such as the DCT. In wavelet-based image coding compression, the entire image

is transformed and compressed as a single data object rather than the block-by-block process used by the DCT techniques. It allows for a uniform distribution of compression errors across the entire image and it can provide better image quality than DCT-based coding, particularly, at higher compression ratios [78]. Other reasons for using wavelet-based techniques include: (i) wavelets in general are efficient in representing nonstationary signals because of the adaptive time-frequency window, (ii) they have high decorrelation and energy compaction efficiency, (iii) blocking artifacts and mosquito noise inherent in DCT-based compression systems are reduced in wavelet-based video coder, and finally, the wavelet multiresolution and direction selective decomposition of images (the wavelet basis functions) offer adaptive spatial−frequency resolution that match and are well suited to the properties of the human visual system [64, 79], resulting in a superior image representation [80].

In addition to the above advantages, the DWT has a direct relation to multiresolution (MR) analysis. MR analysis represents image and video in a scale-space framework where coarse features are large-scale objects and fine-scale features are studied much more locally. It has been shown that wavelets with reasonable time-frequency localization necessarily stem from multiresolution analysis. The multiresolution scheme successfully addresses the following [28]:

- Signal decomposition for coding.
- Scalable image and video compression.
- Representation well suited for fast random access in digital storage devices.
- Robustness and error recovery.
- Suitable signal representation for joint source/channel coding.
- Compatibility with lower resolution representations.

Wavelet Transform

The mathematical treatment of wavelets has been well established [81–87]. Wavelet transformation is a special case of subband decomposition, which is defined as follows. Let $L^2(R)$ denote the vector space of a measurable, square integrable one−dimensional function (that is, the space of square summable functions). If a function say $f(t)$ is an element of $L^2(R)$ then the continuous wavelet transform (CWT) can be obtained by the following:

$$CWT_f(a,b) = \int_{-\infty}^{+\infty} f(t)\Psi^*_{a,b}(t)\,\mathrm{d}t \tag{2.12}$$

where the wavelet basis functions $\Psi_{a,b}(t) \in L^2(R)$ can be expressed as

$$\Psi_{a,b}(t) = a^{-1/2}\Psi\Big(\frac{t-b}{a}\Big) \qquad a \in R^+, b \in R \tag{2.13}$$

These basis functions are what are known as 'wavelets' and can be viewed as dilated and translated versions of the mother wavelet $\Psi(t)$, and have at least one vanishing moment. The arguments a and b denote the *scale* and *location* parameters, respectively. The argument a represents the oscillation in the basis functions, which rapidly increase when a is small in value. The factor $a^{-1/2}$ in Eq. 2.13 maintains the norm of the wavelet function in different scales. The wavelet transform defined Eq. 2.12 represents a function of one variable using functions of two continuous variables a and b. Thus, the transform is highly redundant since a function of one variable t is represented as a function of the two variables a and b. This redundancy, however, is not desirable in image compression applications, as there is no unique way of reconstructing the original signal. The redundancy can be removed by sampling (discretizing) the parameters a and b in the following way [27]:

$$a = a_0^j, \quad b = kb_0a_0^j \qquad j, k \in Z,\ a_0 > 1,\ b_0 \neq 0 \tag{2.14}$$

where Z is the space of integer numbers and b_0 is any real number. In general, however, b_0 is chosen as $b_0 = 1$. The basis function defined in Eq. 2.13 can now be expressed as

$$\Psi_{j,k}(t) = a_0^{-j/2}\Psi(a_0^{-j}t - k) \tag{2.15}$$

Thus, the discretized or sampled form of the CWT in Eq. 2.12 can now be written as

$$CWT_f(j,k) = \int_{-\infty}^{+\infty} a_0^{-j/2}\Psi(a_0^{-j}t - k)f(t)\,\mathrm{d}t \tag{2.16}$$

Although the parameters a and b are discrete in nature, the transform still operates on continuous signals. Orthonormal basis functions can be obtained by carefully choosing a and b. In many applications such as image processing, it is necessary to partition the frequency axis into disjoint frequency bands with little overlap. Therefore, the simplest way to do this is use a binary partition where a_0 is chosen to be equal to 2. When $a_0 = 2$ the transformation is known as *dyadic* wavelet transform.

2−D Discrete Wavelet Transform

In practice, the wavelet transform is applied on discrete data. Thus, one is interested in the discrete versions of the wavelet transform. Image processing applications such as, image compression, require a two-dimensional (2−D) discrete wavelet transform (DWT) for decomposition and reconstruction of image data. Unfortunately, there is no discrete basis function whose translated and dilated versions form a base of $L^2(R)$. Therefore, the wavelet functions for 2−D DWT

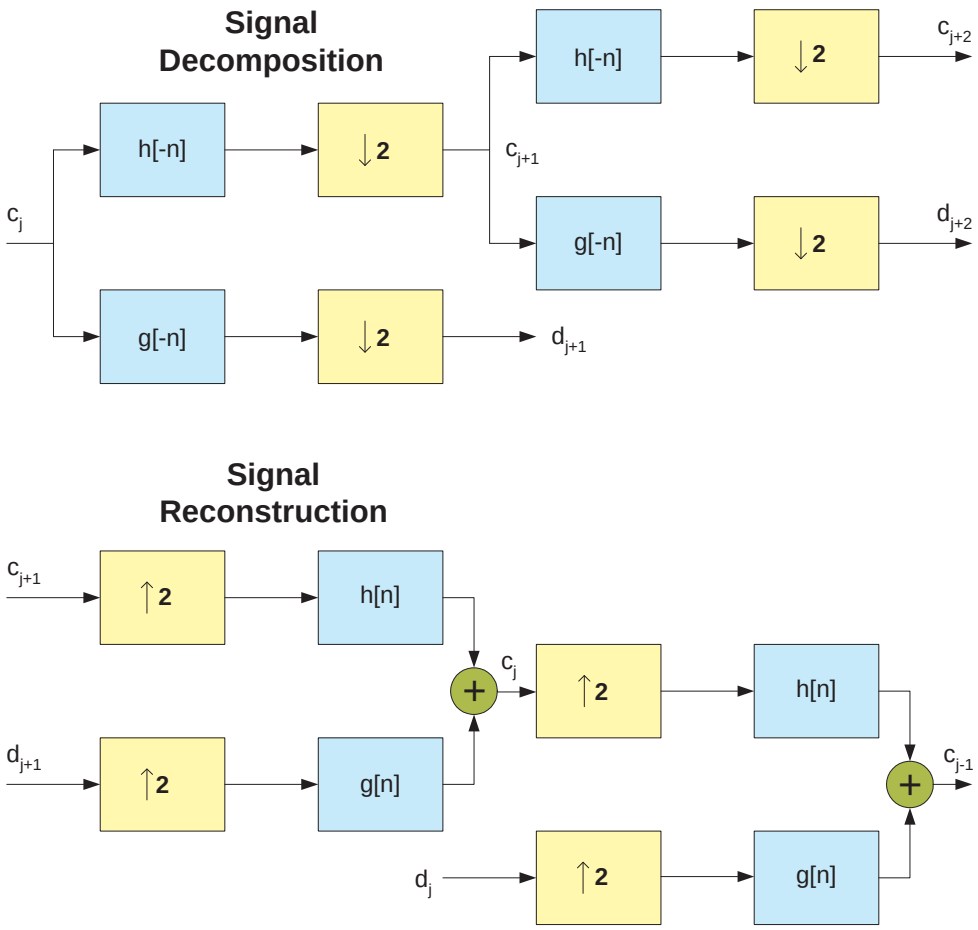

Figure 2.3: 1−D wavelet decomposition using Mallat's tree algorithm.

can be obtained by multiplying two wavelet functions or wavelet and scaling functions used in 1−D analysis. In the case of 1−D decomposition and reconstruction, various approaches such as *Mallat's tree algorithm* have been implemented. Wavelet transformation of a 1−D signal using Mallat's tree algorithm is achieved by passing it through a low-pass filter (LPF) or analysis filter and a high-pass filter (HPF) or synthesis filter, and by decimating the output of the filter by a factor of two. This process is shown in Figure 2.3 [28]. Mathematically, this can be expressed as [28]:

$$c_{j+1,k} = \sum_m c_{j,m} h[m - 2k] \tag{2.17}$$

$$d_{j+1,k} = \sum_m c_{j,m} g[m - 2k] \tag{2.18}$$

where $c_{p,q}$ is the lowpass (or, scaling) coefficient of p th scale at q th location and $d_{p,q}$ is the highpass (or, wavelet) coefficient of p th scale at q th location. The LPF and HPF coefficients corresponding to the mother wavelet are given by $h[.]$ and $g[.]$, respectively. Reconstruction of the original fine scale (detail) coefficients can be extracted from the coarser (approximation)

coefficients, as shown in Figure 2.3. Mathematically this process can be described as follows [28]:

$$c_{j,m} = \sum_{k} c_{j+1,k} h[m-2k] + \sum_{l} d_{j+1,l} g[m-2l] \tag{2.19}$$

Figure 2.3, clearly shows that each level of decomposition produces two bands corresponding to low and high-resolution data. For 2−D transformation, the entire process is carried out by executing a 1−D decomposition twice; one in the 'horizontal' direction and another in the 'vertical' direction. That is, a 2−D separable orthonormal basis can be constructed by taking the tensor product $\bigotimes$ of two 1-D orthonormal wavelet bases. In this approach, three 2−D wavelet basis functions can be obtained from their 1−D counterpart, as follows:

$$\Psi^h(x,y) = \phi(x)\psi(y) \qquad \Psi^v(x,y) = \psi(x)\phi(y) \qquad \Psi^d(x,y) = \psi(x)\psi(y) \tag{2.20}$$

where h, v, d represent the horizontal, vertical, and diagonal component. In the case of image processing, the filtering is performed on the "rows" and "columns" of the two-dimensional image array, which directly correspond to horizontal and vertical directions of the image. Thus, four bands of data is produced; one corresponding to the scaling functions and three corresponding to horizontal, vertical and diagonal wavelets. For multi-level transformation, the low-pass subband (L_i) resulting from the horizontal direction is further decomposed in the vertical direction, creating two new subbands LL_i and LH_i, respectively. Similarly, the high-pass subband (H_i) is further decomposed into the subbands HL_i and HH_i. Where, LL_i is commonly referred to as the low-resolution subband and LH_i, HL_i, HH_i, represent the residual information of the original data set. The decomposition process is repeated iteratively on all the low-pass subbands until the desired level of decomposition is achieved. This results in multiple 'transform' levels.

Figure 2.4, shows an example of a 3−level wavelet decomposition using DWT for an image of size $m \times n$ pixels. In the first level of decomposition, the low-pass subimage/subband LL_1 and three orientation selective high-pass subimages (LH_1, HL_1, HH_1) are created. In second level of decomposition, the lowpass subimage LL_1 is further decomposed into one low-pass and three other high-pass subimages (LH_2, HL_2, HH_2, LL_2). This process is repeated for the low-pass subimage LL_2 to form the third-level transform. Overall, the 2−D DWT decomposes an image into subimages of various resolutions corresponding to the different scales. The inverse discrete wavelet transform (IDWT) is calculated in the reverse manner, i.e. by starting from the lowest resolution subimages and recursively calculating the higher resolution images. The calculation of both the DWT and the IDWT are performed by a series of matrix operations. In practise,

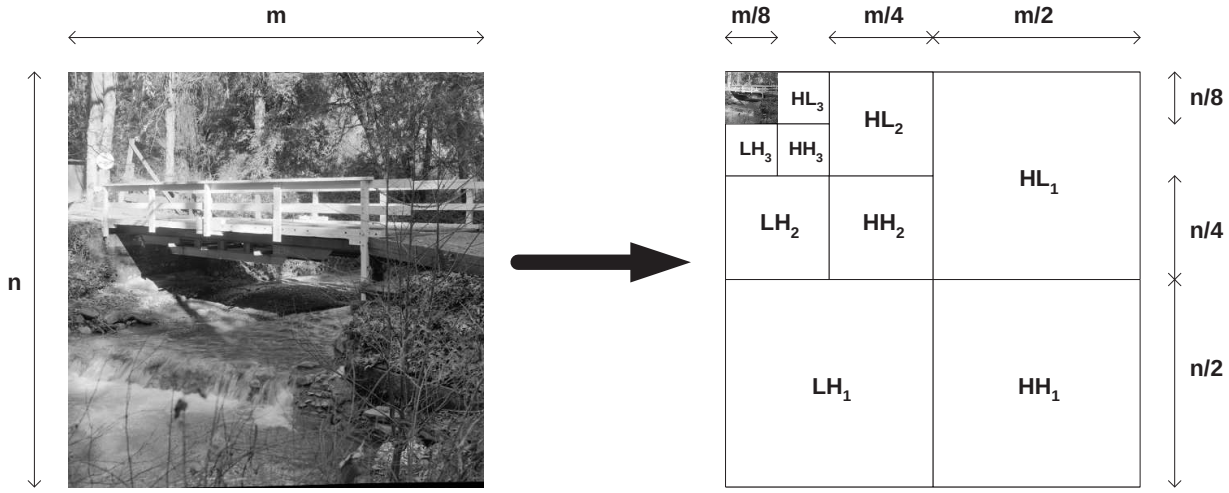

Figure 2.4: Wavelet (3-level) decomposition of a digital image.

however, this is implemented in hardware using a bank of digital filters.

Wavelet-Based Coding

To achieve a high compression ratio in a wavelet-based image compression system an efficient coding technique consisting of a combination of some important processing functions is often required. Figure 2.5 shows a simple coding scheme that demonstrates the main steps necessary in the compression process and is the technique adopted in this thesis. Apart from the application of the wavelet transform, the resulting coefficients are quantized and entropy encoded. In wavelet-based coding there are two quantization methods that can be used: (i) scalar quantization and (ii) vector quantization. Both approaches have their own advantages and disadvantages. It is well known, that a scaler quantizer exploits the fact that high frequency coefficients can be modelled fairly accurately with a generalized Gaussian distribution. On the other hand, it is well known that sharp edges are characterized by frequency components of all resolutions. Hence, there will be some residual correlation among coefficients of different scales. Vector quantizers exploit the correlation among coefficients of different scales resulting in a superior coding performance.

After each band is quantized with its corresponding quantization step size, the DWT coefficients are encoded using an entropy encoding technique such as, Huffman and arithmetic coding. Since, the statistics of different bands vary widely, the bands are generally encoded independently. The remaining nonstationarity within a band is easily handled by an adaptive model. Since adaptive coding is a memory process, the order in which the coefficients are fed into the coder is an important issue. The higher the local stationarity of coefficients the better is the adaptation. We note that various types of scanning, e.g. horizontal, zigzag, and Peano-Hilbert scanning, are employed in practice.

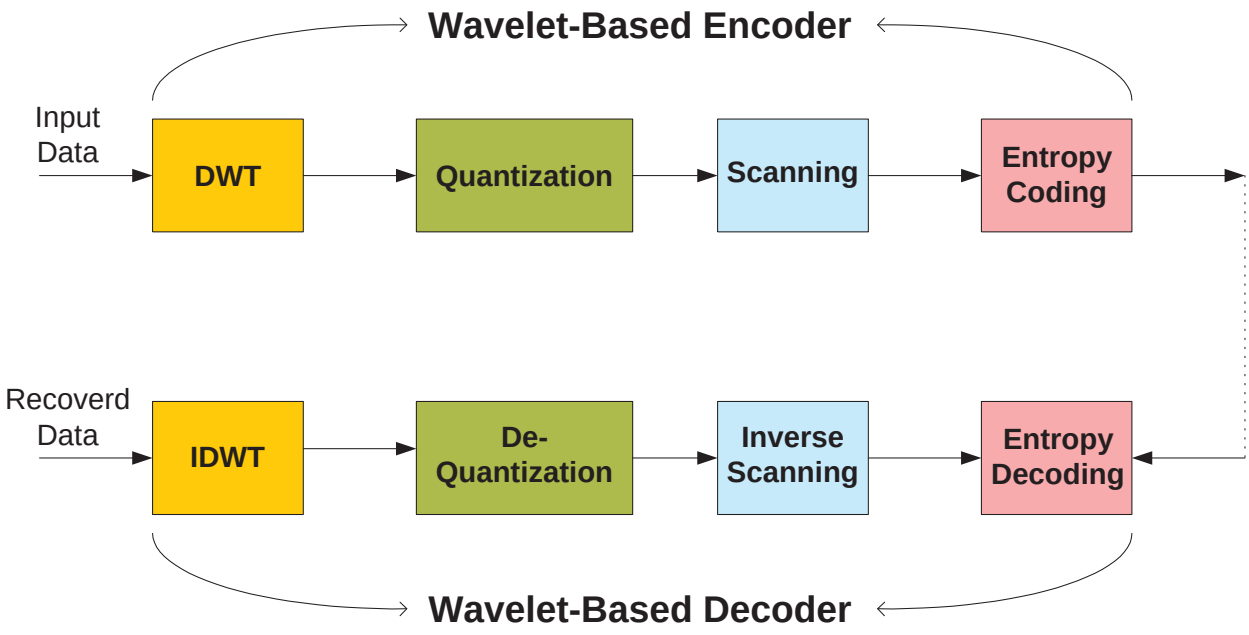

Figure 2.5: Example of a wavelet-based compression system.

The wavelet transform in Figure 2.5 is basically a 2-D orthogonal or bi-orthogonal transform. The decomposition may be dyadic (only the lowest scale is decomposed recursively), regular (full decomposition) or irregular in nature. In practise, the depth of tree is generally determined by the size of the image and the number of wavelet filter taps. With each decomposition, the number of rows and columns of the lowest passband is halved. For efficient decomposition, the number of rows and columns of the band to be decomposed should not be less than the number of filter taps.

2.2.4 Quality Measurement

In image coding/processing, the distortion introduced by the compression system (e.g. quantization of pixel values) is traditionally evaluated using two types of fidelity measures: subjective and objective assessment [22, 26, 29]. The choice of the distortion measurement technique, to assess the visual quality of compressed images, depends on various factors: (i) it should be easily computable, (ii) it should be analytically tractable, and (iii), it should adapt to the human visual system characteristics. As subjective measurement techniques requires extensive visual testing with real subjects (which can be a tedious process), the most widely used distortion measure used in practise is the objective measure known as the Peak Signal-to-Noise Ratio (PSNR),

which is defined as:

$$PSNR(dB) = 10 \log_{10} \left[\frac{(A_{MAX})^2}{MSE} \right] \tag{2.21}$$

and,

$$MSE = \frac{1}{M\,N} \sum_{m=0}^{M-1} \sum_{n=0}^{N-1} \left[x\,(m,n) - y\,(m,n) \right]^2 \tag{2.22}$$

where MSE is the Mean Square Error of the pixel values (pixel-to-pixel difference) between the original image, $x(m,n)$, and the distorted image, $y(m,n)$, of size $M \times N$ (the total number of pixels in the image). In this equation A_{MAX} is the maximum amplitude or peak signal amplitude that can be represented, which for an image with 8-bit/pixel resolution is 255.

In most cases the PSNR does provide useful information, but more importantly, compared to other measurement techniques it can be easily calculated and is mathematically tractable. The mean absolute error (MAE), is another popular distortion measure and is a variant of the SNR metric often used in the field of electrical engineering. It is well known, however, that the values obtained from these performance metrics do not correlate well with the subjective ratings, especially for high compression ratios where the distortion is generally very high [22, 26].

Although new distortion measures have been proposed for better adaption to the properties of the HVS, in this thesis, the performance of the multimedia systems simulated in the work presented are measured in terms of both the PSNR and by evaluating the visual quality of the image data reconstructed. The perceived quality of the reconstructed images are generally estimated by visual comparison of original and reconstructed image. However, in cases where subjective assessment is difficult the PSNR metric is applied.

2.2.5 Standard Test Images

In order to ensure consistency in the evaluation of image processing techniques such as data compression algorithms (developed by the research community and industry) a standard test image is used to facilitate a comparison of performance results; both visually and quantitatively. The images chosen, in most cases, represent natural or typical images that a class of processing techniques would need to deal with. Other test images are chosen because they present a range of challenges to image reconstruction algorithms, such as the reproduction of fine detail and textures, sharp transitions and edges, and uniform regions. In this thesis, we use the most widely published standard test image known as *Lenna*, which has been derived from a 1972 centerfold photograph of the Playboy model Lena Soderberg [88]. Figure 2.6 shows a gray-level version

Figure 2.6: The standard test image, 'Lenna'.

Figure 2.7: The standard test image, 'Bridge'.

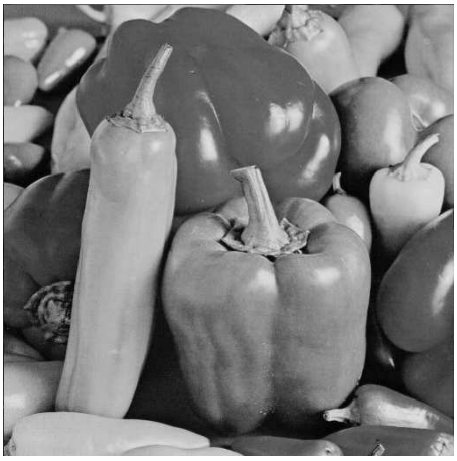

Figure 2.8: The standard test image, 'Peppers'.

of the Lenna image applied to the simulation frameworks developed in this study [89]. Other examples of standard test images widely used such as the images *Bridge* and *Peppers* [90, 91], are shown in Figures 2.7 and 2.8.

2.3 Principles of Mobile Communication Systems

The main elements of a mobile communication system are shown in Figure 2.9. In essence, the network is made up of a number of low-power radio transmitters (generally radio towers for a macrocell environment) which have a power capacity on the order of 100 W or less. Due to the limited range covered by the transmitter, the geographical area that a radio tower serves is divided up into a number of cells with each cell occupied by its own antenna. To avoid interference or crosstalk from neighbouring cells, the base station (BS) or base transceiver station (BTS) that interfaces to the radio tower, is allocated a unique band of frequencies and consists of a transmitter and receiver, and other units to control the communication power to the antennas, etc. The reuse of these frequencies in GSM systems are possible as long as the cells are sufficiently distant from each other. However, this problem does not exist in current CDMA and WCDMA mobile networks, as it is possible for multiple users to utilize the same carrier frequency over the entire bandwidth (passband) available. The same set of frequencies are reused in each cell as unique noise-like codes are used to spread the user information over the allocated passband.

In order to service multiple users and provide enough capacity to avoid traffic congestion, the BS is designed with several transceivers (transmit and receive units), so that communication over a number of channels assigned to the cell is possible. It also controls the radio link between the antenna and mobile station. The base station controller (BSC) unit handles the call process between the mobile station or terminal (MS) and the rest of the network, and manages the radio channel resources (channel setup) and handovers for each BTS, and can control multiple BTS's at any one time. To enable a MS to connect between other mobile units located in the same or different cell a mobile switching center (MSC) is employed. The MSC is the central component of the network and operates all the switching functions required by the MS. It is also connected to the public-switched telephone network (PSTN) which enables call connection between a mobile unit and a fixed subscriber on the public network. Apart from providing an interface between a mobile and other (including fixed) networks it performs a number of functions such as, managing the location of the mobile subscriber, switching and routing calls through the network, managing the security features of a mobile subscriber, controlling handovers between BSC's, collecting call billing data and traffic statistics for performance monitoring, interworks with and manages network databases and manages call processing resources.

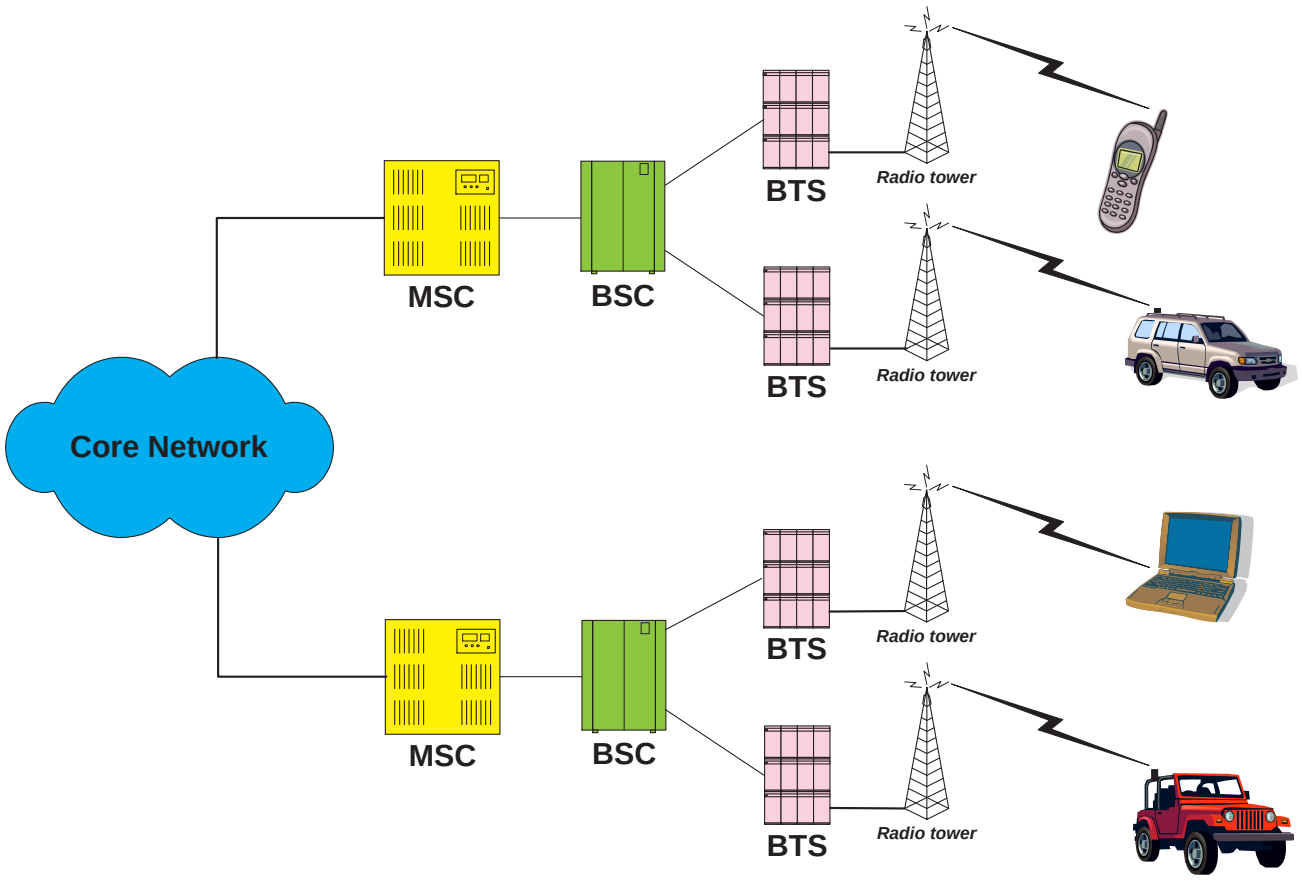

Figure 2.9: Basic elements of a mobile network.

2.3.1 Digital Communication Signal-Processing

In the mobile network presented in Figure 2.9, the BTS performs a key role in the communication of voice and data services between the MS and the rest of the network. Importantly, in the context of mobile multimedia, the transceiver or trasmit/receive unit is critical in ensuring that data applications such as, the transmission of digital images and video over mobile radio links, are received on a MS with high signal fidelity or error-free while mitigating the signal propagation effects of the mobile environment (diffraction, scattering, multiple reflections, etc). To achieve this the transceiver in the BTS is designed using a digital communication system with a basic form similar to the structure shown in Figure 2.10. The main signal-processing functions of the transmitter can be classified into the following nine groups (where the receiver performs the reverse function of the transmitter) as specified in [24]:

1. Formatting and source coding
2. Baseband signalling (modulation)
3. Bandpass signalling (modulation)
4. Equalization

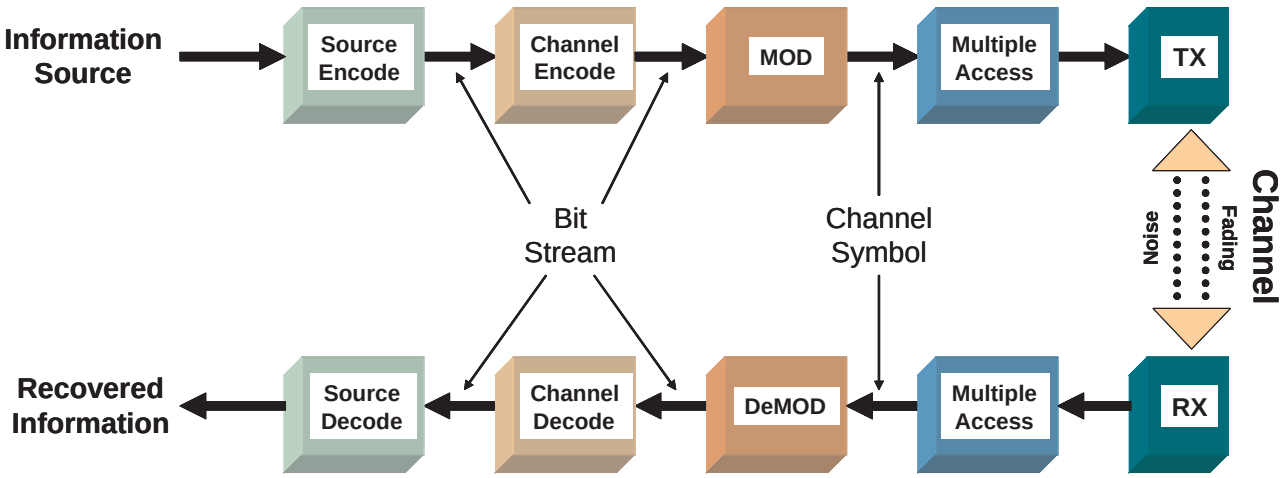

Figure 2.10: Bock Diagram of a digital communication system.

5. Channel coding
6. Multiplexing and multiple access schemes
7. Spreading
8. Encryption
9. Synchronization

One of the most important aspects of a digital communication system is the efficient use of available communication resources such as the bandwidth of the system. The use of 'multiplexing' or 'multiple access' schemes are necessary to ensure that the allocation of resources is shared among the mobile users, such that no block of time or frequency (bandwidth) is wasted. In mobile communication systems, there are three basic ways in which communication resources are distributed across multiple users. These include the following [24]:

1. ***Frequency-division multiple access (FDMA)***: Specific subbands or spectrally separate frequency channels are allocated. Users are assigned to a specific frequency band during the entire transmission period.
2. ***Time-division multiple access (TDMA)***: Periodically recurring timeslots of short duration are allocated. Allows multiple users to share the same frequency channel by dividing the signal into different timeslots and by assigning a fixed portion of the time resource available or timeslot. In some cases, users may access the resource at random times.
3. ***Code-division multiple access (CDMA)***: Considered as a hybrid combination of FDMA and TDMA. A set of orthogonal or nearly orthogonal spread-spectrum (SS) codes (noise-like codes) are allocated so that a mobile user utilises the full channel bandwidth.

In general, mobile communication systems combine multiple access schemes with other digital signal-processing functions such as source coding (lossy/lossless compression), equalization, channel coding (block, convolutional, Turbo) techniques, to overcome both the communication resource limitations inherent of mobile digital transmission and to compensate for the errors/distortion introduced by the effects of multipath propagation, respectively. The most difficult challenge in designing an efficient transmission system is, however, dealing with the problem of *fading* in a mobile environment.

2.3.2 Mobile Radio Propagation Effects

In a mobile environment, the term 'fading' refers to the time variation in the received signal power created by complex transmission effects introduced by changes in the transmission medium, but more often, due to changes in the propagation path. The effects of radio wave propagation are generally characterised by three important mechanisms: reflection, diffraction, and scattering. Reflection occurs when a radio wave (electromagnetic signal) encounters an object or surface whose dimensions are considerable larger than the signal wavelength. These reflected waves may interfere constructively or destructively at the receiver producing multipath interference. Diffraction occurs when radio waves interact with the edges of physical objects whose dimensions are also considerable larger than the signal wavelength, causing a number of waves to propagate in different directions with the edge considered to be the source. This phenomenon is often referred as *shadowing*, since the receiver is shadowed by obstacles. In an urban or rural environment, this mechanism allows reception of radio waves where no line-of-sight (LOS) propagation path exists. When radio waves interact with an obstacle whose size is approximately the same as the signal wavelength such as a lamp post, traffic signs, etc, scattering occurs. The resultant effect of this phenomenon is the dispersion of several weaker signals into different directions, making it very difficult to predict and measure [21, 92].

The effects of these type of propagation mechanisms are commonly referred to as *multipath propagation*. This is illustrated in Figure 2.11, which shows a typical radio propagation environment for mobile communication systems comprising of the following: (i) a set of antennas placed at the top of a radio tower or a tall building, (ii) a single antenna on the MS unit/device located close to ground-level, and (iii) several obstacles located between the BS and the mobile station (MS) which create non-LOS radio waves. In this environment, there are many situations where the propagation path is changing, particularly, due to the movement of the MS antenna relative to the base station (BS) antenna or in the surrounding objects. The strength of the

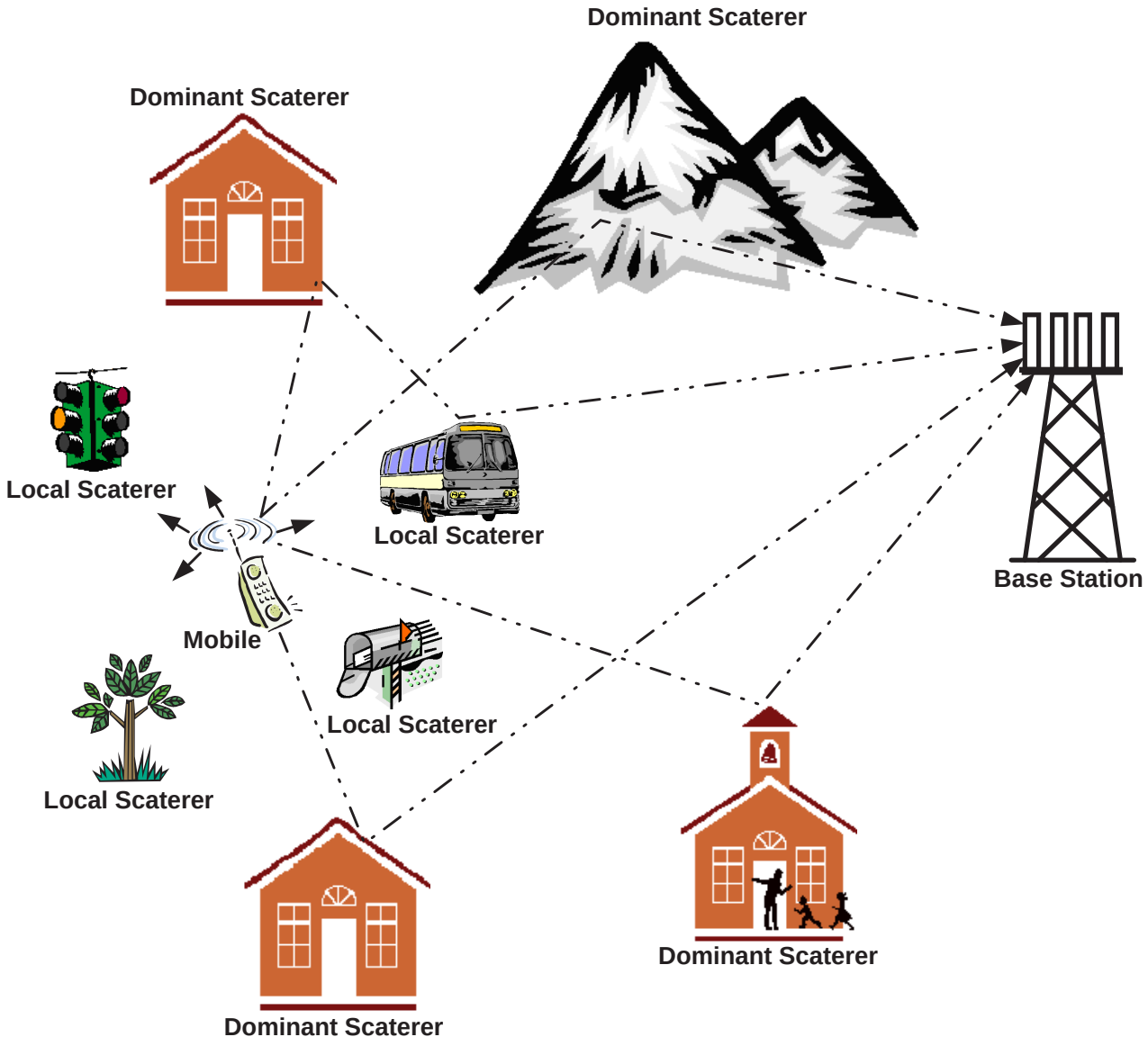

Figure 2.11: An illustration of multipath propagation effects in a mobile environment.

signal between the MS and the BS is generally weak and varies as a function of distance from the two antennas. Moreover, the signal strength varies dynamically as the MS unit moves within the defined coverage area or cell. In addition, multiple signal reflections will arrive at the receiver with its own phase and delay, the interaction between these waves at the receiver will cause destructive or constructive interference resulting in rapid fluctuations in signal amplitude. Commonly, the effects on the received signal strength are characterised by two fading models: large-scale and small-scale fading [21, 24]. The large-scale fading models are traditionally used by mobile operators to estimate the radio coverage area of antenna systems and to aid in the efficient planning of a mobile radio network. On the other hand, the rapid fluctuations in the received signal strength over a short distance or time duration are characterised by the follow-

ing small-scale fading models [21]: *envelope fading* (flat fading), *Doppler spread* (time-selective fading), and *time-delay spread* (frequency-selective fading).

Large-Scale Fading (Path Loss)

The *path loss*, which represents signal attenuation, is defined as the difference between the effective transmitted power and the received power. Equivalently, it is a measure of the amount of power loss in the received signal for a specified distance between the BS and the MS. By using path loss models to estimate the received signal level as a function of distance, it is possible to predict signal-to-noise ratio (SNR). Over the past few years, many important propagation models have been reported, some of which are now widely used to determine the radio coverage area in the design of a mobile communication system.

One of the most popular path loss models proposed for large-scale fading was developed by Okumura et al [93], which is based on a comprehensive range of field measurement data taken of the received signal power over a wide range of separation distances and different antenna heights. This was later refined by Hata who systematically interpreted Okumura's data into parametric formulas [94]. In order to obtain an accurate measurement result for a specific BS-MS separation distance, a typical measurement technique for the local average received power is calculated by averaging signal measurements over a measurement track of $5\lambda_c$ to $40\lambda_c$, where λ_c is the carrier frequency wavelength. Most reported studies have shown that variations in the measured receive signal level is contributed by the shadowing effect which follows a log-normal distribution. In the following, a practical log-normal path loss model is presented.

Log-Normal Shadowing

Many of the path loss models presented in are either based on theoretical prediction or field measurement data. All of them show that the average received signal power decreases logarithmically with distance, whether in outdoor or indoor radio environment. According to [21], an ensemble average large-scale path loss can be estimated using a path loss exponent, n, a reference distance, d_0, and a BS-MS separation distance, d, as

$$\overline{\mathrm{PL}}(d)[dB] = 20\log_{10}\left(\frac{4\pi d_0}{\lambda_c}\right) + 10n\log_{10}\left(\frac{d}{d_0}\right), \tag{2.23}$$

where $\lambda_c = c/f_c$ is the carrier frequency wavelength, c is the speed of light, and f_c is the carrier frequency. The value of n depends on the specific propagation environment and Table 2.1 listed typical path loss exponents obtained in various mobile radio environments [21].

The selection of a reference distance has a major impact on the estimation accuracy and

Table 2.1: Path Loss Exponent for Different Environments.

Environment	Path Loss Exponent, n
Free Space	2
Urban area cellular radio	2.7 to 3.5
Shadowed urban cellular radio	3 to 5
In building line-of-sight	1.6 to 1.8
Obstructed in building	4 to 6
Obstructed in factories	2 to 3

should be appropriately chosen to the propagation environment. For example, 1km reference distances are commonly used in large coverage cellular systems, whereas in micro-cellular systems, much smaller distances (such as 100 meters or 1 meter) are used [95]. However, the log-distance model in (2.1) does not take into consideration the fact that the surrounding scatter may be widely different at two locations having the same BS-MS separation. As a result, the predicted *average* value may be vastly different to the actual measured one. Measurements have shown that at any value of d, the path loss PL(d) at a particular location is random and distributed log-normally about the mean distance-dependent value as [96]

$$\mathrm{PL}(d)[dB] = \overline{\mathrm{PL}}(d)[dB] + X_\sigma, \tag{2.24}$$

where X_σ is a zero-mean Gaussian distributed random variable (in dB) with standard deviation σ (also in dB). Therefore, this log-normal shadowing equation captured not only the log-distance path loss for a specified separation distance d, but it also modelled the random effects of *shadowing* over a large number of measurement locations with different scattering levels.

Figure 2.12 shows the received signal power (dB) as a function of BS-MS separation distance (meters). The bold solid line represents the large-scale fading component which indicates that the average received power decays logarithmically with distance. The thin dotted curve is the small-scale fading component whose amplitude follows a Rayleigh distribution. Thus, it is commonly referred to as *Rayleigh fading*.

Small-Scale Fading (Multipath Fading)

As discussed earlier, due to the reflection, diffraction and scattering mechanisms of radio propagation, the received signal can be considered as a superposition of a large sum of attenuated, delayed, and phase-shifted replicas of the transmitted signal, each interfering one another. Depending on the phase and amplitude of each partial wave, the superposition can be constructive

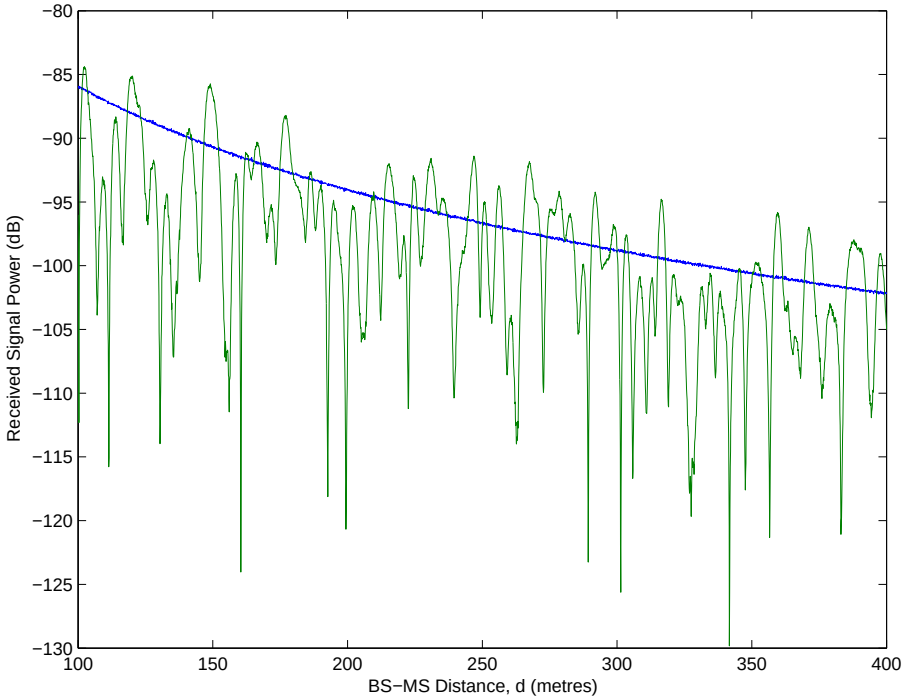

Figure 2.12: Averaged large-scale path loss with small-scale Rayleigh fading amplitude.

or destructive, causing fluctuation in signal strength, thus inducing small-scale fading. In addition, due to large time delays in multipath propagation, the channel often lengthens the time required for the baseband portion of the signal to reach the receiver, smearing signals and hence introducing intersymbol interference (ISI) between the transmitted digital impulses.

Apart from that, since the propagation channel is a constant changing environment, the variability of the channel is contributed by the movement of the MS and/or the surrounding objects, giving rise to a time-variant multipath environment even with the smallest and slowest movement. The rate at which the received signal strength varies depends on the speed of the movement which causes Doppler spread in the received signal. It is reported in [97] that the resulting variations in the signal amplitude, called multipath fading, vary over distances proportional to the signal wavelength and it usually obeys a complex Gaussian process. Therefore, it is clear that small-scale fading is used to describe the rapid fluctuation of the amplitude of a radio signal over a short period of time or travel distance, so that large-scale path loss effect may be ignored. It is shown in [98] that the received signal power may vary by as much as three or four orders of magnitude (30 or 40 dB) when the receiver is moved by only a fraction of a wavelength.

Generally, signal propagation in a multipath channel experience three important small-scale fading effects [21]:

- Rapid fluctuations in signal strength over a small travel distance or time interval.

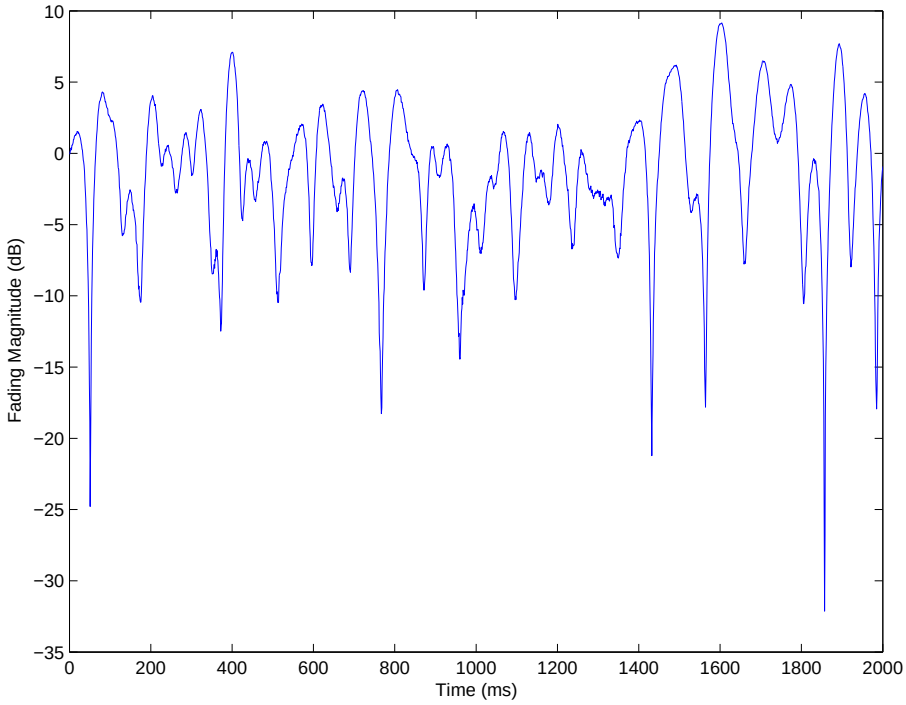

Figure 2.13: Small-scale Rayleigh fading amplitude.

- Random frequency modulation due to varying Doppler shift on different multipath signals.
- ISI due to impulse dispersion (echoes) which is caused by multipath propagation delays.

Delay Spread: Frequency-Selective Fading

In the time domain, due to the phenomenon of multipath propagation, each of radio waves arrived at the receiver with its own time delay. *Delay spread* of the wireless channel is then commonly defined as a statistical measure of a maximum delay difference over which the arriving waves have significant received signal strengths. *Coherence bandwidth* of the wireless channel, B_{C} is, on the other hand, a statistical measure of a maximum frequency separation over which two frequency components of a signal have a strong correlation in amplitude such that the channel can be considered "flat". Although these two channel parameters both describe the time dispersive nature of the wireless channel in different domains, however, they have a distinctive relationship as [95] $B_{\mathrm{C}} \approx \frac{1}{50\sigma_\tau}$, where σ_τ is the rms delay spread of the channel. Therefore, frequency selectivity of the channel is directly related to the physical structure of the multipath propagation environment.

In the case when the coherence bandwidth of the channel is much smaller than the transmitted baseband signal bandwidth, the distorted received signal strength will not fade much over a local area [21]. Meaning the small-scale fading is insignificant. However, the received signal strength will fluctuate rapidly if the channel coherence bandwidth is larger than the transmitted signal

bandwidth. In summary, the probability of the received signal will be corrupted by the ISI and the likelihood of rapid fluctuation in the received signal amplitude are all depend on the bandwidth of the transmitted signal and the delay spread of the multipath channel.

In a frequency-flat multipath fading channel, also referred to as *flat fading* channel in many channel modelling literature, where the coherence bandwidth is larger than the transmitted baseband signal bandwidth, the statistical time varying nature of the received signal envelope is commonly described by two fading distributions; Rayleigh and Rician. When a signal is transmitted over a multipath channel with the absence of a LOS component, the received low-pass signal can be modelled as a zero-mean complex Gaussian random process and the signal envelope obeys a Rayleigh distribution. The probability density function (pdf) of a Rayleigh distribution is given by [99] as

$$P(x) = \frac{x}{\sigma^2} \exp\left\{-\frac{x^2}{\sigma^2}\right\} \quad x \geq 0, \tag{2.25}$$

where x is the received signal amplitude and σ is the rms value of the received signal voltage. This type of fading is normally used for modelling macrocell channel environment. Fig. 2.13 shows a typical rapid variations in the received signal envelope due to Rayleigh fading as a function of time. When there is a dominant LOS component present in the channel, the small-scale fading envelope is Rician. The probability density function (pdf) of a Rician distribution is given by [99] as

$$P(x) = \frac{x}{\sigma^2} \exp\left\{-\frac{x^2 + s^2}{2\sigma^2}\right\} I_o\left\{\frac{xs}{\sigma^2}\right\} \quad x \geq 0, \tag{2.26}$$

where the non-centrality parameter s denotes the peak amplitude of the dominant signal and $I_o(\cdot)$ is the modified Bessel function of the first kind and zero order. This type of fading is normally used for modelling microcell channel environment.

Doppler Spread: Time-Selective Fading

Apart from the delay spread phenomenon in multipath channels, Doppler spread, B_{D}, also has a negative influence on propagating waves as well. Due to the relative motion between the BS and the MS, the Doppler effect introduces random frequency modulation in each of the partial waves and causes spectral broadening of the signal bandwidth. In addition, if objects in the radio channel are in motion, they also induce a time varying Doppler shift on multipath components even when a mobile receiver is stationary.

To illustrate this phenomenon, let us consider a scenario where a MS receives signals from a

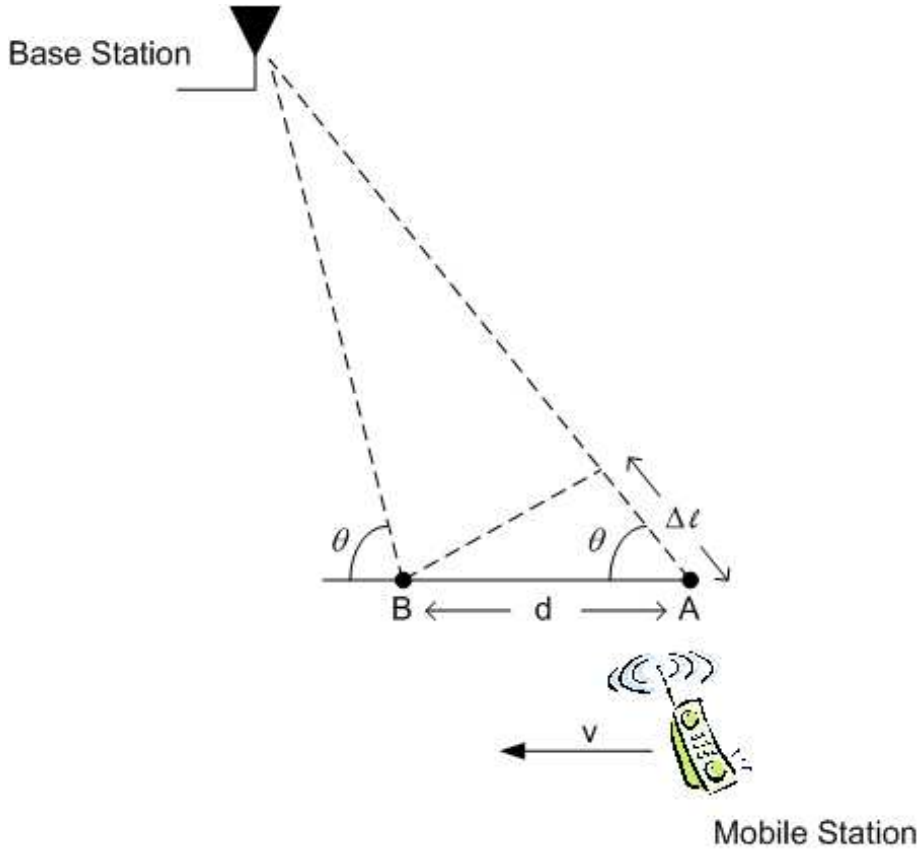

Figure 2.14: Doppler effect of a moving mobile station.

BS while travelling from point A to B with a distance separation of d, as shown in Figure 2.14. Assuming that the angle θ at points A and B is the same and the MS travels at a constant speed of v. Denote the difference in path lengths travelled by the wave as $\Delta\ell$, then the phase change in the received signal due to $\Delta\ell$ can be calculated as $\Delta\phi = \frac{2\pi\Delta\ell}{\lambda_c} = \frac{2\pi v\Delta t}{\lambda_c}\cos(\theta)$, where $\Delta t = d/v$ is the travelling time from A to B. The Doppler shift in the carrier frequency is expressed as

$$f_d = \frac{1}{2\pi}\cdot\frac{\Delta\phi}{\Delta t} = \frac{v}{\lambda_c}\cos\theta. \tag{2.27}$$

The amount of spectral broadening that depends on f_d can be clearly seen as a function of the relative velocity of the mobile, and the angle θ between the direction of motion of the mobile and direction of arrival of the scattered waves. As a rule of thumb, if the MS is moving away from the BS, the channel produces a negative Doppler shift to the carrier frequency and a positive Doppler shift if the MS is moving towards the BS. Thus, the definition of Doppler spread can be described as the range of frequencies over which the received Doppler spectrum is essentially non-zero. According to [21], if the baseband signal bandwidth is much greater than B_D, the effects of Doppler spread are negligible at the receiver. This is a *slow* fading channel.

Apart from the Doppler spread, *coherence time* is commonly used as well to describe the time-varying nature of the channel in the literature [21, 24, 38]. In fact, the coherence time T_{C} is the time domain dual of Doppler spread and they have a relationship being inverse proportional to each other as [21]

$$T_C = \sqrt{\frac{9}{16\pi f_m^2}} = \frac{0.423}{f_m}, \tag{2.28}$$

where f_m is the maximum Doppler shift given by $f_m = v/\lambda_{\mathrm{c}}$. Thus, the definition of coherence time implies that two signals arriving with a time separation greater than T_c are affected differently by the channel. Equivalently, coherence time of the channel can also be thought as the time duration over which two received signals have a strong correlation in signal amplitude.

2.3.3 Space-Time Channel Modelling

To correctly and accurately model previously described characteristics of the wireless channel in different propagation environments, various statistical channel models have been developed for mobile radio systems. These models are often referred as *space-time channel models* and sometimes they are also known as vector channel models in [100] and spatial channel models in [101, 102].

Generally, there are two different approaches in modelling mobile wireless channels; geometrical based and scalar stochastic based. Space-time channel models developed based on these two approaches have significant importance as they not only provide statistical channel information such as received signal strength, Doppler spectra, and power delay profiles, but spatial and temporal information such as angle-of-arrival (AoA) time-of-arrival (ToA) as well. In this thesis, our simulation is developed based on a mixture of these two channel modelling techniques to provide a accurate and reliable framework for performance analysis of different type of mobile transmission systems.

In geometrical based space-time channel modelling, various models have been developed. In [103], Lohse developed a geometrical based exponential channel model for macrocell environment in which it assumes a circular distribution of scatterers around the MS and the distance between the scatterers and the MS are exponentially distributed. In [104–106], Liberti and Rappaport proposed a single bounce geometrical based channel model for microcell environment with line-of-sight multipath components. In this model, scatterers are assumed to be uniformly distributed within an elliptical region where the BS and the MS are the foci of the ellipse. In [107], a uniform-

sectored distribution model is developed and in which all scatterers are uniformly distributed in the region within a certain angular and radial range to the MS. Lee's model assumes that scatterers are uniformly spaced on a radius about the MS and these *effective scatterers* are intended to represent the effect of many scatterers within the region [95,108]. In [109], Mohasseb and Fitz proposed a 3-D spatio-temporal channel model where it is characterised by a set of scattering centers with a given mean AoA, AS (azimuth and elevation), and propagation delay. In addition, it also accommodates either transmitter or receiver motion.

In this thesis, a recently developed space-time channel model is used which is known as, geometrical-based hyperbolically distributed scatterers (GBHDS) [110–113]. This model can be applied to both microcell and macrocell environments and has been validated against practical measurement data and proven to be accurate in modelling realistic channel propagation environments. Therefore, GBHDS channel model is used as one of the channel models for evaluating performances of mobile communication links. A comprehensive study of this model (at theoretical and simulation levels) as well as the validation with practical data reported in [114–116] have been considered. The results have been proved to be more realistic than other models in the literature when tested against practical data [112, 113].

The GBHDS Model for Macrocell Environment

The GBHDS model for macrocell environment is a two-ring ST channel model that assumes both the distance between the MS and local scatterers and the distance between the MS and dominant scatterers are hyperbolically distributed. It also assumes that the scatterers are arranged within a circle of radius R around the mobile. The distances r between the mobile station (MS) and the scatterers are distributed according to the hyperbolic probability density function (pdf) [112]. A diagram showing the various model parameters of the GBHDS macrocell channel model is detailed in Fig. 2.15.

The geometrical scatterer density function (GSDF) for distances r_k and R_k have the form

$$f_{r_k}(r_k) = \begin{cases} \frac{a_1}{\tanh(a_1 R)\cosh^2(a_1 r_k)} & \text{for } 0 \leq r_k \leq R \\ 0 & \text{elsewhere} \end{cases} \tag{2.29}$$

and

$$f_{R_k}(R_k) = \begin{cases} \frac{a_2}{\cosh^2(a_2 R_k)} & \text{for } 0 \leq R_k < \infty \\ 0 & \text{elsewhere} \end{cases} \tag{2.30}$$

where R is the radius of the circle enclosing the local scatterers (scatterers beyond R are consid-

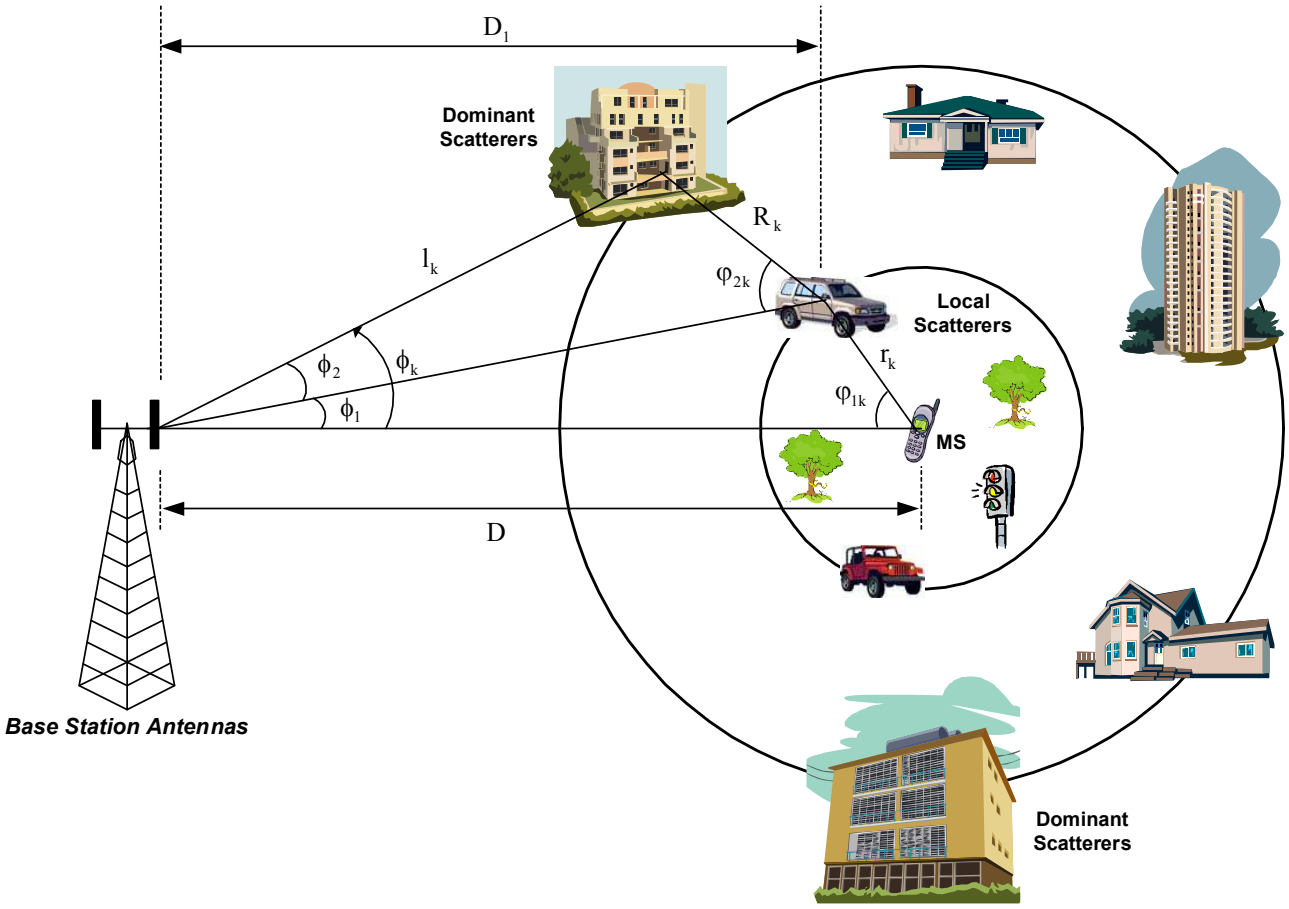

Figure 2.15: Geometry of the GBHDS macrocell channel model.

ered dominant). The parameters a_1 and a_2 control the spread (standard deviation) of the local and dominant scatterers around the MS and are constrained to values that lie in the interval (0,1) [112, 113].

In modelling the mobile propagation channel, there are several important parameters that need to be generated. According to [111], the complex time-variant baseband discrete impulse response as a function of time and delay is described by

$$h(t,\tau) = \sum_{\ell}^{L} \sqrt{P(\tau_\ell)}\alpha_\ell(t)e^{j\phi_\ell(t)}, \tag{2.31}$$

where L is the number of dominant multi-paths, $\alpha_\ell(t)$ is the fading gain which is commonly modelled as Rayleigh or Rician fading, and τ_ℓ is propagation delay for the ℓ^{th} path. Note, that in Fig. 2.15 above the ℓ^{th} path is represented by the variable k. $\sqrt{P(\tau_\ell)}$ is the path attenuation which can be calculated using (2.24) and $\phi_\ell(t) = 2\pi(f_d\cos(\omega_\ell t) - f_c\tau_\ell)$. The term $f_d\cos(\omega_\ell t)$ is the Doppler shift where ω_ℓ is the angle of the ℓ^{th} scatterer with respect to the mobile velocity vector. Note that these parameters vary with time and the received signal $y(t)$ at the MS is

given by

$$y(t) = \sum_{\ell}^{L} \sqrt{P(\tau_\ell)}\alpha_\ell(t)e^{j\phi_\ell(t)}s(t-\tau_\ell) + e(t), \tag{2.32}$$

where $s(t)$ represents the transmitted signal and $e(t)$ is the receiver additive white Gaussian noise (AWGN).

Another important parameter is the AoA of the multipath component. In the GBHDS model, the AoA of the ℓ^{th} path signal impinging on the BS ULA and is generated by $\phi_\ell = \phi_1 + \phi_2$, where

$$\phi_1 = \tan^{-1}\left(\frac{r_\ell \sin(\varphi_{1\ell})}{D - r_\ell \cos(\varphi_{1\ell})}\right) \tag{2.33}$$

and

$$\phi_2 = \begin{cases} \tan^{-1}\left(\frac{R_\ell \sin(\varphi_{2\ell})}{D_1 - R_\ell \cos(\varphi_{2\ell})}\right) & , \text{ for } R_\ell \cos(\varphi_{2\ell}) \leq D_1. \\ \tan^{-1}\left(\frac{R_\ell \sin(\varphi_{2\ell})}{D_1 - R_\ell \cos(\varphi_{2\ell})}\right) + \pi & , \text{ for } R_\ell \cos(\varphi_{2\ell}) > D_1. \end{cases} \tag{2.34}$$

The random variables r_ℓ and R_ℓ with their pdf's given in [6] can be obtained using a random variable ς_ℓ uniformly-distributed over the interval [0,1] with the following transformations:

$$r_\ell = \frac{1}{a_1}\tanh^{-1}(\varsigma_\ell) \tag{2.35}$$

and

$$R_\ell = \frac{1}{a_2}\tanh^{-1}(\varsigma_\ell). \tag{2.36}$$

Moreover, $\varphi_{1\ell}$ and $\varphi_{2\ell}$ are uniformly distributed on the interval $[0, 2\pi]$ [6]. The distance between the BS and the local scatterers can be calculated as:

$$D_1 = \sqrt{r_\ell^2 + D^2 - 2r_\ell D\cos(\varphi_{1\ell})}, \tag{2.37}$$

where D is the distance between the BS and the MS. In our simulation frameworks, we model the multipath propagation channel as a tapped-delay line with time-varying coefficients generated using this ST GBHDS channel model.

This model has been validated against measurement data reported in [114, 115]. In [114], Pedersen et al. conducted a number of outdoor measurement results, collected in a macrocell

typical urban environment. These measurements were performed in Aarhus, Denmark and Stockholm, Sweden. From these results the statistics for the direction of arrival (DOA) and time of arrival (ToA) are measured. These measurements were conducted at 1.8 GHz carrier frequency, 4.096 Mcps chip rate (wideband CDMA), and at 122 ns sampling time. The angular histogram data of DOA had standard deviation of 7° while the delay histogram data for ToA had root mean squared delays of 0.682 μs. The results of the GBHDS channel model has shown that there was a good match between the model result and the measurement data reported in [114] for outdoor environment. In this paper the GBHDS model will be simulated with the same measurement angular spread (angular spread of of 7°).

The GBHDS Model for Microcell Environment

The GBHDS model for a microcell environment is an extension of the macrocell model proposed in [112], however in this model the base station (BS) antenna is relatively low and multipath scattering near the BS is just as likely as multipath scattering near the mobile station (MS). Although in microcell environment there are two types of propagation: LOS and non-LOS propagation, this model assumes that there is a LOS path between the transmitter and the receiver and that the scatterers are arranged in a circle centered on the MS, with the circle radius being R. It is further assumed that the BS lies within this circle [111]. The distances, r, between the scatterers and the MS conform to a hyperbolic distribution as in the macrocell scenario. The GSDF for this model is given by the same equations as in (2.29) and (2.30).

Validation of this model using practical data reported in [116] has been presented in [111]. In [116], Spencer *et al.* conducted a number of indoor measurement results, collected at 7 GHz within office buildings on the BYU campus. The scanning was done mechanically with a 6° horn over a 360° range. At the Clyde building, the angular data measured is for data within one cluster about its mean angle. The angular spread (standard deviations) is 24.5°. As this model shows a good match with measurement data, therefore in this paper we simulate this model with the same measurement angular spread (angular spread of of 24.5°).

2.3.4 Transmit Diversity Techniques

In the previous section, it was shown that multipath propagation often introduces undesirable effects on radio signals which severely degrade the performance of mobile transmission systems or communication over mobile radio channels. To mitigate or alleviate the effect of these channel impairments, space-time processing techniques such as transmit diversity have been developed

which are now an important consideration for next-generation mobile networks [117,118]. Transmit diversity schemes have become increasingly popular as they offer many benefits to mobile communication systems which have been summarised as follows [100, 102, 118]:

- *System capacity enhancement*
- *Interference rejection*
- *Area coverage extension*
- *Spectral efficiency optimisation*
- *Signal quality improvement*
- *Outage probability reduction*

The primary purpose of employing diversity techniques in wireless systems is to exploit diversified branches in propagating paths to overcome the effects of channel deep fading. By providing replicas of transmitted information signal to the receiver, diversity techniques have been proven to be effective in improving performance of wireless links if one of the received replicas is deemed to be unreliable. To accomplish this goal, majority of techniques proposed and developed up to date are either in space, time, or frequency domain.

The most commonly used diversity schemes are delay-diversity, frequency-diversity, multipath diversity, and space diversity. In each of these schemes, the fundamental concept is the same but techniques employed in wireless systems can be very different to each other. We briefly describe each of these techniques in the following.

- **Delay Diversity (Temporal Domain Technique)** - One of the earliest form of diversity techniques is the well-known *channel coding* schemes and sometimes referred to as error correction schemes. The technique used in this scheme is to spread information data or to transmit the same information data in different time slots with a time delay of one channel coherence time to create a scenario where the same information data can experience independent channel fading effect (as oppose to correlated fading). Commonly used coding techniques to achieve delay diversity in wireless transmission are the channel coding schemes such as convolutional coding, turbo coding, and Reed-Solomon coding. In these schemes, duplicate (redundant) bits or symbols are added to the information data sequence before signal transmission, therefore, providing receiver with replicas of the transmitted signal to achieve diversity in time domain. This delay diversity technique is also often used with time interleaving to reassure the channel fading gains for different time slots that contain the same information data are not correlated. Details of these channel coding schemes can be found in [38, 119].

- **Frequency Diversity (Frequency Domain Technique)** - Frequency diversity techniques or wireless systems that are designed to facilitate frequency diversity are multi-carrier code division multiplex access (MC-CDMA), orthogonal frequency division multiplexing (OFDM) frequency-hopping CDMA (FH-CDMA), CDMA-OFDM, and adaptive modulation (also known as adaptive bit and power allocation) scheme. The principle idea behind frequency diversity is to exploit different multipath structure that can be induced if information is transmitted on more than one carrier frequency with at least one coherence bandwidth apart. In turn, frequency diversity techniques and systems can provide the receiver with replicas of the transmitted signal in the form of redundancy in the frequency domain.
- **Multipath Diversity (Spatial Domain Technique)** - One popular technique that is often used to exploit multipath diversity branches in wireless channels is to use the concept of antenna beamforming [118,120] which has a structure that can be configured to produce multiple output-beams simultaneously. Ideally, these output beams are pointing towards dominant propagating paths of the channel that can result in highest receiving signal power at the MS. One major advantage of using such multi-beam structure is that it provides redundancy in the spatial domain of the wireless channel with no bandwidth deficiency. However, depending on the beamforming structure and algorithm used, this scheme can come with a penalty of processing complexity [48]. In Section 2.2.3, we showed the improvement in error-rate performance for systems utilising eigenbeamforming scheme.
- **Space Diversity (Spatial Domain Technique)** - A simpler space diversity technique that can be used is to deploy multiple transmit and receive antennas in wireless systems to exploit additional signal paths in multipath channels to provide redundancy in the spatial domain [121–125]. As oppose to the antenna beamforming scheme where each of the output-beams from the antenna array is considered as a single input to the channel. In this scheme, signal transmitted from each the multiple antenna elements is considered as individual input into the channel, thus creating N_t inputs and N_r outputs. On major advantage of this scheme is that it uses no pre-processing at the transmitter and only a low complexity combiner is needed at the receiver. This type of system is commonly referred as multiple-input multiple-output (MIMO) system. Although its performance is generally lower than antenna beamforming scheme, however, it has been shown that system employed MIMO configuration can greatly enhance system performance and reach up to Gigabit wireless transmission in [124]. An example of MIMO diversity scheme is provided in Section 2.2.2 to illustrate the enhancement in channel capacity for wireless

communication systems.

In addition to the above diversity techniques, two newly developed diversity coding schemes called space-time block coding (STBC) [40] and space-time trellis coding (STTC) [42] were first proposed in 1998. Since then these space-time coding (STC) schemes has attracted considerable attention to researchers around the world and many contributions are made in this area. Due to a large quantity of them, we include those important and often cited references in the bibliography Section. In these two STC schemes, encoding of baseband modulated data symbols is performed across successive time slots and multiple antennas through which they are simultaneously transmitted and are decoded using maximum likelihood sequence estimator at the receiver. The wireless channel is assumed to be quasi-static Rayleigh or Rician fading. By encoding data symbols simultaneously across spatial and temporal domains of the information signal, STC creates redundancy in the multiple dimensions of the signal and results in an additional diversity and coding gains to the system. Apart from its superior performance, another major benefit is that it offers a low complexity encoding and decoding computation to the system when the number of transmit antennas is low.

In the following, we briefly summarise these two types of space-time coding schemes and their extensions in OFDM systems. In particular, the STBC scheme and its extensions in OFDM systems is our primary interest as this has been adopted in the mobile transmission systems presented in subsequent chapters of this thesis.

Space-Time Block Coding

In [40], Alamouti proposed the first space-time block coding (STBC) scheme for systems employing two transmit antennas. The simple encoding and transmission algorithm is carried out by first taking two symbols in a data sequence, denoted by x_0 and x_1, and to format them into the following codeword matrix.

$$\begin{array}{c} \\ \text{Time}\downarrow \end{array} \overset{\text{Space}\longrightarrow}{\begin{bmatrix} x_0 & x_1 \\ -x_1^* & x_0^* \end{bmatrix}}$$

As indicated by the arrows, the transmission of this matrix using two antennas is done by transmitting symbol x_0 and x_1 on antenna 1 and antenna 2, respectively, during the first symbol interval. During the successive symbol interval, encoded symbols $-x_1^*$ and x_0^* are transmitted on antenna 1 and antenna 2, respectively. The encoding process of this STBC scheme and its

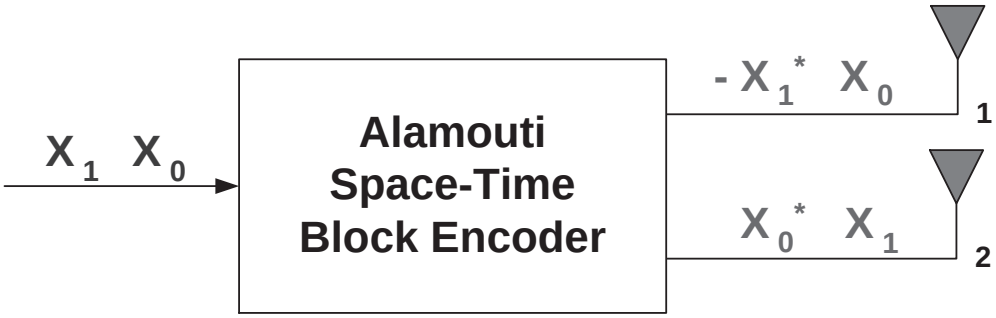

Figure 2.16: Illustration of Alamouti's space-time block encoding scheme.

transmission using two antennas is graphically illustrated in Fig. 2.16 as well. The key feature of this scheme is that it achieves a full rate transmission with full diversity gain and a simple maximum likelihood decoding algorithm to achieve a diversity gain of $N_t N_r$, where N_t and N_r is the number of transmit and receive antennas of the system, respectively. The above encoding structure for Alamouti's STBC scheme is more generally denoted in literature as the 2-by-2 matrix $\boldsymbol{\mathcal{G}}_2$ defined as

$$\boldsymbol{\mathcal{G}}_2 = \begin{pmatrix} x_0 & x_1 \\ -x_1^* & x_0^* \end{pmatrix}$$

Motivated by Alamouti's simple and effective coding scheme, Tarokh *et al.* in [41] and [43] proposed another space-time block coding scheme by applying the theory of orthogonal design to generate output codeword matrices that can be used for systems with more than two transmit antennas, termed orthogonal space-time block coding (OSTBC). Denoting a $N \times N_t$ OSTBC encoded output codeword matrix as $\mathbf{C}$ with its rows are transmitted using the N_t antennas over N symbol intervals. The OSTBC encoding of a data set $\{s_1, \cdots, s_{n_s}\}$ is done according to a *generalised complex orthogonal design* as

$$\mathbf{C} = \sum_{n=1}^{n_s} (s_n \mathbf{A}_n + s_n^* \mathbf{B}_n), \tag{2.38}$$

where $\{\mathbf{A}_n, \mathbf{B}_n\}$ are designed matrices to satisfy the orthogonality condition in [41] such that

$$\mathbf{C}\mathbf{C}^* = \sum_{n=1}^{n_s} \mid s_n \mid^2 \cdot \mathbf{I}_{N_t}. \tag{2.39}$$

The OSTBC encoding matrices reported in [41,43], for encoding complex baseband symbols, are listed in Table 2.2; where the columns in the matrix represent the number of transmit antennas used.

Table 2.2: OSTBC encoding matrices based on generalised complex orthogonal design for different number of transmit antennas.

3 Transmit Antennas	**4 Transmit Antennas**
$\boldsymbol{\mathcal{G}}_3 = \begin{pmatrix} x_1 & x_2 & x_3 \\ -x_2 & x_1 & -x_4 \\ -x_3 & x_4 & x_1 \\ -x_4 & -x_3 & x_2 \\ x_1^* & x_2^* & x_3^* \\ -x_2^* & x_1^* & -x_4^* \\ -x_3^* & x_4^* & x_1^* \\ -x_4^* & -x_3^* & x_2^* \end{pmatrix}$	$\boldsymbol{\mathcal{G}}_4 = \begin{pmatrix} x_1 & x_2 & x_3 & x_4 \\ -x_2 & x_1 & -x_4 & x_3 \\ -x_3 & x_4 & x_1 & -x_2 \\ -x_4 & -x_3 & x_2 & x_1 \\ x_1^* & x_2^* & x_3^* & x_4^* \\ -x_2^* & x_1^* & -x_4^* & x_3^* \\ -x_3^* & x_4^* & x_1^* & -x_2^* \\ -x_4^* & -x_3^* & x_2^* & x_1^* \end{pmatrix}$
$\boldsymbol{\mathcal{H}}_3 = \begin{pmatrix} x_1 & x_2 & \frac{x_3}{\sqrt{2}} \\ -x_2^* & x_1^* & \frac{x_3}{\sqrt{2}} \\ \frac{x_3^*}{\sqrt{2}} & \frac{x_3^*}{\sqrt{2}} & \frac{(-x_1-x_1^*+x_2-x_2^*)}{2} \\ \frac{x_3^*}{\sqrt{2}} & -\frac{x_3^*}{\sqrt{2}} & \frac{(x_2+x_2^*+x_1-x_1^*)}{2} \end{pmatrix}$	$\boldsymbol{\mathcal{H}}_4 = \begin{pmatrix} x_1 & x_2 & \frac{x_3}{\sqrt{2}} & \frac{x_3}{\sqrt{2}} \\ -x_2^* & x_1^* & \frac{x_3}{\sqrt{2}} & -\frac{x_3}{\sqrt{2}} \\ \frac{x_3^*}{\sqrt{2}} & \frac{x_3^*}{\sqrt{2}} & \frac{(-x_1-x_1^*+x_2-x_2^*)}{2} & \frac{(-x_2-x_2^*+x_1-x_1^*)}{2} \\ \frac{x_3^*}{\sqrt{2}} & -\frac{x_3^*}{\sqrt{2}} & \frac{(x_2+x_2^*+x_1-x_1^*)}{2} & -\frac{(x_1+x_1^*+x_2-x_2^*)}{2} \end{pmatrix}$

On close inspection of the OSTBC matrices in Table 2.2, we can clearly see that in systems employing OSTBC and with more than two antennas the data transfer rate requirement is reduced to 1/2 for $\boldsymbol{\mathcal{G}}_3$, and $\boldsymbol{\mathcal{G}}_4$ and 3/4 for $\boldsymbol{\mathcal{H}}_3$ and $\boldsymbol{\mathcal{H}}_4$. In the following section, we will provide a detailed description on the decoding process of Alamouti's STBC scheme and compare the performance between encoding matrices $\boldsymbol{\mathcal{G}}_2$, $\boldsymbol{\mathcal{G}}_3$ and $\boldsymbol{\mathcal{G}}_4$ for systems with a different number of transmit antennas and a single receive antenna.

In [126], Jafarkhani proposed a quasi-orthogonal space-time block code that can achieve a full rate transmission for four transmit antennas. However, only partial diversity is achievable. The decoding algorithm still follows a maximum likelihood estimating algorithm and its encoding matrix has a form

$$\boldsymbol{\mathcal{A}} = \begin{pmatrix} x_1 & x_2 & x_3 & x_4 \\ -x_2^* & x_1^* & -x_4^* & x_3^* \\ -x_3^* & -x_4^* & x_1^* & x_2^* \\ x_4 & -x_3 & -x_2 & x_1 \end{pmatrix} \tag{2.40}$$

Some other important space-time block codes that are not constructed based on orthogonal design are the unitary STBC in [127] which is based on a amicable orthogonal design and

Ganesan's space-time block code based on a maximum signal-to-noise ratio design in [128]. For the sake of completeness, the following is the design rules for constructing amicable orthogonal codes [47] and [127]. In general, an amicable orthogonal design is a set of $N_t \times N$ matrices $\{\mathbf{A}_n\mathbf{B}_n\}$ that satisfy

$$\begin{gathered}\mathbf{A}_n\mathbf{A}_n^H = I_{N_t},\ \mathbf{B}_n\mathbf{B}_n^H = I_{N_t} \\ \mathbf{A}_n\mathbf{A}_p^H = -\mathbf{A}_p\mathbf{A}_n^H,\ \mathbf{B}_n\mathbf{B}_p^H = -\mathbf{B}_p\mathbf{B}_n^H,\quad n \neq p \\ \mathbf{A}_n\mathbf{B}_p^H = \mathbf{B}_p\mathbf{A}_n^H.\end{gathered} \tag{2.41}$$

The following is a codeword example from Ganesan's maximum SNR approach for $N_t = 4$ with a rate of 3/4.

$$\boldsymbol{\mathcal{A}} = \begin{pmatrix} x_1 & 0 & x_2 & -x_3 \\ 0 & x_1 & x_3^* & x_2^* \\ -x_2^* & -x_3 & x_1^* & 0 \\ x_3^* & -x_2 & 0 & x_1^* \end{pmatrix} \tag{2.42}$$

Performance of Orthogonal STBC

Alamouti's space-time block code [40] was originally designed for combatting channel fading effects by introducing a encoding matrix that spreads data symbols simultaneously across space and time domains of the transmitting signal to create diversity in both spatial and temporal domains of the channel using two transmit antennas. This diversity coding scheme proved to be effective in improving system error-rate performance without sacrificing data rate. Its encoding matrix was later generalised as orthogonal space-time block code (OSTBC) by Tarokh *et al.* as $\boldsymbol{\mathcal{G}}_2$. In [41, 43], other encoding matrices, $\boldsymbol{\mathcal{H}}_3$, $\boldsymbol{\mathcal{H}}_4$, $\boldsymbol{\mathcal{G}}_3$, and $\boldsymbol{\mathcal{G}}_4$ as listed earlier, are developed for systems with more than two antennas. These matrices are developed based on a complex orthogonal design such that they can be used for baseband constellations with higher order instead of only *real* dimension. Since then, and together with space-time trellis coding in [42], space-time coding has grabbed every wireless researcher's attention due to its remarkable performances and the simplicity in its algorithms.

To see the error-rate performance improvement from adopting OSTBC technique in wireless communications, we next look at a simple transmission system employing $N_t = 2$ transmit antennas, $N_r = 1$ antenna at the receiver, and Alamouti's $\boldsymbol{\mathcal{G}}_2$ encoding matrix. Such a system is shown in Fig. 2.17. In this diagram, OSTBC encoded information symbols are sent via the

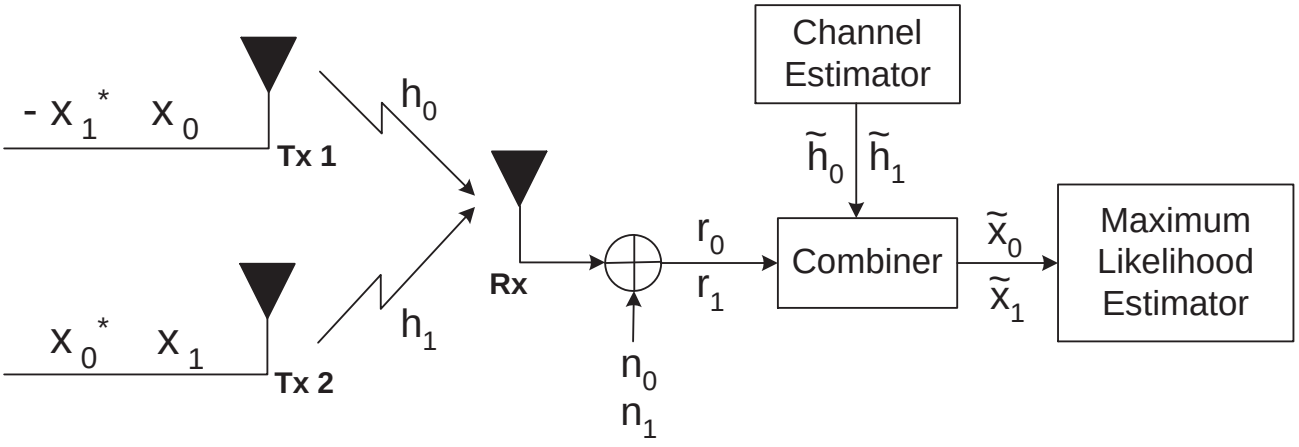

Figure 2.17: Transmission structure for the Alamouti scheme with one receive antenna.

two transmitting antennas occupying two symbol intervals. Let us denote the signal transmitted during the first interval and arrived at the receive antenna as r_0 and the received signal during the second interval as r_1. Assume that the wireless fading channel is quasi-static and the associated fading gains are $h_0 = \alpha_0 e^{j\theta_0}$ and $h_1 = \alpha_1 e^{j\theta_1}$ as indicated in Fig. 2.17. Then the signal model that describes this system's input-output relationship can be expressed as

$$\begin{aligned} \mathbf{r} &= \mathbf{Ch} + \mathbf{e} \\ \begin{bmatrix} r_0 \\ r_1 \end{bmatrix} &= \begin{bmatrix} x_0 & x_1 \\ -x_1 & x_0^* \end{bmatrix} \times \begin{bmatrix} h_0 \\ h_1 \end{bmatrix} + \begin{bmatrix} e_0 \\ e_1 \end{bmatrix} \\ &= \begin{bmatrix} x_0 h_0 + x_1 h_1 + e_0 \\ -x_1^* h_0 + x_0^* h_1 + e_1 \end{bmatrix}, \end{aligned} \tag{2.43}$$

where $\mathbf{e} = [e_0 \ e_1]^T$ is the receiver additive white Gaussian noise vector with zero mean and σ_n^2 variance entries. To decode Alamouti's OSTBC transmission scheme, the receiver first estimates the channel fading gains before it performs the combining process. Denote the estimated version of channel fading gains as $\tilde{h}_0$ and $\tilde{h}_1$. The combining process is carried out by linearly transforming the received signal vector as

$$\tilde{x}_0 = r_0 h_0^* + r_1^* h_1 \tag{2.44}$$

$$\tilde{x}_1 = r_0 h_1^* - r_1^* h_0. \tag{2.45}$$

If ideal channel state information is available, then the above equations are equivalent to

$$\tilde{x}_0 = (\alpha_0^2 + \alpha_1^2)x_0 + e_0 h_0^* + e_1^* h_1 \tag{2.46}$$

$$\tilde{x}_1 = (\alpha_0^2 + \alpha_1^2)x_1 + e_0 h_1^* - e_1^* h_0. \tag{2.47}$$

In Tarokh's decoding scheme, the above combining process is generalised to minimise the following decision matrix

$$\widehat{\mathbf{C}} = \arg \min_{\mathbf{C} \in \boldsymbol{\mathcal{A}}} \|\mathbf{r} - \mathbf{C}\mathbf{h}\|_F^2, \tag{2.48}$$

where $\boldsymbol{\mathcal{A}}$ denotes all possible OSTBC codeword matrices. If multiple-element array is used at the receiver, minimising (2.48) is equivalent to minimising the following for x_0 detection as [43]

$$\left| \left[\sum_{j=1}^{N_r} (r_0(j)h_0^*(j) + r_1^*(j)h_1(j)) \right] - x_0 \right|^2 + \left(-1 + \sum_{j=1}^{N_r} \sum_{i=1}^{2} |h_i(j)|^2 \right) |x_0|^2 \tag{2.49}$$

and

$$\left| \left[\sum_{j=1}^{N_r} (r_0(j)h_1^*(j) - r_1^*(j)h_0(j)) \right] - x_1 \right|^2 + \left(-1 + \sum_{j=1}^{N_r} \sum_{i=1}^{2} |h_i(j)|^2 \right) |x_1|^2 \tag{2.50}$$

for x_1 detection.

The above derivation of the maximum likelihood decoding algorithm can also be extended for the schemes $\boldsymbol{\mathcal{G}}_3$, $\boldsymbol{\mathcal{G}}_4$, $\boldsymbol{\mathcal{H}}_3$, and $\boldsymbol{\mathcal{H}}_4$. These have been provided in Appendix A.

Now, suppose that OSTBC codeword matrix $\mathbf{C}$ was transmitted and ideal channel state information is available at the receiver. Pairwise error probability (PEP) for an erroneous detection in favor of codeword $\widetilde{\mathbf{C}}$ conditioned on the fading channel $\mathbf{H} := [h_1(1), \cdots, h_i(j), \cdots, h_{N_t}(N_r)]$ is well upper bounded by [38]

$$\begin{aligned} P_r(\mathbf{C} \to \widetilde{\mathbf{C}} \mid \mathbf{H}) &= Q\left(\sqrt{\frac{d^2(\mathbf{C}, \widetilde{\mathbf{C}})\varepsilon_s}{2\sigma_n^2}} \right) \\ &\leq \exp\left(\frac{-d^2(\mathbf{C}, \widetilde{\mathbf{C}})\varepsilon_s}{4\sigma_n^2} \right) \end{aligned} \tag{2.51}$$

where $\mathcal{Q}(\cdot)$ is the classical Gaussian $\mathcal{Q}$-function, and $d^2(\mathbf{C}, \widetilde{\mathbf{C}}) := \|\mathbf{H}(\mathbf{C} - \widetilde{\mathbf{C}})\|_F^2$ is commonly known as the squared Euclidean distance between the two codeword matrices.

Defining $\mathbf{h}_j = [h_1(j), \cdots, h_{N_t}(j)] \in \mathbb{C}^{1 \times N_t}$ to be the j^{th} column of $\mathbf{H}$. The squared Euclidean

distance can then be rewritten as

$$d^2(\mathbf{C}, \widetilde{\mathbf{C}}) = \sum_{j=1}^{N_r} \mathbf{h}_j \mathbf{\Psi} \mathbf{h}_j^H, \tag{2.52}$$

where $\mathbf{\Psi} = (\mathbf{C} - \widetilde{\mathbf{C}})(\mathbf{C} - \widetilde{\mathbf{C}})^H$ is the *effective error distance* between two distinct codeword matrices. Recall that the OSTBC encoding matrices are constructed based on a principle of orthogonal design such that they have are full rank matrices and if they multiply by their own conjugation, their product will be a scaler version of an identity matrix. Thus, $\mathbf{\Psi}$ is a non-negative definite Hermitian matrix, and its EVD has a form of $\mathbf{\Lambda \Psi \Lambda}^H = \mathbf{\Omega}$, where $\mathbf{\Lambda}$ is a unitary matrix, $\mathbf{\Omega} = \text{diag}\{\omega_1, \cdots, \omega_r\}$ contains nonzero eigenvalues, and N_t would be the rank of $\mathbf{\Psi}$. Assume that the elements of $\{\mathbf{h}_j\}_{j=1}^{N_r}$ are independent and identically distributed (i.i.d.) complex Gaussian random variables. By averaging the conditional PEP in (2.51) over all channel realizations, the PEP of an OSTBC system can be finally written as

$$P_r(\mathbf{C}_k \to \widetilde{\mathbf{C}}_k) \leq \left(\prod_{m=1}^{r} \omega_m \right)^{-N_r} \left(\frac{\varepsilon_s}{4\sigma_n^2} \right)^{N_t N_r}. \tag{2.53}$$

Therefore, the diversity gain in a OSTBC encoded system is proved to be in the order of $N_t \times N_r$.

The Bit-error rate (BER) and symbol-error rate (SER) performance curves of different OSTBC encoding schemes, $\boldsymbol{\mathcal{G}}_2$, $\boldsymbol{\mathcal{G}}_3$, and $\boldsymbol{\mathcal{G}}_4$, are depicted in Fig. 2.18 with 1 bit/sec/Hz transmission rate and $N_r = 1$ in an independent and identically distributed (i.i.d.), uncorrelated, Rayleigh fading channel. To achieve a constant data transfer rate, in the simulation, we used binary phase shift keying (BPSK) baseband modulated data symbols in $\boldsymbol{\mathcal{G}}_2$ encoding scheme and quadrature phase shift keying (QPSK) in both $\boldsymbol{\mathcal{G}}_3$ and $\boldsymbol{\mathcal{G}}_4$ encoding schemes. Comparing between these error performance curves, it can be clearly seen that the $\boldsymbol{\mathcal{G}}_4$ encoding scheme which requires 4 transmit antennas and offers a diversity gain of $N_t N_r = 4$ has the best error performance and $\boldsymbol{\mathcal{G}}_2$ encoding scheme which requires only 2 transmit antennas and offers a diversity gain of $N_t N_r = 2$ has the worst error performance out of all three schemes. Although, $\boldsymbol{\mathcal{G}}_2$ encoding scheme performed worst, it offers no rate loss in transmission and requires only 2 transmitting antennas. Comparing the error-rate of $\boldsymbol{\mathcal{G}}_2$ to un-coded system also employs 2 transmit and 1 receive antenna, $\boldsymbol{\mathcal{G}}_2$ evidentally improved the error-rate performance dramatically with a simple encoding and decoding algorithm.

The Bit-error rate (BER) and symbol-error rate (SER) performance curves of different OSTBC encoding schemes, $\boldsymbol{\mathcal{G}}_2$, $\boldsymbol{\mathcal{G}}_3$, and $\boldsymbol{\mathcal{G}}_4$, are depicted in Fig. 2.19 with 1 bit/sec/Hz transmission rate and $N_r = 1$ in GBHDS, correlated, macrocell channel with Rayleigh fading gains. Recall

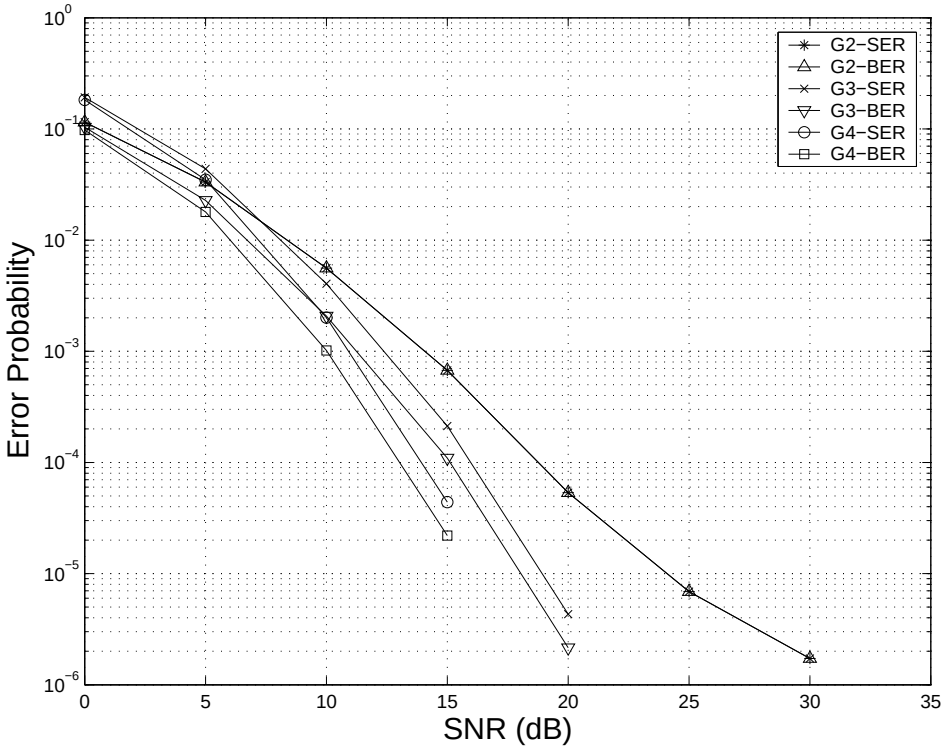

Figure 2.18: BER and SER performances for $\boldsymbol{\mathcal{G}}_2$, $\boldsymbol{\mathcal{G}}_3$, and $\boldsymbol{\mathcal{G}}_4$ encoding schemes in i.i.d. channel with 1 bit/sec/Hz transmission rate and $N_r = 1$.

that wireless systems operating in a correlated channel environment can potentially degrade system performance. In Fig. 2.19, we use computer simulation to show the effect of correlated channel fading on the error-rate performance of OSTBC encoding schemes. Comparing the curves in this figure to the corresponding ones in Fig. 2.18, we can see there is a clear performance loss in all three schemes when OSTBC encoded systems operate in correlated channel environment. This observation is very consistent with findings reported in [45] and [46] and the amount of losses is subject to the degree of correlation which depends on the antenna separation distance and scattering environment, and thus, the angular spread of multipath signals.

Space-Time Trellis Coding

With simple encoding and decoding algorithms, space-time block codes can achieve a maximum diversity order of $N_t N_r$ in frequency-flat channels. However, they provide no coding advantage and may introduce bandwidth expansion when the number of antennas is greater than two. On the other hand, Tarokh *et al.* proposed a different space-time coding scheme called *space-time trellis coding* (STTC) where its codeword construction is based on rank and determinant design criteria to provide a maximum diversity and coding gain. It is shown in [42] that system

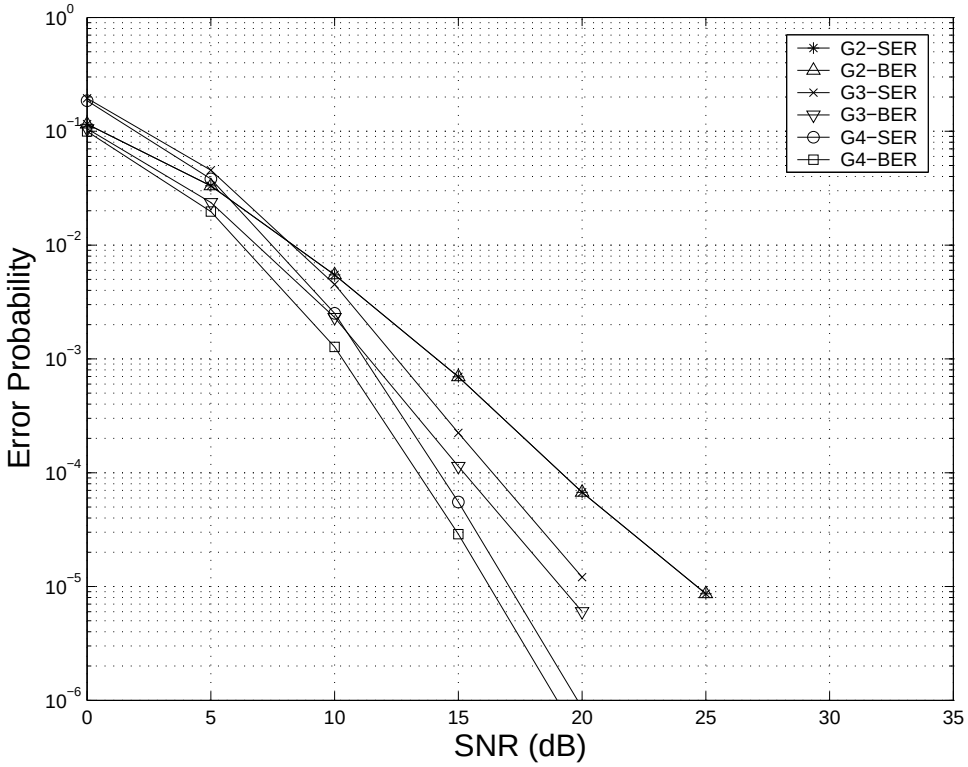

Figure 2.19: BER and SER performances for $\boldsymbol{\mathcal{G}}_2$, $\boldsymbol{\mathcal{G}}_3$, and $\boldsymbol{\mathcal{G}}_4$ encoding schemes in GBHDS macrocell channel with 1 bit/sec/Hz transmission rate and $N_r = 1$.

performance improvement from adopting the STTC scheme is dominated by the diversity gain determined by the rank of certain matrices and the coding gain determined by the determinant of these matrices. In slow fading frequency-flat channels, these matrices can be constructed from pairs of distinct channel codewords. In fast fading frequency-flat channels, system performance improvement is dominated by the diversity gain determined by the generalised Hamming distance of certain sequences and the coding gain determined by the generalised product distance of these certain sequences. These sequences can be constructed from pairs of distinct channel codewords.

The capability of STTC scheme in combating channel fading effects came from its joint design of error correction coding, modulation, transmit and receive diversity to develop an effective signalling scheme [129]. When constructing space-time trellis codes, the encoder maps a sequence of binary data into N_t modulated symbols streams before they are transmitted via N_t transmit antennas. This mapping process is described by a trellis diagram and an example of such mapping for four-states, 4-PSK, $N_t = 2$, and 2 b/s/Hz of transmission is illustrated in Fig. 2.20 (b), assuming 4-PSK signal constellation points are labelled as in Fig. 2.20 (a).

According to [42], the mapping process requires that at the beginning and the end of each frame, the encoder must in the zero state and each transition branch in the trellis representation

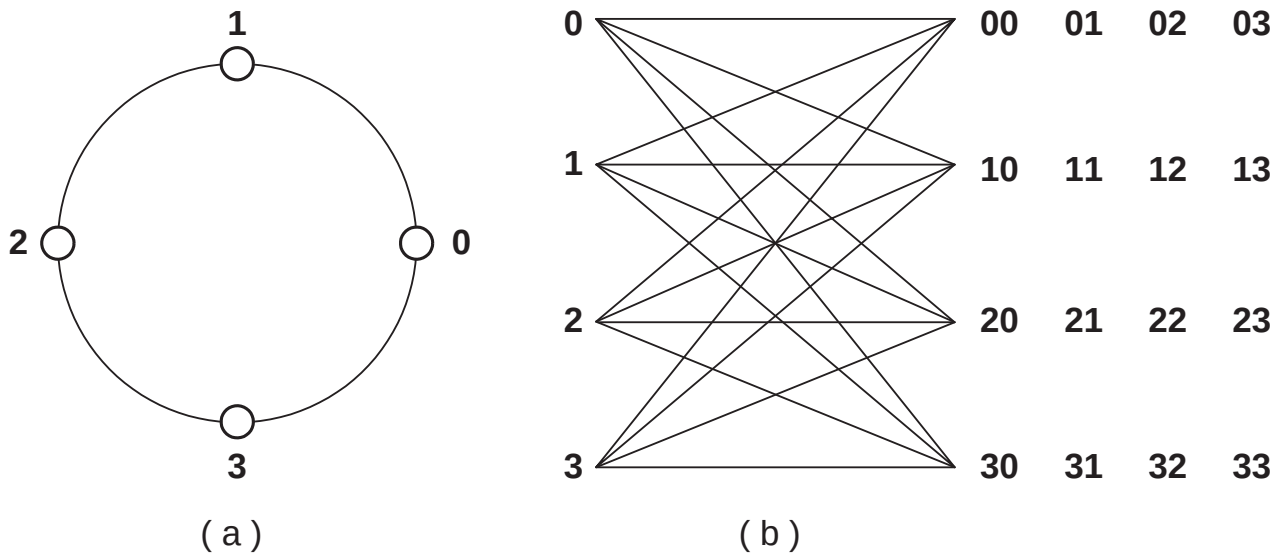

Figure 2.20: (a) 4-PSK signal constellation. (b) 4-PSK space-time code, 4-states, 2 b/s/Hz.

is labelled with a unique sequence of constellation elements. At each time t, depending on the state of the encoder, if the input bits choused a transition branch with a label $c_t^1 c_t^2 \cdots c_t^{N_t}$, then this corresponds to sending the symbol c_t^j via antenna j for all $j = 1, \cdots, N_t$. More mapping examples with different signal constellations and transmission rate can be found in [42].

In principle, decoding of STTC codeword requires a maximum-likelihood sequence estimator and it is generally implemented with the Viterbi algorithm. It is reported in [47] and [129] that the complexity of this decoding algorithm increases dramatically with the memory length of the trellis code, resulting in longer processing time, and making the simpler OSTBC diversity coding scheme is more favorable in practice. For this reason, we study the performance of OSTBC scheme only in the remaining chapters.

Diversity Coding for OFDM Systems

OFDM is a multi-carrier modulation technique that divides the total available frequency spectrum into a large number of overlapping and narrow sub-bands (sub-carriers) which enables parallel transmission of information data [136, 137]. Thus, making this technology very bandwidth efficient (suitable for high-speed communication) and resistance to intersymbol interference (ISI), which commonly exits in broadband single carrier systems. Due to the fact that each of the sub-carriers transports individual information data simultaneously during the transmission, diversity coding for OFDM systems can take an advantage of the additional diversity branches in the frequency domain.

Motivated by the fact that conventional STC encoder can potentially be used for broadband

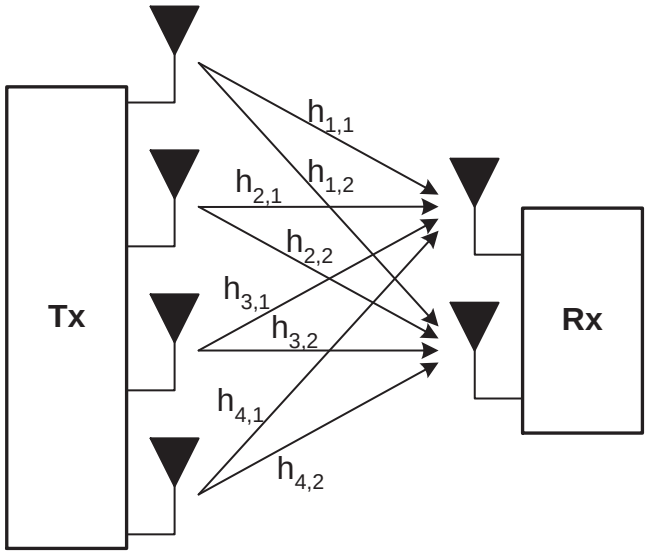

Figure 2.21: Multiple-input multiple-output (MIMO) system.

OFDM systems, there have been enormous amount of study and effort put into developing diversity coding schemes for broadband OFDM systems. Amount them, perhaps Agrawal *el al.* are the first ones to demonstrate this development [138]. Over the time, performance studies and proposals in utilising STC in OFDM system includes [47, 129, 129, 139–145]. Apart from these space-time coding techniques, studies of space-frequency coded OFDM systems have also being report in [146–149]. In order to maximise the diversity gain of diversity coding scheme, encoding across all three space, time, and frequency domains of OFDM system, space-time-frequency (STF) coding techniques have been proposed in [150–153].

In the following sections, other examples of transmit diversity techniques and structures that have been adopted in this thesis are presented. Wireless systems which employ multiple antenna elements at both the transmitter and the receiver are examined. The concept of antenna array is reviewed, in particular, the advanced space-time processing technique called adaptive antenna array or eigenbeamforming.

Capacity Enhancement Using MIMO Configuration

Many performance studies of wireless system employing multi-element antennas at both ends of the communication link have been investigated. In particular, channel capacity analysis of MIMO systems is one of the major topics of interest. In various literature published up to date, they have shown large gains in capacity improvement can be obtained in MIMO systems compared to SISO [121, 122, 124, 154–156], and [157] for OFDM systems.

A generic diagram that shows this type of systems is depicted in Fig. 2.21 with $N_t = 4$

and $N_r = 2$. We consider a simple scenario where the delay spread in the channel is small compared to the signal transmission bandwidth and the communication has no channel coding involved. Thus, frequency-flat Rayleigh fading can be reasonably assumed between the transmit and receive antenna pairs and we denote their time-varying channel impulse response between the i^{th} $(i = 1, 2, \cdots, N_t)$ transmit antenna and the j^{th} $(j = 1, 2, \cdots, N_r)$ receive antenna as shown in the diagram, $h_{i,j}$. Next, we further assume that $\{h_{i,j}\}$ are independent circularly symmetric complex Gaussian random variables with zero mean and unit variance, i.e., i.i.d. $\mathcal{CN}(0, 1)$. This assumption is often used to model the classical frequency-flat Rayleigh fading channel and known to be accurate in non-LOS environments with rich scattering and sufficient antenna spacing at the transmitter and receiver.

Denote ε_s as the total symbol energy at the transmitter and σ_n^2 as the power of noise per Hz. According to Shannon's capacity derivation in [158], the capacity of a band-limited SISO system in AWGN channel is expressed as

$$C = \log_2 \left(1 + \frac{\varepsilon_s}{\sigma_n^2}\right). \tag{2.54}$$

This Shannon capacity expression indicates the maximum possible rate at which information can be transmitted over a channel without any errors. It is often used as the theoretical limit which the spectral efficiency of proposing transmission strategies can be compared.

For a given $\mathbf{H}$, in this case $\mathbf{H} \in \mathbb{C}^{N_t \times N_r}$ is a channel matrix contains the previously described channel impulse responses, the Shannon capacity of a MIMO is given by the maximum mutual information (in bits/sec/Hz) between the $1 \times N_r$ received vector $\mathbf{r}$ and the $1 \times N_t$ transmitted vector $\mathbf{x}$ as [121] and [122]

$$I = \log_2 \det \left(\mathbf{I}_{N_t} + \frac{\gamma}{N_t} \mathbf{H}\mathbf{H}^H\right), \tag{2.55}$$

where $\gamma = \varepsilon_s/\sigma_n^2$ is the average SNR at the received antennas and the input-output relationship between $\mathbf{r}$ and $\mathbf{x}$ can be expressed as

$$\mathbf{r} = \sqrt{\frac{\varepsilon_s}{N_t}}\, \mathbf{x}\, \mathbf{H} + \mathbf{e}. \tag{2.56}$$

$\mathbf{e}$ is $1 \times N_r$ additive white Gaussian noise vector with zero mean and σ_n^2 variance. If signal transmission is spanned over an infinite number of independent fading blocks, the Shannon

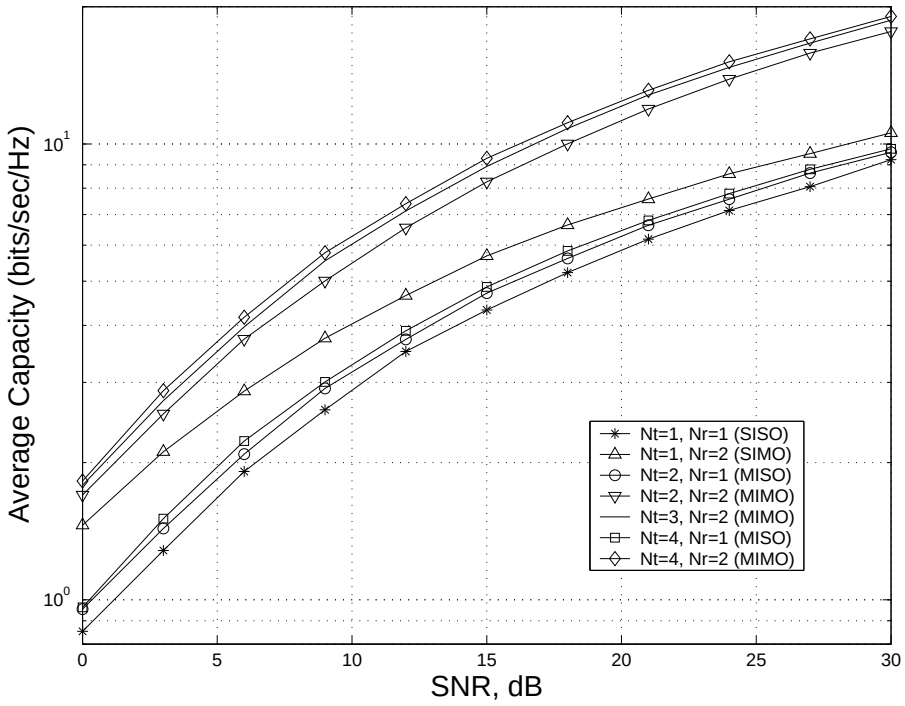

Figure 2.22: Average capacity for a system with different number of transmit and receive antennas.

Capacity, sometimes called *average capacity* or *ergodic capacity* exists and is given by

$$C = \mathcal{E}\{I\} = \mathcal{E}\left\{\log_2 \det\left(\mathbf{I}_{N_t} + \frac{\gamma}{N_t}\mathbf{H}\mathbf{H}^H\right)\right\} = \sum_{i=1}^{N_t} \log_2\left(1 + \frac{\gamma}{N_t}\mu_i\right), \tag{2.57}$$

where $\mu_1 \leq \mu_2 \cdots \leq \mu_{N_t}$ are the ordered eigenvalues of channel's covariance matrix, $\mathbf{H}\mathbf{H}^H$.

In Fig. 2.22, we showed the comparison between the average capacities of systems with different number of transmit and receive antennas as a function of the SNR. It can be easily observed from the graph that there is only a small improvement in capacity for systems employing an additional transmit antenna while there is an approximate 3 dB gain in SNR for an additional receive antenna. This can be explained by the fact that by employing an additional receive antenna in the system effectively doubles the received signal power. For systems with extra transmit antennas can, however, be more effective only in combating channel fading effects. Finally, by comparing the MIMO systems with SISO system, we observed a dramatic capacity enhancement in a order of two, which is a promising result.

2.3.5 Adaptive Antenna Array Systems

The fundamental concept of adaptive antenna array (AAA), also commonly known as *beamforming array*, is the spatial filtering of signals at an antenna array output to provide an enhancement

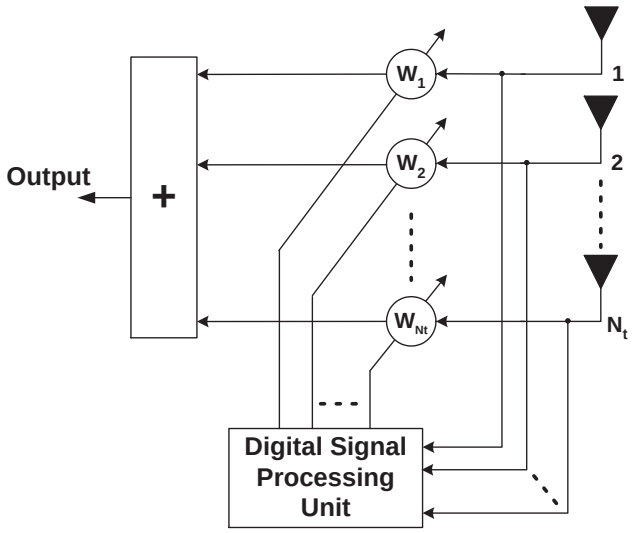

Figure 2.23: Generic diagram of an adaptive antenna array system.

in the signal amplitude coming from a direction of interest and possibly rejection (or "null") in the interfering directions. In general, the array collects samples of propagating wave in space and manipulate by a signal processor to discriminate interference signals from the intended signal to form a desire beam. A generic diagram of a adaptive beamformer is shown in Fig. 2.23, where radio frequency (RF) signal is first captured by the antenna array and down-converted into digital baseband signals before they are processed by a digital signal processor (DSP). Based on the design or performance criteria, the DSP then weights these digital signals from each of the array elements differently such that when they are added together, they form a desire output beam. These description is given as if the adaptive array system is operating in a receive mode. When operating in transmit mode, the system functions in a similar way.

Early studies of adaptive array systems appear in the literature started in late 1950's [159] and in 1960's [160–163]. Their wide range of applications includes radar and anti-jamming systems in [164] and [165], respectively. One of the major contributions in the area of adaptive beamforming was made by Howells who proposed the intermediate frequency sidelobe canceller for adaptive nulling in 1959 [159]. Since then, optimal combining schemes were also introduced in order to minimize different criteria at the beamformer output. These include the minimum mean-square error (MMSE) criterion in least mean-square (LMS) algorithm proposed by Widrow [161] by using a reference signal, the concept of fully adaptive array using the signal-to-interference-and-noise ratio (SINR) criterion proposed by Applebaum [160], and the look-direction constraint that resulted in a minimum variance distortion-less response (MVDR) beamformer proposed by Capon [166]. A rather comprehensive collection of a list of references in array signal processing

can be found in [48, 118, 120, 167]. Besides forming desire antenna output beams, another closely related application of adaptive antenna array systems is AoA estimation for source or target localization purpose. Leading AoA estimation methods are the MUSIC and ESPRIT algorithms in [168, 169] and [170, 171], respectively. Recently, direction finding using higher order statistics can be used to improve the estimation accuracy [130, 131].

Since the radio frequency spectrum is a finite and valuable resource in mobile radio systems, the adaptation of versatile beamforming technique for maximising the SINR and SNR in mobile channel environment is of great interest. It has been shown in [134, 135] that by combatting co-channel interference, it is possible to achieve a high frequency spectrum efficiency.

Two immediate benefits of adopting adaptive beamforming in mobile radio systems are:

- Directional gain - array gain
- Interference cancellation

These ultimately can result in improved system capacity, increased area of coverage, better error-rate performance, and higher spectral efficiency. With all these benefits, it leads to better quality of services and higher earnings for operators. Therefore, it has been widely recognised in the industry that the adaptive beamformer plays an important role in improving the performance of both downlink and uplink transmissions in the future generation of mobile communications.

There are two main types of adaptive beamforming strategies in mobile radio systems; switched-beam and adaptive-beam. Switched-beam strategy antenna system has a pre-defined set of fixed-beams and the BS selects one of these beams patterns that has the strongest signal towards the MS. However, the selected beam may still not be directly pointing to the MS and nulls of the beam may not be pointing to the interfering sources. Adaptive-beam strategy antenna system on the other hand uses algorithms that iteratively adjust its steering weights to track the intended MS with main lobes and interferers with nulls such that the link budget is constantly maximised. In this thesis, we concentrate on the adaptive-beam strategy and use one of its advanced beamforming techniques, eigenspace based adaptive beamformer.

Eigenspace Based Adaptive Beamformer

As the multipath fading is the most undesirable propagation effect from which the wireless systems can experience, the classical maximum-ratio combining (MRC) technique which maximises the SNR at the output of the combiner by linearly weighting the received signal from each of the receiving antennas with channel estimates, is often used as a receive diversity technique to combat multipath fading [172]. In the case where receivers (mobile terminals) do not

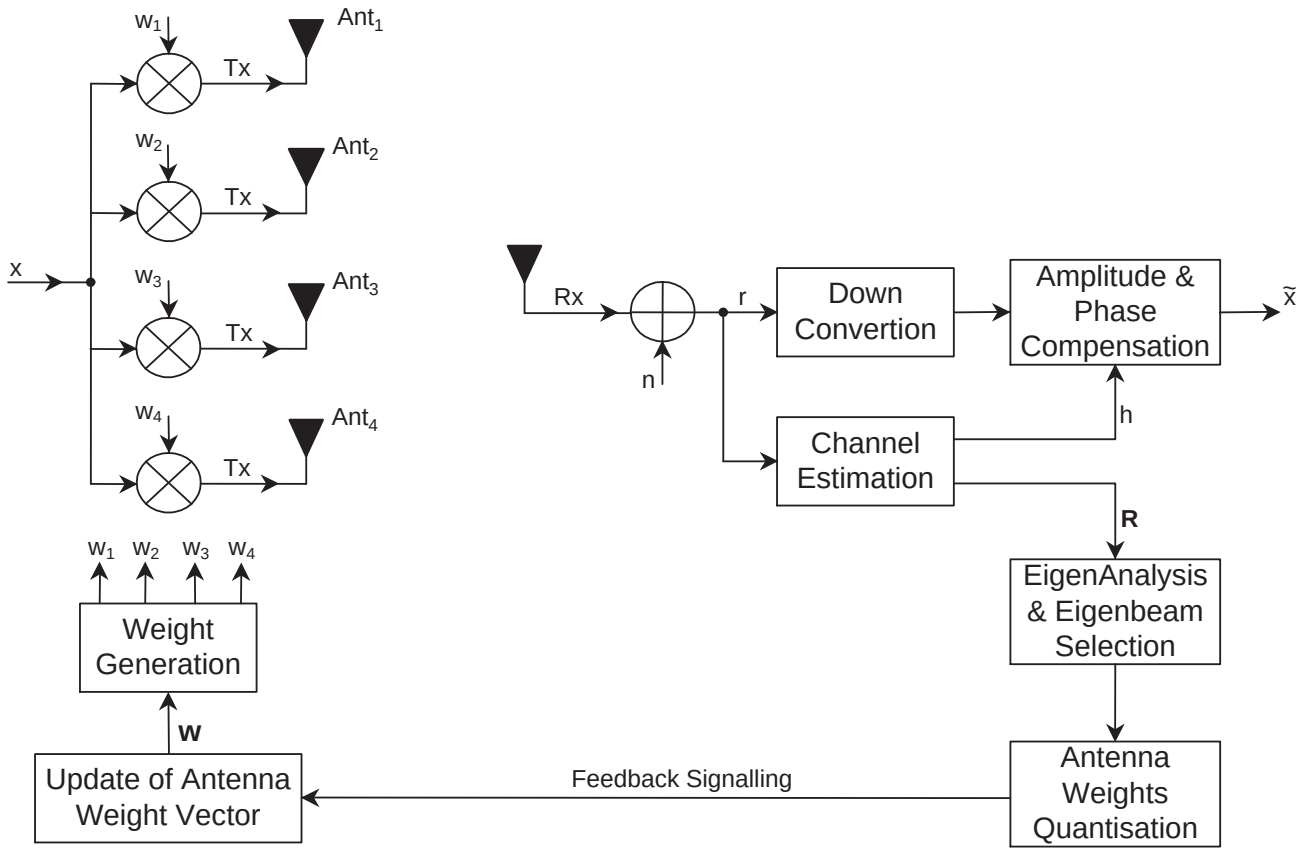

Figure 2.24: General structure of a closed-loop downlink eigenbeamformer.

have the freedom of employing multiple antennas due to limited space, a MRC-like diversity scheme, eigenbeamforming, has recently becoming a popular transmit diversity technique in the application of mobile communications [49, 172–178].

Generally, when instantaneous channel state information is available at the transmitter, the concept of eigenbeamforming can be used to transmit signal in the strongest eigenvector (eigen-mode) of the channel realisations by linearly transforming data symbols with a set of optimal complex antenna weights such that received data signal power is maximised. Over time, this eigenbeamforming scheme has been continuously studied. Until recently, the performance and feasibility studies of adopting this technique in W-CDMA systems have been intensively investigated in [49] references within.

In this thesis, we investigate ways in improving the performance of this eigenbeamforming technique that is adaptive to the wireless fading channel during a downlink transmission. With an exception in chapter 8, the adaptive eigenbeamformer is used for optimising the received SNR during uplink transmissions.

To utilise the eigenbeamforming concept in mobile communication systems, one possible technique is the feedback based downlink eigenbeamforming scheme in [49], where spatial correlation

property of the wireless channel is exploited to achieve a maximum instantaneous SNR at the MS. The principle idea behind this eigenbeamformer is a de-correlation of spatially correlated signal paths by performing eigenanalysis on the spatial covariance matrix of the channel. The eigenbeams that correspond to the largest eigenvalues are determined and quantised before they are fed back to the BS. A general structure of this *closed-loop* eigenbeamforming operation is depicted in Fig. 2.24.

To evaluate the performance of a downlink eigenbeamformer, let us first consider a scenario where BS ULA uses 4 antenna elements. Data transmission via BS antennas comprises of a base-band modulated information symbol which has being transformed by a set of antenna steering weights and a pilot signal that is not being transformed by any steering weights. At the MS, the pilot signal is received by a single antenna and used for estimating channel fading coefficients and temporal taps of the multipath channel. These channel fading estimates are then used for compensation of corrupted information symbols and computation of antenna beamforming weights. Let $\mathbf{h}_\ell := [h_{1,\ell}, h_{2,\ell}, h_{3,\ell}, h_{4,\ell}]^T$ be the channel vector of the ℓ^{th} temporal tap containing channel fading gains from the BS antennas. The channel covariance matrix which describes spatial correlation between signals transmitted from different BS antennas is given as

$$\mathbf{R} = \sum_{\ell=1}^{L} \mathbf{h}_\ell \mathbf{h}_\ell^H. \tag{2.58}$$

Then signal de-correlation is carried out at the MS by performing eigenanalysis (eigen - decomposition) of this spatial covariance matrix as

$$\mathbf{R} = \mathbf{V}\mathbf{D}\mathbf{V}^H, \tag{2.59}$$

where columns of $\mathbf{V} := [\mathbf{v}_1, \mathbf{v}_2, \mathbf{v}_3, \mathbf{v}_4]$ are the eigenvectors (eigenbeams) of $\mathbf{R}$ and $\mathbf{D} := \text{diag}[\mu_1, \mu_2, \mu_3, \mu_4]$ is a diagonal matrix contains the corresponding eigenvalues. According to [49], this eigenbeamformer has an ability to adapt to various channel environments (spatially correlated or uncorrelated). Thus, making it very attractive to adopt in cellular communications.

In order to maximise the instantaneous received SNR at the MS, selection of eigenbeams that are to be fed back and used at the BS is done according to the following calculation as

$$P_m = \mathbf{v}_m^H \mathbf{R}^T \mathbf{v}_m = \sum_{\ell=1}^{L} |\mathbf{v}_m^T \mathbf{h}_\ell|^2. \tag{2.60}$$

Then the eigenbeam that results in the maximum received signal power P_m is quantised and

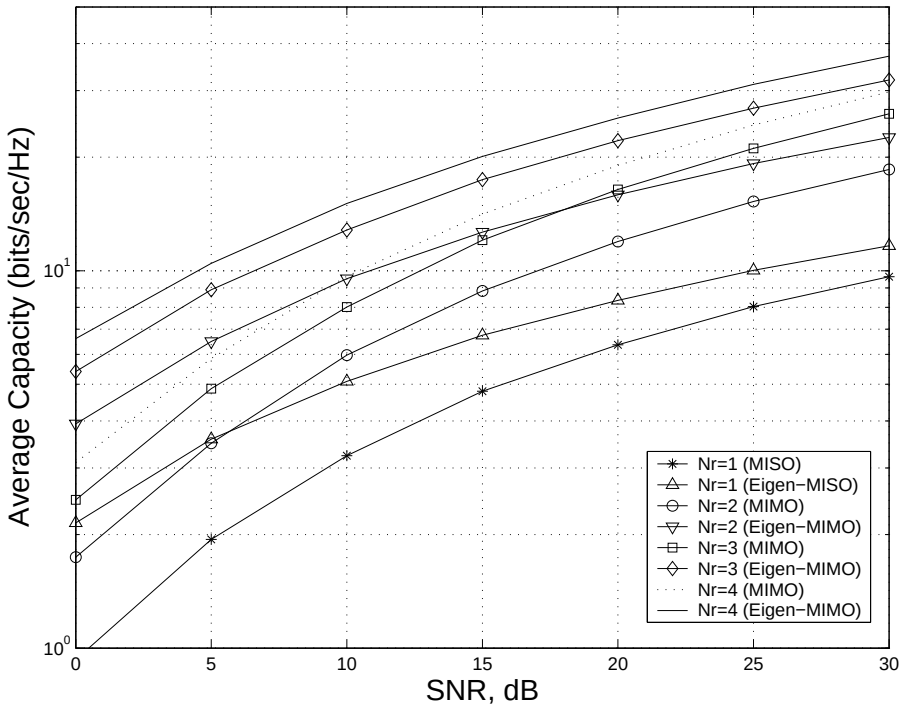

Figure 2.25: Illustration of average capacity improvement of Eigenbeamforming systems with 4 transmit and different numbers of receive antennas in 3GPP correlated fading channels.

signalled to the BS. Alternatively, weighted combining selection can be used as

$$P_m = \mathbf{w}_m^H \mathbf{R}^T \mathbf{w}_m = \sum_{\ell=1}^{L} |\mathbf{w}_m^T \mathbf{h}_\ell|^2, \tag{2.61}$$

where m describes the degree of the combining phase. Let μ_1 and μ_2 be the first and second largest eigenvalue of the covariance matrix $\mathbf{R}$, respectively. Then

$$\mathbf{w}_m = \mathbf{v}_1 + (\sqrt{\mu_2}/\sqrt{\mu_1})\mathbf{v}_2 \exp(j\theta_m) \tag{2.62}$$

$$\theta_m \in \{\pi/2 \; 3\pi/4 \; -3\pi/4 \; -\pi/4\}. \tag{2.63}$$

To demonstrate the improvements that this eigenbeamforming scheme can provide to mobile communication systems, a computer simulation to evaluate the average capacity and error-rate probability performances in a 3GPP specified correlated channel environment [179] has been conducted. For fairer comparison between performance results, it is assumed that the mobile system benefits from no spreading gain, which is an additional gain in W-CDMA systems. In Figure 2.25, the capability of eigenbeamforming scheme in improving the average capacity of mobile wireless systems with four transmit and different number of receive antennas is shown.

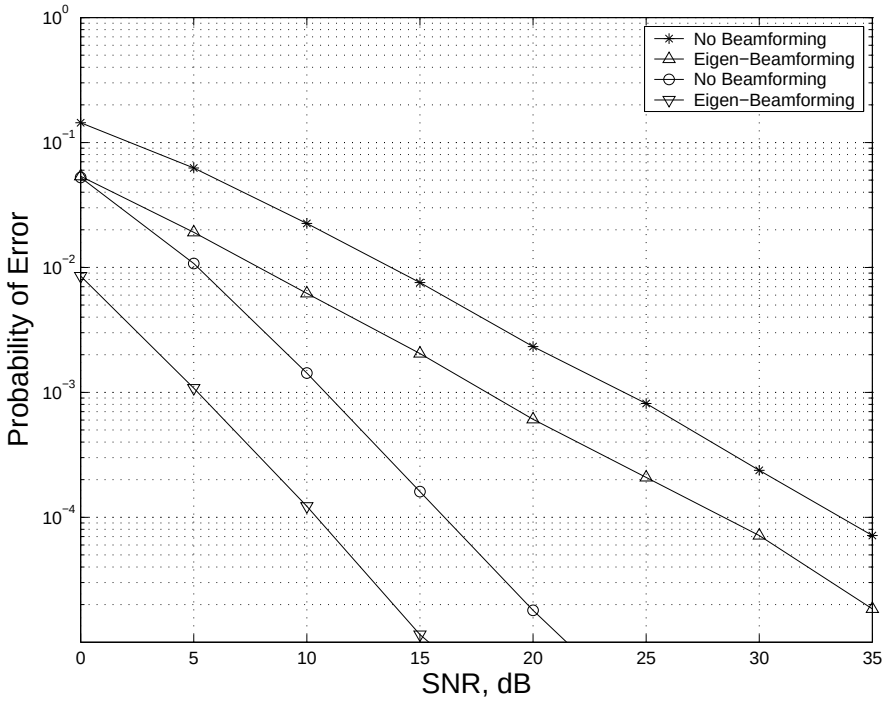

Figure 2.26: BER of Eigenbeamformer.

Comparing the performance curves with the same number of receive antennas, it is observed that there is a 6 dB SNR gain at a capacity of 10 bits/sec/Hz from adopting eigenbeamforming scheme and this gain is uniform across systems with different number of receive antennas.

Figures 2.26 and 2.27, show the bit-error rate (BER) and symbol-error rate (SER) performance improvement using an eigenbeamforming scheme in a system with $N_t = 4$ and different number of receive antennas, respectively. Comparison of performance curves for systems with and without eigenbeamforming scheme, shows that there is a 6 dB difference in SNR uniformly across systems with different number of receive antennas, which is consistent with the performance improvement in average capacity results. In conclusion, the 6 dB improvement in both error-rate probability and average capacity can be explained by the amount of enhancement in the received SNR at the MS as a result of concentrating transmitted radio energy in the direction of dominant multipaths.

2.4 Summary

In the first part of this chapter, a review of various image compression techniques has been presented. A mathematical model for the sampling of digital images was detailed. This was followed by a review of current image coding techniques with a focus on the application of

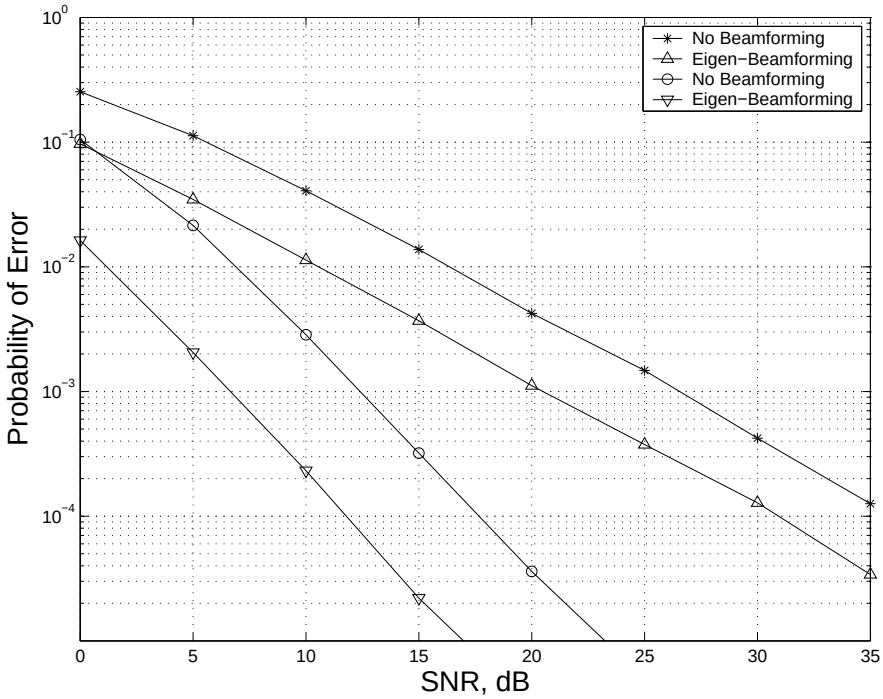

Figure 2.27: SER of Eigenbeamformer.

wavelets for image compression. In addition, the performance metric commonly used to assess the quality of images has been defined. Also, examples of standard test images used in image processing applications are provided.

The second half of this chapter presented an overview of the key elements found in mobile communication systems, particularly the digital signal-processing functions required to support the transmission of user data over mobile radio channels. The characteristics of radio wave propagation (such as multipath fading) in a mobile environment have been described. In order to understand and model the distortion a wireless channel has on radio signals, details of the propagation effects such as log-normal shadowing and small scale multipath fading have been discussed. A recently-developed geometrical channel model, known as the geometrically-based space-time channel (GBHDS) model, has been described. This model will be the basis for testing channel effects in our simulations. In addition, we have also reviewed various transmit diversity techniques such as space-time block coding (STBC) and antenna beamforming.

Chapter 3

Multimedia Communication over Space-Time Beamformed OFDM

3.1 Introduction

Transmit diversity has become one of the most popular and important research areas in the field of wireless communications, particularly, for applications in mobile communication systems. The application of space-time (ST) coding to OFDM systems was first introduced in [138] to achieve high data-rate transmissions for delay-sensitive services. As discussed in Chapter 2, a popular space-time (ST) coding is Alamouti's space-time block code [40], which has proven to be an effective and practical transmit diversity technique in enhancing not only the error performance but also the capacity of wireless systems; an essential requirement for multimedia communication - mobile multimedia. The principal idea behind ST coding is the encoding of data across both space and time such that information is transmitted into different spatial directions including diversity in the temporal domain. The work in [40], later generalized and extended in [41, 42] as orthogonal-STBC (OSTBC), is a well-known ST coding scheme that demonstrates the capability in creating additional spatial and temporal diversity branches, and hence, providing considerable gain in error rate performance in systems with a multiple-input multiple-output (MIMO) channel configuration.

However, it is well known that maximum performance gain is only achievable in spatial uncorrelated channels. Studies in [45], [46], and [146] have shown that the performance of space-time codes and the capacity of multi-antenna systems degrade significantly in the presence of fading correlation. Combining coding with linear processing at the transmitter and the receiver, [180] showed that wireless transmission can be transformed into a set of parallel scalar channels and channel capacity is maximised in multipath environment. A similar approach is also used in [181] and [182], where they combined linear transmit formatting and STC to improve error-

rate performance of narrow-band systems with a feedback link. It has also been shown in [122] and [183], that the use of multiple antennas at both the transmitter and at the receiver can greatly improve the system performance and increase the capacity gain. Traditionally, receiver diversity techniques are employed to combat coherent deep fades of wireless channels by placing additional antennas at the receiver. In practice, however, it is more cost effective to use multiple antennas at the BS only. Therefore, in recent years the focus of transmit diversity techniques has been to optimise transmission at the BS antenna array.

In the context of transmit diversity, adaptive beamforming (AB), also known as adaptive eigenbeamforming, is a different approach to ST coding as it is primarily concerned with the optimisation of the directional gain of an antenna array. In Chapter 2, we have shown how the system performance of wireless communication channels can be enhanced when full or a partial knowledge about the propagation/channel environment is available at the transmitter in order to mitigate the fast fading and multi-path effects of mobile channels. In a multi-antenna array system, the use of both short-term and long-term channel characteristics are important in determining the direction of strongest signal path; which is obtained by performing eigen-analysis (eigenvalue decomposition) of the long-term spatial covariance [49]. This provides a mechanism for de-correlating the spatially correlated signal paths. Antenna weights are computed based on uplink path angle (channel) estimates and adapted to the changing channel conditions, such that an optimal antenna output beam is resolved and the signal power or signal-to-noise ratio (SNR) at the receiver (MS) is maximised.

By combining the STBC and adaptive beamforming techniques as shown in [184–187], greater improvement in error rate performance in a spatially correlated channel environment can be achieved. This is demonstrated in Figure 3.1, which shows the resulting error performance curves in bit-error-rate (BER) and symbol-error-rate (SER) for OFDM systems that are uncoded, systems using O-STBC only, and systems using O-STBC with adaptive beamforming (O-STBC-Eigen). The technique presented by the author in [184, 185] has been extended further and applied to broadband OFDM systems [186].

In this chapter, we introduce a diversity coded OFDM transmission system for multimedia communication that utilises a space-time block coding and an adaptive beamforming strategy. A multimedia simulation framework (MSF) is developed to investigate and analyse the performance characteristics of the system in the application of digital images. This method can be extended to study the transmission of other sources of multimedia information such as digital video. Subsequent sections of this chapter have been organised as follows: In Section 3.2, details of the multimedia framework used as the basis for simulating the transmission of multimedia data

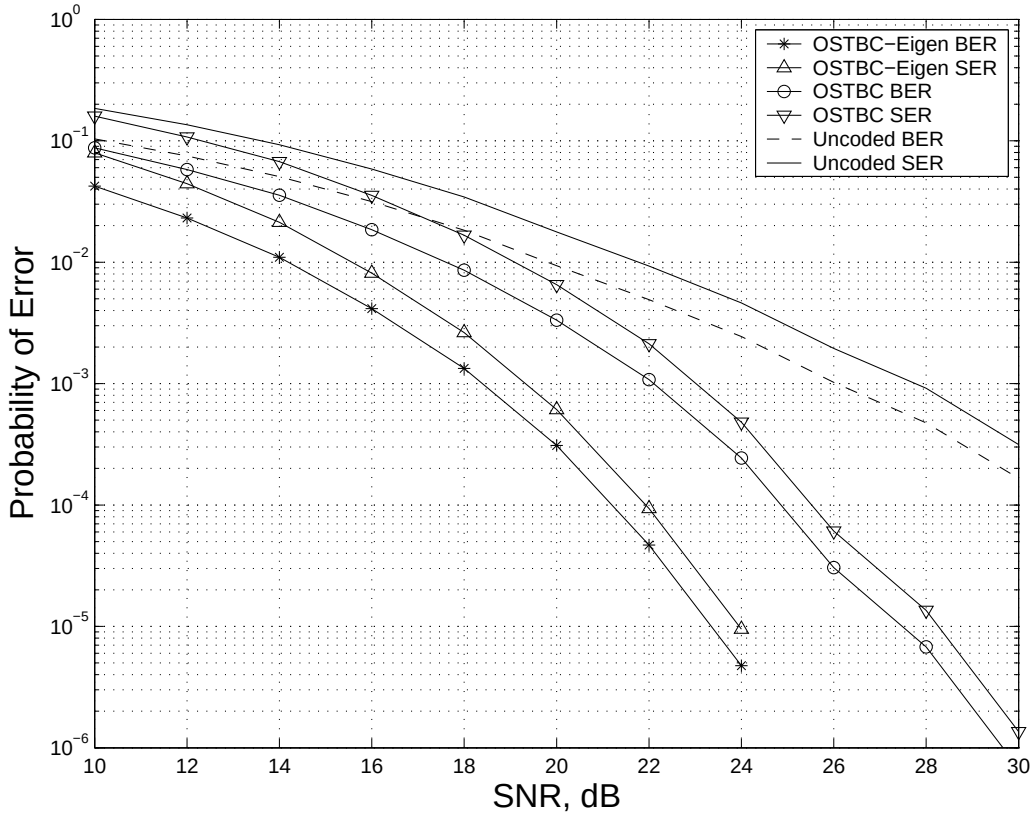

Figure 3.1: Error performance curves of uncoded-OFDM, OSTBC-OFDM, and OSTBC-Eigen-OFDM systems in GBHDS correlated fading channels.

are presented. Importantly, the mathematical treatment of the space-time block coded OFDM model is described in Section 3.2.2 with a review of the adaptive beamforming technique given in Section 3.2.4. Section 3.3, presents the simulation results based on the application of digital images. Concluding remarks are presented in Section 3.4. Note, the following notation has been adopted in this work: $(.)^T$, and $(.)^H$ are vector and Hermitian transpositions, respectively. $\|\mathcal{A}\|_F$ and $\sqrt{\mathcal{A}}$ denote the Frobenius norm and Hermitian square root of matrix $\mathcal{A}$. Finally, capital bold letters represent matrices, and small underlined letters denote vectors.

3.2 Multimedia Simulation Framework

The simulation environment used to create a developmental framework for the analysis and application of 'real' multimedia data over a space-time coded OFDM wireless system with adaptive beamforming has been established using MATLAB® [188]. One of the key advantages of using MATLAB® to simulate the multimedia component of the framework is the availability of a number of 'toolboxes', which provide extensive support for the development of complex multimedia and signal processing models [189]. To enable the simulation of multimedia data over the

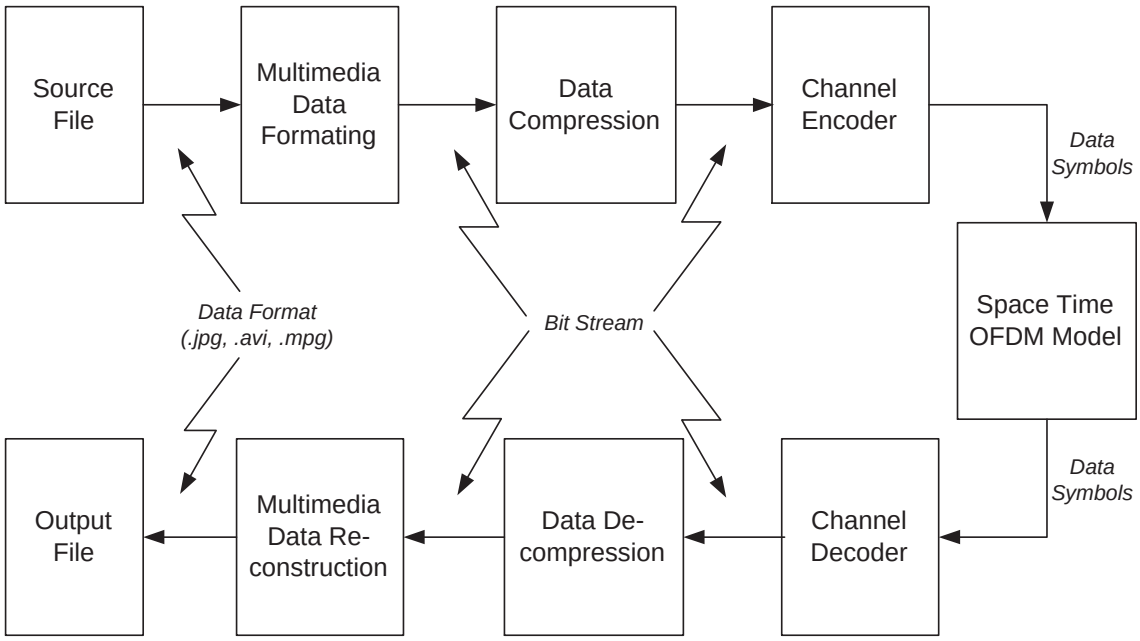

Figure 3.2: Simulation framework (MSF) employing ST-OFDM-AB processing for multimedia communication.

ST-OFDM system, a process for converting multimedia signals from various data sources such as, compressed image and video files (which may be stored on different computing platforms) has been developed. Based on the functional blocks typically found in a digital communication system (as described in Chapter 2), the multimedia processing blocks have been integrated together with the transmission scheme outlined in [185] to form the overall multimedia simulation framework (MSF). Figure 3.2 depicts the general structure of the system model, clearly showing the transformation of multimedia data to a suitable data format which can be further processed by the space-time coded OFDM block with adaptive beamforming (ST-OFDM-AB).

3.2.1 Preprocessing of Multimedia Data

The principal idea behind the MSF system model is to first consider the source file, which is a digitized version of the original multimedia signal with N-bit resolution, as a vector array containing integer quantization levels. For digital audio, these correspond to sampled amplitude values, and for digital image and video coding they correspond directly to pixel values [26]. Before the multimedia data can be further processed by the space-time OFDM block, the source data is converted into a matrix array containing N bit-words which correspond to the sample/ pixel levels. Thus, a bitstream representing the original multimedia data is created. For real systems, the source information can be derived from different computing platforms such as, personal computers, embedded wireless devices, and large data storage systems/servers. In the

case of mobile multimedia, this can be data transmitted from another user's MS or alternatively originating from the core network such as, the Internet.

In order to reduce the transmission bandwidth utilised in the system, the framework includes a source encoder for removing redundant information from the multimedia data by using a compression algorithm such as, transform and subband coding. A channel encoder to convert the bitstream to the required baseband modulated data symbols $\{s(n)\}_{n=0}^{N_s-1}$, as specified by the space-time OFDM model, has also been implemented. In the receiver path, the reverse is performed on the modified data symbols $\{\hat{s}(n)\}$ produced by the space-time OFDM transmission scheme in [185]. Whereby, the data symbols are first converted back to a bitstream by the channel decoder, and are subsequently reconstructed (via the de-compressor) back to the original multimedia data type/ format applied to the system.

It should be noted that, due to practical resource limitations (such as high computational power requirements and the often long simulation times experienced), the multimedia simulation framework has been initially configured for the signal-processing of digital still images.

3.2.2 The Space-Time OFDM Model

Figure 3.3 depicts a general structure of the transmission scheme for an OFDM system in a MIMO channel configuration employing N_t and N_r antennas at the transmitter and receiver, respectively [50]. The OFDM system we consider here utilizes N_c frequency tones and the channel is also assumed to be frequency-selective. Effective spatial correlation between BS uniform linear array (ULA) antennas is assumed. At the transmitter, a sequence of N_s multimedia baseband modulated data symbols $\{s(n)\}_{n=0}^{N_s-1}$ is first space-time (ST) encoded into codewords $\{\mathbf{C}_k \mid k = 1, \cdots, N_c\} \in \mathcal{C}^{p\times N_t}$, using N_t antennas and p adjacent OFDM symbols. Before the stage of inverse Fourier transformation (IFFT) and transmission, encoded subcarriers are split into a set of N_t parallel symbol sequences and linearly transformed by the adaptive beamforming weights.

A uniform linear array (ULA) configuration is assumed for N_t transmit antennas with a spacing of d meters between adjacent antenna elements. In the reverse link (uplink), transmission occurs over a multi-path channel environment. Let the ℓ^{th} path signal impinging on an ULA have an angle-of-arrival (AoA) of ϕ_ℓ. The array propagation vector can be expressed as $\underline{a}(\phi_\ell) := [1,\ e^{j\beta},\ e^{j2\beta},\ \cdots\ , e^{j(N_t-1)\beta}]^T$ where $\beta = (2\pi \cdot d \cdot \sin(\phi_\ell))/\lambda$ and λ being the carrier frequency wavelength. In general, the spacing between the elements of ULA at the transmitter is not large due to the condition at the antenna site to have zero cross-correlation factor, a typical

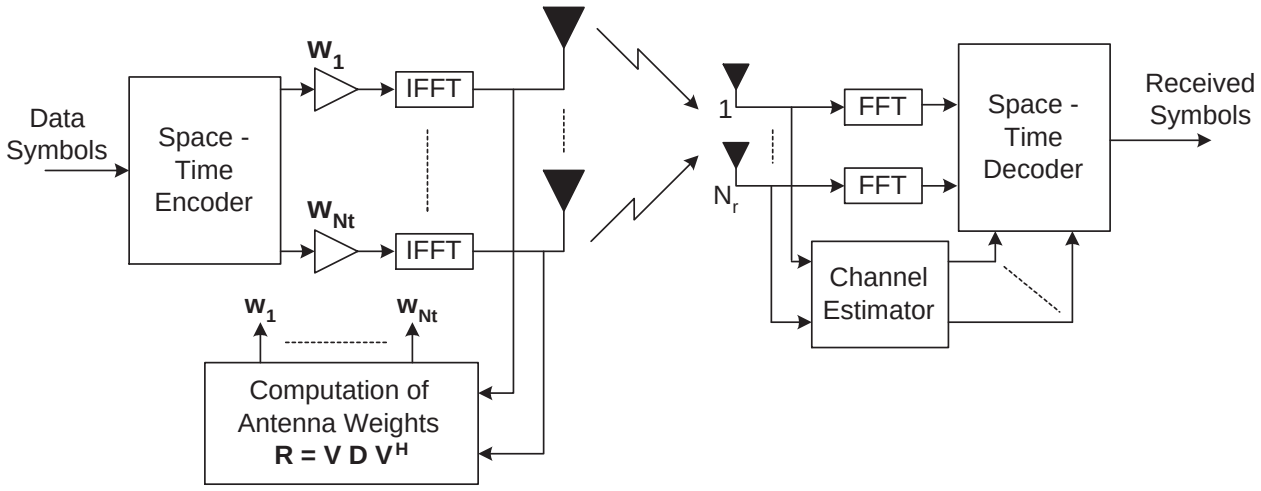

Figure 3.3: The ST-OFDM system model with adaptive beamforming.

scenario in cellular network. Therefore, spatial correlation between antenna elements would be effective. This correlation is defined in [179] based on the geometric scenario characterized by AoA. According to [179], the spatial covariance matrix that specifies the spatial correlation between antenna elements is given by:

$$\mathbf{R} = \frac{1}{L}\sum_{\ell=1}^{L} \underline{a}(\phi_\ell)\underline{a}^H(\phi_\ell) \tag{3.1}$$

where L denotes the number of dominant resolvable paths. In this thesis, we assume that spatial channel correlation at the receiver side is zero, hence, only the transmitter side will be considered. This means that $\mathbf{R}_r = I$, and we use $\mathbf{R}$ to denote $\mathbf{R}_t$ (commonly used notation).

Antenna Weights Computation

To maximize the transmitted signal power along the dominant multipaths, eigen-decomposition of the spatial covariance matrix should be performed, then we apply the resulting antenna weights given by the eigenvector that corresponds to the largest eigenvalue. The eigen-decomposition has the following form:

$$\mathbf{R}_\mathrm{t} = \mathbf{V}\mathbf{D}\mathbf{V}^H \tag{3.2}$$

where $\mathbf{D} := \mathrm{diag}(\mu_1,\ \mu_2,\ \cdots, \mu_{N_t})$ is a diagonal matrix with ordered eigenvalues on the main diagonal and $\mathbf{V}$ is a unitary matrix composed of the corresponding eigenvectors. Hence, the transmit weight vector $\mathbf{w} := [w_1,\ w_2,\ \cdots, w_{N_t}]^T$ can be found as the first column of $\mathbf{V}$ and the

transmission on different eigenvectors will lead to uncorrelated channel fading.

Received Signal Model

Denote $\underline{g}_{i,j} = [g_{i,j}(0), \cdots, g_{i,j}(L-1)]$ to be the L-tap channel impulse response vector between $(i,j)^{\text{th}}$ transmit-receive antenna pair. The elements of this vector are modeled according to the geometrical-based hyperbolically distributed scatterers (GBHDS) channel model in [110] with Jakes power spectral density. The frequency response of the k^{th} subcarrier for the same antenna pair can be expressed as $h_{i,j,k} = \underline{g}_{i,j}\underline{f}_k$, where $\underline{f}_k = [1, e^{-j2\pi(k-1)/N_c}, \cdots, e^{-j2\pi(k-1)\tau_{L-1}/N_c}]^T \in \mathbb{C}^{L\times 1}$ are the corresponding discrete Fourier transform coefficients.

Now, let us represent the antennas weights vector $\underline{w}$ as $\mathbf{W} := \text{diag}(w_1,\ w_2, \cdots\ , w_{N_t})$, and apply $\mathbf{W}^H$ to the space-time encoded codeword $\mathbf{C}_k$ prior to transmission. Then the discrete time baseband equivalent expression of the combined received signal has the form:

$$\mathbf{Y}_k = \mathbf{C}_k\mathbf{W}^H\sqrt{\mathbf{R}}\mathbf{H}_k + \mathbf{E}_k \quad , \quad k = 1, \cdots, N_c. \tag{3.3}$$

$\mathbf{E}_k$ is an additive Gaussian noise matrix at the receiver with each element having zero mean and σ_k^2 variance. $\mathbf{H}_k \in \mathbb{C}^{N_t\times N_r}$ is the channel frequency response matrix for the k^{th} subcarrier.

At the receiver, channel estimation is performed by evaluating pilot tones embedded in the transmitted signal, then it is fed into the maximum likelihood detector (MLD) for ST decoding of data symbols. We assume that the MS receiver has perfect channel knowledge. To decode the received signal matrix, the MLD will evaluate the decision matrix and decide in favor of the codeword as follows:

$$\widehat{\mathbf{C}} = \arg\min_{\mathbf{C}\in\mathcal{C}} \sum_{k=1}^{N_c} \|\mathbf{Y}_k - \mathbf{C}_k\mathbf{W}^H\sqrt{\mathbf{R}}\mathbf{H}_k\|_F^2. \tag{3.4}$$

The received multimedia information bits, $\{\hat{s}(n)\}$, are then recovered through baseband demodulation of the estimated ST codeword $\widehat{\mathbf{C}}$. Thus, the resulting quality of the multimedia data and the system performance depends on the estimation accuracy of the decision matrix (3.4).

Pairwise Error Probability

The SNR at the receive antennas has the form $\gamma = \sqrt{\mu_1}\varepsilon_s/\sigma_n^2$, where ε_s denotes average symbol energy and σ_n^2 is the receiver noise variance [50]. Let us assume that the receiver has perfect knowledge of the channel and the decision matrix in (3.4) is evaluated at the MLD for ST

decoding. The pairwise error probability (PEP) for an erroneous detection of the codeword $\widetilde{\mathbf{C}}$ in favor of transmitted $\mathbf{C}$ is given by:

$$P_r(\mathbf{C} \rightarrow \widetilde{\mathbf{C}} \mid \mathcal{H}) = \mathcal{Q}\left(\sqrt{\frac{d^2(\mathbf{C}, \widetilde{\mathbf{C}})\ \gamma}{2}}\right) \tag{3.5}$$

where $\mathcal{H} \triangleq \{\mathbf{W}^H\mathbf{H}_1, \cdots, \mathbf{W}^H\mathbf{H}_{N_c}\}$ and $d^2(\mathbf{C}, \widetilde{\mathbf{C}}) := \sum_{k=1}^{N_c} \|\mathbf{W}^H\mathbf{H}_k(\mathbf{C}_k - \widetilde{\mathbf{C}}_k)\|_F^2$ is commonly known as the squared Euclidean distance between the two codewords $\mathbf{C}$ and $\widetilde{\mathbf{C}}$. Using the Chernoff bound in [38], (3.5) can be upper bounded as:

$$P_r(\mathbf{C} \rightarrow \widetilde{\mathbf{C}} \mid \mathcal{H}) \leq \exp\left(\frac{-d^2(\mathbf{C}, \widetilde{\mathbf{C}})\ \gamma}{4}\right). \tag{3.6}$$

3.2.3 Achieving Transmit Diversity

For a system employing ST coding to achieve full diversity, two major conditions must be satisfied [47]:

1. The energy of one information symbol must spread over at least as many time intervals as there are transmit antennas. Hence, the ST codeword matrix must have a block length $p \geq N_t$.
2. The propagation channel should be uncorrelated, i.e., channel fading coefficients are identical independently distributed (i.i.d.), this means that $\text{rank}(\mathbf{H}_k) = N_t$.

However, correlation between signal paths always exists in practice; thus the second condition can never be met. Hence, to show that the proposed transmission structure de-correlates the channel covariance matrix (and hence maintain the maximum achievable diversity advantage of ST codes), the system must satisfy the following condition

$$\text{rank}\{\mathbf{W}^H\sqrt{\mathbf{R}_\text{t}}\} = N_t. \tag{3.7}$$

The following Subsections will now consider two special cases of channel correlation including a typical case.

Full Channel Correlation

For the special case of fully correlated channel where $\mathbf{R}_\text{t}(i,j) = 1\ \forall i,j$, the proposed system cannot de-correlate signal paths since elements of $\mathbf{H}_k$ are all the same. The eigen-decomposition of $\mathbf{R}_\text{t}$ will lead to signal transmission with equal transmit power for all antennas, i.e., $\mathbf{W} =$

$\text{diag}(\sqrt{\rho/N_t}) \in \mathbb{R}^{N_t \times N_t}$, ρ being the total transmit power constraint.

No Channel Correlation

Another spacial case: when there is no channel correlation we have $\mathbf{R}_{\text{t}} = \mathbf{I}_{N_t}$. In such a case that satisfies Condition 2 above, no signal paths de-correlation can be performed, and thus the signal transmission should be done in the same way as in the special case of full channel correlation (with equal transmit power for all antennas): $\mathbf{W} = \text{diag}(\sqrt{\rho/N_t}) \in \mathbb{R}^{N_t \times N_t}$. Therefore, no beamforming is utilized again in this case. However, full diversity order can still be obtained for the overall system with $\text{rank}(\mathbf{W}^H) = \text{rank}(\sqrt{\mathbf{R}_{\text{t}}}) = N_t$.

Partial Channel Correlation

This is a typical scenario in the wireless channel environment. In general, without considering the first two idealistic situations, the channel covariance matrix $\mathbf{R}_{\text{t}}$ is a nonnegative definite Hermitian matrix of a Toeplitz form, i.e., $\mathbf{R}_{\text{t}}^H = \mathbf{R}_{\text{t}}$ and $\det(\mathbf{R}_{\text{t}}) > 0$. This means $\sqrt{\mathbf{R}_{\text{t}}}$ will always have full rank equals to N_t. Next, recall that the antenna weight matrix is the dominant eigenvector of the correlation matrix $\mathbf{R}_{\text{t}}$, then it also will have a full rank equals to N_t. Thus, we can clearly see that the condition specified in (3.7) is satisfied, and hence this new transmission structure achieves full diversity order.

Therefore, except for the special case of full channel correlation, the proposed ST-OFDM system can maintain the maximum achievable diversity order as long as the ST codeword matrix has the block length $p \geq N_t$.

3.2.4 Adaptive Beamforming in the ST-OFDM Model

In [48], three adaptive beamforming criteria have been derived. These relationships follow the optimum solution, referred to as Wiener-Hopf equation. These criteria are: maximizing the signal-to-interference noise ratio (SINR) at the output of the beamforming, finding the Maximum Likelihood (ML) estimate of the desired signal power, and finding the minimum variance distortion-less response (MVDR). In this chapter, we adopt the conventional digital beamforming algorithm with the additional criterion of maximizing the desired SNR at the Mobile Station (MS). This criterion will improve the system performance in terms of minimizing the bit error rate (BER). It is shown in [100] that the optimum weight vector $\mathbf{w}$ that maximizes the SNR

according to the following relationship is the principal eigenvector of the covariance matrix.

$$\text{SNR} = \frac{\mathbf{w}^H \mathbf{R}_{ss} \mathbf{w}}{\sigma_n^2 \mathbf{w}^H \mathbf{w}} \tag{3.8}$$

where $\mathbf{R}_{ss}$ is the covariance matrix of the desired signal vector s, σ_n^2 is the noise variance, and $(.)^H$ denotes Hermitian transpose. This is the basis of the eigenbeamforming concept that was originally proposed in the 3GPP standards, to extend the transmit antenna array by more than two antenna elements resulting in greater beamformer resolution. The advantage of the eigenbeamforming algorithm is the effective use of both short-term and long-term channel properties by performing eigen-analysis (eigenvalue decomposition) of the long-term spatial covariance matrix. However, performance results shown in [49] and [174] are based on the channel model given in [179] where there is no specific distribution of local and dominant scatterers are considered for the case of a macrocell environment. This leads to inaccurate estimation of the angle-of-arrival (AoA), angle spread of the incoming wave, and the corresponding degree of spatial correlation between antenna paths.

The space-time channel model proposed in [112, 113] has taken into account the distribution of local and dominant scatterers and models the macrocell environment as hyperbolically distributed scatterers. As discussed in Chapter 2, the GBHDS channel model offers a more accurate and realistic representation of the propagation environment of wireless channels, and thus, has been adopted in this work.

Feedback Signalling of Antenna Beamforming Weights

Traditionally, the antenna weights are based on feedback information embedded in a reverse link signalling channel from the MS to the BS. One of the first schemes to utilize feedback information in adaptive beamforming was proposed by [190]. The MS makes use of a pilot tone in the forward link transmission and signals its estimates of channel characteristics back to the BS. This concept of adaptive beamforming has been adopted by the 3GPP standards [49]. Since the correlation is low between the forward link and reverse link signals, the reverse link channel impulse response estimates cannot be used for forward link beamforming. Hence, the forward link channel estimates are required for the computation of adaptive weights. This process is usually performed at the MS, and then the weights are fed-back to the BS.

In recent years, there have been several different feedback methods proposed. Partial channel feedback was proposed by [191], who derived an algorithm called partial phase combining technique that selects relative antenna phase based on partial channel knowledge. A similar scheme

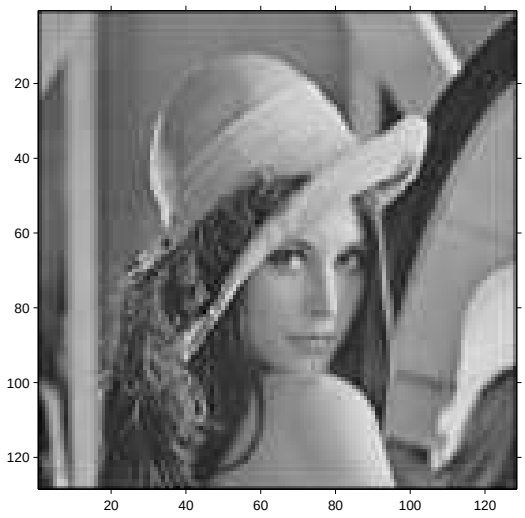

Figure 3.4: Original Lena source image (8-bit gray scale) resized to 128x128.

suggested by [192] where only the relative antenna phases are quantized first before the feedback signalling. Channel covariance feedback and channel mean feedback schemes in [193, 194] and [195] evaluate channel state information and its mean value then derive its optimum beamforming weights and power loading for each of the transmit antennas. In W-CDMA systems, only the quantized version of the weights are then sent back to the BS. In [49], each of the calculated antenna weights is quantized into 3-bit amplitude and 5-bit phase message. Hence, the resultant resolution of the antenna output beams will be greatly affected by the reliability of the reverse link transmission and the amount of quantization error.

The adaptive beamforming weights in this work, however, are computed without the need of the quantization process that is often used before feedback signalling. It utilizes the pilot symbols that are already embedded in the reverse link data channel. The advantage of this scheme, is that these pilot symbols can be better utilised for the transportation of the forward link antenna weights. Furthermore, the need for the feedback (uplink) signalling of the channel estimates from the receiver to the transmitter is eliminated, which reduces the overall computational complexity of the transmission system, particularly, for a transmitter with a large number of antennas. The allocation of dedicated feedback bits in the signalling channel, as would normally be required for computing the antenna weights, can be used for transmitting additional pilot symbols.

3.3 Simulation Results

To evaluate the performance of the space-time OFDM system with adaptive beamforming the MSF was configured for the transmission of digital still images. A standard version of the

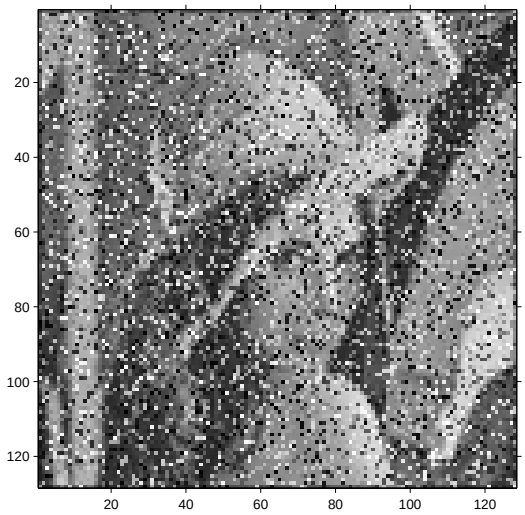

Figure 3.5: Received Lena image with no space-time coding and no adaptive beamforming.

512×512 size gray scale Lena image [89] with 8 bits/pixel resolution was used as the multimedia source data/ file input to the simulation framework. Due to practical computational limitations, however, the Lena image has been resized to 128×128 using 'bilinear' interpolation. Interpolation, in image processing applications, is used to estimate an image value at a location in between image pixels. To determine the value for an interpolated pixel, we find the point in the input image that the output pixel corresponds to. A value to the output pixel is assigned by computing a weighted average of some set of pixels in the vicinity of the point. The weightings are based on the distance each pixel is from the point. In the case of 'bilinear' interpolation, the output pixel value is a weighted average of pixels in the nearest 2-by-2 neighborhood. Other interpolation methods include: Nearest-neighbor and Bicubic interpolation. Bilinear interpolation presents a tradeoff between processing time and quality. Although, this method of reducing the size of the test image introduces slight imperfections (degradation in visual quality), it coincidentally emulates the size of commercially available visual displays for portable hand-held wireless devices. The re-sized Lena image used for simulating the transmission of multimedia data is shown in Figure 3.4.

The ST-OFDM-AB system was configured for QPSK baseband modulation, using the ST encoding matrix $\mathcal{G}4$ in [41], and a GBHDS correlated macrocell channel model developed in [110, 111]. Also, an SNR of 0 dB was assumed for the space-time OFDM simulation model, and the source encoder was configured for lossless compression. In order to determine the effectiveness of the space-time OFDM system over other methods, the framework was configured and simulated for three cases: 1. OFDM with no space-time coding or adaptive beamforming; 2. OFDM with space-time coding and no adaptive beamforming; 3. space-time encoded OFDM

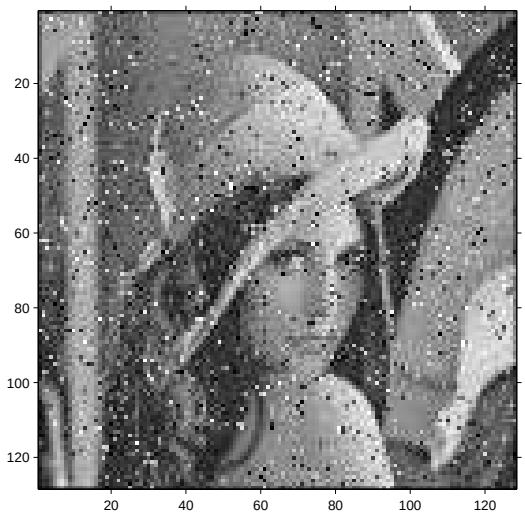

Figure 3.6: Received Lena image using space-time coding but no adaptive beamforming.

with adaptive beamforming. The resulting images produced from the MSF for each case is presented in Figures 3.5, 3.6, and 3.7 respectively. Also, the PSNR value obtained for the resulting images are as follows: $PSNR_1$=14.46 dB, $PSNR_2$=19.84 dB, and $PSNR_3$=27.93 dB.

Figure 3.5, shows the output image received and processed by a simulated OFDM system with no space-time encoding or adaptive beamforming. Visual inspection of the reconstructed Lena image reveals an image which is severely distorted (saturated by noise). Results of reception with ST-OFDM only and ST-OFDM with adaptive beamforming are shown in Figures 3.6 and 3.7, respectively. As we would expect from an analysis of the performance curves presented in Figure 3.1, a visual/subjective comparison of the user perceived quality of these images shows quite clearly that significant improvements in error rate performance (and subsequently image quality) is achieved with an OFDM system using space-time coding and adaptive beamforming (ST-OFDM-AB). This is also consistent with the PSNR values obtained for each simulated case.

3.4 Conclusions

In this chapter, a multimeda framework for the transmission (processing) of digital multimedia signals over a wireless space-time OFDM communication system with adaptive beamforming has been proposed. The performance improvement introduced by the transmit diversity techniques, STBC and AB, confirm their high suitability for mobile multimedia systems and are further complemented by being integrated with a compression system. Simulation results based on the application of digital still images, using a space-time coded OFDM scheme and GBHDS channel model, showed a good match between performance curves obtained through numerical studies

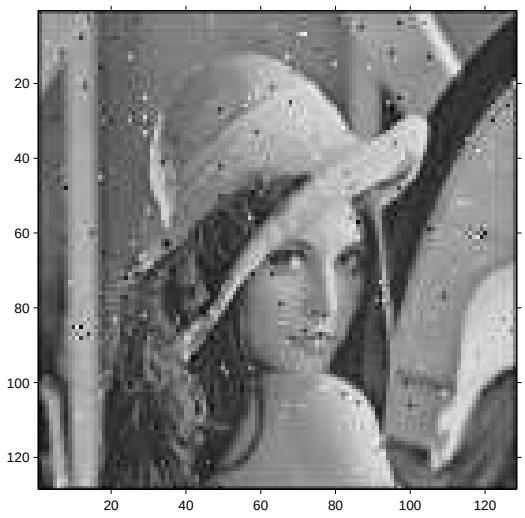

Figure 3.7: Received Lena image using space-time coding and adaptive beamforming.

and subjective fidelity measures (human visual perception). This analysis has been achieved without the need of an objective performance metric such as, the peak signal-to-noise ratio (PSNR), commonly used in image processing literature.

In general, this study has demonstrated the use of the multimedia framework as a validation tool for determining the subjective performance - user perceived quality - of multimedia data received through transmission over wireless communication channels utilizing ST-OFDM with adaptive beamforming.

Chapter 4

Integrated Source and Diversity Coding for Multimedia Communication

4.1 Introduction

In the previous chapter, we have shown that the use of a space-time block coded STBC-OFDM system with an adaptive eigenbeamforming scheme is well suited to the application of multimedia data, and that a significant BER perfomance gain readily facilitates the transmission of high-quality/high data-rate multimedia signals. By integrating transmit diversity techniques with a lossy compression system such as wavelet-based coding, further enhancements in overall system performance can be achieved due to the additional control provided over the communication bandwidth and channel capacity requirements [52]. Thus, the first part of this chapter, presents a transmission system for multimedia communication employing STBC-OFDM with adaptive beamforming incorporating the use of a perceptually-based image compression coder consisting of the following: a 2-D discrete wavelet transform (DWT), an adaptive quantizer (with thresholding) and variable-length entropy encoding.

Traditionally, diversity coding for (OFDM) systems have been mainly focused only on the spatial and temporal domain of transmitted signals. More recently, however, the authors in [146], [151], and [152] have shown that additional diversity branches in broadband multipath channels can be exploited using space-frequency (SF) and space-time-frequency (STF) coding, which encode data symbols across the frequency domain of the signal to be transmitted. The second part of this chapter, therefore, focuses on a new transmission strategy that integrates space-time-frequency (STF) coding with a wavelet-based compression system [53]. Like the other methods proposed, this approach can be extended to study the transmission of various other multimedia sources such as digital images and video data.

Subsequent sections of this chapter have been organized as follows: Section 4.2, details

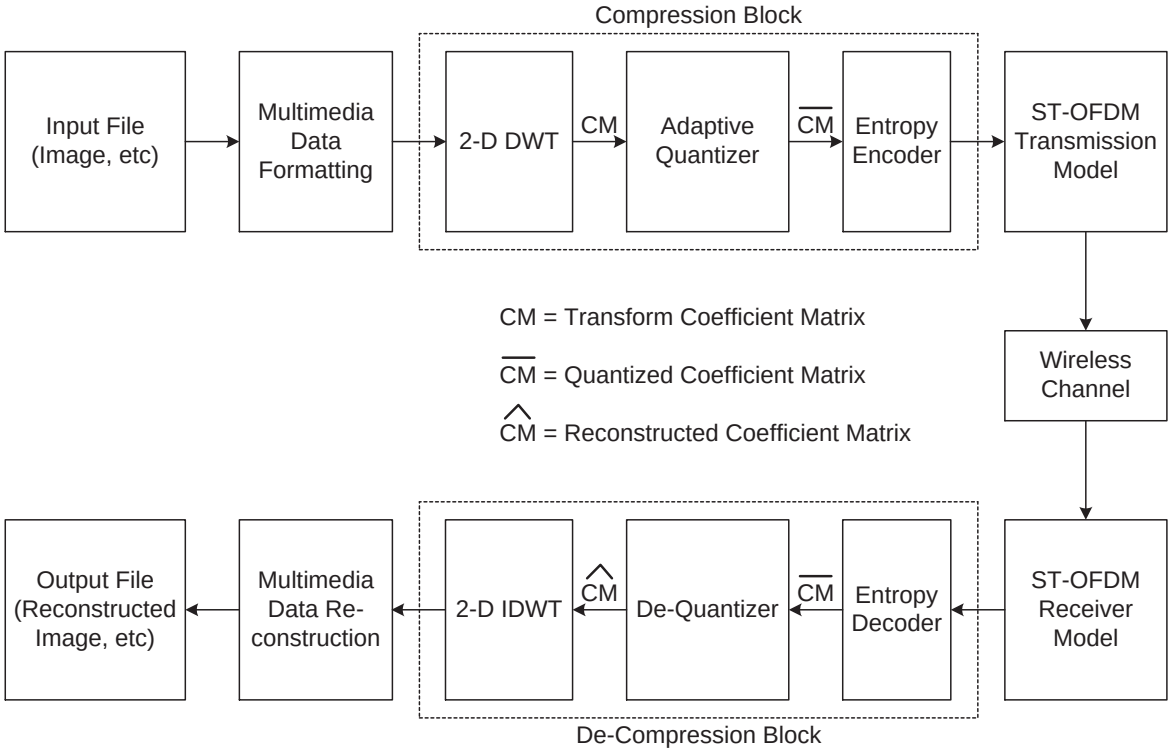

Figure 4.1: Block diagram of the Source-STBC OFDM transmission system model.

the structure of the proposed source-STBC coded OFDM system. In particular, Section 4.2.2 provides a description of the wavelet-based compression technique employed in the multimedia framework. Performance results based on the simulation and analysis of compressed digital images using both subjective and objective measures (visual comparison and PSNR metric) are presented in 4.2.4. Similarly, the system models and simulation results for the source-STF coded OFDM schem are presented in Section 4.3. Finally, Section 4.4 provides concluding remarks.

4.2 Integrated Source-STBC OFDM System Model

The elements of the transmission system model proposed, consists mainly of 3 blocks: multimedia data formatting, data compression, and an adaptive ST-OFDM model. Note, that a channel encoder such as turbo coding is not employed, as an initial baseline performance of the system is required. Channel encoding schemes provide forward error correction and only add redundancy to the entropy coded data to achieve a BER close to the shanon limit. A block diagram of the system model is shown in Figure 4.1. This is based on the STBC-OFDM-AB simulation scheme already outlined in Chapter 3. A description of the main blocks is provided in the following sections.

4.2.1 Multimedia Data Formatting

As described in section 3.2.1, to enable the simulation of multimedia (image) data over the adaptive space-time OFDM transmission scheme, multimedia signals from various data sources (such as, compressed audio/ image/ video files), which may be stored on a PC, are converted to a suitable format which can be further processed by the compression block (transform/entropy coder).

The principal idea behind the multimedia data model developed is to consider the source file (digitized version of the original multimedia signal with n-bit resolution) as a vector array containing integer quantization levels. For digital audio, these correspond to sampled amplitude values, and for digital image and video coding they correspond directly to pixel values. In the case of monochrome digital still images (with 8-bit/pixel resolution), the source data is converted into a matrix array ($M \times N$) containing 8-bit integer values which correspond to intensity information of the image.

The output - after transform/subband coding, adaptive quantization, and entropy coding - of the compression block provides a vector array of integers representing the bitstream required for conversion to a vector array of baseband modulated data symbols $\{s(n)\}_{n=0}^{N_s-1}$, as specified by the space-time OFDM model. In the receiver path, the reverse operation is performed on the modified data symbols $\{\hat{s}(n)\}$ produced by the space-time OFDM transmission scheme. Whereby, the data symbols are first converted back to a bitstream and subsequently to an integer array, which can be reconstructed (via inverse operations by the de-compressor) back to the original multimedia data format applied to the system.

4.2.2 Data Compression

The use of the discrete wavelet transform (DWT) in the compression of multimedia signals, such as image/video compression applications, has been well documented [22, 26, 29]. For example, wavelet transform coding has been accepted as the core processing tool in the JPEG2000 image compression standard, as it has a number of advantages over other compression techniques (DCT subband coding, vector quantization, fractal coding, etc). Some of the main benefits of wavelet transform coding include, the high decorrelation and energy compaction capability, reduction in image distortion due to blocking artifacts and mosquito noise, and the adaptive spatial-frequency resolution offered which is well suited to the properties of the human visual system (HVS) - psychovisual redundancy (HVS properties which can be exploited to achieve superior compression). In general, image compression applications based on wavelet transform coding provide better

image quality over other subband coding techniques such as block DCT, particularly, for large compression ratios [78]. Referring to Figure 4.1, in this work signal compression of image data consists of the following steps:

1. Wavelet decomposition using 2D-DWT.
2. Adaptive quantization, with threshold.
3. Entropy coding (Huffman coder).

In the case of transmitting digital images, a multiresolution 2D-DWT decomposition based on dyadic scales and positions (dilations and translations) of the wavelet basis function (mother wavelet) is obtained using two subband filters. After each level of decomposition four bands of data are produced, one corresponding to the low-pass band and three others corresponding to horizontal, vertical, and diagonal high-pass bands - with all subbands providing spatial and frequency information simultaneously. This subband information can be iteratively decomposed resulting in multiple 'transform levels'. In theory this process can be continued indefinitely, however, in practice a suitable number of levels is chosen based on a suitable entropy-based criterion.

In wavelet analysis, we represent the low-resolution subband by approximation coefficients ($\mathbf{cA_n}$) and high-pass subband spatial-frequency information with horizontal, vertical, and diagonal detail coefficients ($\mathbf{cH_n}$, $\mathbf{cV_n}$, $\mathbf{cD_n}$) respectively. For an n-level decomposition, the coefficient matrix **CM** consists of the following coefficients:

$$\mathbf{CM} = [\mathbf{cA_n}, \mathbf{cH_n}, \mathbf{cV_n}, \mathbf{cD_n}, \cdots, \mathbf{cH_1}, \mathbf{cV_1}, \mathbf{cD_1}] \tag{4.1}$$

During transmission, the transform coefficients (DWTC) are adaptively mapped to a finite set of values using a uniform scalar quantizer. Spatial redundancy of the detail coefficients can be exploited, as many of the coefficients will be either small in value or contain a high number of elements close to or equal to zero. A threshold can be adaptively set to remove coefficients below a preset value. Since the statistics of the detail DWTC can vary, a different threshold can be applied independently to each band/level or a 'global' threshold parameter for all subbands can be applied. For lossless compression, the DWTC are quantized with their actual values. In contrast, however, to achieve high compression ratios a lossy compression technique which uses an aggressive quantization scheme is required. After the data has been adaptively quantized, additional lossless compression is achieved by further removing spatial and statistical redundancy of the DWTC using a run-length and entropy encoding respectively. In this paper, we use an

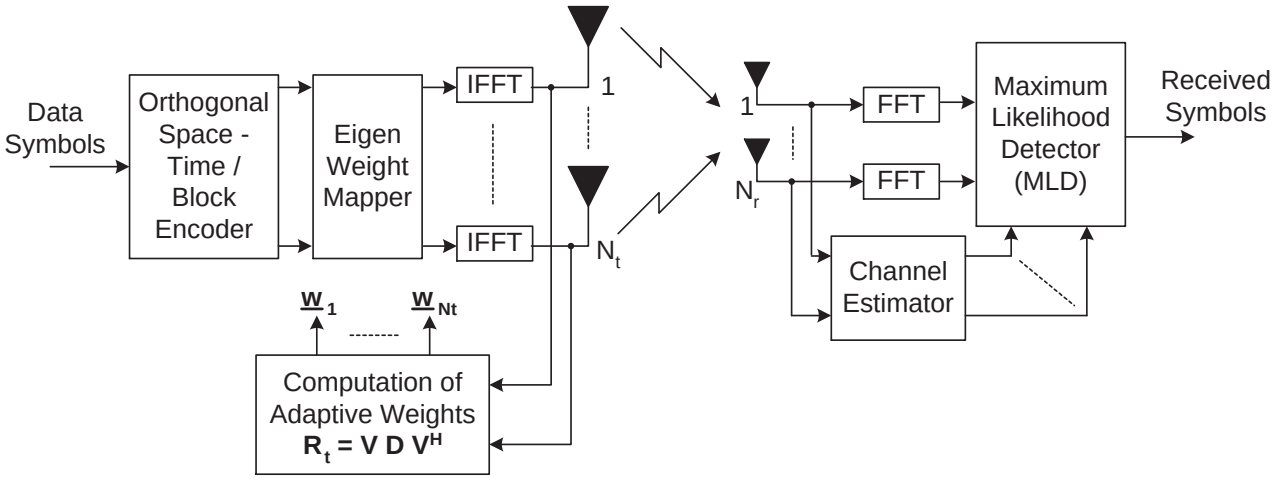

Figure 4.2: Structure of the Adaptive STBC-OFDM transmission model with eigenbeamforming.

entropy coder based on an improved Huffman coding scheme using recursive splitting of symbol sequences [202].

4.2.3 Adaptive Space-Time OFDM Model

The general structure of the ST-OFDM transmission model with adaptive eigenbeamforming in a MIMO channel configuration employing N_t and N_r antennas at the transmitter and receiver, is shown in Figure 4.2. The OFDM system we consider in this work utilizes N_c frequency tones. The channel is assumed to be frequency-selective having quasi-static fading. At the transmitter, a sequence of N_s multimedia baseband modulated data symbols $\{s_k(n)\}_{n=0}^{N_s-1}$ is first orthogonal space-time block (OSTB) encoded into codeword matrices $\{\mathbf{C}_k \mid k = 1, \cdots, N_c\} \in \boldsymbol{\mathcal{C}}^{p\times N_t}$, which spans across N_t spatial dimensions and p adjacent OFDM symbol intervals. $\mathbf{C}_k$ is the OSTB encoded output matrix to be transmitted on the k^{th} subcarrier and $\boldsymbol{\mathcal{C}}$ denotes all possible codeword matrices that can be constructed. Before the stage of inverse Fourier transformation (IFFT) OSTB codeword $\mathbf{C}_k$ is linearly transformed by the adaptive beamforming weights as shown in Fig. 4.2.

For the N_t BS antennas, we assume a uniform linear array (ULA) configuration is used with an element spacing of d meters apart. In general, the spacing between the elements of the ULA at the transmitter is not large due to the condition at the antenna site to have zero cross-correlation factor, a typical scenario in mobile networks. Therefore, spatial correlation between antenna elements would be effective. This correlation is defined in [179] based on the geometric scenario characterized by AoA. To model this spatial correlation, we let the ℓ^{th} path signal impinging on an ULA have an angle-of-arrival (AoA) of ϕ_ℓ during reverse link signalling.

Then the array propagation vector can be expressed as $\underline{a}(\phi_\ell) := [1,\ e^{j\beta},\ e^{j2\beta},\ \cdots\ , e^{j(N_t-1)\beta}]^T$ where $\beta = (2\pi \cdot d \cdot \sin(\phi_\ell))/\lambda$ and λ being the carrier frequency wavelength. According to [179], the spatial covariance matrix that specifies the spatial correlation between antenna elements is given by:

$$\mathbf{R}_t = \frac{1}{L}\sum_{\ell=0}^{L-1} \underline{a}(\phi_\ell)\underline{a}^H(\phi_\ell) \tag{4.2}$$

where L denotes the number of dominant resolvable paths. In this paper, we assume that spatial channel correlation at the receiver side is zero, hence, only the transmitter side will be considered. This means that $\mathbf{R}_r = \mathbf{I}_{N_r}$, where $\mathbf{I}_M$ is an identity matrix having a size of $M \times M$.

Denote $\mathbf{h}_{i,j} = [h_{i,j}(0), \cdots, h_{i,j}(L-1)]$ to be the L-tap channel impulse response vector between $(i,j)^{\text{th}}$ transmit-receive antenna pair. The elements of this vector are modelled according to the geometrical-based hyperbolically distributed scatterers (GBHDS) channel model in [112] with Jakes power spectral density. The spatially correlated frequency response matrix for the k^{th} subcarrier frequency can then be expressed as $\mathbf{H}_k = \sqrt{\mathbf{R}_t}\overline{\mathbf{H}}_k$, where the $(i,j)^{\text{th}}$ element of $\mathbf{H}_k$ is given by $\mathbf{H}_k(i,j) = \mathbf{h}_{i,j}\mathbf{f}_k$ and $\mathbf{f}_k = [1, e^{-j2\pi(k-1)/N_c}, \cdots, e^{-j2\pi(k-1)\tau_{L-1}/N_c}]^T \in \mathbb{C}^{L\times 1}$ is the corresponding discrete Fourier transform coefficients. $\overline{\mathbf{H}}_k \in \mathbb{C}^{N_t \times N_r}$ is the uncorrelated channel fading gain for the k^{th} subcarrier.

Maximizing the signal power along the dominant multipaths of the channel, eigen-decomposition of the spatial correlation matrix should be performed. The eigen-decomposition has the following form:

$$\mathbf{R}_t = \mathbf{V}\mathbf{D}\mathbf{V}^H \tag{4.3}$$

where $\mathbf{D} := \text{diag}(\lambda_d,\ \lambda_2,\ \cdots\ , \lambda_{N_t})$ is a diagonal matrix with ordered eigenvalues and $\mathbf{V} := [\boldsymbol{\upsilon}_1, \cdots, \boldsymbol{\upsilon}_{N_t},]$ is a unitary matrix composed of the corresponding eigenvectors. To facilitate signal transmission in the eigen-modes of the correlation matrix, eigen weight mapping is performed across the space dimension of the OSTB codewords $\{\mathbf{C}_k\}_{k=1}^{N_c}$ prior to transmission. Mathematically, it can be expressed as $\mathbf{W}^H\mathbf{C}_k$, where $\mathbf{W} = [\mathbf{w}_1, \cdots, \mathbf{w}_{N_t}]$ is the eigen weight mapping matrix and $\mathbf{w}_i = \boldsymbol{\upsilon}_i$. Hence, signal transmission on different eigenvectors of $\mathbf{R}_t$ amounts for transmitting N_t orthonormal beams in the direction of the dominant multipaths seen by the BS. Then the discrete time baseband equivalent expression of the combined received signal has the

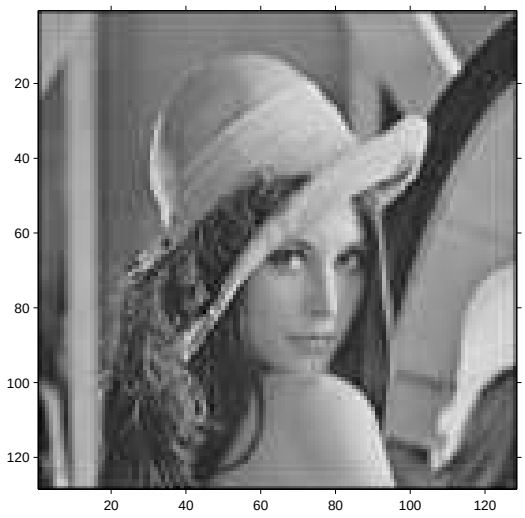

Figure 4.3: Original Lena source image (8-bit gray scale) resized to 128×128.

form:

$$\mathbf{Y}_k = \mathbf{C}_k \mathbf{W}^H \mathbf{H}_k + \mathbf{E}_k \ , \tag{4.4}$$

where $\mathbf{E}_k$ is a additive Gaussian noise matrix at the receiver with each element having zero mean and σ_k^2 variance.

At the receiver, channel estimation is performed by evaluating pilot tones embedded in the transmitted signal, then it is fed into the maximum likelihood detector (MLD) for OSTB decoding of data symbols. Assume that the receiver has an ideal knowledge of the channel state information. To decode the received signal matrix, the MLD will evaluate the decision matrix and decide in favor of the codeword as follows:

$$\widehat{\mathbf{C}}_k = \arg \min_{\mathbf{C}_k \in \boldsymbol{\mathcal{C}}} \sum_{k=1}^{N_c} \|\mathbf{Y}_k - \mathbf{C}_k \mathbf{W}^H \mathbf{H}_k\|_F^2. \tag{4.5}$$

The multimedia information data can then be recovered through baseband demodulation of the estimated OSTB codeword $\widehat{\mathbf{C}}_k$. The adaptive ST-OFDM system performance and thus the resulting quality of the multimedia data depends on the estimation accuracy of the decision matrix (4.5).

4.2.4 Simulation Results & Discussion

To evaluate the performance of the transmission system for image applications, a standard version of the 512x512 size gray scale (monochrome) Lena image with 8 bits/pixel resolution,

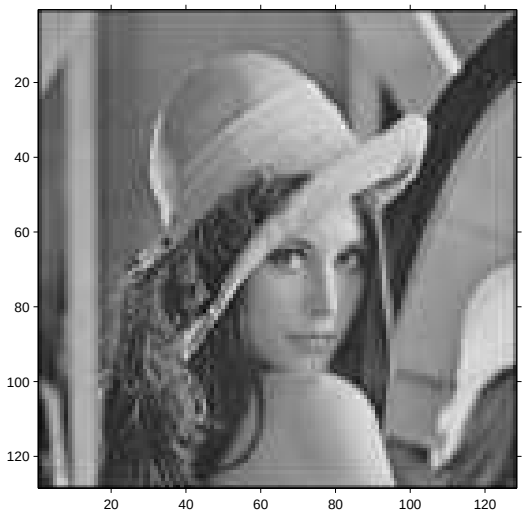

Figure 4.4: Reconstructed Lena image from the OFDM system with space-time coding and adaptive beamforming: SNR=20 dB.

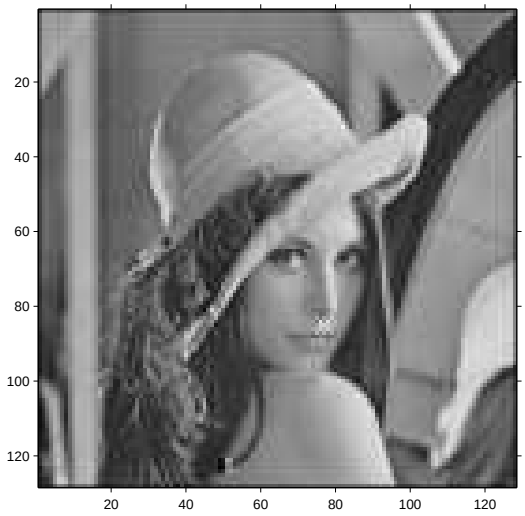

Figure 4.5: Reconstructed Lena image from the OFDM system with no space-time coding and no adaptive beamforming: SNR=20 dB.

was used as the multimedia source data/file input to the simulation framework. As stated in section 3.3, due to practical computational limitations the Lena image is resized to 128x128 using 'bilinear' interpolation. This introduces only slight imperfections in the image (visual quality). The re-sized Lena image used for data compression is shown in Figure 4.3. In order to maintain a linear phase of the reconstructed image, the source data was transformed using biorthogonal wavelets and a level 4 wavelet decomposition was performed.

The space-time OFDM model is configured for QPSK baseband modulation, using the ST encoding matrix $\mathcal{G}4$ in [41], and a GBHDS correlated macrocell channel model developed in [112]. Also, the source coder (compression block) was configured to provide a compression ratio (CR)

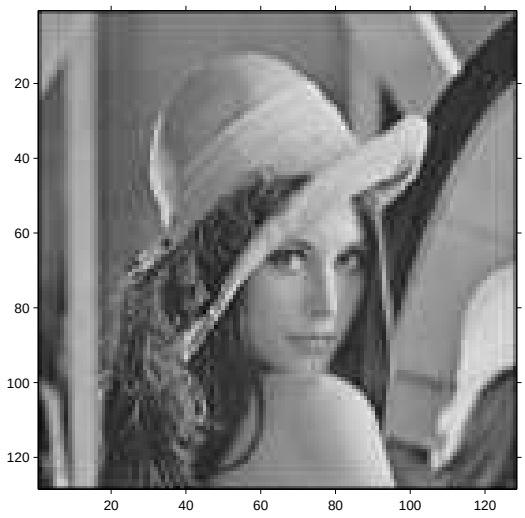

Figure 4.6: Reconstructed Lena image from the OFDM system with space-time coding and adaptive beamforming: SNR=10 dB.

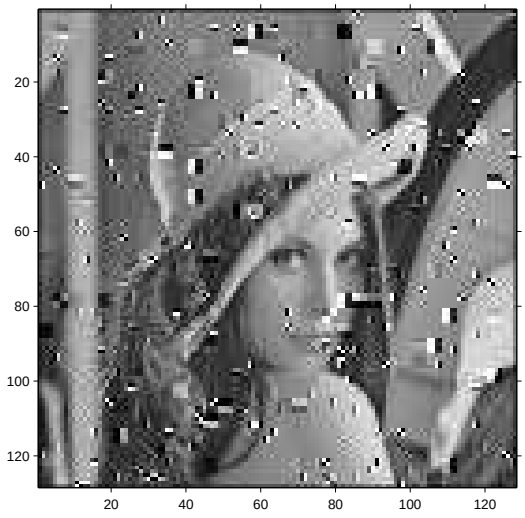

Figure 4.7: Reconstructed Lena image from the OFDM system with no space-time coding and no adaptive beamforming: SNR=10 dB.

of 20.21 using a DWTC threshold of 10, and the Huffman coder in [202]. In order to determine the effectiveness of the adaptive space-time OFDM system over other methods, the framework was simulated and compared for two cases: OFDM with no space-time coding or adapative beamforming and a space-time coded OFDM system with adaptive beamforming. Objective performance metrics commonly used in image processing literature, such as the MSE and PSNR, was recorded for both cases using an initial system SNR of 20 dB, and subsequently repeated for a SNR of 10 dB.

For the case where an OFDM system model with no space-time coding or adaptive beamforming is utilised, the MSE/PSNR degrades from a value of MSE = 4.62/ PSNR = 41.48 dB

(at SNR = 20 dB) to a MSE = 1376.27/ PSNR = 16.74 dB (at SNR = 10 dB). When the transmission system is configured for space-time OFDM system with adaptive beamforming, the MSE/ PSNR remains the same at MSE = 0.22/ PSNR = 54.77 dB for both values of SNR.

These results are confirmed by inspecting the subjective quality of the images obtained, as shown in the accompanying Figures 4.4, 4.5, 4.6, and 4.7. Visual inspection and comparison of the received Lena images at a SNR of 10dB, shows severe image distortion is introduced by OFDM systems with no space-time coding or adaptive beamforming - mainly due to the large errors occurring in the received DWTC. As expected, significant performance gains in the transmission of compressed images is achieved with an OFDM system using space-time coding and adaptive beamforming.

4.3 Integrated Source-STF coded OFDM System Model

In this section, we present an adaptive transmission scheme that combines the use of transmitter eigenbeamforming and STF coding (Eigen-STF) to provide an array weighting gain (AWG) and preserve the diversity and coding gains offered by the STF scheme for broadband OFDM systems [196]. Based on uplink AoA estimates, spatial correlation structure of the propagation channel is first estimated at the base station (BS), then STF encoded information is transmitted in the eigen-directions of this channel and lead to uncorrelated fading for each antenna. The resultant effect is an enhancement of SNR at the mobile station (MS); this gives an improvement in system error-rate performance. The proposed solution depends only on the channel correlation matrix, and thus can be applied without any feedback mechanism or channel reciprocity assumption. This makes it more practical as compared to the traditional beamforming schemes in [181] and [182], where output beam resolution can suffer greatly from channel estimation, quantization, and feedback errors and delay.

This can be seen in Figure 4.8, which shows the resulting error performance curves in bit-error rate (BER) and symbol-error-rate (SER) for OFDM systems that are STBC and STF coded respectively.

4.3.1 STF Coding

The general structure of a MIMO-OFDM system employing the proposed Eigen-STF transmission structure is similar to that shown in Fig. 4.2 with N_t transmit and N_r receive antennas (except the STBC encoder is replaced by STF). The OFDM system we consider here uses N_c

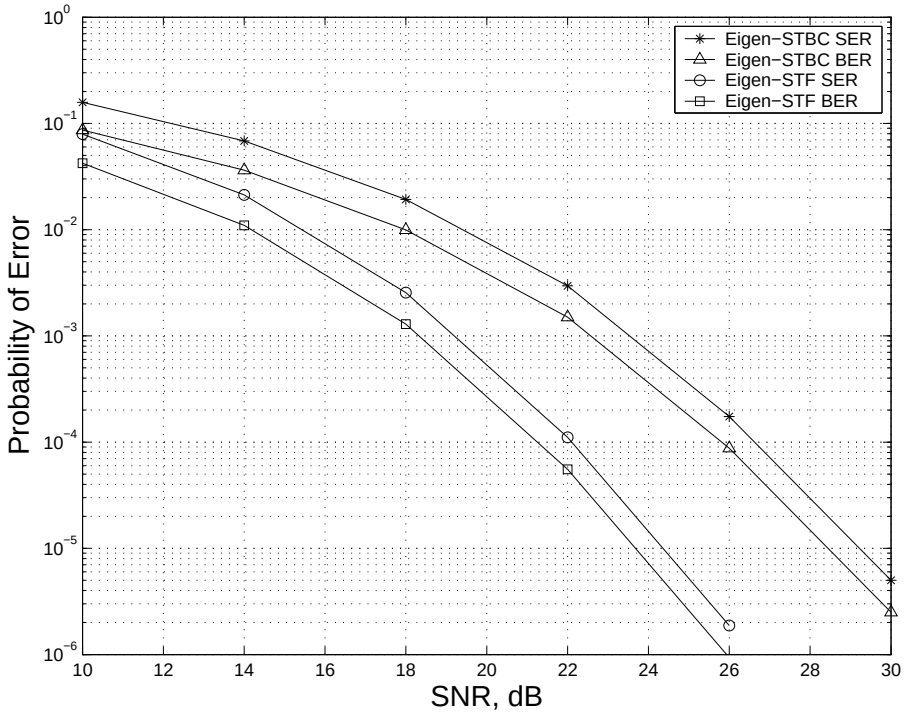

Figure 4.8: Comparison of performance curves between STBC-OFDM-AB and STF-OFDM-AB systems in correlated fading channels.

frequency tones and the channel is assumed to be frequency-selective with L dominant paths. At the BS, STF encoding is performed by formatting the compressed multimedia data symbols into a codeword matrix $\boldsymbol{\mathcal{C}} := [\mathbf{C}_1, \cdots, \mathbf{C}_k, \cdots, \mathbf{C}_{N_c}] \in \mathbb{C}^{N_t \times pN_c}$, where $\mathbf{C}_k$ is a $N_t \times p$ sub-matrix (which spans across p OFDM-symbol intervals and N_t transmit antennas) to be transmitted on the k^{th} subcarrier. Because the number of baseband constellation points is finite, there is a limited number of possible STF codeword matrices and we denote this finite set as $\boldsymbol{\Upsilon} \ni \boldsymbol{\mathcal{C}}$. Details of the design criteria and the formatting of STF codewords can be found in [151] and [152].

4.3.2 Spatial Correlated Frequency-Selective Fading Channel

Consider a typical cellular communication scenario where the BS antennas are placed at the building roof-top in an unobstructed environment and the MS is located at the street level and surrounded by dense distribution of local scatterers. It is stated in [47] that signal transmission in such an environment over a multipath channel leads to uncorrelated signal paths arriving at the MS but partially correlated in spatial domain at the BS. Assuming that a uniform linear array (ULA) configuration is used for N_t BS antennas with a spacing of d meters, the normalized transmit spatial covariance matrix that specifies the spatial correlation between antenna elements

is defined as [179]

$$\mathbf{R}_{\mathrm{t}} = \frac{1}{L}\sum_{\ell=1}^{L}\mathbf{a}(\phi_\ell)\mathbf{a}^H(\phi_\ell)\ , \tag{4.6}$$

where L denotes the number of dominant resolvable paths (i.e., arriving signal paths that are more than one symbol length apart with significant received power),

$$\mathbf{a}(\phi_\ell) := [1, e^{j\beta}, e^{j2\beta}, \cdots, e^{j(N_t-1)\beta}]^T \tag{4.7}$$

is the array propagation vector for the ℓ^{th} tap with an AoA of ϕ_ℓ, and $\beta = [2\pi \cdot d \cdot \sin(\phi_\ell)]/\lambda$ with λ being the carrier frequency wavelength. To estimate these uplink AoA's, one practical technique is the virtual array concept with space diversity in [130]. By applying a MUSIC-like algorithm in [131], the forth-order statistics of the uplink arriving signals can be computed using an array of sensors that is larger than the actual number of antenna elements to improve the estimation accuracy. It is observed that $\mathbf{R}_{\mathrm{t}}$ has a distinct characteristic of slow varying. To further improve the accuracy of $\mathbf{R}_{\mathrm{t}}$ (additional to the virtual array concept), another practical approach is by averaging $\mathbf{R}_{\mathrm{t}}$ on a long-term using a forgetting factor.

In general, $\mathbf{R}_{\mathrm{t}}$ is a nonnegative-definite Hermitian matrix and its eigenvalue-decomposition (EVD) can be expressed as

$$\mathbf{R}_{\mathrm{t}} = \mathbf{V}\mathbf{D}\mathbf{V}^H, \tag{4.8}$$

where

$$\mathbf{V} = [\boldsymbol{v}_1, \cdots, \boldsymbol{v}_{N_t}] \tag{4.9}$$

is a unitary matrix with columns that are the eigenvectors of $\mathbf{R}_{\mathrm{t}}$ and

$$\mathbf{D} = \mathrm{diag}\{\mu_1, \mu_2, \cdots, \mu_{N_t}\} \tag{4.10}$$

contains the corresponding eigenvalues. Define

$$\mathbf{g}_{i,j} = [g_{i,j}(0), \cdots, g_{i,j}(L-1)] \tag{4.11}$$

as the L-tap channel impulse response vector for the $(i,j)^{\mathrm{th}}$ receive-transmit antenna pair. The

channel frequency response matrix can be expressed as $\mathbf{H}_k \in \mathbb{C}^{N_r \times N_t}$ with its $(i,j)^{\text{th}}$ entry

$$h_{i,j,k} = \mathbf{g}_{i,j}\mathbf{f}_k, \tag{4.12}$$

where

$$\mathbf{f}_k = [1, e^{-j2\pi(k-1)/N_c}, \cdots, e^{-j2\pi(k-1)\tau_{L-1}/N_c}]^T \tag{4.13}$$

is the corresponding discrete Fourier transform coefficients and τ_ℓ is the integer delay of the ℓ^{th} tap. The correlated channel frequency response can then be given as $\mathbf{H}_k\sqrt{\mathbf{R}_{\text{t}}}$. We assume that the spatial correlation is the same for all subcarriers.

4.3.3 Adaptive Transmit Eigenbeamforming

To facilitate STF codeword transmission in the eigen-modes of the correlation matrix, eigen weight mapping is performed across the space dimension of the STF codeword $\{\mathbf{C}_k\}_{k=1}^{N_c}$ prior to transmission. Mathematically, it can be expressed as $\mathbf{W}^H\mathbf{C}_k$, where $\mathbf{W} = [\mathbf{w}_1, \cdots, \mathbf{w}_{N_t}]$ is the eigen weight mapping matrix and $\mathbf{w}_j = \boldsymbol{\upsilon}_j$. Then signal transmission on different eigenvectors of $\mathbf{R}_t$ amounts for transmitting N_t orthonormal beams in the direction of the dominant multipaths seen by the BS. In the case when $\mathbf{R}_t$ is not the same for all subcarriers, beamforming should be performed individually for all subcarriers or groups of subcarriers with approximately one coherent bandwidth apart.

4.3.4 Received Signal Model

At the receiver, discrete Fourier transformation (DFT) is applied to the received signals from N_r antennas. The discrete time baseband equivalent expression of the received signal has the form

$$\mathbf{Y}_k = \mathbf{H}_k\sqrt{\mathbf{R}_{\text{t}}}\mathbf{W}^H\mathbf{C}_k + \mathbf{E}_k \ , \tag{4.14}$$

where $\mathbf{E}_k$ is the receiver noise matrix and its elements are modelled as uncorrelated additive white Gaussian random variables having $\mathcal{N}(0, \sigma_n^2)$. At the receiver, channel estimation is performed by correlating pilot tones embedded in the transmitted signal. The result is then fed into the MLD for STF decoding of data symbols by evaluating the decision matrix as follows

$$\widehat{\boldsymbol{\mathcal{C}}} = \arg\min_{\boldsymbol{\mathcal{C}}\in\boldsymbol{\Upsilon}} \sum_{k=1}^{N_c} \|\mathbf{Y}_k - \mathbf{H}_k\sqrt{\mathbf{R}_{\text{t}}}\mathbf{W}^H\mathbf{C}_k\|_F^2 \ . \tag{4.15}$$

4.3.5 Performance Analysis

Assuming that the receiver has perfect knowledge of the channel and that the decision matrix in (4.15) is evaluated at the MLD for symbol detection, the pairwise error probability (PEP) for an erroneous detection of the codeword $\widetilde{\boldsymbol{\mathcal{C}}}$ in favor of $\boldsymbol{\mathcal{C}}$ conditioned on the fading channel $\mathcal{H} = \{h_{i,j,k}\}_{i=1,\ j=1,\ k=1}^{N_r,\ N_t,\ N_c}$ can be expressed as

$$P_r(\boldsymbol{\mathcal{C}} \rightarrow \widetilde{\boldsymbol{\mathcal{C}}} \mid \mathcal{H}) = \mathcal{Q}\left(\sqrt{\frac{d^2(\boldsymbol{\mathcal{C}}, \widetilde{\boldsymbol{\mathcal{C}}})\ \rho}{2}}\right), \tag{4.16}$$

where $\rho = \varepsilon_s/\sigma_n^2$, ε_s is the average symbol energy, $\mathcal{Q}(\cdot)$ is the classical Gaussian Q-function, and

$$d^2(\boldsymbol{\mathcal{C}}, \widetilde{\boldsymbol{\mathcal{C}}}) := \sum_{k=1}^{N_c} \|\mathbf{H}_k \sqrt{\mathbf{R}_{\mathrm{t}}} \mathbf{W}^H (\mathbf{C}_k - \widetilde{\mathbf{C}}_k)\|_F^2 \tag{4.17}$$

is commonly known as the squared Euclidean distance between the two codeword matrices. Using the Chernoff bound in [38], (4.16) can be upper-bounded as

$$P_r(\boldsymbol{\mathcal{C}} \rightarrow \widetilde{\boldsymbol{\mathcal{C}}} \mid \mathcal{H}) \leq \exp\left(\frac{-d^2(\boldsymbol{\mathcal{C}}, \widetilde{\boldsymbol{\mathcal{C}}})\ \rho}{4}\right). \tag{4.18}$$

Defining $\mathbf{g}_i = [\mathbf{g}_{i,1}, \cdots, \mathbf{g}_{i,N_t}] \in \mathbb{C}^{1 \times N_t L}$ and $\mathbf{F}_k := \mathrm{diag}\{\mathbf{f}(k), \cdots, \mathbf{f}(k)\} \in \mathbb{C}^{N_t L \times N_t}$, the squared Euclidean distance can be rewritten as

$$d^2(\boldsymbol{\mathcal{C}}, \widetilde{\boldsymbol{\mathcal{C}}}) = \sum_{i=1}^{N_r} \mathbf{g}_i \boldsymbol{\Psi} \mathbf{g}_i^H, \tag{4.19}$$

where

$$\boldsymbol{\Psi} = \sum_{k=1}^{N_c} \mathbf{F}_k \sqrt{\mathbf{R}_t} \mathbf{W}^H \mathbf{B}_k \mathbf{B}_k^H \mathbf{W} \sqrt{\mathbf{R}_t}^H \mathbf{F}_k^H \in \mathbb{C}^{N_t L \times N_t L} \tag{4.20}$$

is the *effective error distance* between two distinct codeword matrices and $\mathbf{B}_k = \mathbf{C}_k - \widetilde{\mathbf{C}}_k$. It is observed that $\boldsymbol{\Psi}$ is a non-negative definite Hermitian matrix, and thus, EVD of $\boldsymbol{\Psi}$ has a form of $\boldsymbol{\Lambda}\boldsymbol{\Psi}\boldsymbol{\Lambda}^H = \boldsymbol{\Omega}$, where $\boldsymbol{\Lambda}$ is a unitary matrix, $\boldsymbol{\Omega} = \mathrm{diag}\{\omega_1, \cdots, \omega_r\}$ contains nonzero eigenvalues, and r is the rank of $\boldsymbol{\Psi}$. We assume that the elements of $\{\underline{g}_i\}_{i=1}^{N_r}$ are independent and identically distributed (i.i.d.) complex Gaussian random variables. By averaging the conditional PEP in (4.18) over all channel realizations, the PEP of an Eigen-STF OFDM system can be finally

written as

$$P_r(\boldsymbol{\mathcal{C}} \to \widetilde{\boldsymbol{\mathcal{C}}}) \leq \left(\prod_{m=1}^{r} \omega_m \right)^{-N_r} \left(\frac{\gamma}{4} \right)^{-rN_r}, \tag{4.21}$$

where $\gamma = \rho \| \sqrt{\mathbf{R}_t} \mathbf{W}^H \|_F^2$ denotes the effective receiver SNR. Then the SNR gain of this system over systems without beamforming can be found as

$$\sum_{j=1}^{L} \mathbf{w}_j \mathbf{R}_t \mathbf{w}_j^H. \tag{4.22}$$

Diversity Order

Based on the above error probability analysis, a few remarks are now in order. First, by checking the dimensionality of $\boldsymbol{\Psi}$, the maximum diversity order in our system is $N_t L N_t$. Suppose that $\mathbf{B}$ has full rank for all pairs of matrices $\mathbf{C}_k \neq \widetilde{\mathbf{C}}_k$, which is a necessary assumption for the design of STF codeword to exploit the space diversity. If $\mathbf{R}_t$ has a rank of N_t, the system will achieve the maximum diversity order since the weight mapping matrix $\mathbf{W}$ is constructed with eigenvectors of $\mathbf{R}_t$ on its columns (so $\mathbf{W}$ has full rank as well). Second, when $\mathbf{R}_t$ is not a full rank matrix, the rank of $\mathbf{R}_t$ reduces to L; this implies that only L eigenvectors should be used, and thus the spatial domain encoding of STF codeword should be done across L dimensions instead of N_t, giving a new $\{\mathbf{C}_k\}_k \in \mathbb{C}^{L \times p}$. In this case the maximum diversity order of $N_t L N_r$ is still achievable. Third, when $L > N_t$, the eigenbeamformer outputs only N_t beams, which results in a diversity order of $N_t^2 N_r$, and thus incurs a loss of $L - N_t$. So, in order to achieve the maximum diversity order, it is necessary to have $N_t \geq L$, or to have an eigen-weight mapping scheme that will always generate L output beams.

Coding Gain

At a high SNR, Eqn. (4.21) can be expressed as

$$P_r(\boldsymbol{\mathcal{C}} \to \widetilde{\boldsymbol{\mathcal{C}}}) \leq \frac{\gamma^{-rN_r}}{\det\left(\sqrt{\mathbf{R}_t} \mathbf{W}^H \mathbf{W} \sqrt{\mathbf{R}_t}\right) \det\left(\mathbf{B}\mathbf{B}^H\right)}. \tag{4.23}$$

The coding gain can be found as

$$\left[\det\left(\sqrt{\mathbf{R}_t} \mathbf{W}^H \mathbf{W} \sqrt{\mathbf{R}_t} \right) \det\left(\mathbf{B}\mathbf{B}^H \right) \right]^{-r}. \tag{4.24}$$

Since STF codewords have already been chosen, we can assume $\det(\mathbf{B}\mathbf{B}^H)$ to be a constant.

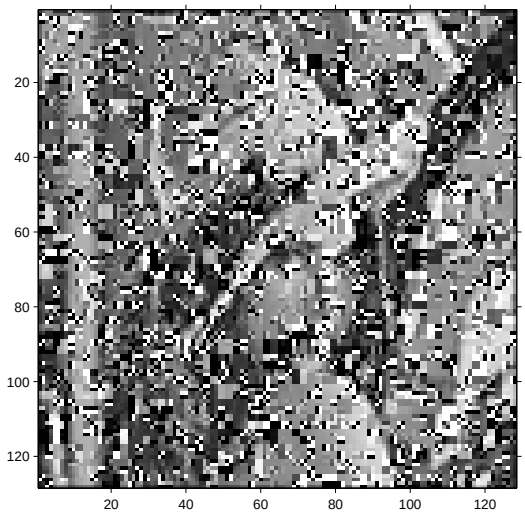

Figure 4.9: Reconstructed Lena image from the STBC-OFDM system with adaptive beamforming: SNR = 3 dB.

Given that $\mathbf{W}^H\mathbf{W} = I_{N_t}$, the coding gain is clearly affected by the correlation matrix. In general, it often results in coding gain penalty as shown in [46] where the performance reduction is proportional to the degree of spatial correlation. Thus, the coding gain is retained in our system.

From the channel capacity point of view, there is a possible technique in enhancing the AWG by loading unequal powers on the eigen-weighting matrix. It is shown in [47] that if power loading follows the waterpouring strategy, then the received SNR and the mutual information are maximised. In this case the joint use of transmit eigenbeamforming and diversity coding will not make sense anymore since this technique gives a reduction in the coding gain and the error rate performance can be achieved by using just beamforming.

4.3.6 Simulation Results

The performance of the overall ST-coded OFDM transmission system was evaluated using the application of compressed images. As in Section 4.2.4, a resized (128×128) version of the standard 512×512 gray scale Lena image with 8 bits/pixel resolution was used as the multimedia source data. The Lena image used for processing is shown in Figure 4.3. This was compressed using biorthogonal wavelets and a level 4 DWT decomposition.

The STF-OFDM-AB scheme was configured for QPSK baseband modulation and simulated using a maximum Doppler frequency of 100 Hz and a ULA with $N_t = 4$ and $N_r = 2$ (with a spacing of 0.5λ employed at the transmitter), over a correlated fading channel with a system SNR of 3 dB. Also, the source coder was configured for a compression ratio (CR) of 32.2 using

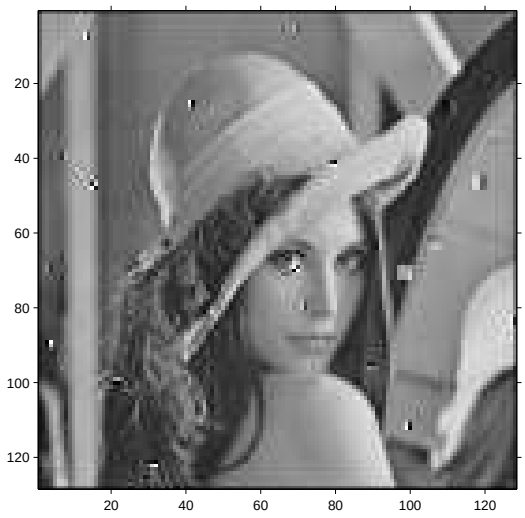

Figure 4.10: Reconstructed Lena image from the STF-OFDM system with adaptive beamforming: SNR = 3 dB.

a global DWTC threshold of 5. In order to determine the effectiveness of the STF-OFDM-AB system, this was simulated and compared to the STBC-OFDM-AB scheme presented in [52]. The resulting images obtained are shown in the accompanying Figures 4.9 and 4.10.

As expected, analysis of the performance curves and visual inspection (comparison of subjective fidelity measures) of the resulting images simulated, show quite clearly that significant improvements in system performance are achieved with an OFDM system using STF coding and adaptive beamforming.

4.4 Conclusions

In this chapter, we introduced two transmission systems for multimedia communication over wireless channels using a combined source coding scheme based on wavelet compression integrated with STBC-OFDM-AB and STF-OFDM-AB. The performance of these schemes have been analysed over the GBHDS channel model. Our study has shown that the diversity order and the coding gain are retained in the proposed structure while the received SNR is enhanced and the error performance is improved. Simulation results have also demonstrated that the STF-based scheme provides superior performance in terms of SER and BER as compared to that with only STBC in correlated channels.

In terms of practical implementation, the additional cost introduced by the proposed techniques in combining space-time coding and beamforming for narrowband systems would be minimal, especially when the required processing for the proposed beamforming scheme is now

transferred to the base station (traditionally, it is done at the mobile station), hence, reducing the amount of computational load/complexity at the mobile station. Therefore, the overall cost from adopting this new transmission technique in the system would remain the same as compared to systems employing the traditional beamforming scheme.

Chapter 5

An Optimised Transmission Technique for Mobile Multimedia

5.1 Introduction

In Chapter 4, it was shown that the performance of a mobile multimedia system could be significantly enhanced by combining a wavelet-based coding system with a STBC-OFDM-AB or STF-OFDM-AB system. A major problem with this scheme, however, is that the data encoded from the compression system is not optimised when transmitted over a mobile radio channel. One way to enhance or optimise the spectral efficiency and error performance of diversity coded OFDM systems is to use an adaptive modulator based on a *lookup matrix*-adaptive bit and power allocation scheme (LM-ABPA) proposed in [197–199]. Adaptive bit and power allocation (ABPA), also known as adaptive modulation (AM), is a modulation scheme that individually assigns an optimal symbol constellation size and power across subcarriers in a multi-carrier system such as OFDM to achieve a high spectral efficient transmission while maintaining system performance at a target level.

Current video/image source coders, on the other hand, such as those designed in the JPEG-2000 and MPEG standards [29], employ data compression techniques to encode information that are not equally important. Transform based or subband coders, compress data into their respective low-frequency and high-frequency components. In the case of wavelet-based coding, the resulting data from the data from the encoding process carry information which can be classified into two main classes: important data, that is, the low-frequency components/approximate coefficients - which are very sensitive to transmission errors; and less important data, that is, the high-frequency components/detail coefficients. It is well known, that in a mobile environment, data representing the low-frequency components are more sensitive to the time-varying nature of channel conditions and propagation environments.

Furthermore, in current wireless (MIMO-OFDM) transmission systems with combined source-channel coders, the data representing the low-frequency information of compressed signals are encoded and transmitted together with the high-frequency components using a sub-optimal transmit power level, signal constellation size, and modulation type. This can lead to a significant degradation in system performance as a large number of low-frequency components can be subjected to subchannels with a low SNR value, resulting in a loss of signal quality during the reconstruction/decoding process at the receiver. Consequently, for multimedia communication this means degradation in overall system performance, a reduction in data throughput, and a constraint on achieving high data-rate transmission.

In this chapter, we extend the previous framework presented in Chapter 4, to propose an optimized transceiver structure with a combined source-modulation coded adaptive MIMO-OFDM system using an unequal adaptive modulation scheme; where a LM-ABPA scheme is used to modulate the low and high frequency components from the compression stage separately. A modified version of the LM-ABPA algorithm, sorts and allocates subcarriers with the highest SNR to low-frequency data and the remaining to the least important data before allocating appropriate signal constellation sizes and transmit power levels. In this system, knowledge of the subchannel gain is also used to maximize the instantaneous channel-to-noise ratio (CNR) such that an optimal number of antenna beams are selected with a corresponding power splitting ratio. Thus, minimizing the symbol-error-rate (SER) and eliminating the multipath fading effect of the entire system. Although initial simulations are based on the application of digital images, this approach can be extended to study the transmission of other sources of multimedia data such as digital video.

The chapter is organised as follows. A system model representing the new transmission strategy that incorporates the LM-ABPA scheme with the wavelet-based compression system to enhance the error-rate performance for multimedia OFDM systems is presented in Section 5.2. In particular, Section 5.2.2 describes the procedure used by the unequal adaptive modulator to optimise the SNR of the transmitted data from the wavelet-based coder. The details of the constrained optimization problem is given in Section 5.2.4. In Section 5.3, simulation results based on the transmission of digital images are presented. Performance measurements such as the analysis of the user-perceived quality and PSNR metric are used to compare results. Finally, Section 5.4 provides concluding remarks.

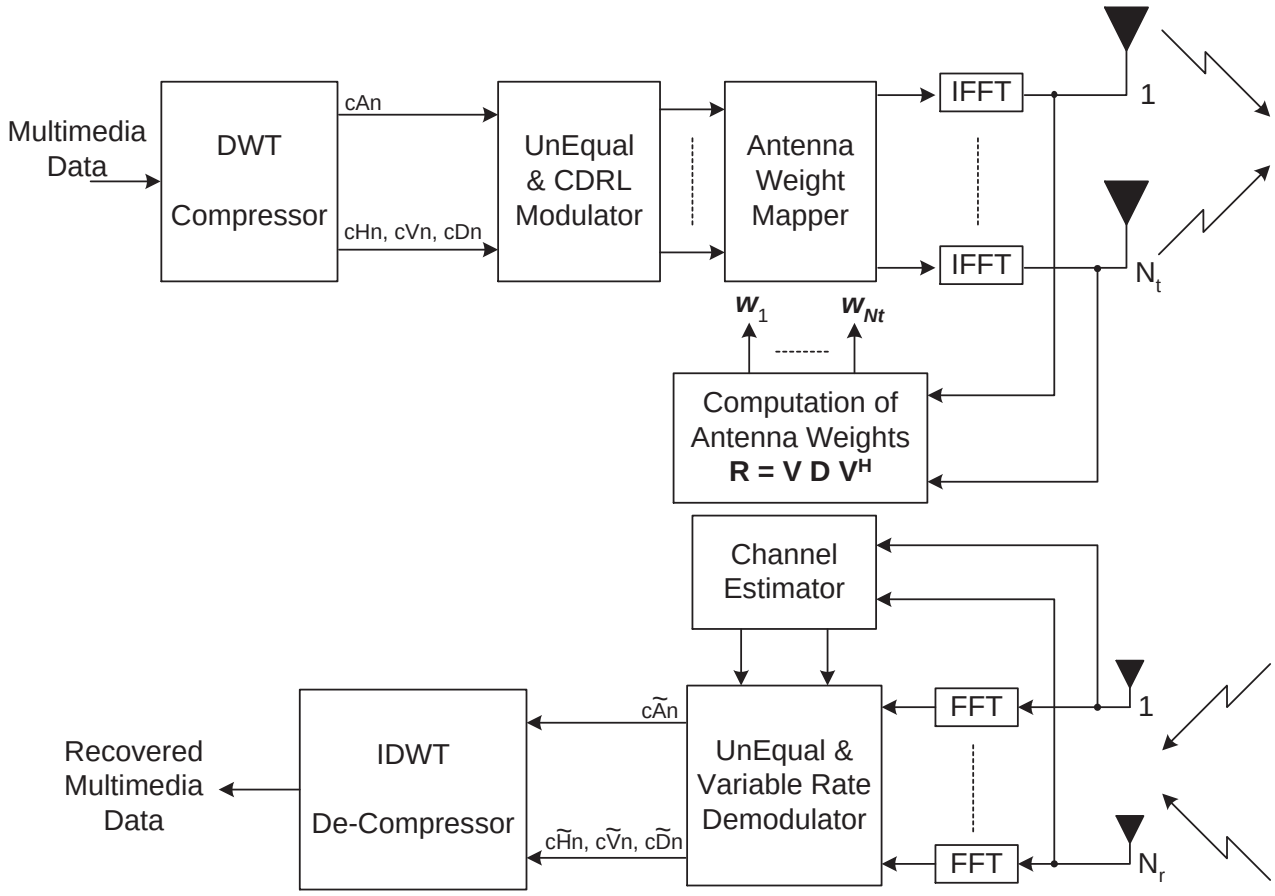

Figure 5.1: Transceiver structure of a combined source coder and unequal modulator for adaptive MIMO-OFDM systems with transmitter beamforming.

5.2 System Model

The transceiver structure proposed consists of 3 main blocks: data compression using a transform based coder, an unequal adaptive modulator, and a MIMO-OFDM transmission model with adaptive eigen-beamforming. As stated in the previous chapters, a channel encoder such as turbo coding, is not considered as we are only interested in the baseline performance of the system. Channel encoding schemes provide error correction capability and only add redundancy to the entropy coded data to achieve a BER close to the Shannon limit. A block diagram of the system model is shown in Figure 5.1 below. A description of the various processing elements are provided in the following sections.

5.2.1 Transform-Based Source Encoder

Referring to the system diagram in Figure 5.1, multimedia data is compressed using a source coder based on discrete wavelet transformation (DWT). In the case of transmitting digital images, a multiresolution 2D-DWT decomposition is performed using biorthogonal wavelets. In

wavelet analysis, we represent the low-resolution subband (low-frequency information) by approximation coefficients ($\mathbf{cA_n}$) and high-pass subband spatial-frequency data (high-frequency information) with horizontal, vertical, and diagonal detail coefficients ($\mathbf{cH_n}$, $\mathbf{cV_n}$, $\mathbf{cD_n}$) respectively. For an n-level decomposition, the coefficient matrix **CM** consists of the following coefficients

$$\mathbf{CM} = [\mathbf{cA_n}, \mathbf{cH_n}, \mathbf{cV_n}, \mathbf{cD_n}, \cdots, \mathbf{cH_1}, \mathbf{cV_1}, \mathbf{cD_1}] \tag{5.1}$$

During transmission, transform coefficients (DWTC) are adaptively mapped to a finite set of values using a uniform scalar quantizer. Additional lossless compression is achieved by further removing spatial and statistical redundancy of the DWTC using a combined run-length and entropy encoder. In this work, we use an improved Huffman coding scheme described in [202]. Unlike other systems, however, the coefficients resulting from the compression stage are not encoded together but are processed separately. That is, the approximate coefficients are transmitted over OFDM subchannels using an optimal transmit power level, constellation size, and modulation type. While, the less important data - detail coefficiets - are allocated the remaining sub-optimal channel resources.

5.2.2 Unequal Adaptive Modulation

Based on different system requirements, adaptive modulation schemes that allocate different transmit power and modulation constellation size across all subcarriers in a multicarrier system are commonly classified into two major categories: *constant error performance loading* & *constant data rate loading*. For systems designed for constant error performance loading, the system error rate performance is maintained at a prescribed target level while maximising the data rate at the same time without exceeding available total transmit power. In the case of constant data rate loading, the guaranteed system data rate is specified to be achieved with a minimum system error at the same time without exceeding available total transmit power.

To ensure that the SNR of the multimedia data recovered at the receiver is optimized, sensitive low-frequency data from the compressor is transmitted by making use of a desirable subchannel state. In this work, we maximize the instantaneous channel-to-noise ratio (CNR) based on a lookup matrix-adaptive bit and power allocation (LM-ABPA), and constant data rate loading (CDRL) scheme in [200]. The adaptive modulator is employed to first sort subcarrier information from the LM-ABPA process into subchannels with the highest SNR values to the

lowest. To achieve a target system SNR level, we allocate subcarriers with the highest SNR values to the approximate coefficients and the remaining data to the detail coefficients, such that, an optimal modulation signal is transmitted with a constellation size determined for the required subchannel SNR and target SER/BER. Thus, the term 'unequal adaptive modulation'. This process is then adapted to the varying channel conditions using the following MIMO-OFDM transmission system.

For a MIMO channel configuration, with N_t transmit and N_r receive antennas, and a wireless fading channel assumed to be frequency-selective (i.e., channel gains for subcarriers are independent) but spatially correlated, the transmit spatial covariance matrix that specifies the spatial correlation between antenna elements is defined as $\mathbf{R}_t$ [179] - assuming that a uniform linear array (ULA) configuration is used for N_t BS antennas. Let $\mathbf{H}_k$ be the channel frequency response matrix. Thus, the correlated channel frequency response is given by $\sqrt{\mathbf{R}_t}\mathbf{H}_k$, where $\sqrt{\boldsymbol{\mathcal{A}}}$ denotes the Hermitian square root of matrix $\boldsymbol{\mathcal{A}}$.

To maximize the transmitted signal power along the dominant multi-paths, eigen-beamforming strategy in [50] is utilized and eigen-decomposition of the spatial covariance matrix is performed. The resultant antenna weights are given by the eigenvector that corresponds to the largest eigenvalue. The eigen-decomposition of $\mathbf{R}_t$ has the form $\mathbf{R}_t = \mathbf{V}\mathbf{D}\mathbf{V}^H$, where $\mathbf{D} := \text{diag}(\mu_1, \mu_2, \cdots, \mu_{N_t})$ is a diagonal matrix with ordered (non-increasing) eigenvalues on the main diagonal and $\mathbf{V} := [\boldsymbol{\nu}_1, \cdots, \boldsymbol{\nu}_{N_t}]$ is a unitary matrix whose columns are the corresponding eigenvectors. Thus, the transmit weight vector $\mathbf{w} = \boldsymbol{\nu}_1$ can be found as the first column of $\mathbf{V}$.

Based on the channel estimation feedback message, a baseband signal constellation size and a transmit power level are computed during the CDRL process and allocated to each subcarrier. Thus, the number of information bits γ_k transmitted from the k^{th} subcarrier may be different from other subcarriers.

Let x_k be the CDRL output baseband symbol to be transmitted on the k^{th} subcarrier and ρ_k be the amount of power allocated. At the receiver, DFT is applied to signals received from N_r antennas and the discrete-time baseband equivalent expression for the received signal can be written as

$$\boldsymbol{y}_k = x_k\sqrt{\rho_k}\mathbf{w}\sqrt{\mathbf{R}_t}\mathbf{H}_k + \boldsymbol{\eta}_k \tag{5.2}$$

where $\boldsymbol{\eta}_k$ is the receiver noise vector with zero mean and σ_k^2 variance. At the receiver, channel estimation is performed by correlating pilot tones embedded in the transmitted signal. This estimate is then fed into the variable rate demodulator (VRD), which consists of a maximum

ratio combiner (MRC) and a maximum likelihood detector (MLD).

5.2.3 Error Performance Analysis

The receive SNR for the k^{th} subcarrier at the output of MRC can be found from (2) as $\text{SNR}_k = \varepsilon_s \rho_k \mu_1 \|\mathbf{H}_k\|_F^2 / \sigma_k^2$, where $\|\cdot\|_F$ denotes the Frobenius norm and ε_s is the average baseband symbol energy.

Next, we define the instantaneous channel-to-noise ratio (CNR) for the k^{th} frequency tone as $\text{CNR}_k = \mu_1 \|\mathbf{H}_k\|_F^2 / \sigma_k^2$.

For a M-QAM baseband modulated system, the average BER can be approximated as [203], $\text{BER}_{k,M-\text{QAM}} \approx 0.2 \exp[1.6 \cdot \text{SNR}_k / (2^{\gamma_k} - 1)]$ and $\text{BER}_{k,M-\text{PSK}} \approx \text{erfc}(\sqrt{\text{SNR}_k} \sin(\pi / 2^{\rho_k})) / \rho_k$ for M-PSK. Using these BER_k approximation, we can express the required SNR as a function of a target BER (BER_{tar}) for a particular M-QAM constellation size as

$$\text{SNR}_{\text{req},M-\text{QAM}} \approx \frac{(\ln(\frac{\text{BER}_{\text{tar}}}{0.2}))(1 - M)}{1.6}. \tag{5.3}$$

and M-QAM constellation size as

$$\text{SNR}_{\text{req},M-\text{PSK}} \approx \frac{-\ln(2 \cdot \text{BER}_{\text{tar}})}{\sin^2(\frac{\pi}{M})} \ . \tag{5.4}$$

5.2.4 Constant Data Rate Loading

As the unequal modulator is configured for a constant data rate load, the constrained optimization problem can be written as

$$\begin{aligned} \textbf{minimize} \quad & \text{BER}_k \ , \quad \forall \ k = 1, \cdots, N_c \\ \textbf{subject to} \quad & \text{C1.} \quad \sum_{k=1}^{N_c} \log_2 M_k = \mathcal{R}_{\text{T,tar}} \ \text{ and} \\ & \text{C2.} \quad \sum_{k=1}^{N_c} \rho_k = P_{\text{T}}, \end{aligned} \tag{5.5}$$

where $\mathcal{R}_{\text{T,tar}}$ is the target system data rate. The CDRL algorithm is divided into two major stages. Details of the loading techniques can be found in [201].

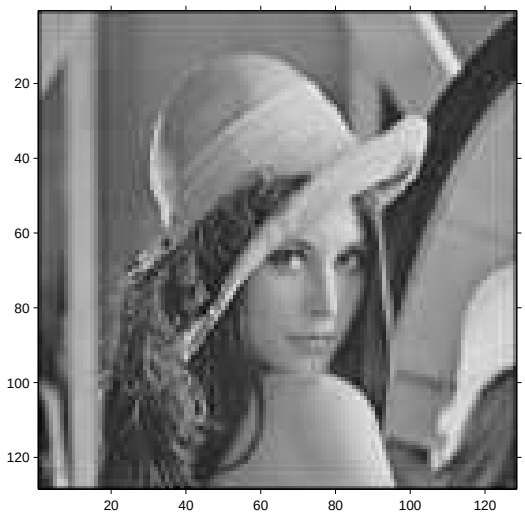

Figure 5.2: Original 128×128 Lena source image (8-bit gray scale).

5.3 Simulation Results

The performance of the proposed transmission structure was evaluated using the application of compressed images. A resized version (128×128) of the standard 512×512 gray scale Lena image was used for processing, and is shown in Figure 5.2. This was compressed using biorthogonal wavelets and a level 4 decomposition. The system model was configured for M-ary PSK modulation and simulated using a ULA with $N_t = 4$ and $N_r = 2$ (with a spacing of 0.5λ employed at the transmitter), over a correlated fading channel with a system SNR of 15dB. Also, the source encoder was configured for a compression ratio (CR) of 40.6 using a global DWTC threshold of 10.

In order to determine the effectiveness of the proposed unequal modulator scheme, the system was simulated and compared to a MIMO-OFDM system with a typical adaptive modulator. The resulting images and PSNR values obtained are shown in the accompanying Figures 5.3 and 5.4. As expected, visual inspection (subjective quality) of the images simulated, show quite clearly that a significant gain in system performance of approximately 3 dB is achieved for a combined source-modulation coded adaptive MIMO-OFDM system using an unequal adaptive modulator.

5.4 Conclusions

In this chapter, we have proposed an unequal modulation scheme for adaptive MIMO-OFDM systems with eigen-beamforming for the application of multimedia data over wireless/mobile channels. A discrete wavelet transform compression system is used to encode data into their respective low-frequency and high-frequency components. However, unlike other methods, data

Figure 5.3: Received image with non-adaptive modulation (PSNR = 11.8 dB).

Figure 5.4: Received image with unequal adaptive modulation (PSNR = 14.9 dB).

representing the low-frequency components (wavelet coefficients) are processed and modulated separately due to their sensitivity to noise/distrotion particularly during the wavelet decoding process. To ensure a desirable subchannel state, such that the quality (SNR) of the multimedia data recovered at the receiver is maximised, a lookup matrix-adaptive bit and power allocation (LM-ABPA) algorithm has been applied.

Apart from improving the spectral efficiency of OFDM, the LM-ABPA scheme optimises the transmission of multimedia data by sorting and allocating subcarriers with the highest SNR to

low-frequency data and the remaining data (high-frequency components). Appropriate signal constellation sizes and transmit power levels (modulation type) are then assigned across all subcarriers and is adapted to the varying channel conditions such that the average system error-rate (SER/BER) is minimised. When the system is configured using a constant data-rate constraint, simulation results for the application of compressed digital images show significant performance gains over non-adaptive or general OFDM systems.

Chapter 6

Application of a Blind Equalization Technique for Wireless Multimedia

6.1 Introduction

In a mobile radio environment, any signal transmitted over a wireless channel is subjected to various impairments caused by the effects of multipath propagation. Even in the absence of noise, *intersymbol interference* (ISI) has become a major obstacle in the reliable communication of high-speed applications such as, digital video. Arising from the time dispersive nature of channels, this type of distortion can be limited by placing a channel equaliser at the receiver [38]. This serves to maximise the transmission rate through the channel by compensating for the linear distortion introduced by the radio communication link. Even though a receiver comprises of various filtering stages, it is not surprising to find most of the computational load of a receiver system dominated by a channel equaliser [204]. As ISI is produced by time-varying multipath fading effects, the degradation caused can be severe depending on the changes in the reflective environment surrounding the receiver such as, reflections from physical structure of building, ground and water, moving vehicles, and foliage [21]. Naturally, the characteristic of this propagation channel is varying very fast, therefore, it necessitates the use of an *adaptive equaliser* to track the rapid time variation of the channel.

Traditionally, channel equalisation employs the use of training sequences for adapting its coefficients. Using this approach is attractive in handling time-variant mobile communication channels, but part of the communication bandwidth is wasted as a fraction of the transmission time must be allocated to process the training sequences. This obviously leads to a high cost implementation. In a point-to-multipoint or broadcast network, it is apparent that transmitting a training sequence for each new client (in order to establish a communication link between server and client) is not practical since it interrupts the transmission of communication data,

and requires a backward link from each receiver to request the training sequences [205].

Therefore, to overcome this problem, much research effort in modern digital communication systems has focused on the development of *blind equalisation* techniques. In contrast to the conventional adaptive equalisation methods, the blind adaptive equalisation schemes do not require training sequences. Since the 1980's, some applications have been deployed employing blind equalisation techniques where full bandwidth utilization of the channel is necessary, particularly, in meeting the demand for high rate multimedia applications such as, microwave radio [206], broadband access for high definition television (HDTV) [205], digital subscriber line (xDSL) [207], and point-to-multipoint access fiber-to-the-curb (FTTC) [208]. Although, implementation of orthogonal frequency division multiplexing (OFDM) in next-generation mobile communication networks is able to resolve the channel selectivity by transmitting the signal through a large number of carriers, the fact that the channel affects the carriers individually such that each carrier exhibits various attenuation and phase offset also necessitates the use of equalisation techniques to remedy the distorted signal [209, 210].

In recent years, there have been various algorithms developed for blind equalisation in mobile radio environements. The Constant Modulus Algorithm (CMA), originally proposed in [211], has attracted the main research effort as a suitable blind wireless channel equalizer. This is mainly due to its robustness over the violation of perfect blind equalization (PBE) conditions state in [212]. To achieve the low complexity requirement of the CMA algorithm, recent studies associated with the fractionally-spaced equalization constant modulus (FSE-CM) algorithm have lead to the development of the dithered signed-error constant modulus algorithm (DSE-CMA) and its applications [213–215]. In this scheme, the input signal to the equalizer is dithered by a non-subtractive sinusoidally-distributed signal before a sign operation is applied.

In this chapter, we investigate the characteristics and system performance of a wireless multimedia communication system using the sinusoidally-distributed dithered signed-error constant modulus algorithm (S-DSE-CMA) blind equalisation technique [216] in the application of compressed digital still images. The framework developed can be extended to study the transmission of other types of multimedia signals such as, high rate digital video. Empirical results obtained are used to determine subjective (perceptual-based) quality issues, without the need for an extensive numerical analysis as is often required in most research studies.

The system model comprising of the mobile communication channel, the $T/2$-spaced equaliser and the blind equalisation algorithm are presented in Sections 6.2 & 6.3 , while the framework for the simulation of multimedia data is described in Section 6.4. As the Peak Signal-to-Noise Ratio (PSNR) fidelity metric is used to measure the image quality of the restored image, the definition

of the PSNR is recalled again in Section 6.4.1. Finally, Section 6.5 discusses the performance analysis and results of the S-DSE-CMA blind equalisation technique based on the transmission of compressed images through a GBHDS mobile communication channel. Concluding remarks are given in Section 6.6.

6.2 System Model

Figures 6.1 and 6.2 depict a multirate model of a baseband communication system comprising of a transmitter and receiver part, where subscript n denotes baud-spaced quantities and subscript k represents $T/2$ fractionally-spaced quantities. Through this system, a sequence of formatted multimedia data symbolised as $\{x(n)\}$ with T symbol period is transmitted through the $T/2$-spaced channel $\mathbf{h}$ of a length N_h. In many communication systems, even in the absence of noise the effects of filtering and channel-induced distortion lead to intersymbol interference (ISI). Therefore, in addition to the white Gaussian noise the received signal is also corrupted by ISI. These distorted signals can only be removed by employing an equaliser in the receiver. Following the figures, the system output of the equalisation may be expressed as:

$$\begin{aligned} y(n) &= \mathbf{r}^H(n)\mathbf{f}(n) + \mathbf{w}^H(n)\mathbf{f}(n) \\ &= \mathbf{x}^H(n)\mathcal{H}\,\mathbf{f}(n) + \mathbf{w}^H(n)\mathbf{f}(n), \end{aligned} \tag{6.1}$$

where $\mathbf{x} = [x(n), x(n-1), \cdots, x(n-N_q+1)]^T$ denotes a finite-length source symbol vector of a length $N_q = \lfloor (N_h + N_f - 1)/2 \rfloor$, while $\mathbf{f}$ is representing a column vector of fractionally-spaced equaliser coefficients with a length N_f. A column vector $\mathbf{r}(n)$ and $\mathbf{w}(n)$ be the symbol of time-decimated of N_f received samples and white Gaussian noise, respectively. A Hermitian operator is denoted by $(.)^H$, and matrix transposition is symbolized by $(.)^T$. The matrix $\mathcal{H}$ symbolises a $N_q \times N_f$ time-decimated channel convolution, defined as follows:

$$\begin{bmatrix} c_1 & c_0 & & & & & \\ \vdots & \vdots & c_1 & c_0 & & & \\ c_{N_c-1} & c_{N_c-2} & \vdots & \vdots & \ddots & c_1 & c_0 \\ & & c_{N_c-1} & c_{N_c-2} & \ddots & \vdots & \vdots \\ & & & & & c_{N_c-1} & c_{N_c-2} \end{bmatrix}. \tag{6.2}$$

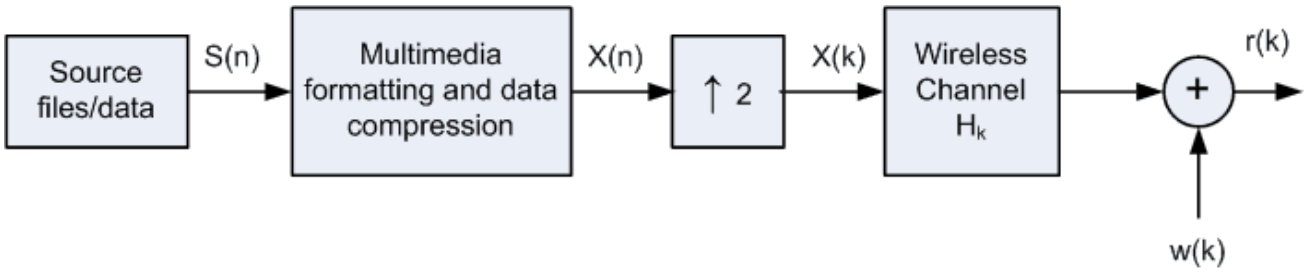

Figure 6.1: Transmitter block for $T/2$ baseband communication system.

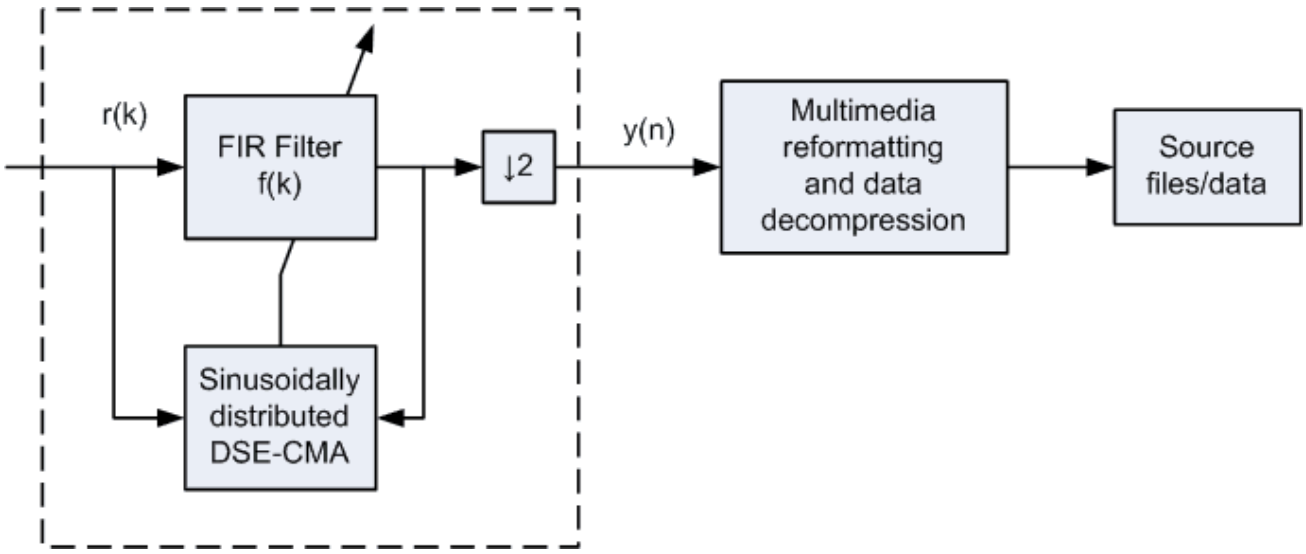

Figure 6.2: Receiver block with a linear equaliser for $T/2$ baseband communication system.

6.3 Blind Adaptive Algorithm

Most of blind adaptive equalizers update their coefficient vectors utilizing the stochastic gradient descent minimization method, which has also been used in this thesis. The equalizer coefficients are updated according to the following algorithm:

$$\mathbf{f}(n+1) = \mathbf{f}(n) + \mu \mathbf{r}(n) \psi_{\text{cma}}(y_n), \tag{6.3}$$

where μ is a small constant called the step-size, and $\psi_{\text{cma}}(y_n)$ is the CMA error function.

A complex-valued error function of CMA is described in [211] as:

$$\psi_{\text{cma}}(y_n) = y_n^*(\gamma - \mid y_n \mid^2), \tag{6.4}$$

where γ is a dispersion constant defined as

$$\gamma = E[|x(n)|^4]/E[|x(n)|^2]. \tag{6.5}$$

The objective that the equalizer minimizes the CM cost function (under a perfect blind equalization (PBE) condition [212]) is to remove all the linear distortion incurred by the channel such that the the output of the original source symbols are recovered for some system delay δ ($0 \leq \delta \leq N_x - 1$) and phase shift θ ($\theta \in [0, 2\pi]$). Hence, the filter output for perfect equalization becomes:

$$y_n = e^{j\theta} x_{n-\delta}. \tag{6.6}$$

Recently, advanced study of blind equalizers moved towards the achievement of complexity reduction. Primarily it is motivated by low cost implementation of the blind systems. One of the methods is transforming the error function in eq. (6.4) into a sign function. As it can be seen clearly, the multiplication of every regressor element with the error function becomes a multiplication with +1 and -1 only. However, in order to preserve information lost in the quantization process, a small perturbation random signal is added; this is called dithering [217]. Thus the error function in eq. (6.4) for complex-valued case is modified to:

$$\begin{aligned} \psi_{\text{dse-cma}}(y_n) &= \alpha \,\text{sign}\left(\psi^r_{\text{cma}}(y_n) + \nu^r_n(\alpha)\right) + \\ &\quad j\alpha \,\text{sign}\left(\psi^i_{\text{cma}}(y_n) + \nu^i_n(\alpha)\right), \end{aligned} \tag{6.7}$$

where α is a dither amplitude selected large enough to satisfy $\alpha \geq \max\{|\psi^r_{\text{cma}}(y_n)|, |\psi^i_{\text{cma}}(y_n)|\}$, $\nu^r_n(\alpha)$ and $\nu^i_n(\alpha)$ are real-valued i.i.d process sinusoidally distributed in $(-\alpha, \alpha)$ [216], where the superscripts r and i refer to the real and imaginary components, respectively.

In order to guarantee that the sinusoidally-distributed dithered signed-error CMA (DSE-CMA) algorithm resembles the behavior of the CMA, the theorems of the average transient behavior DSE-CMA in [217] will be imposed, in which α is selected in accordance with the values of $\{\alpha_{\text{c}}, \alpha_{\text{ZF}}, \alpha_{\text{OE}}\}$. These parameters are constellation and modulation dependent. The choice of $\alpha > \max\{\alpha_{\text{c}}, \alpha_{\text{ZF}}\}$ guarantees the zero-forcing solutions of the equalizer to be in the vicinity of CMA minima, while selections of $\alpha > \alpha_{\text{OE}}$ ensure the mean trajectory within $\mathcal{F}_\alpha$ (that there exists a neighbourhood around every open-eye equaliser). The convex hull $\mathcal{F}_\alpha$ is formed by the hyper planes $\mathcal{B}_\alpha := \{\mathbf{f} :| \mathbf{r}^H\mathbf{f} |= \psi^{-1}_{\text{cma}}(\alpha) \text{ for } \mathbf{r} \in \mathcal{R}\}$ in the absence of channel noise, where $\mathcal{R}$ is the set of all possible received vector $\mathbf{r}$. The reader is referred to [218] for the complete design guidelines of α.

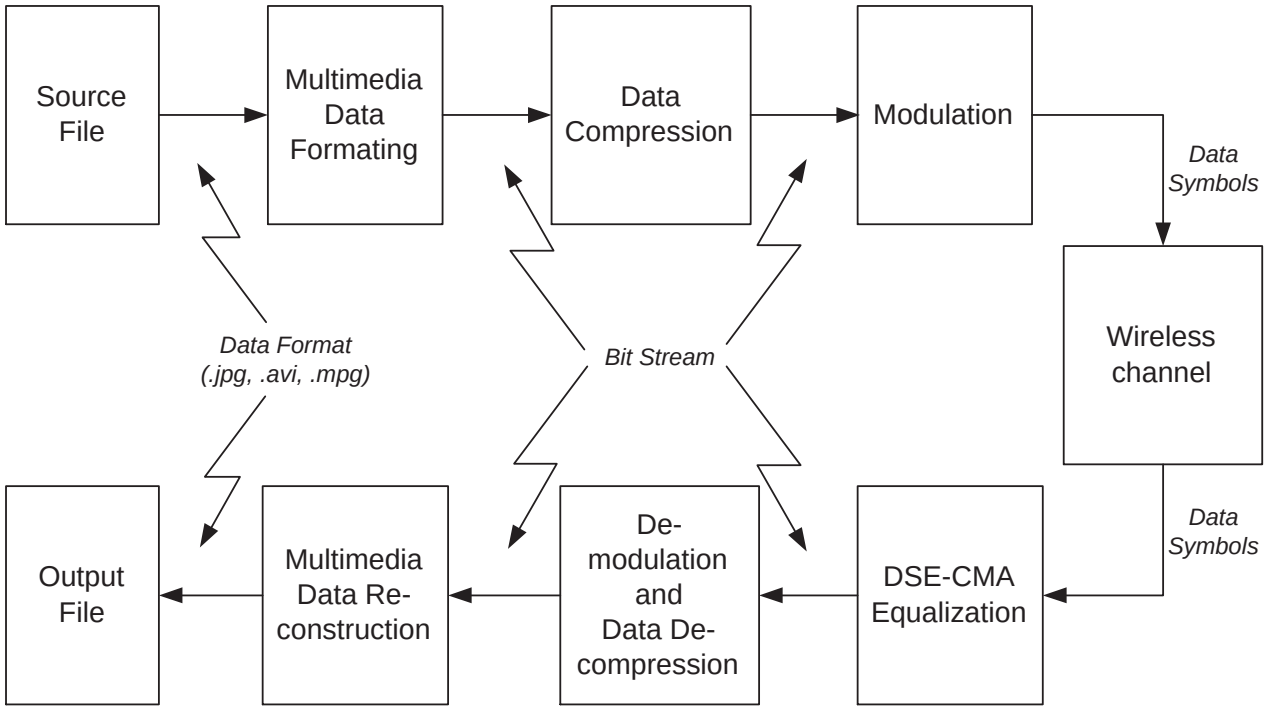

Figure 6.3: Framework for wireless multimedia communication using DSE-CMA.

6.4 Preprocessing of Multimedia Data

To enable the simulation of multimedia data using the proposed blind adaptive algorithm, the framework developed in the previous chapters is adopted. That is, the same method of converting multimedia signals from various data sources (such as compressed audio/image/video) and signal-processing using digital communication techniques such as source coding, baseband modulation, etc, is applied. This has been integrated together with the S-DSE-CMA blind equalisation scheme, to form the overall multimedia framework as depicted in Figure 6.3 (showing a general structure of the conversion process).

Recalling from Chapters 3, 4 & 5, the principal idea behind the preprocessing of multimedia data is to consider the source file (digitised version of the original multimedia signal with N-bit resolution) as a vector array containing integer quantisation levels. In the case, of digital image and video coding these correspond directly to pixel values [26]. Before the multimedia data can be processed by the multirate communication model, the source data is converted into a matrix array containing N bit-words which correspond to the sample/pixel levels. Thus, a bitstream representing the original multimedia data is created.

The simulation framework includes source coding for system development along with investigating new adaptive compression algorithms. A channel encoder to convert the bitstream to the required baseband modulated data symbols $\{x(n)\}$ as specified by the multirate model has been

implemented. In the receiver path, the reverse is performed on the modified data symbols $\{y(n)\}$ produced by the S-DSE-CMA equaliser. Whereby, the data symbols are first converted back to a bitstream by the channel decoder, and are subsequently reconstructed (via the de-compressor) to the original multimedia data format applied to the system.

6.4.1 Measurement of Image Quality

The performance of the S-DSE-CMA algortihm is evaluated using the objective measurement technique (Peak Signal-to-Noise Ratio) described in Chapter 2. Although the $PSNR$ metric is not an ideal measurement technique to quantify the quality of the image (as it does not account for complex distortion effects), it is commonly used in the field of image processing for quickly comparing restoration results for the same image. Thus, in this work, we utilise the $PSNR$ to compare the transmitted image with the restored image after the blind equalisation process. We recall from section 2.2.4, that the $PSNR$ is defined as:

$$PSNR(dB) = 10\ \log_{10}\left[\frac{(A_{MAX})^2}{MSE}\right]$$

and,

$$MSE = \frac{1}{M\,N}\sum_{m=0}^{M-1}\sum_{n=0}^{N-1}\left[x\,(m,n) - y\,(m,n)\right]^2$$

where, MSE is the Mean Square Error of the pixel values (pixel-to-pixel difference) between the original image, $x(m,n)$, and the distorted image, $y(m,n)$, of size $M\ \times\ N$ (the total number of pixels in the image). In this equation A_{MAX} is the maximum amplitude or peak signal amplitude that can be represented, which for an image with 8-bit/pixel resolution is 255.

6.5 Performance Analysis and Results

To evaluate the performance of the S-DSE-CMA equalisation algorithm in the application of multimedia data, a test image is transmitted over various wireless communication channels using the geometrically-based hyperbolically distributed scatterers (GBHDS) channel model in [110]. Two kind of channels simulating urban environments are used, where Channel A is generated with a path loss exponent ($epl = 2.8$) and Channel B is generated with a path loss exponent ($epl = 4$). The frequency and phase responses of the channels are depicted in Figure 6.4. It can be clearly seen that both model frequency selective fading channels, with a very deep null produced

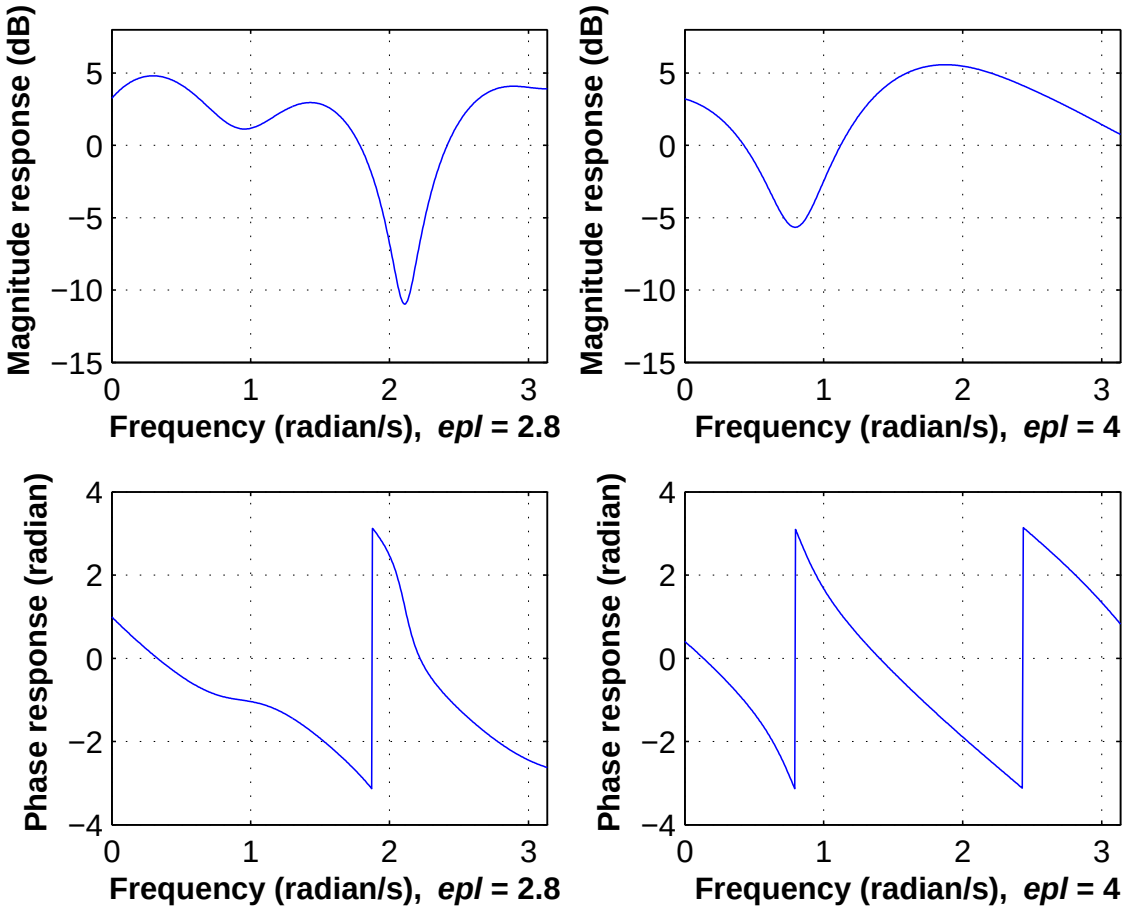

Figure 6.4: Frequency responses of Channel A and Channel B with path loss exponent ($epl = 2.8$) and ($epl = 4$), respectively.

by Channel A. These kind of channels obviously give rise to ISI as expected for multipath propagation in wireless environments, which deteriorate the received signal significantly.

A standard version of the 512×512 size gray scale Lena image with 8 bits/pixel resolution was used as the multimedia source data (test image) to the simulation framework. However, as discussed in the previous chapters, to reduce the computational load of the simulations the image was resized to 128×128 using 'bilinear' interpolation. The re-sized Lena image used for transmission is shown in Figure 6.5. The overall communication framework was configured for QPSK baseband modulation. The remaining parameters of the fractionally-spaced equaliser were set as follows: $N_f = 16$ and $\alpha = 1$. The dither amplitude α was set to be large enough to guarantee the existence of the zero-forcing solutions of the equalizers.

Figure 6.6 shows the recovered image from the output of the channel with $epl = 2.8$, where there was no equaliser used at the input of the receiver. It was simulated with a SNR = 50 dB. As expected, this results an image which is severely distorted. Through visual inspection we can confirm that even in the absence of noise, channel-induced distortion leads to ISI and corruption

Figure 6.5: Lena image source file (8-bit gray scale) after resizing to 128×128.

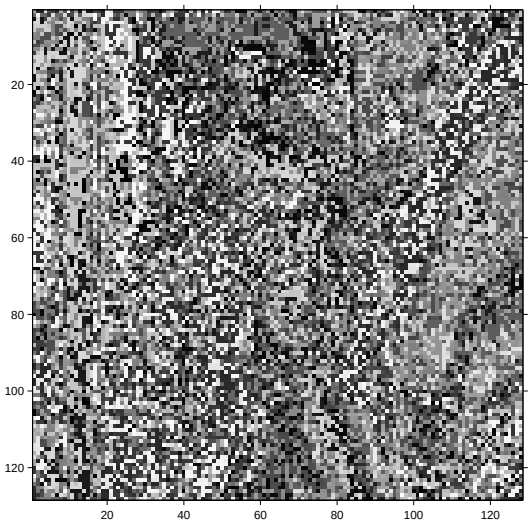

Figure 6.6: Received Lena image file (8-bit gray scale) after passing it through the GBHDS channel ($epl = 2.8$) without employing an equaliser, SNR = 50 dB.

of the original image.

In order to determine the effectiveness of the proposed S-DSE-CMA technique, the multirate model was configured and simulated for a SNR = 20 dB over a GBHDS channel ($epl = 2.8$) using a blind adaptive equaliser based on two schemes. In the first scheme, we used the uniformly-distributed dithered signed-error CMA, and in the second case we employed our proposed sinusoidally-distributed dithered signed-error CMA algorithm. Figure 6.7 and Figure 6.8 show the significant improvement obtained in using a sinusoidally-distributed DSE-CMA algo-

Figure 6.7: Equalized Lena image file after passing it through the GBHDS channel ($epl = 2.8$), SNR = 20 dB with blind adaptive equalisation utilizing sinusoidally-distributed DSE-CMA.

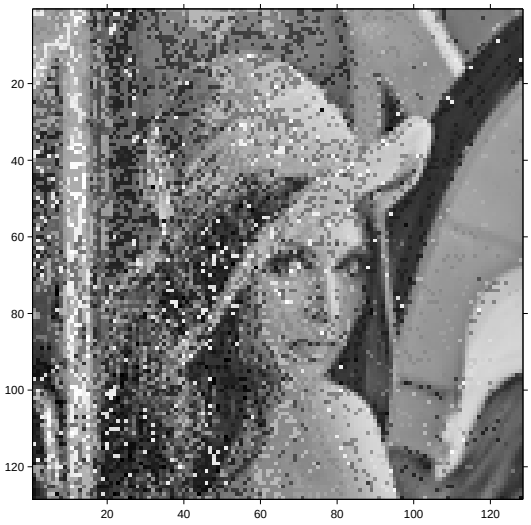

Figure 6.8: Equalized Lena image file after passing it through the GBHDS channel ($epl = 2.8$), SNR = 20 dB with blind adaptive equalisation utilizing uniformly-distributed DSE-CMA.

rithm as opposed to the uniformly-distributed DSE-CMA method. This is due to the faster convergence rate of sinusoidally-distributed DSE-CMA as compared to uniformaly-distributed DSE-CMA [216].

Clearly, for different channel conditions the results obtained are similar. Figure 6.9 and Figure 6.10 show the equalized images recovered after employing the two algorithms, both simulated using the GBHDS channel model ($epl = 4$). Under the condition when the thermal noise heavily

Figure 6.9: Equalized Lena image file after passing it through the GBHDS channel ($epl = 4$), SNR = 20 dB with blind adaptive equalisation utilizing sinusoidally-distributed DSE-CMA.

Figure 6.10: Equalized Lena image file after passing it through the GBHDS channel ($epl = 4$), SNR = 20 dB with blind adaptive equalisation utilizing uniformly-distributed DSE-CMA.

corrupts the channel, Figure 6.11 shows the degradation in user perceived quality of the received images. However, it can be seen that the equaliser is very efficient in removing the effect of ISI. Further analysis was performed using an objective performance metric such as, the peak signal-to-noise ratio (PSNR), commonly used in image processing literature [29]. The PSNR performance curves of the received images, transmitted over various wireless GBHDS channels using the two blind equalisation schemes, are plotted against different values of SNR. Each

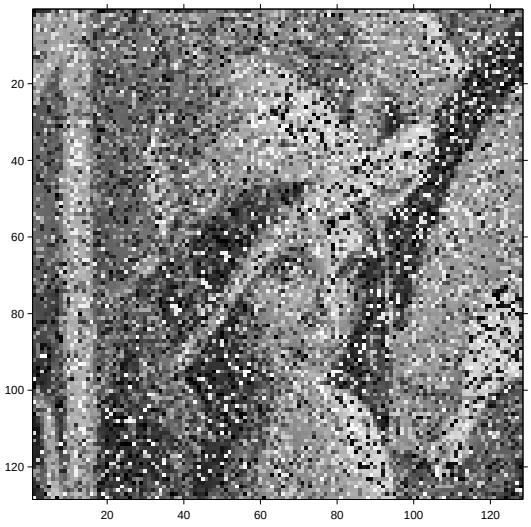

Figure 6.11: Equalized Lena image file after passing it through the GBHDS channel ($epl = 4$), SNR = 5 dB with blind adaptive equalisation utilizing sinusoidally-distributed DSE-CMA.

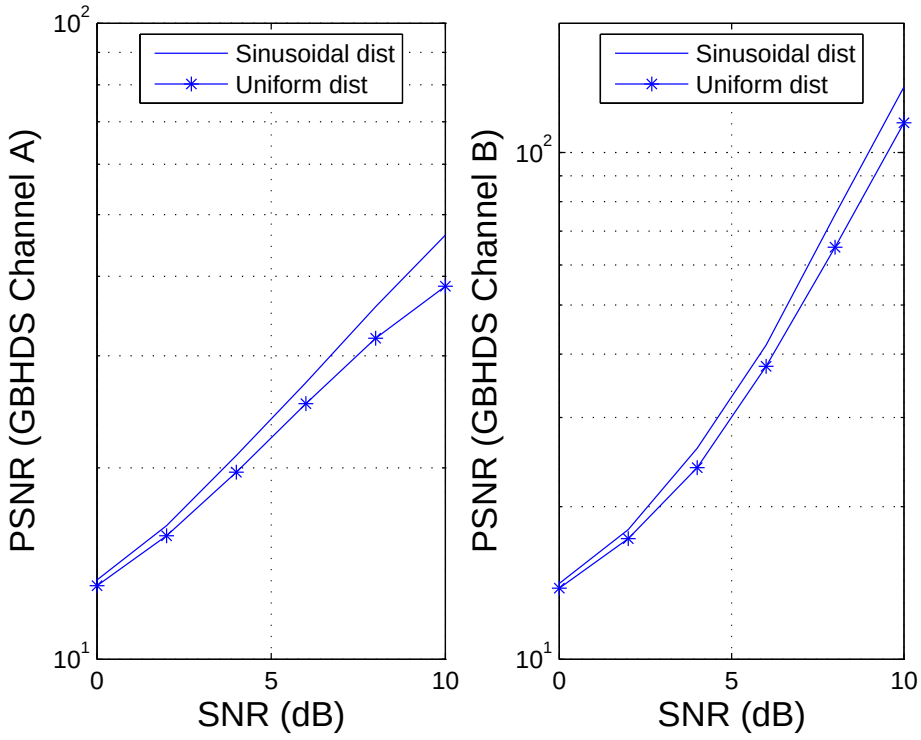

Figure 6.12: Peak signal-to-noise ratio (PSNR) of the received Lena image after equalisation for different values of SNR.

value of the PSNR for certain SNR values was averaged over 100 realizations. It can be seen in Figure 6.12, that the sinusoidally-distributed DSE-CMA algorithm outperforms the uniformly-distributed DSE-CMA algorithm in both cases.

6.6 Conclusion

In this chapter, we presented a multimedia communication framework to investigate the characteristics of the S-DSE-CMA blind equalisation technique in the transmission of compressed images over wireless communication channels. Simulation results, based on both user-perceived quality and the PSNR performance metric, showed that the recently proposed S-DSE-CMA algorithm outperforms other DSE-CMA blind equalisation techniques.

Chapter 7

Chaos for Secure Multimedia Communication

7.1 Introduction

The analysis of any dynamic system may be considered as a non-linear behavioral problem, and one of the easiest ways to model the security aspects of a communication system is to use a deterministic modeling technique such as Chaos Theory [219]. The application of a chaotic modeling technique is simple yet provides a characteristic that is close to a dynamic non-linear system. Over the past few years, there has been much of research effort devoted to the use of Chaos Theory in communication engineering [220–228]. In addition to its bifurcation property, the non-linear behavior of a chaotic system is well-suited in enhancing the security performance of existing communication systems. Chaos Theory has also offered several possibilities for new applications and other performance enhancements [229, 230].

In today's climate of increased criminal attacks on the privacy of personal or confidential data and with the rapid growth and use of multimedia applications (digital images/video) to convey information over digital communication systems, there is an impeding need for a more secure physical communication link. A review of current literature shows that a chaotic generator exhibits a set of properties which are suitable for use in spread spectrum (SS) communication systems. The basic principle of a spread spectrum system is to extend the original information data over a broad bandwidth of frequencies. To be able to perform spreading on the information data, the system requires a spreading code or sequence that provides auto- and cross-correlation behaviors similar to those of white noise. In a conventional spread spectrum communication system, a pseudorandom or a pseudo-noise (PN) sequence generator is used to produce the spreading code. Some systems use specially designed codes such as, Gold codes, Kasami codes, Walsh Hadamard, and OVSF codes [231] for spreading the information data. However, one of the

main issues with these types of spreading code generators is that they suffer from the 'periodicity' problem. This is due to the fact that the generated code sequences have a fixed number of states and the state-machine utilized runs through each sequence in a deterministic manner. It is this periodicity behavior of pseudorandom sequences which compromises the overall security of the system. Moreover, it reduces the system capacity [232]. In contrast, a chaotic generator can produce these noise-like sequences in a non-repeating fashion [222–224, 228].

A chaotic generator can be considered as an unlimited state-machine. Therefore, it can produce non-repeating sequences which are non-deterministic. This non-periodic behavior of chaotic generators offers significant advantages over the conventional pseudo-noise based SS systems in terms of security, synchronization, and system capacity. The bifurcation behavior of a chaotic generator (depending on some initial condition) can be readily exploited to enhance the security of a communication system. It can produce disordered sequences that provide auto- and cross-correction properties similar to random white noise, which are used to scramble data in spread spectrum systems. These sequences can be created from only a single mathematical relationship and is neither restricted in length nor repetitive/cyclic. Interception of information data depends on the estimation of the chaos sequence. It is very difficult to predict a long-term chaotic pattern unless the exact initial condition of the chaotic generator is known. Even a small error in the estimation of the initial condition used by the interceptor will lead to a very different chaotic sequence. Since the solution of the synchronization offered by Pecora and Carroll in 1990 [225], there have been an increasing number of proposed schemes that utilize chaos theory in SS communication systems. Such schemes include but are not limited to: chaotic masking, analog chaos modulation, digital chaos modulation (e.g., Chaos Shift Keying - CSK), and Chaotic CDMA sequences [220–228].

In this chapter, we use a chaos approach to develop a communication technique that provides a secure channel (guarded from interception) for the transmission of multimedia data with a high spectral efficiency and improved system capacity. We propose a modified logistic chaotic map for CSK spread spectrum communication in the application of 'real' multimedia data. This is compared with two different widely-used logistic chaotic maps. Subsequent sections of this chapter have been divided as follows: Section 7.2 provides an overview of the Chaos Shift Keying (CSK) modulation technique; Section 7.3 formulates CSK theoretical performance; Section 7.4 provides two commonly-used chaos generators with a modified chaos generator for CSK; Section 7.5 provides multimedia performance results using the proposed CSK system; Section 7.6 discusses the security aspects of the CSK system. Concluding remarks are presented in 7.7.

7.2 Chaos Shift Keying (CSK)

Spread spectrum communication is produced by directly multiplying the information bits (in the time domain) with a known spreading sequence running at a much higher rate, in order to spread the information over the bandwidth of the transmitted signal. The spreading sequence can be generated using a pseudorandom noise generator or some other specially-designed code generator. However, these generators produce repeating sequences and lead, over a long period of time, to a very predictable fashion which reduces the system capacity and security. To provide a secure communication channel, a chaos generator can be used to generate Chaos Shift Keying (CSK) sequences, where a different sequence can be generated using a different initial condition. Due to its bifurcation behavior, the chaotic sequence is very sensitive to the initial condition chosen. An exact value must be known in the receiver side to be able to demodulate the transmitted CSK signal

Chaos Shift Keying modulation uses a pair of chaotic sequences (g_1 and g_2) with different bit energies to transmit the binary information [226, 227]. If the l^{th} data bit which occupies the l^{th}-bit period is, $\alpha_l = +1$, then g_1 sequence is radiated from the transmitter, while for $\alpha_l = -1$, g_2 sequence is transmitted. The number of chaotic symbols transmitted for one data bit is dependent on the spreading factor (2β) [220]. The output of the CSK transmitter can be written as

$$s_k = \alpha_l g_{v,k} \tag{7.1}$$

where, v decides which chaos sequence is to be sent.

The chaotic sequence for CSK, g_1 and g_2, can be generated in three different ways. First method: it uses two different chaotic generators. Second method: generating the two sequences using different initial conditions of the same chaotic generator. And the last method: the two sequences are generated by the same chaotic generator with the same initial condition, but multiplied by two different constants. For simplicity, we use the latter method to generate the two chaotic sequences. In this work, the two chaotic sequences are related as $g_2 = -g_1$. Assuming we are only dealing a with binary system, where the sign of the binary signal is used to determine the chaotic sequences, the transmitted CSK signal from equation 7.1 can be simplify to

$$s_k = \alpha_l g_k \tag{7.2}$$

The demodulation process is simply a coherent correlator at the receiver as shown in Figure (7.1)

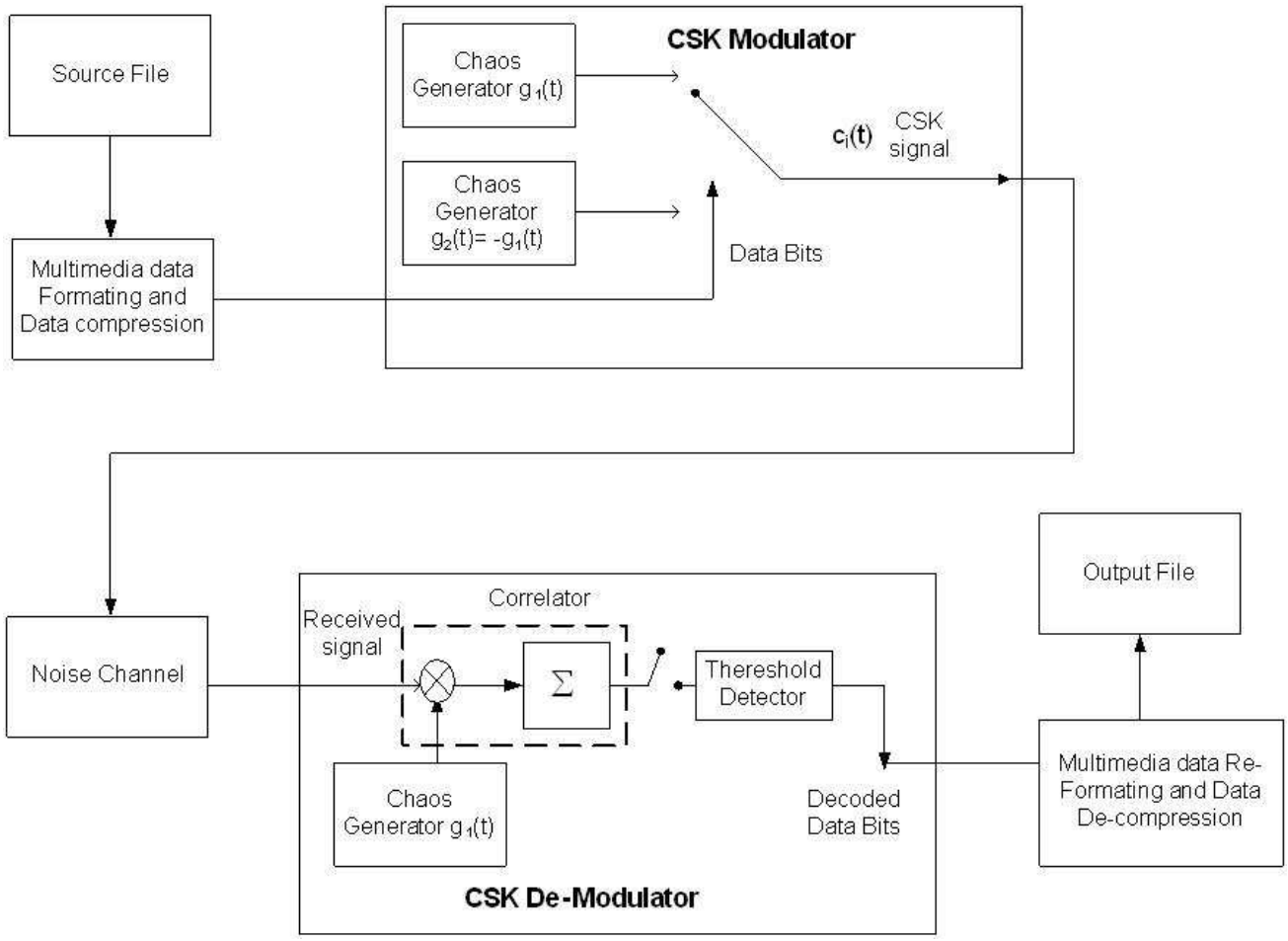

Figure 7.1: A multimedia framework for the CSK communication system.

7.3 CSK Theoretical Background

The performance of the CSK system in an AWGN environment can be derived following the method used in [220, 221]. For a correlator based receiver, the correlator output for the l^{th} bit y_l is given by

$$y_l = \sum_{k=2\beta(1-l)+1}^{2\beta l} r_k g_k \tag{7.3}$$

where, $r_k = s_k + \eta_k$, is the received signal in an AWGN environment during the k^{th} chip period and η_k being additive Gaussian white noise. Now we have:

$$y_l = \alpha_l \sum_{k=2\beta(1-l)+1}^{2\beta l} g_k^2 + \sum_{k=2\beta(1-l)+1}^{2\beta l} \eta_k g_k \tag{7.4}$$

The first term is the required signal and second term is noise. According to the Central Limit Theorem, if we consider a sum of a large number of random variables in the system, we can assume that the system to follow a normal distribution. Hence the BER for the CSK can be

formulated as follows:

$$\begin{aligned}
\mathrm{BER}_{CSK} &= \mathrm{Prob}(\alpha_l = 1) \times \mathrm{Prob}(y_l \leq 0 \mid \alpha_l = 1) \\
&+ \mathrm{Prob}(\alpha_l = -1) \times \mathrm{Prob}(y_l > 1 \mid \alpha_l = -1) \\
&= \frac{1}{4}\left[\mathrm{erfc}\left(\frac{\mathrm{E}[y_l \mid (\alpha_l = +1)]}{\sqrt{2\mathrm{var}[y_l \mid (\alpha_l = +1)]}}\right)\right. \\
&\left. + \mathrm{erfc}\left(\frac{-\mathrm{E}[y_l \mid (\alpha_l = -1)]}{\sqrt{2\mathrm{var}[y_l \mid (\alpha_l = -1)]}}\right)\right] \qquad (7.5)
\end{aligned}$$

From [220, 221], the variance of $y_l|(\alpha_l = +1)$ equals to the variance of $y_l|(\alpha_l = -1)$ and we have $\mathrm{E}[y_l|(\alpha_l = +1)] = -\mathrm{E}[y_l|(\alpha_l = -1)]$, where E is the expectation function. Hence, equation (7.5) can be simplified to:

$$\begin{aligned}
\mathrm{BER}_{CSK} &= \frac{1}{4}\left[\mathrm{erfc}\left(\frac{\mathrm{E}[y_l \mid (\alpha_l = +1)]}{\sqrt{2\mathrm{var}[y_l \mid (\alpha_l = +1)]}}\right)\right. \\
&\left. + \mathrm{erfc}\left(\frac{\mathrm{E}[y_l \mid (\alpha_l = +1)]}{\sqrt{2\mathrm{var}[y_l \mid (\alpha_l = +1)]}}\right)\right] \\
&= \frac{1}{2}\left[\mathrm{erfc}\left(\frac{\mathrm{E}[y_l \mid (\alpha_l = +1)]}{\sqrt{2\mathrm{var}[y_l \mid (\alpha_l = +1)]}}\right)\right] \qquad (7.6)
\end{aligned}$$

Where, erfc(.), is the complementary error function defined as

$$\mathrm{erfc}(\psi) \equiv \frac{2}{\sqrt{\pi}} \int_{\psi}^{\infty} e^{-\lambda^2} d\lambda. \qquad (7.7)$$

The mean value of y_l when $\alpha_l = +1$ in equation (7.4) is given as

$$\mathrm{E}[y_l|\alpha_l = +1] = \sum_{k=2\beta(1-l)+1}^{2\beta l} \mathrm{E}[g_k^2] + \sum_{k=2\beta(1-l)+1}^{2\beta l} \mathrm{E}[g_k][\eta_k] \qquad (7.8)$$

We Know that the mean of AWGN is zero, that is, $\mathrm{E}[\eta_k] = 0$. So the mean, therefore, for equation (7.8) can be simplified to:

$$\mathrm{E}[y_l|\alpha_l = +1] = 2\beta P_s + 0 \qquad (7.9)$$

where, $P_s = \mathrm{E}[g_k^2]$, is the average power of the chaotic signal.

As for the variance of y_l in equation (7.4), we know from [220, 221] that

$$\begin{aligned} 2\text{cov}\left[\sum_{k=2\beta(l-1)+1}^{2\beta l} g_k^2, \sum_{k=2\beta(l-1)+1}^{2\beta l} \eta_k g_k\right] &= 0 \\ \text{var}\left[\sum_{k=2\beta(l-1)+1}^{2\beta l} \eta_k g_k\right] &= \beta N_o P_s \\ \text{var}\left[\sum_{k=2\beta(l-1)+1}^{2\beta l} g_k^2\right] &= 2\beta\Lambda \end{aligned}$$

where, $\Lambda = \text{var}[g_k^2]$. Hence, the variance of y_l when $\alpha_l = +1$ for equation (7.4) is given by:

$$\begin{aligned} \text{var}\left[y_l \mid \alpha_l = +1\right] &= 2\text{cov}\left[\sum_{k=2\beta(l-1)+1}^{2\beta l} g_k^2, \sum_{k=2\beta(l-1)+1}^{2\beta l} \eta_k g_k\right] \\ &+ \text{var}\left[\sum_{k=2\beta(l-1)+1}^{2\beta l} \eta_k g_k\right] \\ &+ \text{var}\left[\sum_{k=2\beta(l-1)+1}^{2\beta l} g_k^2\right] \\ &= 0 + \beta N_o P_s + 2\beta\Lambda. \end{aligned} \tag{7.10}$$

Substituting (7.9) and (7.10) into equation (7.6), the BER for CSK can be found as follows:

$$\begin{aligned} \text{BER}_{CSK} &= \frac{1}{2}\text{erfc}\left(\frac{2\beta P_s}{\sqrt{4\beta\Lambda + 2\beta N_o P_s}}\right) \\ &= \frac{1}{2}\text{erfc}\left(\frac{1}{\sqrt{\frac{\Lambda}{\beta P_s^2} + \frac{N_o}{E_b}}}\right) \\ &= \frac{1}{2}\text{erfc}\left(\frac{1}{\sqrt{\left(\frac{E_b^2}{4\beta\Lambda}\right)^{-1} + \left(\frac{E_b}{N_o}\right)^{-1}}}\right) \end{aligned} \tag{7.11}$$

where, $E_b = 2\beta P_s$. Equation (7.11) shows that the BER performance of the CSK system can be improved by either reducing Λ (variance of g_k^2), increasing the spreading factor (2β), or increasing the signal power P_s (that is, $\text{E}[g_k^2]$).

7.4 Chaotic Sequences and Their Performance

Two commonly used chaotic generators and our proposed modified chaotic generator are studied in this section. To obtain the BER performance for each chaos logistic map or sequence, the signal power P_s and the variance Λ are either calculated from their invariant probability density function (pdf) or numerically obtained from simulation.

7.4.1 Logistic Chaos Generator 1 (LCG1)

This is one of the simplest chaos logistic maps used in generating chaotic sequences for digital communication [220–222] in which:

$$g_{n+1} = 1 - 2g_n^2 \tag{7.12}$$

with the invariant probability density function given in [220–222, 228] as follows:

$$\rho(g) = \begin{cases} \frac{1}{\pi\sqrt{1-g^2}} & \text{, if } \mid g \mid < 1 \\ 0 & \text{, otherwise} \end{cases} \tag{7.13}$$

Hence, the values of P_s and Λ for LCG1 can be mathematically calculated using its invariance probability density function as shown by [220]:

$$P_s = \mathrm{E}[g_k^2] = \int_{-\infty}^{\infty} g^2 \rho(g) dg = \int_{-1}^{1} g^2 \frac{1}{\pi\sqrt{1-g^2}} dg = \frac{1}{2} \tag{7.14}$$

$$\Lambda = \mathrm{var}[g_k^2] = \mathrm{E}[g_k^4] - \mathrm{E}^2[g_k^2] = \int_{-1}^{1} g^4 \rho(g) dg - \frac{1}{4} = \frac{1}{8} \tag{7.15}$$

7.4.2 Logistic Chaos Generator 2 (LCG2)

Another dynamic system that is capable of exhibiting chaotic properties for spreading spectrum communication is proposed in [223, 224] in which:

$$g_{n+1} = a g_n (1 - g_n) \tag{7.16}$$

where, a is the bifurcation parameter (or control) parameter, which is considered to be in the interval of $3.57 < a \leq 4$; for a non-periodic chaos system.

In this work, the bifurcation parameter is identified as the 'security key' of the system. This security key can only be known to the authorized user. Without this key the transmitted signal cannot be demodulated. However, a drawback of this system is that the output of the above

Table 7.1: Statistics of Logistic Map 3 (LCG3)

a	$\mathrm{E}[g_k^2]$ or P_s	Λ
4	$\frac{1}{2}$	$\frac{1}{8}$
3.97	$\frac{9}{20}$	0.111
3.95	0.410	$\frac{1}{10}$
3.90	0.392	0.095

sequence lies in the interval $0 \leq g_n \leq 1$, which decreases P_s and increases Λ (as compared to LCG1). This will lead to a lower BER performance. The probability density function for this system is not provided. Numerical simulation is used to obtain, $P_s = \frac{3}{8}$, and $\Lambda = 1\frac{1}{3}$, when $a = 4$. To Increase the system performance, a modified version of this logistic is proposed in the next Section and is shown to have a higher value of P_s and a lower value for Λ .

7.4.3 The Proposed Logistic Chaos Generator 3 (LCG3)

The proposed chaos generator (LCG3) in this section is a modification of the logistic chaos generator 2 (LCG2), which is a scaled and shifted version of LCG2. Scaling and shifting the chaos sequence will not change the chaotic properties of the generator but will provide an increase in P_s and a decrease in the Λ value. This will improve the BER performance over LCG2. The proposed logistic chaos generator is as shown below:

$$\begin{aligned} g_{n+1} &= a g_n (1 - g_n) \\ j_{n+1} &= 2(g_{n+1} - 0.5) \end{aligned} \tag{7.17}$$

where, j_n is the output chaotic sequence for the CSK modulator and a is the chaotic or security parameter, as discussed previously, and is considered to be in the interval $3.57 < a \leq 4$. Again, the probability density function for this system is not provided. Numerical simulation is used to obtain P_s and Λ; which are shown in Table 7.1.

It should be noted, that when $a = 4$ both LCG1 and LCG3 provide the same values for P_s and Λ. From Table 7.1, we can see that LCG3 can provide the same performance characteristics as LCG1, but as will be shown in section 7.6, can significantly improve the security of the system by simply modifying the parameter, a.

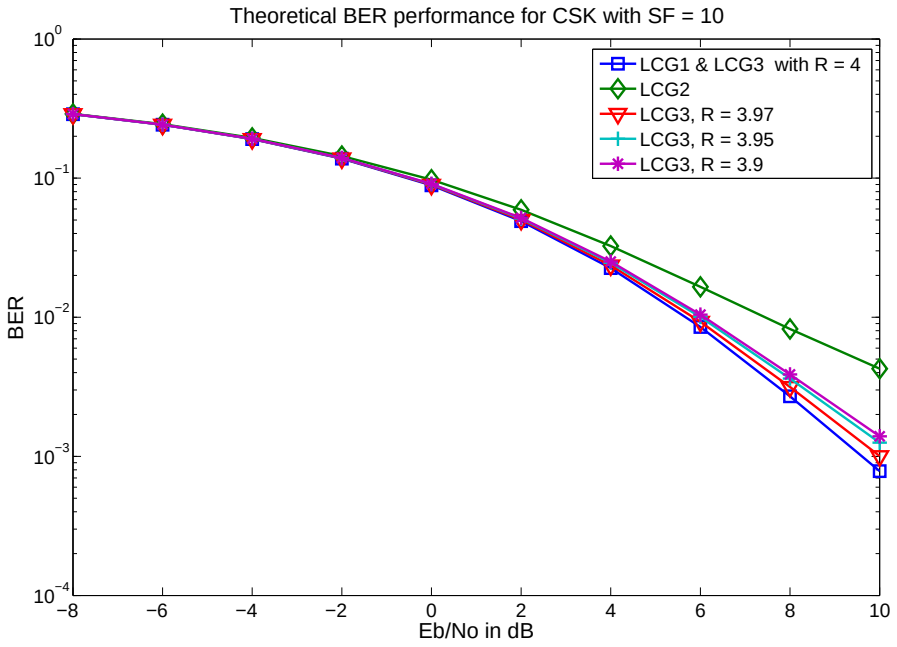

Figure 7.2: Theoretical BER performance of CSK in AWGN Channel with SF=10.

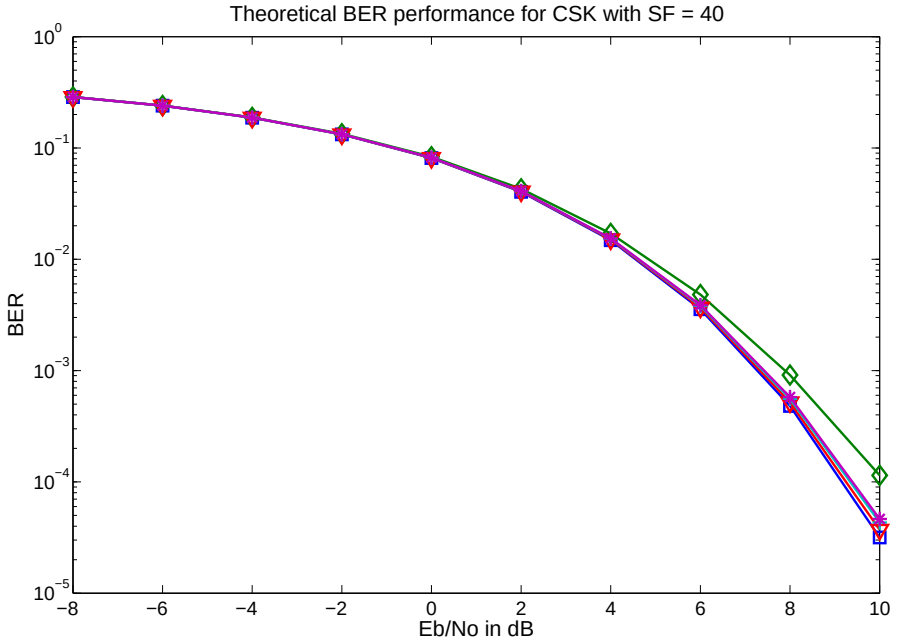

Figure 7.3: Theoretical BER performance of CSK in AWGN Channel with SF=30.

7.4.4 Performance of the CSK System

Using equation (7.11), the theoretical BER performance of the CSK system can be plotted against Eb/No as shown in figures (7.2, 7.3, 7.4, 7.5).

From the theoretical curves and simulated results shown in figures (7.6 & 7.7), one can clearly see that the performance of CSK in an AWGN channel can be improved by utilizing a higher spreading factor (SF). Comparing LCG1 to LCG3 based on theoretical BER performance,

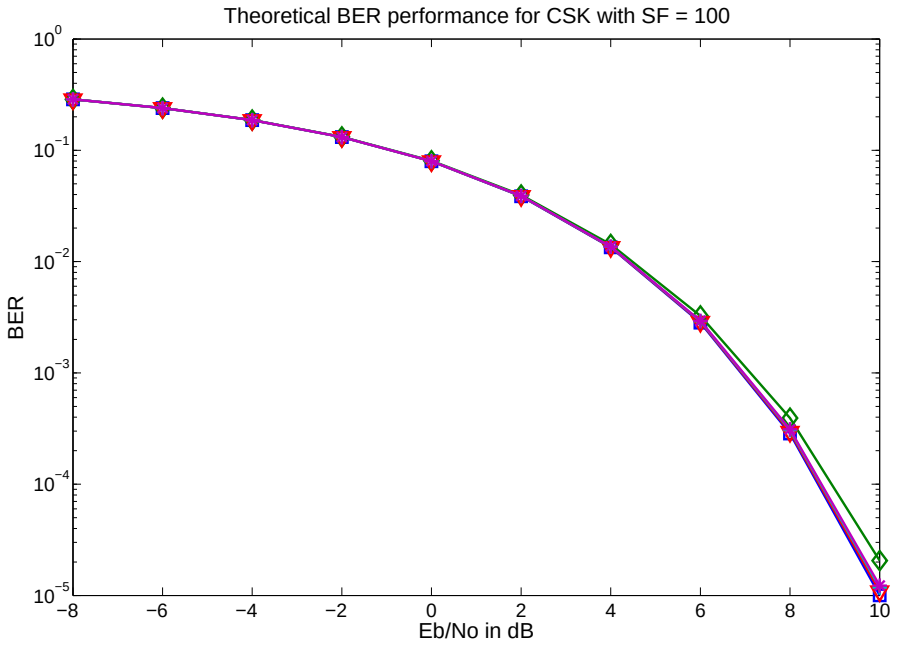

Figure 7.4: Theoretical BER performance of CSK in AWGN Channel with SF=100.

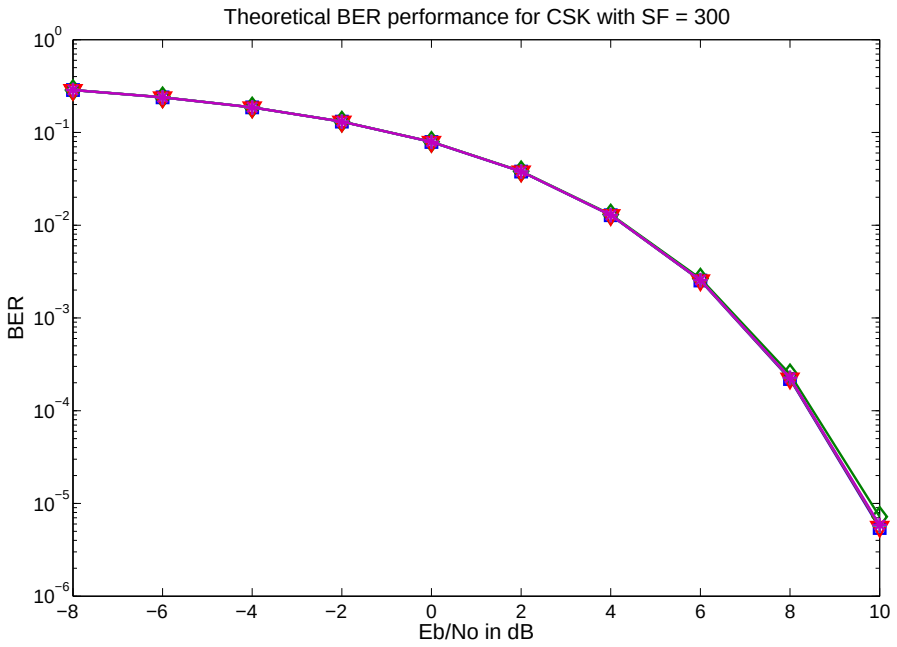

Figure 7.5: Theoretical BER performance of CSK in AWGN Channel with SF=300.

there is not much difference even when the security parameter a is varied. Both theoretical and simulated BER results show that LCG2 performance drops one order of magnitude when a small value of SF is used. Hence, LCG3 can perform as well as LCG1 with the advantage of an additional parameter for enhancing the security of a communication channel. Figure (7.8), shows the performance of the CSK system for different SF values in a 10 dB AWGN channel. When a large SF value is employed we can virtually see no difference between all three generators.

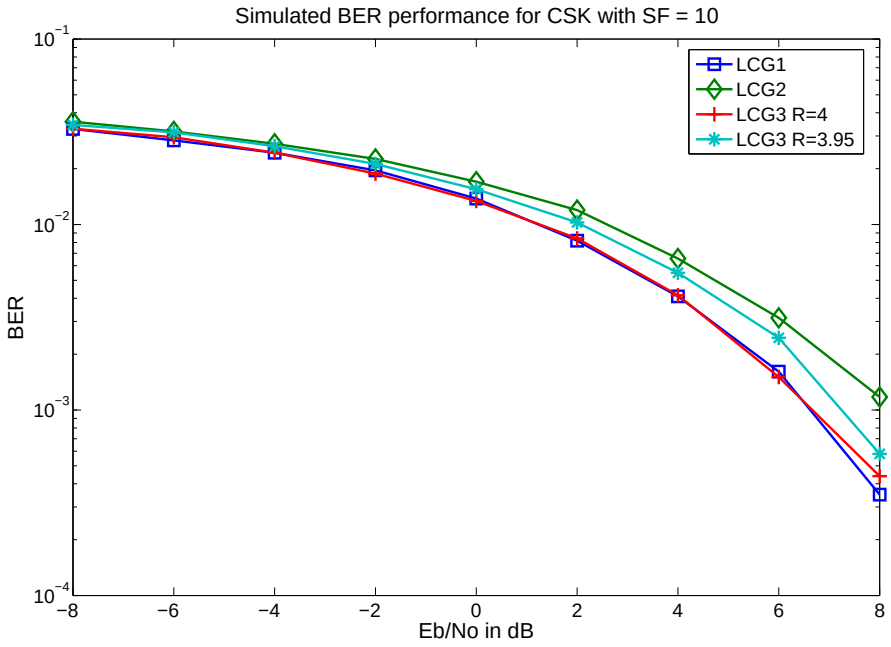

Figure 7.6: Simulated BER performance of CSK in AWGN Channel with SF=10.

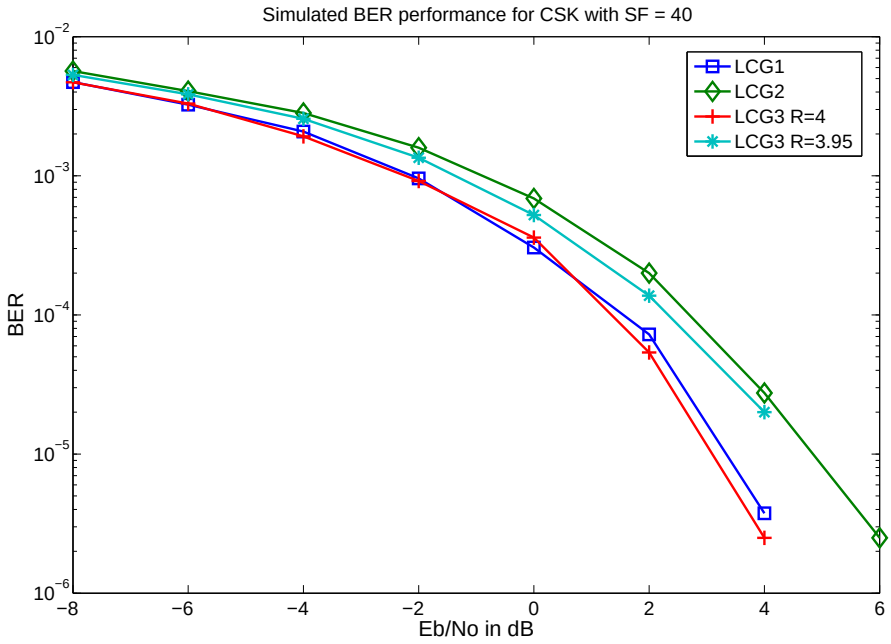

Figure 7.7: Simulated BER performance of CSK in AWGN Channel with SF=40.

However, when the SF value is small (around 50 - 100), the BER performance shows a significant difference even for a simple increase in the SF value. Note, that an optimum value of SF for CSK should be around 50 - 100 for an AWGN channel environment.

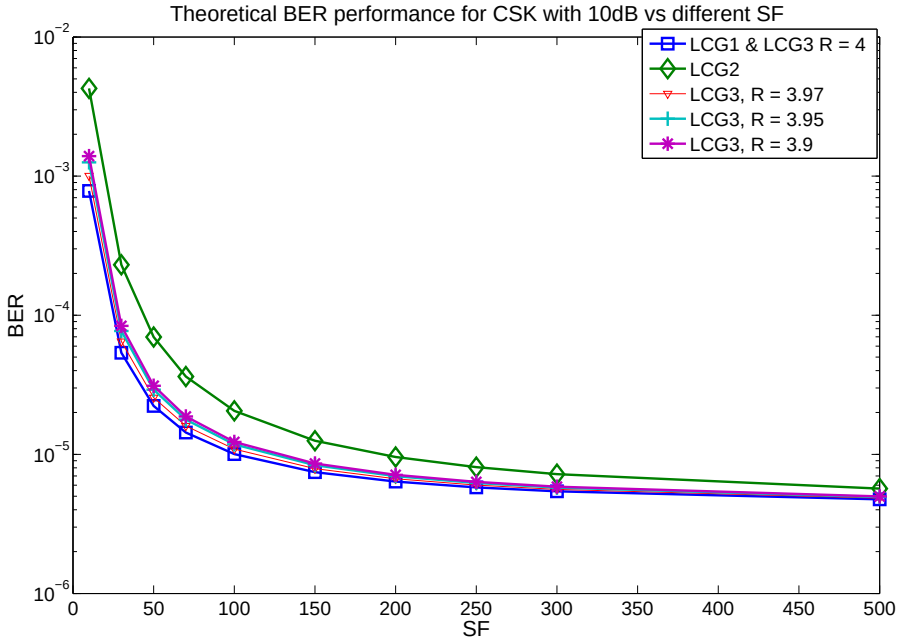

Figure 7.8: Theoretical BER performance of CSK versus different SF with AWGN Channel ($E_b/N_o = 10$ dB).

7.5 Multimedia Framework and Performance Analysis

To enable the simulation of multimedia data over the proposed CSK system, the framework developed in the previous chapters is adopted. That is, the same process of converting multimedia signals from various data sources (such as, compressed audio/ image/ video), which may be stored as files on a PC, is used. This has been integrated together with the CSK modulator, to form the overall multimedia simulation framework; refer to Figure (7.1). A generic transmission system for multimedia data using the CSK scheme has been implemented using a conversion process which transforms multimedia content to a suitable data format which can be further processed by the CSK modulator.

As detailed previously in Chapter 3, the principal idea behind the multimedia preprocessing stage developed is to first consider the source data (digitized version of the original multimedia signal with N-bit resolution) as a vector array containing integer quantization levels. For digital image and video coding these correspond directly to the sampled pixel values [26]. Before the multimedia information can be processed by the CSK modulator, the source data is converted into a matrix array containing N bit-words which correspond to the sample/pixel levels. Thus, a bit-stream representing the original multimedia data is created. This is subsequently encoded into the required baseband modulated data symbols, as specified by the CSK modulator. In the receiver structure, the reverse functions of the transmitter are performed on the modified data

symbols produced by the CSK scheme. Data symbols are first converted back to a bit-stream and are subsequently reconstructed back to the original multimedia data format applied to the system.

7.5.1 Performance Measurement

The performance of the CSK system in the application of multimedia data can be measured in terms of both user perception (human perceived quality) and the use of the fidelity criterion known as the Peak Signal-to-Noise Ratio, as defined in section 2.2.4. Traditionally, performance analysis of communication systems is based on objective measures such as the BER or MSE criteria. These metrics alone, however, cannot be used to determine the overall effectiveness of the 'security' of the system nor the quality of the received (decoded) multimedia data. To illustrate the misuse of the BER performance measurement technique in this situation, Figure (7.9) shows that both the shifted image (image pixel is shifted one line to the top) and the noise-added image (original image with white noise) provide a similar BER or MSE result. While, perception-wise, it can be clearly seen that the noise-added image is very different from the original.

Subjective assessment of the visual or perceived quality of individual images using an ensemble of test subjects can often be a tedious process. As stated in section 2.2.4, the $PSNR$ metric can thus be used to quickly quantify the resulting image distortion when compared to the original. It is also important to note, that the BER of the physical channel (in a communication system) can provide control over the user-perceived quality. For digital image applications, for example, the most important quality measure is how the image appears to the end user. This will differ depending on the type of multimedia content being transmitted, and in this situation can be used to ascertain a suitable BER for a particular CSK scheme and a given target application.

7.5.2 Simulation Results

To evaluate/demonstrate the transmission of multimedia data over a secure communication channel using the proposed CSK system, the simulation framework was configured for the application of digital still images. A standard version of the 512x512 size gray scale Lenna image with 8 bits/pixel resolution [89] was used as the multimedia source data/ file input. Due to practical computational limitations, however, the Lena image was resized to 128x128. Although, this introduces slight imperfections in the image, it has a very minor effect on the results obtained. The re-sized Lena image used is shown in Figure 7.9 - labeled as 'Original Image'. Figures 7.10,

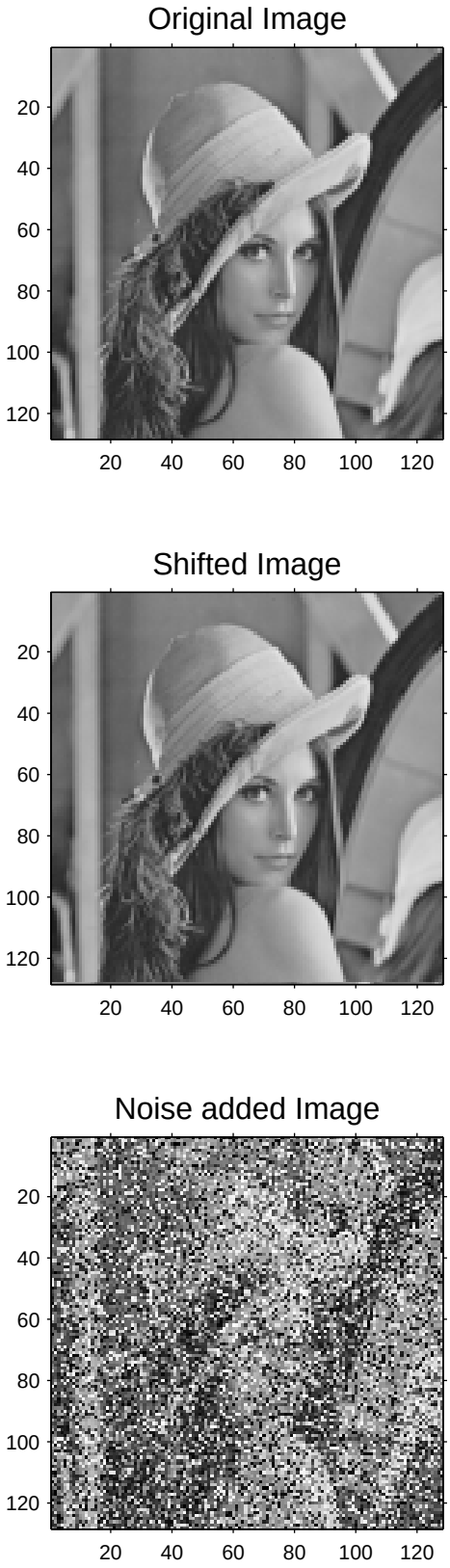

Figure 7.9: Illustrating the misuse of traditional BER performance over user (human) perception.

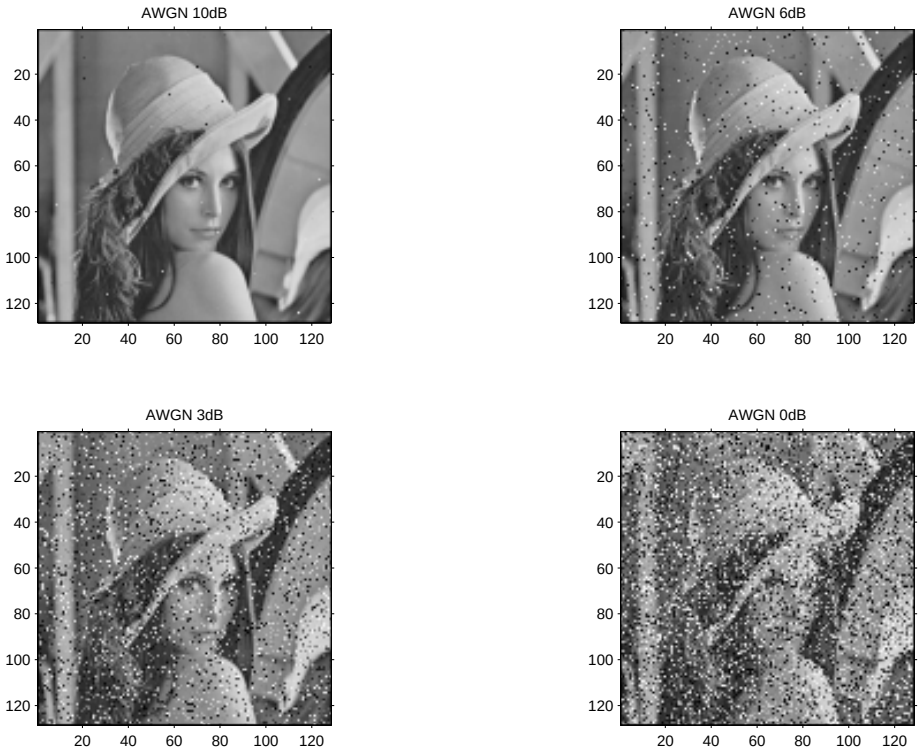

Figure 7.10: Multimedia performance of the LCG1 CSK system in different AWGN environments (SF = 10).

Table 7.2: Comparison of PSNR Values for Different CSK Systems and Images

PSNR	LCG1	LCG2	LCG3
Lenna	17.16 dB	15.49 dB	16.90 dB
Bridge	17.07 dB	15.38 dB	16.71 dB
Peppers	17.09 dB	15.28 dB	17.01 dB

7.11, 7.12, 7.13 show the performance of different CSK systems for multimedia transmission. On close inspection of the resulting images, we notice that the performance of the LCG2 based CSK system is slightly worse than the LCG1 and LCG3 CSK systems.

To support the performance results presented in Figures 7.10, 7.11, 7.12, 7.13, the simulations were repeated for different test images - Lenna, Bridge, Peppers [90, 91] - and the PSNR of the reconstructed images was evaluated. Figures 7.14, 7.15, 7.16 and Table 7.2 show the resulting images obtained for CSK systems using LCG1, LCG2, and LCG3, and their respective PSNR values. As expected, from Table 7.2, we can clearly see that the PSNR difference between the CSK system using LCG2 and the other systems is not significant and is normally not very noticeable.

Although Section 7.4 shows that the three systems provide different BER performance curves, the small variation in BER performance may not be too apparent perception-wise for multimedia

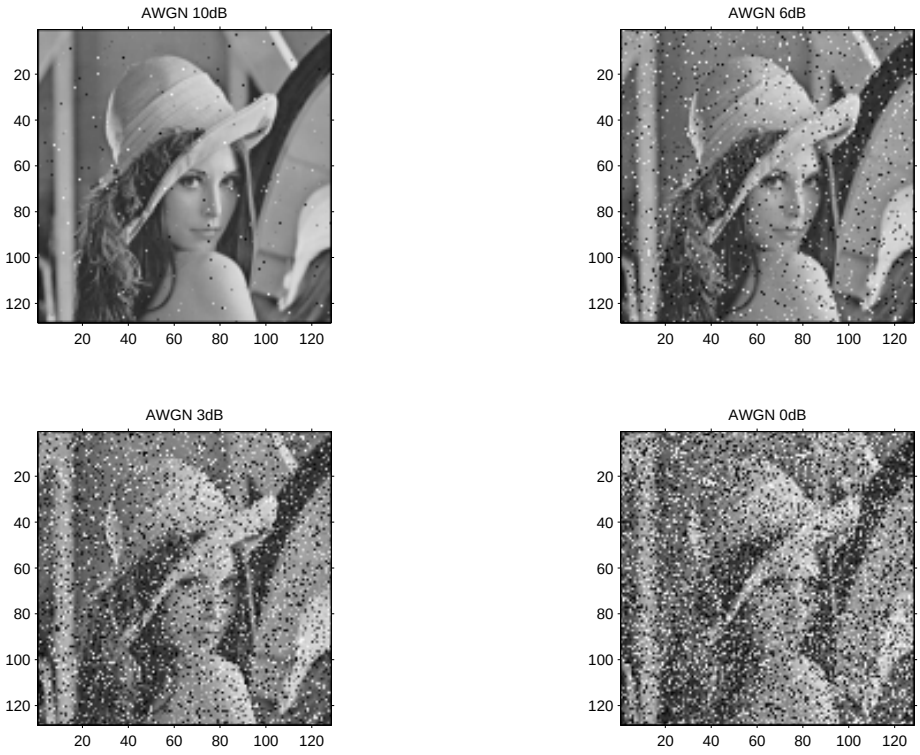

Figure 7.11: Multimedia performance of the LCG2 CSK system in different AWGN environments (SF = 10).

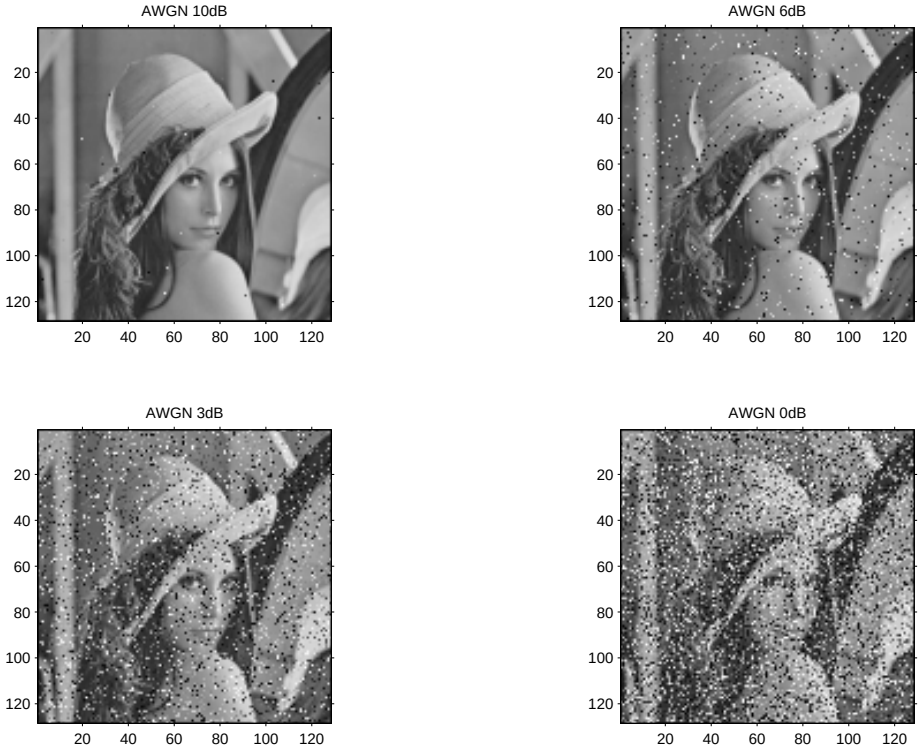

Figure 7.12: Multimedia performance of the LCG3 CSK system in different AWGN environments (a = 4, SF=10).

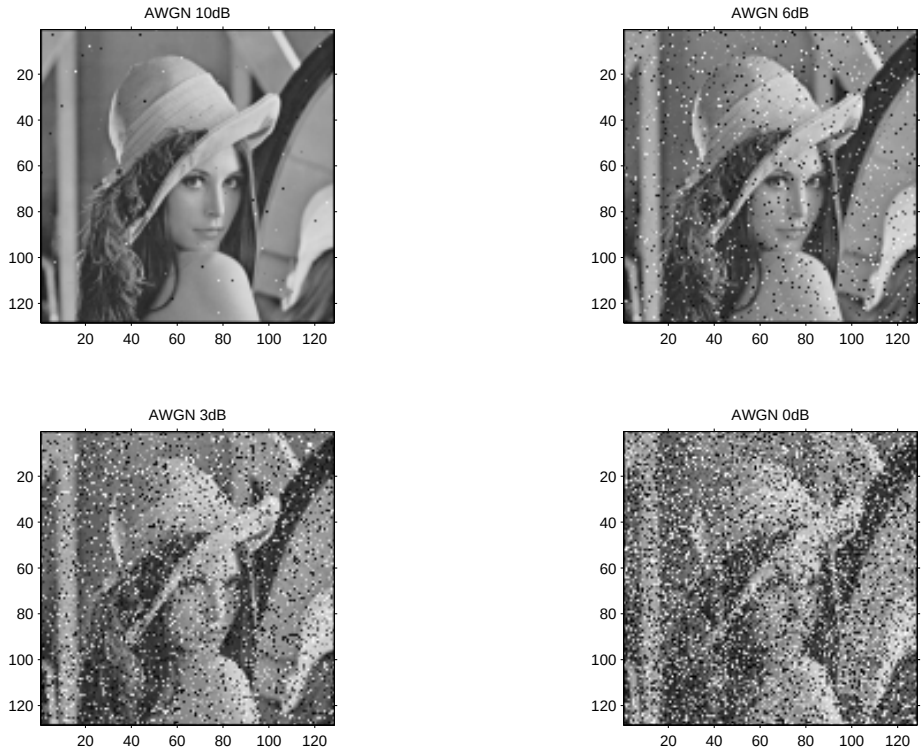

Figure 7.13: Multimedia performance of the LCG3 CSK system in different AWGN environments (a = 3.9, SF=10).

applications. Importantly though, it provides a means of determining an acceptable E_b/N_o required for a suitable user-perceived quality. For an AWGN channel environment, simulation results of the proposed CSK system show that good image quality is maintained generally at a minimum of 10 dB required for E_b/N_o.

7.6 Security Overview

Measurement of the 'security' aspects of any communication system is not an easy task to undertake. However, we can view security in a few different ways. To begin with, the auto- and cross- correlation property is used. This is the simplest security measure for any spread spectrum communication system. If a spreading sequence provides an auto and cross-correlation characteristic not similar to white noise, we can conclude that this would be unsuitable for spread spectrum communication. Also, since there is some correlation between two sequences, it could be easily intercepted by an attacker.

Figures (7.17) and (7.18) show the auto- and cross-correlation performance for all three chaos generators with different values for the initial condition, and the security parameter defined in section 4. It is quite evident that LCG1 and LCG3 have auto- and cross-correlation properties

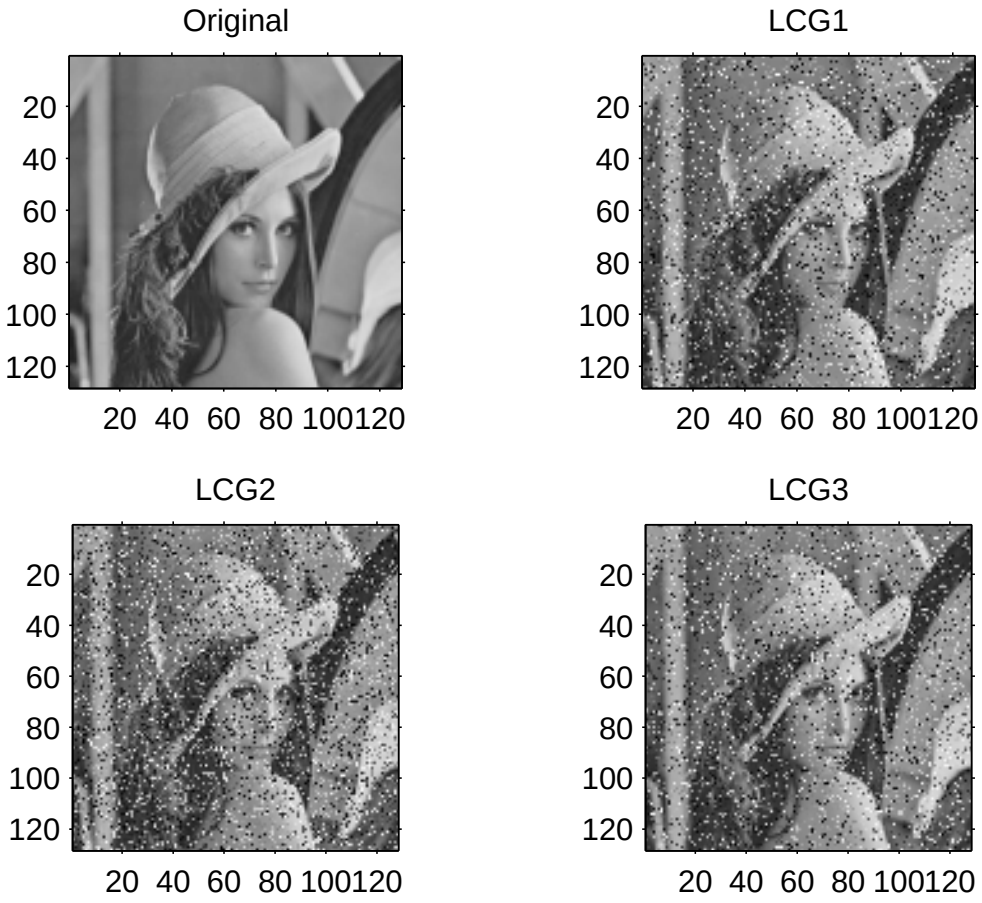

Figure 7.14: Multimedia performance of LCG1, LCG2, and LCG3 for the image, Lenna (a = 4, SF = 10).

similar to those of random white noise, despite the fact that their initial conditions are just slightly different. This indicates that LGC1 and LGC3 can generate sequences that are uncorrelated. However with LCG3, more security is embedded with its extra security parameter (even small variations in provide uncorrelated sequences). Hence, the generation of a chaos sequence is very sensitive to the initial condition. A slight difference in the initial condition will generate a totally different chaotic sequence.

In the case of an unauthorized attacker trying to gain access to the communication system using LCG3, as compared to LCG1, an attacker would need to know not only the exact initial condition for the chaos generator but also the security 'key' (parameter) before interception/demodulation of any information could be possible; even if the sequence generating method was also known to the attacker. This process is fairly similar to other encryption processes where a unique security key is needed. This additional security parameter, therefore, enhances the security performance of the communication physical link.

The simulation results in Figure (7.19) demonstrate the orbits generated when using two

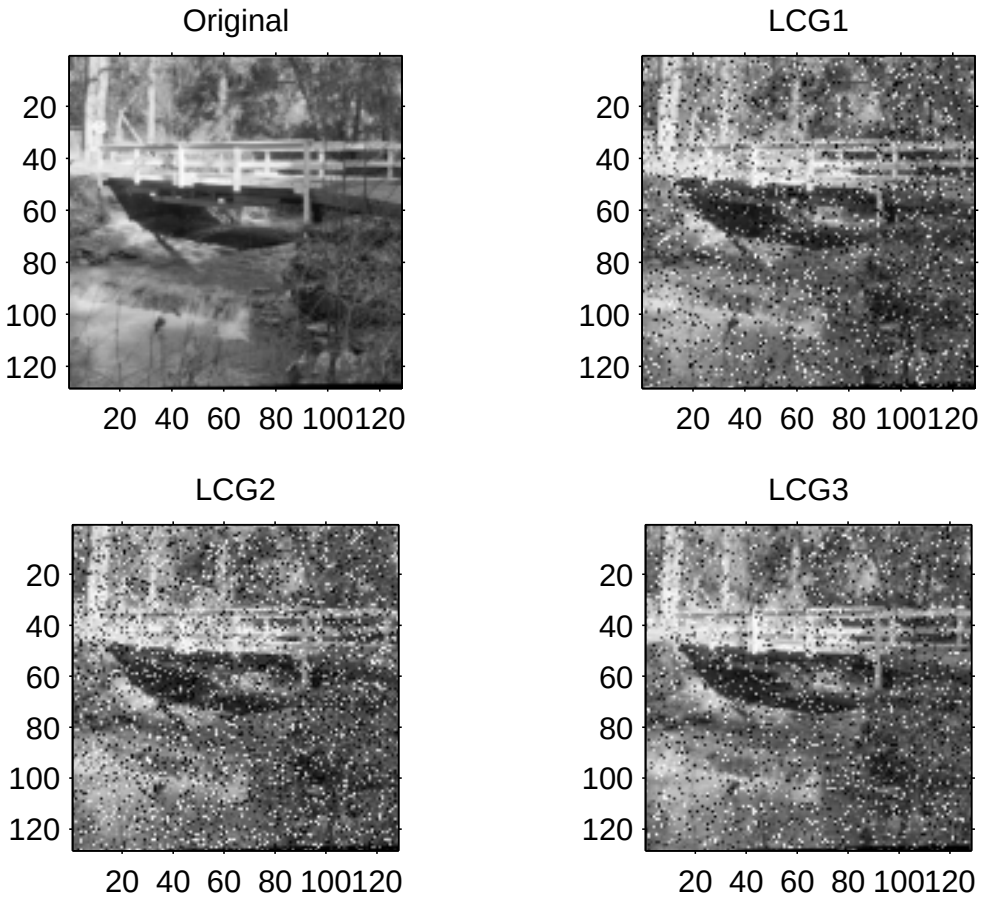

Figure 7.15: Multimedia performance of LCG1, LCG2, and LCG3 for the image, Bridge (a = 4, SF = 10).

very close initial conditions and two very close security parameters for each chaotic logistic map. More importantly, it shows how fast or how long a sequence is generated for before it is out of the orbit of similarity. These results also show that an exact initial condition is required and that no long-term prediction is possible in all three chaos generators. In particular, Figure (7.19) confirms that LCG3 provides the most secure communication, where only 10 iterations are needed (for a different value of a) to cause the sequences to go out of orbit.

In general, all three generators provide a very secure communication channel, as approximately 25 iterations are needed for the sequences to go off orbit. The shorter the sequence for SF the more vulnerable it is for the attacker to decipher the transmitted signal. A larger SF can ensure prediction of the spreading sequence is increasingly more difficult. Hence, using a chaotic generator can ensure higher security of the physical channel due to it's bifurcation property. In other words, it is hard to predict or even estimate its chaotic spreading sequence. As a result, to enhance the robustness in the security of transmitted data, it is more practical to use a larger spreading factor (more than 25) [219]. For optimum performance, it is recommended that the

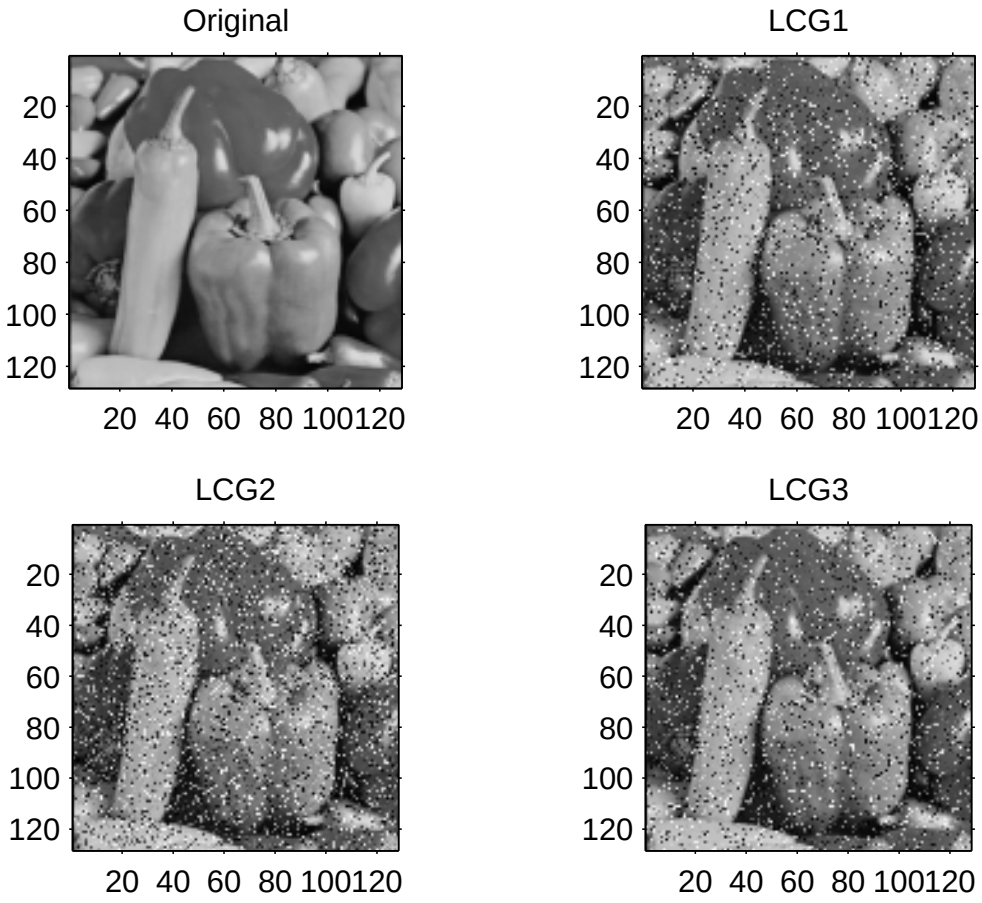

Figure 7.16: Multimedia performance of LCG1, LCG2, and LCG3 for the image, Peppers (a = 4, SF = 10).

system be designed with a spreading factor between 50 and 100.

To illustrate the security performance of the CSK system using LCG1 and LCG3, the system was simulated with the Lenna image by deliberately estimating the initial condition and security parameter - emulating the process that would otherwise be used by an attacker. Figure (7.20) and Figure (7.21) show the resulting image (error) obtained in estimating the initial sequence for LCG1 and in estimating the security parameter for LCG3 respectively. The demodulated multimedia data (image) for both cases is totally unrecognizable even though the BER of the system is very small (almost 0.05). Hence, we can confirm that the analysis of BER performance data is not suitable in determining the effectiveness of secure communications in the system. Instead, security measurement can be readily extracted from simple observation - user perception. Moreover, Figure (7.20) shows the additional level of security achieved in multimedia communication due to the bifurcation property of the proposed CSK system using LCG3.

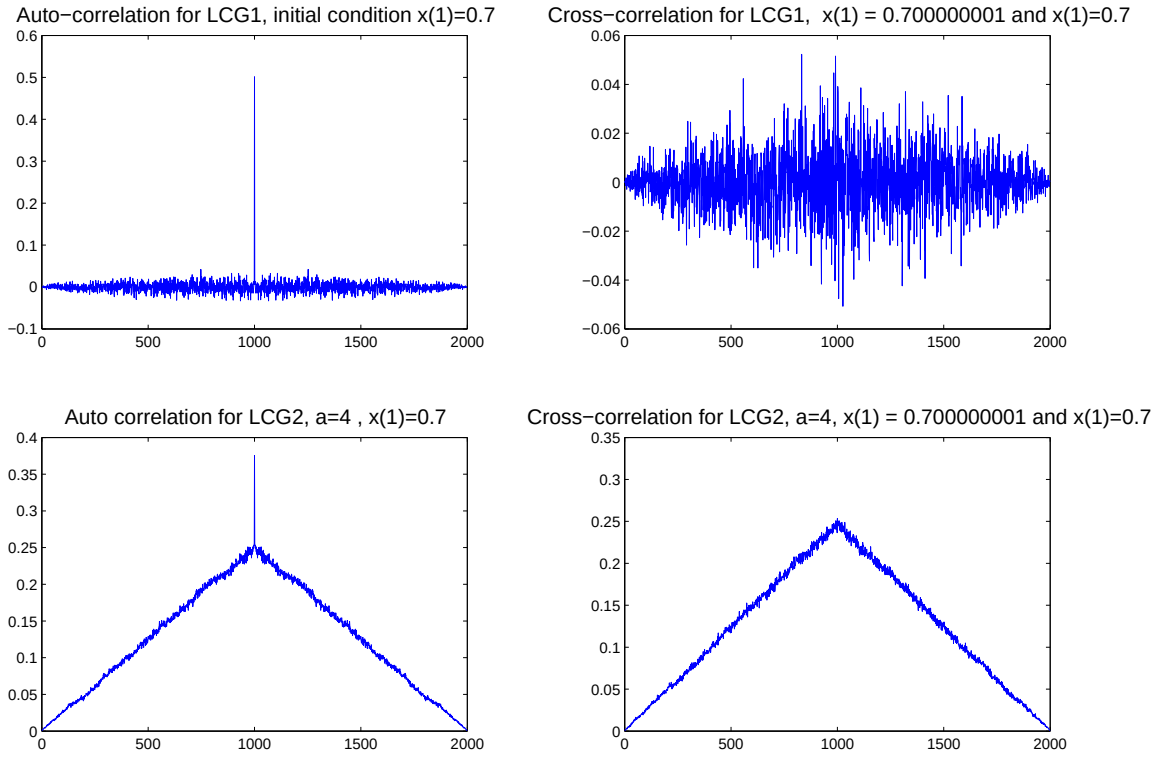

Figure 7.17: Correlation performance for LCG1 and LCG2.

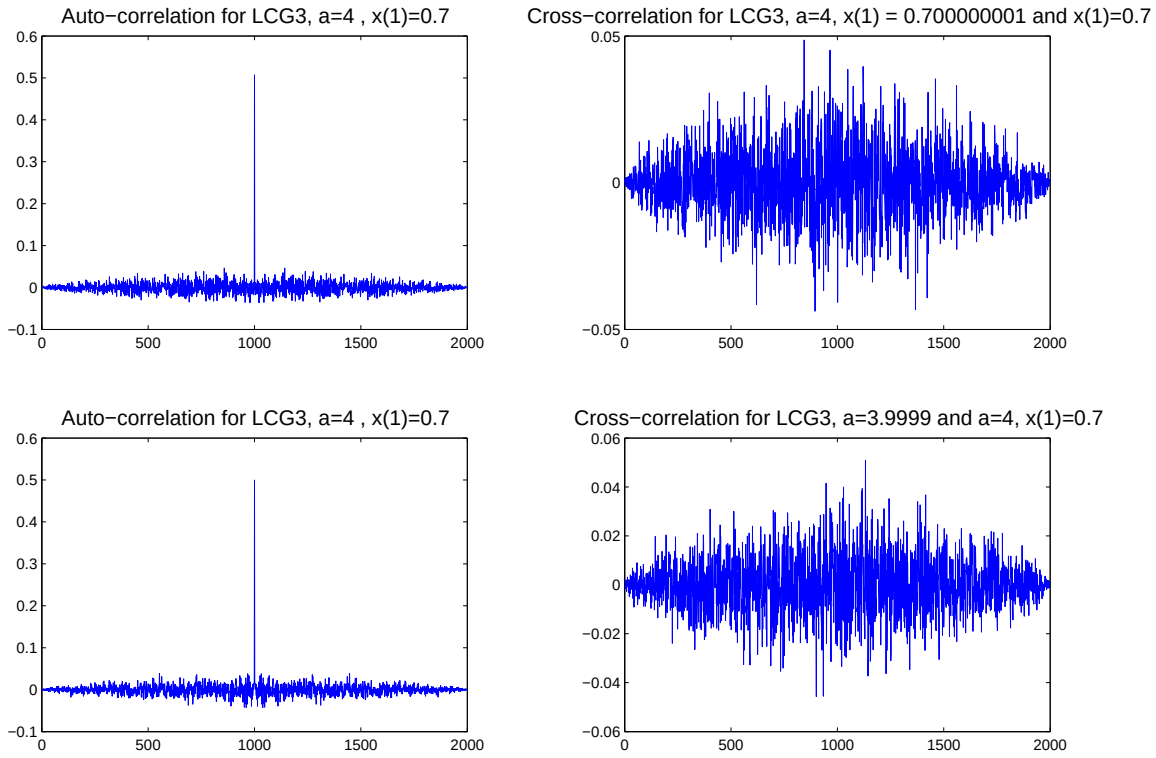

Figure 7.18: performance for LCG3.

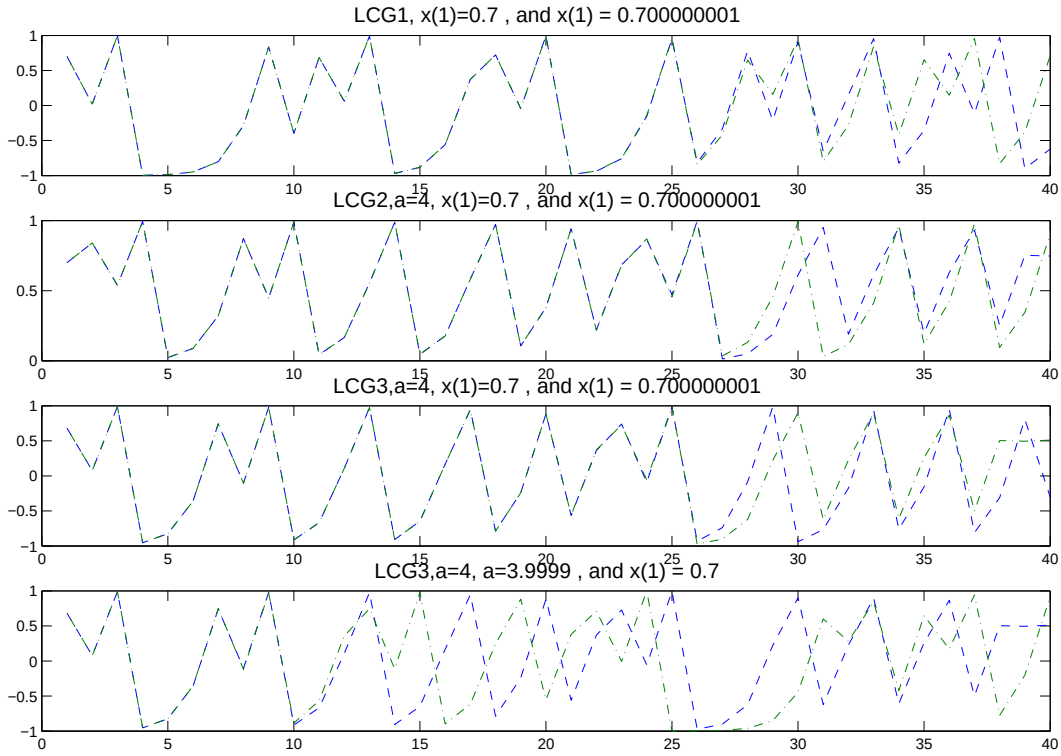

Figure 7.19: Different chaotic sequences generated by each chaotic generator with different initial values and bifurcation parameters.

7.7 Conclusion

In this chapter, a modified logistic chaotic map for chaos-shift-keying (CSK) to transmit multimedia data over a highly-secure spread spectrum communication system has been proposed. This approach was compared with two commonly used logistic chaotic maps. The proposed logistic chaotic map shows BER performance similar to the optimum performance obtained for CSK modulation. Simulation results, based on the application of digital images, showed that the additional bifurcation parameter inherent in the proposed logistic chaotic map provides another level of security for spread spectrum communication while maintaining a target system SNR.

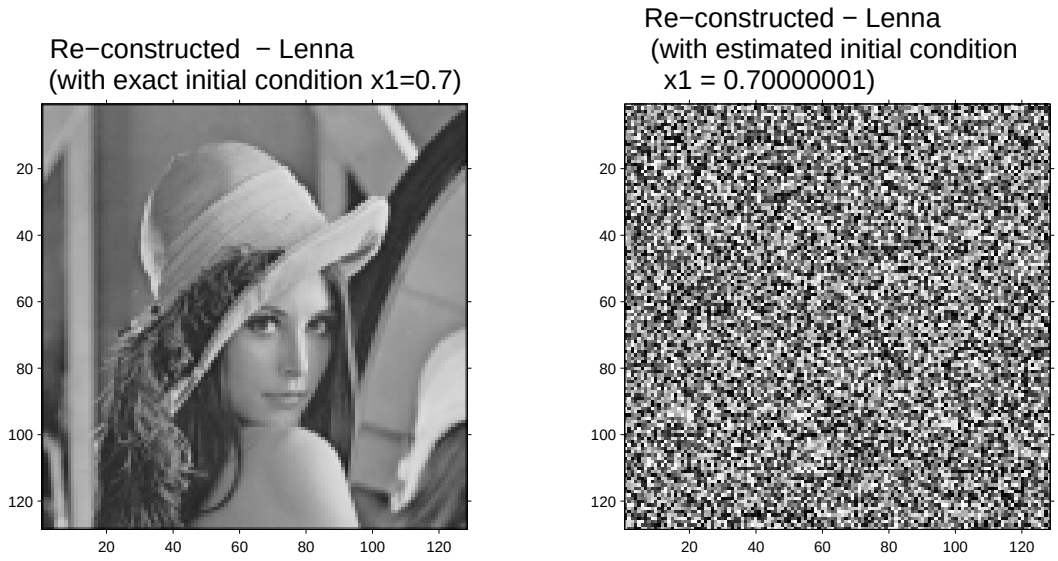

Figure 7.20: Multimedia secure communication using LCG1.

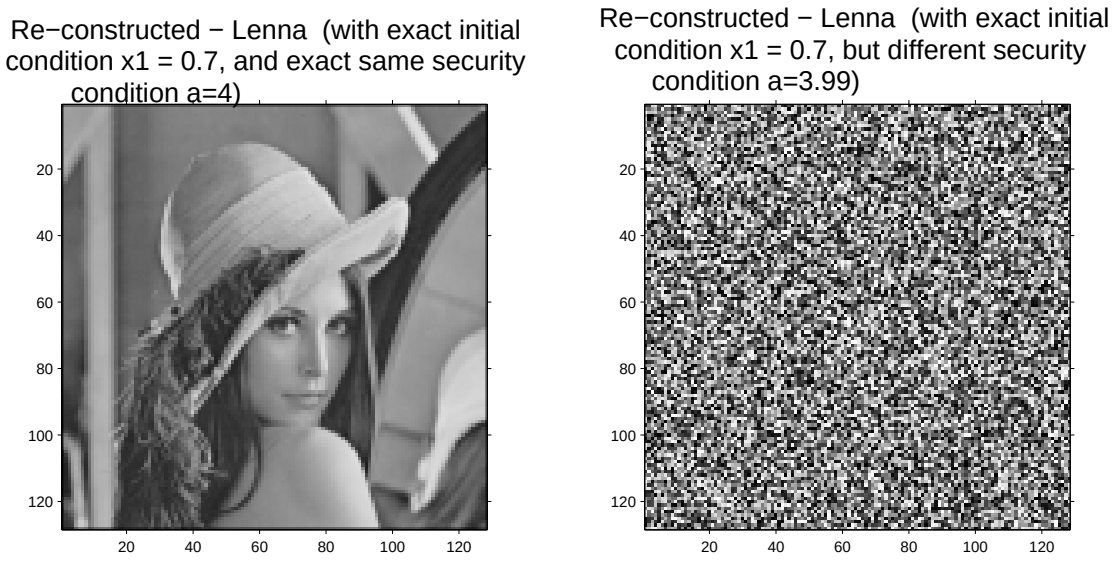

Figure 7.21: Multimedia secure communication using LCG3 with a different security condition (bifurcation parameter).

Chapter 8

Conclusions and Future Directions

During the past few years, there has been a significant paradigm shift in both the use and in the requirements of mobile technologies. Trends in mobile communications suggest that this is due to a rapid growth in the generation, transmission, and use of multimedia data to communicate a diverse range of information. The efficient transmission of high speed multimedia applications over mobile radio channels have, thus, become essential in meeting the demands for next-generation mobile communication systems. It is well known, however, that multimedia data such as high quality digital images and video place enormous constraints on the communication system bandwidth, transmission power, latency, and processing resources. Furthermore, the reliability and data throughput performance of mobile radio links is often impaired by the presence of noise, interference and the multipath fading effects of wireless channel conditions and propagation environments. To overcome these bottlenecks for mobile multimedia, various signal-processing techniques have been adopted such as data compression, adaptive modulation, and channel coding.

Recently, however, transmit diversity such as space-time coding and antenna beamforming have emerged as valuable processing techniques for mobile transmission systems with a multi-element antenna array configuration. Additional gains have been reported in terms of both the channel capacity and the error-rate performance for diversity coded systems combined with the spectral efficiency of OFDM. Furthermore, by adapting system parameters to match the instantaneous channel conditions, even greater improvement in overall system performance can be expected. We also recall from chapter 1, that by jointly developing and applying adaptive transmit diversity techniques to deal with the problem of efficient mobile transmission, significant performance gains can be achieved [50]. These and other signal-processing functions such as data compression are, therefore, crucial considerations for the enhancement of mobile multimedia systems and have been the main focus of this thesis.

8.1 Summary and Conclusions

This dissertation has introduced and investigated the use of several signal-processing techniques to deal with the problems associated with the transmission of multimedia applications in mobile communication systems - mobile multimedia. In particular, a novel approach using wavelet compression and unequal adaptive modulation to optimise the performance of multimedia data transmitted over mobile radio channels has been presented. The proposed techniques have been implemented and simulation results (based on the transmission of digital still images) have demonstrated their superior performance. A summary of the outcomes resulting from this research study is provided below.

An overview of some of the key aspects concerning the processing and compression of multimedia signals, particularly, the use of wavelet-based coding for image compression was presented in Chapter 2. In addition, a review of the key signal processing functions of mobile transmission systems for digital communications have also been provided. This included a survey on existing transmit diversity techniques and channel models, some of which were used throughout the thesis.

In Chapter 3, a simulation framework to model the transmission of multimedia data over diverity-coded OFDM systems with a multi-antenna configuration was introduced. A space-time block coding (STBC) and an adaptive beamforming (AB) strategy were integrated with a source encoded OFDM transmission system (STBC-OFDM-AB) to maximise the received signal power and overall system performance (error-rate performance and channel capacity). The diversity gain offered by the STBC-OFDM-AB system is maintained as the adaptive antenna weighting scheme effectively mitigates the fast fading and multi-path effects of mobile channels. When compared to other methods, superior performance gains were demonstrated using the simulation of compressed digital images over a geometrical space-time channel model (GBHDS), and could be readily observed by inspecting the perceived quality of the reconstructed images; without the need for extensive numerical analysis as traditionally required. This showed STBC-OFDM-AB based systems to be well suited to mobile multimdia communication.

The work in Chapter 3 was further extended in Chapter 4, by combining the STBC-OFDM-AB transmission system for multimedia communication with a wavelet-based compression technique, consisting of a 2-D discrete wavelet transform (DWT) based on biorthogonal wavelets, an adaptive quantizer (with thresholding) and variable-length entropy encoding. Simulation results based on the transmission of compressed images over a GBHDS space-time channel model, showed that greater control over system characteristics could be achieved and provided improve-

ments in overall system performance. The simulation framework was then modified to include a space-time-frequency coding (STF-OFDM-AB), such that additional diversity branches could be exploited in both the space, time, and frequency domains of OFDM systems. When compared to other methods, STBC-OFDM-AB & STF-OFDM-AB, simulation results showed superior performance from both the analysis of objective or fidelity criteria ($PSNR$) and subjective measurements (user-perceived quality).

In Chapter 5, a communication system to optimise the transmission of multimedia applications over mobile radio channels was proposed. This chapter introduced a novel approach to the processing of multimedia data by combining a source encoder with an adaptive modulator based on a lookup matrix-adaptive bit and power allocation (LM-ABPA) scheme, and was further integrated with a diversity-coded MIMO-OFDM system. However, unlike other systems, the adaptive modulator was configured such that the low-frequency and high-frequency components produced by the wavelet-based coder were encoded separately - unequal adaptive modulation. This was achieved by sorting and allocating OFDM subcarriers with the highest SNR to the low-frequency components representing the compressed multimedia data, as they are more sensitive to the channel impairments produced by wireless propagation environments. Using a loading algorithm from the LM-ABPA process, OFDM subcarriers were adaptively assigned with a signal constellation size and required power so that the channel-to-noise ratio (CNR)is maximised, and the target system error-rate performance (data transfer rate) is satisfied. Simulation results based on the application of compressed images showed that in comparison to other non-adaptive methods the proposed transmission system for multimedia communication achieved superior performance under a constant data rate load.

The ideas and concepts applied in the earlier chapters, in particular, the multimedia simulation frameworks developed were then applied to study and investigate the performance of other signal-processing strategies in mobile communication systems. In Chapter 6, we showed how a blind channel equalisation technique known as the, sinusoidally-distributed dithered signed-error constant modulus algorithm (S-DSE-CMA), could overcome the effects of intersymbol interference (ISI) in mobile radio channels. This algorithm proved to outperform other DSE-CMA schemes due to a faster convergence rate and was demonstrated by simulating the transmission of compressed digital images.

Finally, in Chapter 7, a secure communication system based on the use of chaotic generator for CSK spread spectrum communication was presented. A modified version of a chaotic generator (LCG3) from two common chaotic logistic maps was developed, to provide an additional security parameter for the control of its bifurcation property. Based on the transmission of digital still

images, simulation results clearly showed the performance enhancements introduced by LCG3 in maintaining a bit error-rate (BER) performance of the system close to the best logistic map, but more importantly, demonstrated the greater level of security achievable in terms of multimedia communication. This could be readily observed from analysis of both the perceived quality of the reconstructed images and objective measurement based on the $PSNR$ metric.

8.2 Future Research Directions

In this thesis, we have addressed several issues in dealing with the efficient transmission of multimedia data over mobile/wirless communication channels, particularly, when combining adaptive transmit diversity and modulation techniques with wavelet-based coding. However, many of the ideas presented in this dissertation can be extended through further research. Some of the unresolved research challenges that remain to be investigated and that follow from this work are:

- Mobile and wireless communication systems currently support the transport of both image and video data. The multimedia framework and coding techniques proposed in this thesis have been based on the application of gray-level digital still images. Their adaptation to digital video and color images needs to be explored.
- In Chapter 5, we proposed a novel approach to the transmission of multimedia data over MIMO-OFDM channels based on an unequal adaptive modulation scheme employing a LM-ABPA algorithm. To further reduce the bandwidth requirement for multimedia communication, the choice of different wavelet bases (the filter coefficients, number of decomposition levels, etc.) and their adaptation to the varying channel conditions of mobile/wireless environments needs to be investigated. This includes, jointly developing an unequal adaptive modulation scheme and transmit diversity technique which is content dependent, as future mobile networks will support a multitude of high-speed mobile multimedia services and applications.
- Neuro-Fuzzy techniques for image/video compression have attracted serious attention by the research community, as an alternative to current object-based and predictive coding approaches [233]. Many of these techniques, particularly in the case of video coding, require a mechanism for clustering or prediction. While fuzzy theory deals with the problem of defining categorical boundaries for a given dataset, neural networks have learning capabilities which can be designed to detect and label clusters. Neuro-fuzzy approaches combine the advantages of both fuzzy theory and neural networks for data clustering in image and

video coding. There use in adaptive diversity coded MIMO-OFDM transmission systems needs to be explored and performance evaluated in comparison to wavelet-based coding methods.

- The relatively new field of multiwavelets has recently emerged as a powerful tool in overcoming some of the limitations of standard wavelets. Multiwavelets and multiwavelet packets offer greater design flexibility and are able to combine several desirable transform features - orthogonality, symmetry, etc. Published results show that multiwavelet transforms can exhibit performance gains superior to the current wavelet filters [234]. Thus, further research work is required to explore the use of multiwavelet-based compression in adaptive diversity coded MIMO-OFDM transmission systems.
- The multimedia framework proposed in this thesis has been applied to investigate some of the problems commonly associated with the transmission of multimedia data in mobile communication systems which include, channel impairment due to multi-path fading, low bandwidth utilisation and spectral efficiency, inter-symbol interference, and secure communications in spread spectrum systems. There are, however, other issues which the multimedia framework can be used to explore such as, dynamic power and error control and intercarrier interference (carrier frequency offset) [235, 236], etc.
- As with any system proposed, various implementation issues involving hardware design and computational complexity need to be evaluated.

We note, that most of the current techniques developed to enhance the performance of the physical layer in mobile/wirless communications predominantly exploit the benefits of a FFT/IFFT-based OFDM multicarrier/mulichannel system. More recently, however, there has been an increasing interest by the research community in the development of an equivalent wavelet-based OFDM transmission system, which claims to offer superior performance gains over traditional methods; including the potential to dramatically decrease implementation and computational complexity. This presents a unique opportunity for future research work in the area of mobile multimedia, as new signal processing techniques and transmission strategies for the integration of wavelet-based coders (and other compression technologies) with wavelet-based OFDM will need to be developed and studied.

Appendix A

Maximum Likelihood for Space-Time Codes

Maximum Likelihood Decision Rule for OSTBC

The maximum likelihood decision rule in [43] for decoding a $\mathcal{G}_3$ orthogonal space-time block code in Table 2.2 can be expressed as

$$\left| \left[\sum_{j=1}^{N_r} r_0(j)h_0^*(j) + r_1(j)h_1^*(j) + r_2(j)h_2^*(j) + r_4^*(j)h_0(j) + r_5^*(j)h_1(j) + r_6^*(j)h_2(j) \right] - x_0 \right|^2 + \left(-1 + 2\sum_{j=1}^{N_r}\sum_{i=1}^{3} |h_i(j)|^2 \right) |x_0|^2 \tag{A.1}$$

for x_0 detection,

$$\left| \left[\sum_{j=1}^{N_r} r_0(j)h_1^*(j) - r_1(j)h_0^*(j) + r_3(j)h_2^*(j) + r_4^*(j)h_1(j) - r_5^*(j)h_0(j) + r_7^*(j)h_2(j) \right] - x_1 \right|^2 + \left(-1 + 2\sum_{j=1}^{N_r}\sum_{i=1}^{3} |h_i(j)|^2 \right) |x_1|^2 \tag{A.2}$$

for x_1 detection,

$$\left| \left[\sum_{j=1}^{N_r} r_0(j)h_2^*(j) - r_2(j)h_0^*(j) - r_3(j)h_1^*(j) + r_4^*(j)h_2(j) - r_6^*(j)h_0(j) - r_7^*(j)h_1(j) \right] - x_2 \right|^2 + \left(-1 + 2\sum_{j=1}^{N_r}\sum_{i=1}^{3} |h_i(j)|^2 \right) |x_2|^2 \tag{A.3}$$

for x_2 detection, and

$$\left|\left[\sum_{j=1}^{N_r} -r_1(j)h_2^*(j) + r_2(j)h_1^*(j) - r_3(j)h_0^*(j) - r_5^*(j)h_2(j) + r_6^*(j)h_1(j) - r_7^*(j)h_0(j)\right] - x_3\right|^2 + \left(-1 + 2\sum_{j=1}^{N_r}\sum_{i=1}^{3}|h_i(j)|^2\right)|x_3|^2 \tag{A.4}$$

for x_3 detection.

The maximum likelihood decision rule in [43] for decoding $\boldsymbol{\mathcal{G}}_4$ orthogonal space-time block code in Table 2.2 can be expressed as

$$\left|\left[\sum_{j=1}^{N_r} r_0(j)h_0^*(j) + r_1(j)h_1^*(j) + r_2(j)h_2^*(j) + r_3(j)h_3^*(j) + r_4^*(j)h_0(j) + r_5^*(j)h_1(j) + r_6^*(j)h_2(j) + r_7^*(j)h_3(j)\right] - x_0\right|^2 + \left(-1 + 2\sum_{j=1}^{N_r}\sum_{i=1}^{4}|h_i(j)|^2\right)|x_0|^2 \tag{A.5}$$

for x_0 detection,

$$\left|\left[\sum_{j=1}^{N_r} r_0(j)h_1^*(j) - r_1(j)h_0^*(j) - r_2(j)h_3^*(j) + r_3(j)h_2^*(j) + r_4^*(j)h_1(j) - r_5^*(j)h_0(j) - r_6^*(j)h_3(j) + r_7^*(j)h_2(j)\right] - x_1\right|^2 + \left(-1 + 2\sum_{j=1}^{N_r}\sum_{i=1}^{4}|h_i(j)|^2\right)|x_1|^2 \tag{A.6}$$

for x_1 detection,

$$\left|\left[\sum_{j=1}^{N_r} r_0(j)h_2^*(j) + r_1(j)h_3^*(j) - r_2(j)h_0^*(j) - r_3(j)h_1^*(j) + r_4^*(j)h_2(j) + r_5^*(j)h_3(j) - r_6^*(j)h_0(j) - r_7^*(j)h_1(j)\right] - x_2\right|^2 + \left(-1 + 2\sum_{j=1}^{N_r}\sum_{i=1}^{4}|h_i(j)|^2\right)|x_2|^2 \tag{A.7}$$

for x_2 detection, and

$$\left|\left[\sum_{j=1}^{N_r} r_0(j)h_3^*(j) - r_1(j)h_2^*(j) + r_2(j)h_1^*(j) - r_3(j)h_0^*(j) + r_4^*(j)h_3(j) - r_5^*(j)h_2(j) + r_6^*(j)h_1(j) - r_7^*(j)h_0(j)\right] - x_3\right|^2 + \left(-1 + 2\sum_{j=1}^{N_r}\sum_{i=1}^{4}|h_i(j)|^2\right)|x_3|^2 \tag{A.8}$$

for x_3 detection.

The maximum likelihood decision rule in [43] for decoding $\boldsymbol{\mathcal{H}}_3$ orthogonal space-time block code in Table 2.2 can be expressed as

$$\left|\left[\sum_{j=1}^{N_r} r_0(j)h_0^*(j) + r_1^*(j)h_1(j) + \frac{\big(r_3(j) - r_2(j)\big)h_2^*(j)}{2} - \frac{\big(r_2(j) + r_3(j)\big)^* h_2(j)}{2}\right] - x_0\right|^2 + \left(-1 + \sum_{j=1}^{N_r}\sum_{i=1}^{3} |h_i(j)|^2\right)|x_0|^2 \tag{A.9}$$

for x_0 detection,

$$\left|\left[\sum_{j=1}^{N_r} r_0(j)h_1^*(j) - r_1^*(j)h_0(j) + \frac{\big(r_3(j) + r_2(j)\big)h_2^*(j)}{2} + \frac{\big(-r_2(j) + r_3(j)\big)^* h_2(j)}{2}\right] - x_1\right|^2 + \left(-1 + \sum_{j=1}^{N_r}\sum_{i=1}^{3} |h_i(j)|^2\right)|x_1|^2 \tag{A.10}$$

for x_1 detection, and

$$\left|\left[\sum_{j=1}^{N_r} \frac{\big(r_0(j) + r_1(j)\big)h_2^*(j)}{\sqrt{2}} + \frac{r_2^*(j)\big(h_0(j) + h_1(j)\big)}{\sqrt{2}} - \frac{r_3^*(j)\big(h_0(j) - h_1(j)\big)}{\sqrt{2}}\right] - x_2\right|^2 + \left(-1 + \sum_{j=1}^{N_r}\sum_{i=1}^{3} |h_i(j)|^2\right)|x_2|^2 \tag{A.11}$$

for x_2 detection.

The maximum likelihood decision rule in [43] for decoding $\boldsymbol{\mathcal{H}}_4$ orthogonal space-time block code in Table 2.2 can be expressed as

$$\left|\left[\sum_{j=1}^{N_r} r_0(j)h_0^*(j) + r_1^*(j)h_1(j) + \frac{\big(r_3(j) - r_2(j)\big)\big(h_2^*(j) - h_3^*(j)\big)}{2} - \frac{\big(r_2(j) + r_3(j)\big)^*\big(h_2(j) + h_3(j)\big)}{2}\right] - x_0\right|^2 + \left(-1 + \sum_{j=1}^{N_r}\sum_{i=1}^{4} |h_i(j)|^2\right)|x_0|^2 \tag{A.12}$$

for x_0 detection,

$$\left|\left[\sum_{j=1}^{N_r} r_0(j)h_1^*(j) - r_1^*(j)h_0(j) + \frac{\big(r_3(j)+r_2(j)\big)\big(h_2^*(j)-h_3^*(j)\big)}{2} + \frac{\big(-r_2(j)+r_3(j)\big)^*\big(h_2(j)+h_3(j)\big)}{2}\right] - x_1\right|^2 + \left(-1+\sum_{j=1}^{N_r}\sum_{i=1}^{4}|h_i(j)|^2\right)|x_1|^2 \quad \text{(A.13)}$$

for x_1 detection, and

$$\left|\left[\sum_{j=1}^{N_r} \frac{\big(r_0(j)+r_1(j)\big)h_2^*(j)}{\sqrt{2}} + \frac{\big(r_0(j)-r_1(j)\big)h_3^*(j)}{\sqrt{2}} + \frac{r_2^*(j)\big(h_0(j)+h_1(j)\big)}{\sqrt{2}} + \frac{r_3^*(j)\big(h_0(j)-h_1(j)\big)}{\sqrt{2}}\right] - x_2\right|^2 + \left(-1+\sum_{j=1}^{N_r}\sum_{i=1}^{4}|h_i(j)|^2\right)|x_2|^2 \quad \text{(A.14)}$$

for x_2 detection.

Maximum Likelihood Decision Rule for FT codes

The maximum likelihood decision rule for decoding FT code, if the $\boldsymbol{\mathcal{G}}_3$ orthogonal space-time block code is used, can be expressed as

$$\left|\left[\sum_{j=1}^{N_r}\Big(y_{i,j}(n)h_{i(1)}^*(j) + y_{i,j}(n+1)h_{i(2)}^*(j) + y_{i,j}(n+2)h_{i(3)}^*(j) + y_{i,j}^*(n+4)h_{i(1)}(j) + y_{i,j}^*(n+5) h_{i(2)}(j) + y_{i,j}^*(n+6)h_{i(3)}(j)\Big)\right] - s_1\right|^2 + \left(-1+2\sum_{j=1}^{N_r}\sum_{m=1}^{3}|h_{i(m)}(j)|^2\right)|s_1|^2 \quad \text{(A.15)}$$

for s_1 detection,

$$\left|\left[\sum_{j=1}^{N_r}\Big(y_{i,j}(n)h_{i(2)}^*(j) - y_{i,j}(n+1)h_{i(1)}^*(j) + y_{i,j}(n+3)h_{i(3)}^*(j) + y_{i,j}^*(n+4)h_{i(2)}(j) - y_{i,j}^*(n+5) h_{i(1)}(j) + y_{i,j}^*(n+7)h_{i(3)}(j)\Big)\right] - s_2\right|^2 + \left(-1+2\sum_{j=1}^{N_r}\sum_{m=1}^{3}|h_{i(m)}(j)|^2\right)|s_2|^2 \quad \text{(A.16)}$$

for s_2 detection,

$$\left|\left[\sum_{j=1}^{N_r}\Big(y_{i,j}(n)h_{i(3)}^*(j) - y_{i,j}(n+2)h_{i(1)}^*(j) - y_{i,j}(n+3)h_{i(2)}^*(j) + y_{i,j}^*(n+4)h_{i(3)}(j) - y_{i,j}^*(n+6) h_{i(1)}(j) - y_{i,j}^*(n+7)h_{i(2)}(j)\Big)\right] - s_3\right|^2 + \left(-1+2\sum_{j=1}^{N_r}\sum_{m=1}^{3}|h_{i(m)}(j)|^2\right)|s_3|^2 \quad \text{(A.17)}$$

for s_3 detection, and

$$\left|\left[\sum_{j=1}^{N_r}\Big(-y_{i,j}(n+1)h^*_{i(3)}(j)+y_{i,j}(n+2)h^*_{i(2)}(j)-y_{i,j}(n+3)h^*_{i(1)}(j)-y^*_{i,j}(n+5)h_{i(3)}(j)\right.\right.$$
$$\left.\left.+y^*_{i,j}(n+6)h_{i(2)}(j)-y^*_{i,j}(n+7)h_{i(1)}(j)\Big)\right]-s_4\right|^2+\left(-1+2\sum_{j=1}^{N_r}\sum_{m=1}^{3}|h_{i(m)}(j)|^2\right)|s_4|^2 \quad \text{(A.18)}$$

for s_4 detection.

The maximum likelihood decision rule for decoding FT code, if $\boldsymbol{\mathcal{G}}_4$ orthogonal space-time block code is used, can be expressed as

$$\left|\left[\sum_{j=1}^{N_r}\Big(y_{i,j}(n)h^*_{i(1)}(j)+y_{i,j}(n+1)h^*_{i(2)}(j)+y_{i,j}(n+2)h^*_{i(3)}(j)+y_{i,j}(n+3)h^*_{i(4)}(j)+y^*_{i,j}(n+4)\right.\right.$$
$$\left.\left.h_{i(1)}(j)+y^*_{i,j}(n+5)h_{i(2)}(j)+y^*_{i,j}(n+6)h_{i(3)}(j)+y^*_{i,j}(n+7)h_{i(4)}(j)\Big)\right]-s_1\right|^2$$
$$+\left(-1+2\sum_{j=1}^{N_r}\sum_{m=1}^{4}|h_{i(m)}(j)|^2\right)|s_1|^2 \quad \text{(A.19)}$$

for s_1 detection,

$$\left|\left[\sum_{j=1}^{N_r}\Big(y_{i,j}(n)h^*_{i(2)}(j)-y_{i,j}(n+1)h^*_{i(1)}(j)-y_{i,j}(n+2)h^*_{i(4)}(j)+y_{i,j}(n+3)h^*_{i(3)}(j)+y^*_{i,j}(n+4)\right.\right.$$
$$\left.\left.h_{i(2)}(j)-y^*_{i,j}(n+5)h_{i(1)}(j)-y^*_{i,j}(n+6)h_{i(4)}(j)+y^*_{i,j}(n+7)h_{i(3)}(j)\Big)\right]-s_2\right|^2$$
$$+\left(-1+2\sum_{j=1}^{N_r}\sum_{m=1}^{4}|h_{i(m)}(j)|^2\right)|s_2|^2 \quad \text{(A.20)}$$

for s_2 detection,

$$\left|\left[\sum_{j=1}^{N_r}\Big(y_{i,j}(n)h^*_{i(3)}(j)+y_{i,j}(n+1)h^*_{i(4)}(j)-y_{i,j}(n+2)h^*_{i(1)}(j)-y_{i,j}(n+3)h^*_{i(2)}(j)+y^*_{i,j}(n+4)\right.\right.$$
$$\left.\left.h_{i(3)}(j)+y^*_{i,j}(n+5)h_{i(4)}(j)-y^*_{i,j}(n+6)h_{i(1)}(j)-y^*_{i,j}(n+7)h_{i(2)}(j)\Big)\right]-s_3\right|^2$$
$$+\left(-1+2\sum_{j=1}^{N_r}\sum_{m=1}^{4}|h_{i(m)}(j)|^2\right)|s_3|^2 \quad \text{(A.21)}$$

for s_3 detection, and

$$\left|\left[\sum_{j=1}^{N_r}\Big(y_{i,j}(n)h^*_{i(4)}(j)-y_{i,j}(n+1)h^*_{i(3)}(j)+y_{i,j}(n+2)h^*_{i(2)}(j)-y_{i,j}(n+3)h^*_{i(1)}(j)+y^*_{i,j}(n+4)\right.\right.$$
$$\left.\left.h_{i(4)}(j)-y^*_{i,j}(n+5)h_{i(3)}(j)+y^*_{i,j}(n+6)h_{i(2)}(j)-y^*_{i,j}(n+7)h_{i(1)}(j)\Big)\right]-s_4\right|^2$$
$$+\left(-1+2\sum_{j=1}^{N_r}\sum_{m=1}^{4}|h_{i(m)}(j)|^2\right)|s_4|^2 \tag{A.22}$$

for s_4 detection.

The maximum likelihood decision rule for decoding FT code, if $\boldsymbol{\mathcal{H}}_3$ orthogonal space-time block code is used, can be expressed as

$$\left|\left[\sum_{j=1}^{N_r}\left(y_{i,j}(n)h^*_{i(1)}(j)+y^*_{i,j}(n+1)h_{i(2)}(j)+\frac{\Big(y_{i,j}(n+3)-y_{i,j}(n+2)\Big)h^*_{i(3)}(j)}{2}-\right.\right.$$
$$\left.\left.\frac{\Big(y_{i,j}(n+2)+y_{i,j}(n+3)\Big)^*h_{i(3)}(j)}{2}\right)\right]-s_1\right|^2+\left(-1+\sum_{j=1}^{N_r}\sum_{m=1}^{3}|h_{i(m)}(j)|^2\right)|s_1|^2 \tag{A.23}$$

for s_1 detection,

$$\left|\left[\sum_{j=1}^{N_r}\left(y_{i,j}(n)h^*_{i(2)}(j)-y^*_{i,j}(n+1)h_{i(1)}(j)+\frac{\Big(y_{i,j}(n+3)+y_{i,j}(n+2)\Big)h^*_{i(3)}(j)}{2}+\right.\right.$$
$$\left.\left.\frac{\Big(-y_{i,j}(n+2)+y_{i,j}(n+3)\Big)^*h_{i(3)}(j)}{2}\right)\right]-s_2\right|^2+\left(-1+\sum_{j=1}^{N_r}\sum_{m=1}^{3}|h_{i(m)}(j)|^2\right)|s_2|^2 \tag{A.24}$$

for s_2 detection, and

$$\left|\left[\sum_{j=1}^{N_r}\left(\frac{\Big(y_{i,j}(n)+y_{i,j}(n+1)\Big)h^*_{i(3)}(j)}{\sqrt{2}}+\frac{y^*_{i,j}(n+2)\Big(h_{i(1)}(j)-h_{i(2)}(j)\Big)}{\sqrt{2}}+\right.\right.$$
$$\left.\left.\frac{y^*_{i,j}(n+3)\Big(h_{i(1)}(j)+h_{i(2)}(j)\Big)}{\sqrt{2}}\right)\right]-s_3\right|^2+\left(-1+\sum_{j=1}^{N_r}\sum_{m=1}^{3}|h_{i(m)}(j)|^2\right)|s_3|^2 \tag{A.25}$$

for s_3 detection.

The maximum likelihood decision rule for decoding FT code, if $\boldsymbol{\mathcal{H}}_4$ orthogonal space-time block

code is used, can be expressed as

$$\left|\left[\sum_{j=1}^{N_r}\left(y_{i,j}(n)h^*_{i(1)}(j)+y^*_{i,j}(n+1)h_{i(2)}(j)+\frac{\Big(y_{i,j}(n+3)-y_{i,j}(n+2)\Big)\Big(h^*_{i(3)}(j)-h^*_{i(4)}(j)\Big)}{2}-\right.\right.$$
$$\left.\left.\frac{\Big(y_{i,j}(n+2)+y_{i,j}(n+3)\Big)^*\Big(h_{i(3)}(j)+h^*_{i(4)}(j)\Big)}{2}\right)\right]-s_1\Bigg|^2+\left(-1+\sum_{j=1}^{N_r}\sum_{m=1}^{4}|h_{i(m)}(j)|^2\right)|s_1|^2 \tag{A.26}$$

for s_1 detection,

$$\left|\left[\sum_{j=1}^{N_r}\left(y_{i,j}(n)h^*_{i(2)}(j)-y^*_{i,j}(n+1)h_{i(1)}(j)+\frac{\Big(y_{i,j}(n+3)+y_{i,j}(n+2)\Big)\Big(h^*_{i(3)}(j)-h^*_{i(4)}(j)\Big)}{2}-\right.\right.$$
$$\left.\left.\frac{\Big(-y_{i,j}(n+2)+y_{i,j}(n+3)\Big)^*\Big(h_{i(3)}(j)+h^*_{i(4)}(j)\Big)}{2}\right)\right]-s_2\Bigg|^2+\left(-1+\sum_{j=1}^{N_r}\sum_{m=1}^{4}|h_{i(m)}(j)|^2\right)|s_2|^2 \tag{A.27}$$

for s_2 detection, and

$$\left|\left[\sum_{j=1}^{N_r}\left(\frac{\Big(y_{i,j}(n)+y_{i,j}(n+1)\Big)h^*_{i(3)}(j)}{\sqrt{2}}+\frac{\Big(y_{i,j}(n)-y_{i,j}(n+1)\Big)h^*_{i(4)}(j)}{\sqrt{2}}+\right.\right.$$
$$\left.\left.\frac{y^*_{i,j}(n+2)\Big(h_{i(1)}(j)+h_{i(2)}(j)\Big)}{\sqrt{2}}+\frac{y^*_{i,j}(n+3)\Big(h_{i(1)}(j)-h_{i(2)}(j)\Big)}{\sqrt{2}}\right)\right]-s_3\Bigg|^2$$
$$+\left(-1+\sum_{j=1}^{N_r}\sum_{m=1}^{4}|h_{i(m)}(j)|^2\right)|s_3|^2 \tag{A.28}$$

for s_3 detection.

Bibliography

[1] D. Myers, *Mobile Video Telephony*, McGraw- Hill Professional, 2005.

[2] S. C. Guthery and M. J. Cronin, *MMS Wireless Application Development*, McGraw-Hill Professional, 2003.

[3] A. Jamalipour, *The Wireless Mobile Internet - Architectures, Protocols, and Services*, John Wiley & Sons, 2003.

[4] H. Holma and A. Toskala, *WCDMA for UMTS: Radio Access for Third Generation Mobile Communications*, 3rd ed., West Sussesx, England, John Wiley & Sons, 2004.

[5] T. Ojanperä and R. Prasad, *Wideband CDMA for Third Generation Mobile Communications*, Norwood, MA: Artech House, 1998.

[6] S. Hartwig, et al, "Mobile mulimedia - challenges and opportunities," *IEEE Transactions on Consumer Electronics*, vol. 46, no. 4, pp. 1167-1178, Nov. 2000.

[7] L. Hanzo, et al, *Wireless Video Communications: Second to Third Generation and Beyond*, IEEE Series on Mobile & Digital Communications, 2001.

[8] J. F. Huber, "Mobile next-generation networks", *IEEE Multimedia*, vol. 11, pp. 72-83, Jan. 2004.

[9] A. Bria, F. Gessler, O. Queseth, R. Stridh, M. unbehaun, J. Wu, and J. Zander, "4th-generation wireless infrastructures: scenarios and research challenges," *IEEE Personal Commun.*, pp. 25-31, Dec. 2001.

[10] B. G. Evans and K. Baughan, "Visions of 4G," *Electronics & Communication Engineering Journal*, pp. 293-303, Dec. 2000.

[11] Webiste of the Mobile Operators Assocaition (MOA):
http://www.mobilemastinfo.com/information/history.htm

[12] Website of GSM^{TM}World:
http://www.gsmworld.com/technology/3g/statistics.shtml

[13] M. Mouly and M.-B. Pautet, *The GSM System for Mobile Communications*, France, Cell & Sys, 1992.

[14] P. Stuckmann, *The GSM Evolution - Mobile Packet Data Services* , John Wiley and Sons, Chichester, 2002.

[15] Webiste of the 3rd Generation Partnership Project 2:
http://www.3gpp2.org/

[16] H. Holma and A. Toskala, *HSDPA/HSUPA for UMTS: High Speed Radio Access for Mobile Communications*, West Sussesx, England, John Wiley & Sons, 2006.

[17] Website of the Global mobile Suppliers Association (GSA):
http://www.gsacom.com/news/statistics.php4

[18] K. Y. Kyun and R. Prasad, *4G Roadmap and Emerging Communication Technologies*, Artech House, 2006.

[19] Website of the Wi-Fi Alliance:
http://www.wi-fi.org/

[20] Website of the WiMax Forum:
http://www.wimaxforum.org/home/

[21] T. S. Rappaport, *Wireless Communications Principles and Practice*, 2nd edition, Delhi, India: Pearson Education Inc., 2002.

[22] J. -R. Ohm, *Multimedia Communication Technology: Representation, Transmission and Identification of Multimedia Signals*, Germany: Springer-Verlag Berlin Heidelberg, 2004.

[23] K. Sayood, *Introduction to Data Compression*, 2nd edition, Morgan Kaufmann, 2000.

[24] B. Sklar, *Digital Communications: Fundamental and Applications*, 2nd edition, New Jersey: Prentice Hall PTR, 2001.

[25] A. N. Akansu and R. A. Haddad, *Multiresolution Signal Decomposition: Transform, Subbands and Wavelets*, Academic Press, 1993.

[26] M. Kr. Mandal, "*Multimedia Signals and Systems*," Massachusetts, USA: Kluwer Academic, 2003.

[27] M. K. Mandal, *Wavelets for Image Compression*, Master's Thesis, Department of Electrical Engineering Faculty of Engineering, University of Ottawa OTTAWA, 1994.

[28] M. K. Mandal, *Wavelet Based Coding and Indexing of Images*, Ph.D. Thesis, School of Information Technology and Engineering, University of Ottawa October, 1998.

[29] M. Ghanbari, "*Standard Codecs: Image Compression to Advanced Video Coding*," Herts, UK: The Institution of Electrical Engineers, IEE Telecommunications Series 49, 2003.

[30] W. B. Pennebaker and J. L. Mitchell, *JPEG Still Image Compression Standard*, Van Nostrand Reinhold, New York, 1992.

[31] Website of the Joint Photographic Experts Group, JPEG: http://www.jpeg.org/

[32] D. L. Gall, "MPEG: a video compression standard for multimedia applications," *Communications of the ACM*, vol.34, pp. 46-58, April 1991.

[33] J. L. Mitchell, *MPEG Video: Compresssion Standard*, Chapman & Hall, New York, 1996.

[34] Webiste of the Moving Picture Experts Group, MPEG: http://www.mpeg.org/MPEG/index.html

[35] S. Catreux, V. Erceg, D. Gesbert, and R. W. , Jr. Heath, "Adaptive modulation and MIMO coding for broadband wireless data networks," *IEEE Commun. Magazine* vol. 40, pp. 108-115, June 2002.

[36] C. N. Taylor and S. Dey, "Adaptive image compression for wireless multimedia communication," in *IEEE ICC*, pp. 1925 - 1929, 2001.

[37] J. Yang, M. H. Lee, M. Jiang, and J. Y. Park, "Robust wireless image transmission based on turbo-coded OFDM," *IEEE Trans. Consumer Elec.*, vol. 48, no. 3, pp. 724-730, Aug. 2002.

[38] J. G. Proakis, *Digital Communications*, New York, N.Y.: McGraw-Hill Inc., Fourth Edition, 2001.

[39] J. Hagenauer and T. Stockhammer, "Channel coding and transmission aspects for wireless multimedia," *Proc. IEEE*, vol. 87, pp. 1764-1777, Oct. 1999.

[40] S. M. Alamouti, "A simple transmit diversity technique for wireless communications," *IEEE J. Select. Areas Commun.*, vol. 16, pp. 1451-1458, Oct. 1998.

[41] V. Tarokh, H. Jafarkhani, and A. R. Calderbank, "Space-time block codes from orthogonal designs," *IEEE Trans. Inform. Theory*, vol. 45, pp. 1456-1467, Jul. 1998.

[42] V. Tarokh, N. Seshadri, and A. R. Calderbank, "Space-time codes for high data rate wireless communication: Performance criterion and code construction," *IEEE Trans. Inform. Theory*, vol. 44, pp. 744-764, Mar. 1998.

[43] V. Tarokh, H. Jafarkhani, and A. R. Calderbank, "Space-time block coding for wireless communications: Performance results," *IEEE J. Select. Areas in Commun.*, vol. 17, pp. 451-460, Mar. 1999.

[44] B. Vucetic and J. Yuan, *Space-Time Coding*, John Wiley & Sons, West Sussex, England, 2003.

[45] D-S. Shiu, G. J. Foschini, M. J. Gans, and J. M. Khan, "Fading correlation and its effect on the capacity of multielement antenna systems," *IEEE Trans. Commun.*, vol. 48, pp. 502-513, Mar. 2000.

[46] H. Bölcskei and A. J. Paulraj, "Performance of space-time codes in the presence of spatial fading correlation," in *Proc. 34th Asilomar Conf. on Signals, Systems and Computers*, vol. 1, 2000, pp. 687-693.

[47] E. G. Larsson and P. Stoica, *Space-Time Block Coding for Wireless Communications*, Cambridge, U.K.: Cambridge Univ. Press, 2003.

[48] J. Litva and T. K. Lo, *Digital Beamforming in Wireless Communications*, Boston, MA: Artech House, 1996.

[49] 3GPP, *Tx Diversity Solutions for Multiple Antennas*, 3GPP TR25.869, Release 5, V0.1.1, Feb. 2002.

[50] K. H. Lin, *Adaptive Transmit Diversity for Mobile Communication Systems*, Ph.D. Thesis, RMIT University, Aug. 2005.

[51] T. Athanasiadis, K. H. Lin, and Z. M. Hussain, "Space-time OFDM with Adaptive Beamforming for Wireless Multimedia Applications," *Proc. IEEE International Conference on Information Technology and Applications - ICITA 2005*, vol. 2, pp. 381-386, July 2005.

[52] T. Athanasiadis, K H. Lin, and Z. M. Hussain, "Transmission of Compressed Multimedia Data over Wireless Channels using Space-time OFDM with Adaptive Beamforming," *IEEE Region 10 Conference - TENCON 2005*, Nov. 2005.

[53] T. Athanasiadis, K. H. Lin, and Z. M. Hussain, "Multimedia Transmission over Wireless Space-Time-Frequency coded OFDM Systems with Adaptive Beamforming," *Asia-Pacific Conference on Communications - APCC '06*, Aug. 2006.

[54] T. Athanasiadis, K. H. Lin, and Z. M. Hussain, "An Unequal Modulation Scheme for the Transmission of Compressed Multimedia Data over Adaptive MIMO-OFDM Systems," *IEEE Region 10 Conference - TENCON 2006*, Nov. 2006.

[55] J. Jusak, T. Athanasiadis, Z. M. Hussain, "A Blind Equalization Algorithm for Wireless Multimedia Communication," *Asia-Pacific Conference on Communications - APCC 2005*, Oct. 2005.

[56] Y.-S. Lau, T. Athanasiadis, and Z. M. Hussain, "A Secure Digital Communication System for Multimedia Applications Using a Chaotic Generator," *Multimedia Cyberscape Journal*, vol. 5, no. 1, pp. 30-42, 2007.

[57] R. Freeman, *Radio System Design for Telecommunciations*, New York: Wiley, 1997.

[58] J. Gibson, *The Communications Handbook*, Boca Raton, FL: CRC Press, 1997.

[59] A. K. Jain, *Fundamentals of Digital Image Processing*, Prentice Hall, 1989.

[60] A. N. Netravali and B. G. Haskell, *Digital Pictures: Representation, Compression, and Standards*, Plenum Press, New York, 1994.

[61] R. C. Gonzalez and R. C. Woods, *Digital Image Processing*, Addison Wesley, 1992.

[62] H. Nyquist, "Certain topics in telegraph transmission theory," *Trans. AIEE*, vol. 47, pp. 617-644, Apr. 1928. Reprint as classic paper in: *Proc. IEEE*, vol. 90, no. 2, Feb 2002.

[63] C. E. Shannon, "Communication in the presence of noise," *Proc. Institute of Radio Engineers*, vol. 37, no.1, pp. 10-21, Jan. 1949. Reprint as classic paper in: *Proc. IEEE*, vol. 86, no. 2, pp. 447-457, 1998.

[64] M. K. Mandal, S. Panchanathan and T. Aboulnasr, "Wavelet-based image coding using HVS characteristics," *Proc. of SPIE: Wavelets Applications in Signal and Image Processing III*, vol. 2569, pp. 345-352, San Diego, July 1995.

[65] J. A. Saghri, P. S. Cheatham, and A. Habibi, "Image quality measure based on a human visual system model," in *Journal of Optical Engineering*, pp. 813-818, July 1989.

[66] N. S. Jayant, J. Johnston, and R. Safranek, "Signal compression based on models of human perception," in *Proc. of IEEE*, vol. 81, no. 10, Oct. 1993.

[67] ISO/IEC/ JTC1/SC29/WG1, Document N1646R, *JPEG Part I Final Committee Draft*, Version 1, March 16, 2000.

[68] ITU-T Recommendation H.263, *Video Coding for low bitrate communications*, 1996.

[69] B. B. Hubbard, *The World According to Wavelets: A Story of a Mathematical Technique in the Making*, A K Peters: Wellesley, Massachusetts, 1996.

[70] J. S. Walker, *Wavelets and their Scientific Applications*, Chapmann & Hall/CRC Press LLC, 1999.

[71] M. Antonini et al., "Image coding using wavelet transform," *IEEE Trans. on Image Processing*, vol. 1, pp. 205-220, April 1992.

[72] R. A. Devore, B. Jawerth and B. J. Lucier, "Image compression through wavelet coding," *IEEE Trans. on Information Theory*, vol. 38, pp. 719-746, March 1992.

[73] G. Ling, "Wavelet image modelling and its application in model-based image coding," *Proc. of SPIE: VCIP*, vol. 2308, pp. 526-534, 1994.

[74] A. Averbuch, D. Lazar and M. Israeli, "Image compression using wavelet transform and multiresolution decomposition," *IEEE Transactions on Image Processing*, vol. 5, no. 1, pp. 4-15, Jan. 1996.

[75] I. Rabinovitch, A. N. Venetsanopoulos, "High quality image compression using the wavelet transform," *Proc. International Conference on Image Processing*, vol. 1, pp. 283-286, Oct. 1997.

[76] O. O. Khalifa, S. S. Dlay, "Wavelets image data compression," *Proc. IEEE International Symposium on Industrial Electronics*, vol. 2, pp. 407-410, July 1998.

[77] S. Grgic, K. Kers, M. Grgic, "Image compression using wavelets," *Proc. IEEE International Symposium on Industrial Electronics*, vol. 1, pp. 99-104, July 1999.

[78] Z. Xiang, K. Ramchandran, M. T. Orchard, and Y. Q. Zhang, "A comparative study of DCT and wavelet-based image coding," *IEEE Transactions on Circuits and Systems for Video Technology*, vol. 9, pp. 692-695, April 1999.

[79] S. S. Hermami, "Robust image communication over wireless channels," *IEEE Communications Magazine*, vol. 39, no. 11, pp. 120-124, Nov. 2001.

[80] S. Grgic, M. Grgic, and B. Zovko-Cihlar, "Performance analysis of image compression using wavelets," *IEEE Transactions on Industrial Electronics*, vol. 48, no. 3, pp. 682-695, June 2001.

[81] I. Daubechies, *Ten Lectures on Wavelets*, SIAM, 1992.

[82] S. Mallat, "A theory for multiresolution signal decomposition: the wavelet representation," *IEEE Pattern Anal. and Machine Intell.*, vol. 11, no. 7, pp. 674-693, 1989.

[83] S. Mallat, *A Wavelet Tour of Signal Processing*, Academic Press, 1998.

[84] A. Cohen, *Wavelets and Multiscale Signal Processing*, Chapman and Hall, 1995.

[85] R. R. Coifman and M. V. Wickerhauser, "Entropy-based algorithms for best basis selection," *IEEE Trans. on Inf. Theory*, vol. 38, no. 2, pp. 713-718, 1992.

[86] G. Kaiser, *A Friendly Guide to Wavelets*, Birkhauser, 1994.

[87] F. Keinert, *Wavelets and Multiwavelets*, Chapmann & Hall/CRC Press LLC, 2004.

[88] Website of 'The Lenna Story', availble online at: http://www.cs.cmu.edu/* *chuck/lennapg/

[89] Website of Rice University, Digital Signal Processing Group: http://www.dsp.ece.rice.edu/ *wakin/images/

[90] Website of University of Southern California, The USC-SIPI Image Database: http://sipi.usc.edu/database/

[91] Website of University of Waterlo, Fuzzy Image Processing Group: http://pami.uwaterloo.ca/tizhoosh/images.htm

[92] J. B. Andersen, T. S. Rappaport, and S. Yoshida, "Propagation measurements and models for wirless communications channels," *IEEE Commun. Mag.*, pp. 42-49, Jan. 1995.

[93] T. Okumura, et. al., "Field strength and its variability in VHF and UHF land mobile radio services," *Rev. Elec. Communication Lab*, 1968.

[94] R. Price and P. E. Green, Jr., "A communication technique for multipath channels," in *Proc. IRE*, vol. 46, Mar. 1958, pp. 555-70.

[95] W. C. Y. Lee, *Mobile Cellular Telecommunications Analog and Digital Systems*, Singapore: McGraw Hill Inc., Second Edition, 1995.

[96] B. Sklar, "Rayleigh fading channels in mobile digital communication systems Part 1: Characterization," *IEEE Commun. Mag.*, pp. 90-100, July 1997.

[97] A. F. Naguib, V. Tarokh, N. Seshadri, and A. R. Calderbank, "A space-time coding modem for high-data-rate wireless communications," *IEEE J. Select. Areas Commun.*, vol. 16, pp. 1459-1478, Oct. 1998.

[98] M. Pätzold, *Mobile Fading Channels*, West Sussex, U.K.: John Wiley & Sons, 2002.

[99] G. L. Stüber, J. R. Barry, S. W. McLaughlin, Y. Li, M. A. Ingram, and T. G. Pratt, "Broadband MIMO-OFDM wireless communications," *Proc. IEEE*, vol. 92, pp. 271-294, Feb. 2004.

[100] F. Alam, *Space Time Processing for Third Generation CDMA Systems*, Ph.D. Dissertation, Virginia Polytechnic Institute & State University, USA, Nov. 2002.

[101] R. B. Ertel, P. Cardieri, K. W. Sowerby, T. S. Rappaport, and J. H. Reed, "Overview of spatial channel models for antenna array communication systems," *IEEE Personal Commun.*, Feb. 1998.

[102] R. B. Ertel, *Antenna Array Systems: Propagation and Performance*. Ph.D. Dissertation, Virginia Polytechnic Institute & State University, USA, July 1999.

[103] N. Lohse, M. Bronzel, J. Jelitto, D. Hunold, and G. Fettweis, "Analyse des delay/Doppler spread bei raumlicher filterung anhand eines Kanalmodells und Messungen," *ITG-Diskussionssitzung: Systeme mit intelligenten Antennen für UMTS und GMS*, Universität Karlsruhe, June 1998.

[104] J. C. Liberti, *Analysis of CDMA Cellular Radio Systems Employing Adaptive Antennas*. Ph.D. Dissertation, Virginia Polytechnic Institute and State University, Sept. 1995.

[105] J. C. Liberti and T. S. Rappaport, "An analysis of CDMA cellular radio systems employing adaptive antennas," in *Proc. IEEE Veh. Tech. Conf.*, Atlanta, GA, 1996.

[106] J. C. Liberti and T. S. Rappaport, "A geometrically based model for line-of-sight multipath radio channels," in *Proc. IEEE Veh. Tech. Conf.*, Atlanta, GA, 1996, pp. 844-848.

[107] O. Nørklit and J. B. Anderson, "Mobile radio environments and adaptive arrays," in *Proc. of IEEE PIMRC*, vol. 2, 1994, pp. 725-728.

[108] W. C. Y. Lee, "Spectrum efficiency in cellular," *IEEE Trans. Veh. Tech.*, vol. 38, pp. 69-75, May 1989.

[109] Y. Z. Mohasseb and M. P. Fitz, "A 3-D spatio-temporal simulation model for wireless channels," *IEEE J. Select. Areas Commun.*, vol. 20, pp. 1193-1203, Aug. 2002.

[110] S. S. Mahmoud, Z. M. Hussain, and P. O'Shea, "A space-time model for mobile radio channels with hyperbolically distributed scatterers," *IEEE Antennas and Wireless Propagation Letters*, vol. 1, pp. 211-214, 2002.

[111] S. S. Mahmoud, *Space-time Channel Modelling for CDMA Mobile Communications*, Ph.D. Dissertation, RMIT University, Australia, July 2004.

[112] S. S. Mahmoud, Z. M. Hussain, and P. O'Shea, "A Geometrical-Based Channel Model with Hyperbolically Distributed Scatterers for a Macrocell Mobile Environment with Antenna Array," *Multimedia Cyberscape Journal*, vol. 2, pp.1-10, 2004.

[113] S. S. Mahmoud, Z. M. Hussain, and P. O'Shea, "A geometrical-based microcell mobile radio channel model," In press, *Kluwer Journal on Wireless Networks*.

[114] K. I. Pedersen, P. E. Mogensen, and B. Fleury, "A stochastic model of the temporal and azimuthal dispersion seen at the base station in outdoor propagation environments,"*IEEE Trans. Veh. Technol.*, vol. 49, pp. 437-447, Mar. 2000.

[115] R. Janaswamy, "Angle and Time of Arrival Statistics for the Gaussian Scatter Density Model,"*IEEE Trans. Wireless Commun.*, vol. 1, pp. 488-497, July 2002.

[116] Q. H. Spencer, B. D. Jeffs, M. A. Jensen, and A. L. Swindlehurst, "Modeling the Statistical Time and Angle of Arrival Characteristics of an Indoor Multipath Channel,"*IEEE J. Select. Areas Commun.*, vol. 18, pp. 347-360, Mar. 2000.

[117] P. V. Rooyen, M. Lötter, and D. V. Wyk, *Space-Time Processing for CDMA Mobile Communications*, Norwell, Massachusetts: Kluwer Academic, 2000.

[118] A. J. Paulraj and C. B. Papadias, "Space-time processing for wireless communications: Improving capacity, coverage, and quality in wireless network by exploiting the spatial dimension," *IEEE Personal Commun.*, vol. 14, pp. 49-83, Nov. 1997.

[119] B. Sklar, *Digital Communications; Fundamentals and Applications*, Upper Saddle River, NJ: Prentice-Hall Inc., Second Edition, 2000.

[120] J. H. Winters, "Smart antennas for wireless systems," *IEEE Personal Commun.*, pp. 23-27, Feb. 1998.

[121] G. J. Foschini and M. J. Gans, "On limits of wireless communications in a fading environment when using multiple antennas," *Wireless Pers. Commun.*, vol. 6, no. 3, pp. 311-335, Mar. 1998.

[122] I. E. Telatar, "Capacity of multi-antenna Gaussian channels," *Eur. Trans. Tel.*, vol. 10, no. 6, pp. 585-595, Nov./Dec. 1999.

[123] J. Winters, "The diversity gain of transmit diversity in wireless systems with Rayleigh fading," *IEEE Trans. Veh. Technol.*, vol. 47, pp. 119-123, Feb. 1998.

[124] A. J. Paulraj, D. A. Gore, R. U. Nabar, and H. Bölcskei, "An overview of MIMO communications - A key to gigabit wireless," *Proc. IEEE*, vol. 92, pp. 198-218, Feb. 2004.

[125] R. S. Blum, J. H. Winters, and N. R. Sollenberger, "On the capacity of cellular systems with MIMO," *IEEE Commun. Lett.*, vol. 6, pp. 242-244, June 2002.

[126] H. Jafarkhani, "A quasi-orthogonal space-time block code," *IEEE Trans. Commun.*, vol. 49, pp. 1-4, Jan. 2001.

[127] G. Ganesan and P. Stoica, "Space-time diversity using orthogonal and amicable orthogonal designs," in *Proc. IEEE ICASSP'00*, vol. 5, June 2000, pp. 2561-2564.

[128] G. Ganesan and P. Stoica, "Space-time block codes: A maximum SNR approach," *IEEE Trans. Inform. Theory*, vol. 47, pp. 1650-1656, May 2001.

[129] Y. Li, B. Vucetic, Y. Tang, and Q. Zhang, "Space-time trellis codes with linear transformation for fast fading channels," *IEEE Signal Processing Lett.*, vol. 11, pp. 895-898, Nov. 2004.

[130] P. Chevalier and A. Ferreol, "On the virtual array concept for the fourth-order direction finding problem," *IEEE Trans. Signal Processing*, vol. 47, pp. 2592-2595, Sept. 1999.

[131] B. Porat and B. Friedlander, "Direction finding algorithms based on higher order statistics," *IEEE Trans. Signal Processing*, vol. 39, pp. 2016-2024, Sept. 1991.

[132] Siemens, *Simulation Parameters for Tx diversity simulations using correlated antennas*, 3GPP Document TSG-RAN WG1 #16, R1-00-1180, Pusan, Korea, Oct. 2000.

[133] S. Siwamogsatham and M. P. Fitz, "Robust space-time codes for correlated Rayleigh fading channels," *IEEE Trans. Signal Processing*, vol. 50, pp. 2408-2416, Oct. 2002.

[134] Y. S. Yeh and D. O. Reudink, "Efficient spectrum utilization for mobile radio systems using space diversity," in *IEE Int. Conf. Radio Spectrum Conservation Techniques*, London, 1980, pp. 12-16.

[135] Y. S. Yeh and D. O. Reudink, "Efficient spectrum utilization for mobile radio systems using space diversity," in *IEEE Trans. Commun.*, vol. COM-30, pp. 447-455, Mar. 1982.

[136] Z. Wang, X. Ma, and G. B. Giannakis, "OFDM or single-carrier block transmissions?," *IEEE Trans. Commun.*, vol. 52, pp. 380-394, Mar. 2004.

[137] Z. Wang and G. B. Giannakis, "Wireless multicarrier communications; where Fourier meets Shannon," *IEEE Signal Processing Mag.*, pp. 29-48, May 2000.

[138] D. Agrawal, V. Tarokh, A. Naguib, and N. Seshadri, "Space-time coded OFDM for high data-rate wireless communication over wideband channels," in *Proc. IEEE VTC*, 1998, pp. 2232-2236.

[139] S. Zhou and G. B. Giannakis, "Space-time coding with maximum diversity gains over frequency-selective fading channels," *IEEE Signal Processing Lett.*, vol. 8, pp. 269-272, Oct. 2013.

[140] S. Zhou and G. B. Giannakis, "Space-time coded transmissions with maximum diversity gains over frequency-selective multipath fading channels," in *Proc. IEEE GLobeCom'01*, Nov. 2001, pp. 440-444.

[141] B. Lu, X. Wang, and K. R. Narayanan, "LDPC-based space-time coded OFDM systems over correlated fading channels: Performance analysis and receiver design," *IEEE Trans. Commun.*, vol. 50, pp. 74-88, Jan. 2002.

[142] B. Lu and X. Wang, "Space-time code design in OFDM systems," in *Proc. IEEE GlobeCom'00*, vol. 2, Nov.-Dec. 2000, pp. 1000-1004.

[143] Z. Hong and B. L. Hughes, "Robust space-time codes for broadband OFDM systems," in *Proc. IEEE WCNC'02*, vol. 1, Mar. 2002, pp. 105-108.

[144] D. Gesbert, M. Shafi, D.-S. Shiu, P. J. Smith, and A. Naguib, "From theory to practice: An overview of MIMO space-time coded wireless systems," *IEEE J. Select. Areas Commun.*, vol. 21, pp. 281-302, Apr. 2003.

[145] M. Qin and R. S. Blum, "Properties of space-time codes for frequency-selective channels," *IEEE Trans. Signal Processing*, vol. 52, pp. 694-702, Mar. 2004.

[146] H. Bölcskei and A. J. Paulraj, "Space-frequency coded broadband OFDM systems," in *Proc. IEEE WCNC2000*, Sept. 2000, pp. 1-6.

[147] Y. Gong and K. B. Letaief, "An efficient space-frequency coded OFDM system for broadband wireless communications," *IEEE Trans. Commun.*, vol. 51, pp. 2019-2029, Nov. 2003.

[148] Y. Gong and K. B. Letaief, "An efficient space-frequency coded wideband OFDM system for wireless communications," in *Proc. IEEE ICC'02*, Apr. 2002, pp. 475-479.

[149] K. F. Lee and D. B. Williams, "A space-frequency transmitter diversity technique for OFDM systems," in *Proc. IEEE GlobeCom'00*, vol. 3, Nov.-Dec. 2000, pp. 1473-1477.

[150] A. F. Molisch, M. Z. Win, and J. H. Winters, "Space-time-frequency coding for MIMO-OFDM systems," *IEEE Commun. Lett.*, vol. 6, no. 9, pp. 370-372, Sep. 2002.

[151] Y. Gong and K. B. Letaief, "Space-frequency-time coded OFDM for broadband wireless communications," in *Proc. IEEE GLOBECOM'01*, vol. 1, Nov. 2001, pp. 519-523.

[152] Z. Liu, Y. Xin, and G. B. Giannakis, "Space-time-frequency coded OFDM over frequency-selective fading channels," *IEEE Trans. Signal Processing*, vol. 50, pp. 2465-2476, Oct. 2002.

[153] Z. Liu, Y. Xin, and G. B. Giannakis, "Space-time-frequency block coded OFDM with subcarrier grouping and constellation precoding," in *Proc. IEEE ICASSP'02*, vol. 3, 2002, pp. 2205-2208.

[154] A. Goldsmith, S. A. Jafar, N. Jindal, and S. Vishwanath, "Capacity limits of MIMO channels," *IEEE J. Select. Areas Commun.*, vol. 21, pp. 684-702, June 2003.

[155] J. W. Shao, M.-S. Alouini, and A. J. Goldsmith, "Impact of fading correlation and unequal branch gains on the capacity of diversity systems," *IEEE 49th Vehicular Technology Conference*, 1999, pp. 2159-2163.

[156] R. K. Mallik, M. Z. Win, J. W. Shao, M.-S. Alouini, and A. J. Goldsmith, "Channel capacity of adaptive transmission with maximal ratio combining in correlated Rayleigh fading," *IEEE Trans. Wireless Commun.*, vol. 3, pp. 1124-1133, July 2004.

[157] H. Bölcskei, D. Gesbert, and A. J. Paulraj, "On the capacity of OFDM-based spatial multiplexing systems," *IEEE Trans. Commun.*, vol. 50, pp. 225-234, Feb. 2002.

[158] C. E. Shannon, "A mathematical theory of communication," *Bell Syst. Tech. J.*, vol. 27, pp. 379-423, July/Oct. 1948.

[159] P. W. Howells, "Intermediate frequency sidelobe canceller," Technical report, U.S. Patent 3202990, May 1959.

[160] S. P. Applebaum, "Adaptive arrays," Technical Report SPL TR 66-001, Syracuse Uni. Research Corp., 1965 (reprinted in *IEEE Trans. Antennas Propagat.* vol. AP-24, pp. 650-662, Sept. 1976).

[161] B. Widrow and M. E. Hoff, "Adaptive switch circuits," in *IRE WESCOM, conv. Rec.*, Part 4, pp. 96-104, 1960.

[162] B. Widrow, P. E. Mantey, L. J. Griffiths, and B. B. Goode, "Adaptive antenna systems," *Proc. IEEE*, vol. 55, pp. 2143-2159, Dec. 1967.

[163] L. J. Griffiths, "A simple adaptive algorithm for real-time processing in antenna arrays," *Proc. IEEE*, vol. 57, pp. 64-78, Oct. 1969.

[164] T. E. Curtis, "Digital beam forming for sonar system," *IEE Proc. Pt. F*, vol. 127, pp. 257-265, Aug. 1980.

[165] P. Barton, "Digital beamforming for radar," *IEE Proc. Pt. F*, vol. 127, pp. 257-265, Aug. 1980.

[166] J. Capon, "High-resolution frequency-wavenumber spectrum analysis," *Proc. IEEE*, vol. 57, pp. 1408-1418, Aug. 1969.

[167] B. D. Van Veen and K. M. Buckley, "Beamforming: A versatile approach to spatial filtering," *IEEE ASSP Magazine*, pp. 4-24, Apr. 1988.

[168] R. O. Schmidt, "Multiple emitter location and signal parameter estimation," in *Proc. RADC Spectrum Estimation Workshop*, Griffiths AFB, NY, 1979, pp. 243-258.

[169] R. O. Schmidt, *A signal subspace approach to multiple emitter location and spectral estimation*. Ph.D. dissertation, Stanford Univ., Stanford, CA, 1981.

[170] A. Paulraj, R. Roy, and T, Kailath, "Estimation of signal parameters via rotational invariance techniques - ESPRIT," in *Proc. 19th Asilomar Conf. Circuits, Syst. Comput.,* Asilomar, CA, Nov. 1985.

[171] R. Roy, A. Paulraj, and T, Kailath, "ESPRIT - A subspace rotation approach to estimation of parameters of cisoids in noise," *IEEE Trans. ASSP*, vol. ASSP-34, pp. 1340-1342, Nov. 1986.

[172] T. K. Y. Lo, "Maximum ratio transmission," *IEEE Trans. Commun.*, vol. 47, pp. 1458-1461, Oct. 1999.

[173] C.-C. Lee and J.-H. Lee, "Eigenspace-based adaptive array beamforming with robust capabilities," *IEEE Trans. Antennas Propagat.*, vol. 45, pp. 1711-1716, Dec. 1997.

[174] A. Seeger, A. Lobinger, R. Widemann, and B. Raaf, "Downlink Eigenbeamformer with combining of eigenbeams," in *Proc. IEEE GlobeCom'01*, vol. 5, 2001, pp. 3211-3216.

[175] A. Seeger, A. Lobinger, R. Widemann, and B. Raaf, "Performance of downlink eigenbeamformer with realistic feedback transmission," in *Proc. IEEE 54th Vehicular Technology Conference*, vol. 3, Oct. 2001, pp. 7-11.

[176] C. Brunner, J. S. Hammerschmidt, A. Seeger, and J. A. Nossek, "Space-time eigenrake and downlink eigenbeamformer: Exploiting long-term and short-term channel properties in WCDMA," in *Proc. IEEE GlobeCom'00*, vol. 1, Nov.-Dec. 2000, pp. 138-142.

[177] C. Brunner, *Efficient Space-Time Processing Schemes for WCDMA*, Ph.D. Dissertation, Munich University of Technology, Germany, June 2000.

[178] J. S. Hammerschmidt, C. Brunner, and C. Drewes, "Eigenbeamforming - a novel concept in array signal processing," in *Proc. IEEE European Wireless 2000*, Dresden, Germany, Sept. 2000.

[179] Siemens, *Channel Model for Tx Diversity Simulations using Correlated Antennas*, 3GPP Document TSG-RAN WG1 #15, R1-00-1067, Berlin, Germany, Aug. 2000.

[180] G. G. Raleigh and J. M. Cioffi, "Spatio-temporal coding for wireless communication," *IEEE Trans. Commun.*, vol. 46, pp. 357-366, 1998.

[181] G. Jöngren, M. Skoglund, and B. Ottersten, "Combining beamforming and orthogonal space-time block coding," *IEEE Trans. Inform. Theory*, vol. 48, pp. 611-627, Mar. 2002.

[182] H. Sampath and A. Paulraj, "Linear precoding for space-time coded systems with known fading correlations," *IEEE Commun. Lett.*, vol. 6, pp. 239-241, June 2002.

[183] W. C. Jakes, *Microwave Mobile Communications*, New York, John Wiley & Sons, 1974.

[184] K. H. Lin, Z. M. Hussain, and R. Harris, "Orthogonal space-time block coding with adaptive transmit diversity for correlated MIMO channels," in *Proc. Second WSEAS International Conference on Electronics, Control, and Signal Processing (ICECS'03)*, Singapore, Dec. 2003.

[185] K. H. Lin, Z. M. Hussain, and R. Harris, "Adaptive transmit eigenbeamforming with orthogonal space-time block coding in correlated space-time channels," in *Proc. IEEE ICASSP'04*, Montreal, May 2004, pp. 817-820.

[186] K. H. Lin, Z. M. Hussain, and R. J. Harris, "Space-time OFDM with adaptive beamforming: Performance in spatially correlated channels," in *Proc. IEEE TENCON'04*, Chiang-Mai, Nov. 2004, pp. 617-620.

[187] S. S. Mahmoud, K. H. Lin, and Z. M. Hussain, "Performance of adaptive transmit diversity with orthogonal space-time block coding in microcell and macrocell channel environments," accepted in *IEEE TENCON'05*, Melbourne, Nov. 2005.

[188] Website of MathWorks - MATLAB®:
http://www.mathworks.com/products/matlab/

[189] Website of MathWorks - MATLAB®Product List:
http://www.mathworks.com/products/product_listing/

[190] D. Gerlach and A. Paulraj, "Adaptive transmitting antenna arrays with feedback," *IEEE Signal Processing Lett.*, vol. 1, no. 10, Oct. 1994.

[191] R. W. Heath Jr. and A. Paulraj, "A simple scheme for transmit diversity using partial channel feedback," in *Proc. Thirty-Second Asilomar Conference on Signals, Systems, and Computers*, 1998, pp. 1073-1078.

[192] K. K. Mukkavilli, A. Sabbarwal, and B. Aazhang, "Design of multiple antenna coding schemes with channel feedback," in *Proc. Thirty-Fifth Asilomar Conference on Signals, Systems, and Computers*, 2001, pp. 1009-1013.

[193] S. Zhou and G. B. Giannakis, "Adaptive modulation for multi-antenna transmissions with channel mean feedback," in *Proc. IEEE ICC'03*, May 2003, pp. 2281-2285.

[194] S. Zhou and G. B. Giannakis, "Adaptive modulation for multiantenna transmissions with channel mean feedback," in *IEEE Trans. Wireless Commun.*, vol. 3, pp. 1626-1636, Sept. 2004.

[195] E. Visotsky and U. Madhow, "Space-time transmit precoding with imperfect feedback," *IEEE Trans. Inform. Theory*, vol. 47, no. 6, Sept. 2001.

[196] K. H. Lin and Z. M. Hussain, "Performance of STF coded OFDM with transmit eigenbeamforming in correlated fading channels," revised version submitted to *IEEE Signal Processing Lett.*, 2005.

[197] K. H. Lin and Z. M. Hussain, "Adaptive bit and power allocation with sub-channel grouping for OFDM systems," in *Proc. Third Workshop on the Internet, Telecommunications and Signal Processing (WITSP'04)*, Adelaide, Dec. 2004.

[198] K. H. Lin, S. S. Mahmoud, and Z. M. Hussain, "Adaptive modulation with space-time block coding for MIMO-OFDM systems," in *Proc. IEEE International Conference on Information Technology and Applications (ICITA'05)*, Sydney, July 2005, pp. 299-304.

[199] K. H. Lin and Z. M. Hussain, "Space-time block coded OFDM with adaptive modulation and transmitter beamforming," in *Proc. IEEE GlobeCom'05*, St. Louis, Nov. 2005, pp 3487-3492.

[200] K. H. Lin and Z. M. Hussain, "An adaptive bit and power allocation algorithm for OFDM systems with eigenbeamforming," submitted to *WSEAS Trans. Communi*, 2005.

[201] K. H. Lin and Z. M. Hussain, "Adaptive modulation for space-time block coded OFDM with transmitter beamforming," submitted to *Australian Journal of Electrical and Electronics Engineers*, 2005.

[202] K. Skretting, J. H. Husoy, and S. O. Aase, "Improved huffman coding using recursive splitting," *NORSIG 1999, Proc. Norwegian Signal Proc. Symp.*, Asker, Norway, Sept. 1999.

[203] P. S. Chung and A. J. Goldsmith, "Degrees of freedom in adaptive modulation: A unified view," *IEEE Trans. Commun.*, vol. 49, no. 9, pp. 1561-1571, Sep. 2001.

[204] J. R. Treichler, I. Fijalkow and C. R. Johnson, Jr., "Fractionally spaced equalizers: How long should they really be?," *IEEE Signal Processing Magazine*, vol. 13, no. 3, pp. 65-81, May 1996.

[205] J. R. Treichler, M. G. Larimore and J. C. Harp, "Practical blind modulators for high-order QAM signals," *Proccedings of IEEE*, vol. 86, no. 10, pp. 1907-1925, Oct. 1998.

[206] M. G. Larimore and M. J. Goodman, "Implementation of the constant modulus algorithm at RF bandwidths," *Proccedings of Asilomar Conference on Signals, Systems and Computers*, pp. 626-630, Nov. 1985.

[207] Gi Hong Im, Cheol Jin Park and Hui Chui Won, "A blind equalization with the sign algorithm for broadband access," *IEEE Communications Letters*, vol. 5, no. 2, pp. 70-72, Feb. 2001.

[208] J.-Jacques Werner, J. Yang, D. D. Harman and G. A. Dumont, "Blind equalization for broadband access," *IEEE Communications Magazine*, vol. 37, no. 4, pp. 87-93, Apr. 1999.

[209] H. Sari, G. Karam and I. Jeanclaude, "Transmission techniques for digital terrestrial TV bradcasting," *IEEE Communications Magazine*, vol. 32, no. 2, pp. 100-109, Feb. 1995.

[210] S. L. Ariyavisitakul and G. M. Durant, "A broadband wireless packet technique base on coding, diversity, and equalization," *IEEE Communications Magazine*, vol. 36, no. 7, pp. 110-115, Jul. 1998.

[211] D. Godard, "Self-recovering equalization and carrier tracking in two dimensional data communication systems," *IEEE Trans. Commun.*, vol. 28, pp. 1867-1875, 1980.

[212] C. R. Johnson, Jr., P. Schniter, T. J. Endres, J. D. Behm, D. R. Brown, and R. A. Casas, "Blind equalization using the constant modulus criterion: A review," *Proc. IEEE*, vol. 86, no. 10, pp. 1927-1950, Oct. 1998.

[213] J. Jusak and Z. M. Hussain, "Evaluation of a sinusoidally-distributed dithering for signed-error constant modulus algorithm: performance comparison with uniformly-distributed dithering," *Proccedings of The 3rd Workshop on the Internet, Telecommunications and Signal Processing (WITSP)*, pp. 53-57, Dec. 2004.

[214] J. Jusak and Z. M. Hussain, "Blind Adaptive Multiuser Detection for DS-CDMA Utilizing Sinusoidally-Distributed DSE-CMA," *IEEE Region 10 Conference - TENCON 2005*, Nov. 2005.

[215] J. Jusak and Z. M. Hussain, "Blind Adaptive Multiuser Detection for Chaos CDMA Communication," *IEEE Region 10 Conference - TENCON 2005*, Nov. 2005.

[216] J. Jusak and Z. M. Hussain, "Performance of Sinusoidally-Distributed Dithering for Signed-Error Constant Modulus Algorithm," *Proccedings of IEEE International Conference on Information Technology and Applications (ICITA 2005)*, vol. 2, pp. 626-629, Jul. 2005.

[217] P. Schniter and R. J. Johnson, Jr., "Dithered signed-error CMA: the complex-valued case," *Proc. 32nd Asilomar Conf. on Signals, Systems, and Computers*, pp. 1143-1147, 1998.

[218] P. Schniter and R. J. Johnson, Jr., "Dithered signed-error: robust, computationally efficient blind adaptive equalization," *IEEE Trans. Signal Processing*, vol. 47, no. 6, pp. 1592-1603, 1999.

[219] Y.-S. Lau and Z. M. Hussain, "A new approach in chaos shift keying for secure communication," *Proc. IEEE International Conference on Information Technology and Applications - ICITA 2005*, July 2005.

[220] F. C. M. Lau, C. K. Tse, M. Ye, and S. F. Hau, "Coexistence of chaos-based and conventional digital communication systems of equal bit rate," *IEEE Trans. Circuits and Systems*, vol. 51, pp. 391-408, Feb. 2004.

[221] F. C. M. Lau and C. K. Tse, "Coexistence of chaos-based and conventional digital communication system," *Proc. IEEE ISCAS*, vol. 3, pp. 204-207, May 2003.

[222] S. S. Rao and S. P. Howard, "Correlation performance of chaotic signals in spread spectrum systems," *Proc. IEEE Digital Signal Processing Workshop*, pp. 506-509, Sept. 1996.

[223] G. Heidari-Bateni and C. D. McGillem, "A chaotic direct-sequence spread-specturm communication system," *IEEE Trans. Communications*, vol. 42, no. 234, pp. 1524- 1527, Apr. 1994.

[224] G. Heidari-Bateni and C. D. McGillem, "Chaotic sequences for spread spectrum: an alternative to PN-sequences," *Proc. ICWC*, pp. 437-440, Jun. 1992.

[225] L. Pecora and T. Carroll, "Synchronization in chaotic systems," *Phys. Rev. Letters*, vol. 64, pp. 821-824, 1990.

[226] G. Kolumban, M. P. Kennedy, Z. Jako, and G. Kis, "Chaotic communications with correlator receivers: theory and performance limits," *Proc. of the IEEE*, vol. 90, pp. 711-732, 2002.

[227] M. P. Kennedy and G. Kolumban, "Digital communications using choas," *Elsevier Signal Processing Journal*, vol. 80, pp. 1307-1320, 2000.

[228] T. Kohda and A. Tsuneda, "Even- and odd-correlation fucntions of chaotic chebyshev bit sequences for CDMA," *Proc. IEEE Int. Symp. Spread Specturm Technology and Applications*, pp. 391-395, 1994.

[229] Y.-S. Lau and Z. M. Hussain, "Chaos Shift Keying Spread Spectrum with Multicarrier Modulation for Secure Digital Communication," *WSEAS Transactions on Communications*, vol. 4, no. 1, Jan. 2005.

[230] Y.-S. Lau, K. H. Lin, and Z. M. Hussain, "Space-Time Encoded Secure Chaos Communications with Transmit Beamforming," *Proc. IEEE Region 10 Conference - TENCON 2005*, Nov. 2005.

[231] M. Ibnkahla, *Signal Processing for Mobile Communications Handbook*, CRC Press, ch. 10, 2005.

[232] Y.-S. Lau and Z. M. Hussain, "Chaotic-based OFDM-CDMA for secure digital communications: Performance comparison with PN-based OFDM-CDMA," *Proc. The 3rd Workshop on the Internet, Telecommunications and Signal Processing (WITSP)*, Adelaide, Australia, Dec. 2004.

[233] P. Stavroulakis, *Neuro-Fuzzy and Fuzzy-Neural Applications in Telecommunications*, Springer-Verlag Berlin Heidelberg, Germany, 2004.

[234] M. B. Martin and A. E. Bell, "New image compression techniques using multiwavelets and multiwavelet packets," *IEEE Transactions on Image Processing*, vol. 10, no. 4, pp. 500-510, Apr. 2001.

[235] J. Armstrong, P. M. Grant, and G. Povey, "Polynomial cancellation coding of OFDM to reduce intercarrier interference due to Doppler spread," in *IEEE GlobeCom*, vol. 5, Nov. 1998, pp. 2771 - 2776.

[236] J. Armstrong, "Analysis of new and existing methods of reducing intercarrier interference due to carrier frequency offset in OFDM ," *IEEE Trans. Commun.* vol. 47, pp. 365 - 369, March 1999.

VITA

Tasso Athanasiadis was born in Wangaratta (Victoria), Australia on May 20, 1971. He received his B.Eng. degree in electronic engineering (with honours) and M.Eng. degree both from RMIT University, Melbourne, Australia in June 1993 and October 2000, respectively. From 1993 to 2000 he undertook various academic positions at RMIT University, including sessional teaching at the School of Infrastructure, Electrotechnology and Building Services (SIEBS), delivering advanced diploma courses in electronics and computer systems. He was also a tutor/laboratory supervisor at the School of Electrical and Computer Engineering (SECE), delivering classes for undergraduate courses in electronics, communication systems, and engineering design. From 1999 to 2002 he worked as a systems integration and test engineer at NEC Australia on the development of a global mobile-satellite communications network (known as, ICO Net). During this time he was also a sessional teacher at SIEBS, delivering specialized classes in electronics and computer networking (organized primarily for students working in industry). In 2002, he took up a position as a research engineer at SECE, where he worked on the implementation of the 3GPP WCDMA mobile standards for NEC Australia in a joint RMIT/NEC project. From mid 2002 to 2004, he was appointed as the principal lecturer and coordinator for the 2nd year undergraduate course Engineering Design & Innovation, where he delivered lectures, laboratory and tutorial classes, and supervised major student projects. In 2004, he was awarded a 3-year scholarship from SECE to undertake his PhD research. During his PhD candidacy, he continued working as a sessional teacher at SIEBS delivering advanced diploma courses in electronics and digital systems, and also as a sessional academic at SECE delivering classes at both undergraduate and postgraduate levels in digital signal processing, communication systems, and engineering design. He also authored and published 5 technical papers at various IEEE conferences and a paper in the *Multimedia Cyberscape Journal*. He received two consecutive IEEE (Victoria Chapter) First Awards at the 2005 & 2006 RMIT Annual Postgraduate Conferences. His research interests include multimedia signal processing, data compression techniques for image/video coding, and digital wireless communications. Mr. Athanasiadis is a valued member of the IEEE. Currently he holds a position as a technical specialist with Telstra, Australia's leading telecommunications and information services company, providing high-level technical support and fault management for three core mobile networks - GSM, CDMA, and 3G-850 (WCDMA).